

**UNIVERSITY OF CALIFORNIA**

**Los Angeles**

**Adaptive Diversity Combining, Equalization and  
Sequence Decoding for Time-Varying Dispersive  
Channels**

A dissertation submitted in partial satisfaction of the  
requirements for the degree of Doctor of Philosophy  
in Electrical Engineering

by

**Heung-No Lee**

1999

© Copyright by Heung-No Lee, 1999

All Rights Reserved

The dissertation of Heung-No Lee is approved.

---

Kirby A. Baker

---

Babak Daneshrad

---

Kung Yao

---

Gregory J. Pottie, Committee Chair

University of California, Los Angeles

1999

# Contents of the Dissertation

**Contents of the Dissertation iii**

**List of Figures x**

**List of Tables xviii**

**Acknowledgments xix**

**Vita xxi**

**Abstract of the Dissertation xxii**

<b>1. Introduction .....</b>	<b>1</b>
1.1 Recent Advances in Communications Technologies .....	1
1.1.1 The advent of the Internet .....	1
1.1.2 The wireless networks .....	2
1.1.3 The hybrid networks and emergence of the universal computing systems .....	3
1.1.4 Need for spectrally efficient, robust wireless modem technologies .....	4
1.2 Overview of Dissertation .....	5
1.3 Roadmap of Dissertation .....	7

<b>2.</b>	<b>Wireless Channels and Simulation Models .....</b>	<b>13</b>
2.1	Characterization of Multipath Channels .....	13
2.1.1	Multipath fading: the small-scale variation of the signal strength	14
2.1.2	Shadow fading: the large-scale variation of the signal strength	16
2.1.3	Multipath delay spread .....	17
2.1.4	Time-variation of a fading component .....	18
2.2	Wireless Propagation Channels .....	20
2.2.1	Typical multipath delay profiles .....	20
2.2.2	Basic mechanism of signal propagation .....	21
2.2.3	Building a suitable channel model for a geographic region .....	23
2.2.4	Frequency-selective channels due to multipath spread .....	26
2.2.5	Time-varying channel due to Doppler spreading .....	29
2.3	The Diversity FIR Channel Model .....	36
2.3.1	FIR representation of the channel, transmit and receive filters	36
2.3.2	Diversity receive antennas .....	40
2.3.3	Diversity antenna channel model .....	40
2.3.4	Generation of independent diversity channels .....	43
2.4	Concluding Remarks .....	44
<b>3.</b>	<b>Background and Equalizers .....</b>	<b>47</b>
3.1	Simulation of Digital Communication Systems .....	48
3.1.1	Baseband Representation of the Bandpass Systems .....	49

3.2	LE, DFE and TH-precoder .....	54
3.2.1	Ideal output SNR comparison of LE and DFE .....	58
3.2.2	Output SNR for finite length DFE .....	61
3.2.3	TH-Precoder .....	62
3.2.4	Simulation comparison of DFE and TH-Precoder .....	64
3.3	LMS and RLS training of DFE filter .....	65
3.3.1	LMS training of DFE filters .....	67
3.3.2	RLS training of DFE filters .....	72
3.4	Concluding Remarks .....	75
<b>4.</b>	<b>Feedforward Channel Estimation and Tracking .....</b>	<b>78</b>
4.1	Why Not Symbol-By-Symbol Recursive Adaptation? .....	79
4.1.1	Recursive adaptation of DFE filters using LMS and RLS .....	79
4.1.2	Recursive channel estimation using LMS and RLS .....	80
4.2	The Structure of Feedforward Channel Estimation .....	85
4.3	Parametric Channel Estimation .....	88
4.3.1	Construction of channel estimation equation .....	90
4.3.1.1	Constructing the SRRC matrix .....	93
4.4	Novel Channel Estimators .....	93
4.4.1	The Least Squares Estimator .....	94
4.4.2	The Maximum Likelihood Estimator .....	94
4.4.3	The Maximum A Posteriori Estimator .....	95

4.5	The Mean Squares Channel Estimation Errors .....	96
4.6	The Optimal Training Sequences .....	98
4.7	Simulation Results and Discussion .....	100
4.8	Concluding Remarks .....	104
<b>5.</b>	<b>Diversity Combining DFE .....</b>	<b>106</b>
5.1	Robust Signal Detection over Fast Multipath Fading, ISI Channels ..	107
5.2	Baseband Equivalent Channel Model .....	109
5.3	Diversity-Combining DFE .....	111
5.3.1	The Wiener-Hopf normal equation .....	112
5.3.2	A straightforward solution .....	116
5.3.3	A matched filtered diversity combining DFE solution .....	118
5.3.4	The equivalent single channel .....	123
5.4	Simulation Results and Discussion .....	125
5.4.1	BER performance in slow fading .....	125
5.4.2	BER performance in fast fading .....	127
5.4.3	The sources of BER floor .....	129
5.4.4	The suboptimal T-DFE and the DFE update periods. ....	132
5.4.5	Computational complexities .....	133
5.5	Concluding Remarks .....	133
<b>6.</b>	<b>Matched Filter Bounds and Spectral Efficiency .....</b>	<b>137</b>

6.1	Matched Filter Bound .....	138
6.1.1	Sampled, matched filter output .....	141
6.1.2	Square-QAM symbol error probability .....	142
6.1.3	Average symbol error probability for square-QAM .....	144
6.1.3.1	Distinct eigenvalues (no eigenvalues in multiplicity)	147
6.1.3.2	Eigenvalues occurring in multiplicity .....	149
6.1.3.3	Combination of distinct and multiple poles .....	154
6.2	Spectral Efficiency of the Fading ISI Channels .....	160
6.2.1	Maximum Spectral Efficiency Calculation .....	161
6.3	Concluding Remarks .....	171
<b>A.</b>	<b>Integration of erfc-function over Chi-square distribution.....</b>	<b>172</b>
<b>7.</b>	<b>Sequential Detection .....</b>	<b>176</b>
7.1	Introduction .....	177
7.1.1	Motivation for sequence based detection .....	177
7.1.2	Reduced complexity sequence based detection techniques ....	178
7.1.3	The pre-processing filters .....	181
7.2	Optimum Diversity Combining MLSD .....	184
7.2.1	The baseband channel model .....	184
7.2.2	Derivation of the optimum diversity combining MLSD .....	188
7.2.3	The Ungerboeck's receiver .....	191

7.2.4	Forney's MLSD receiver .....	193
7.2.5	The finite length whitening filter .....	196
7.2.6	The mean-square whitening filter .....	199
7.3	The Proposed MLSD Postprocessor .....	205
7.3.1	The equivalent input/output equation .....	205
7.3.2	The proposed T-algorithm .....	206
7.3.3	Why T-algorithm is efficient? .....	207
7.4	Per-Survivor Tracking of the Channel Mismatch .....	208
7.4.1	The channel mismatch and optimal tracking .....	210
7.4.2	Modeling and suboptimal tracking of the channel mismatch ..	213
7.5	Simulation Results and Discussion .....	215
7.5.1	Static channel simulation .....	216
7.5.2	The Rayleigh fading ISI channel .....	218
7.6	Concluding Remarks .....	227
<b>8.</b>	<b>Decoding of Trellis Coded Modulated Signals .....</b>	<b>231</b>
8.1	Introduction .....	232
8.2	The system description .....	234
8.3	The receivers .....	238
8.3.1	The Euclidean distance metric from MLSE .....	238
8.3.2	Joint decoder without the use of interleaver .....	238
8.3.3	Separate equalization and decoding with the use of an interleaver	

	239
8.3.4	The proposed joint tree searching T-algorithm receiver ..... 240
8.4	Simulation Results and Discussion ..... 243
8.5	Concluding Remarks ..... 249
<b>9.</b>	<b>Conclusion ..... 251</b>
9.1	Research Contributions ..... 252
9.2	Future Work ..... 254
	<b>Glossary 256</b>
	<b>References 262</b>

# List of Figures

Figure 1-1	Overview of the transceiver techniques over the multipath fading ISI channels .....	7
Figure 1-2	Roadmap of the dissertation .....	10
Figure 2-1	Angle of incident of the incoming signal to the direction of mobile.	19
Figure 2-2	Outdoor wireless communication channels in cellular structure for the typical rural area. ....	21
Figure 2-3	Outdoor wireless communication channels in cellular structure for the typical urban area. ....	22
Figure 2-4	Outdoor wireless communication channels in cellular structure for the Hilly Terrain area. ....	23
Figure 2-5	Typical propagation models defined in GSM 05.05 version 4.13.0.	25
Figure 2-6	Response of the typical urban channel to the 1.25 MHz pulse.	28
Figure 2-7	Narrowband pulse response of the typical urban area channel.	30
Figure 2-8	Response of the HT channel to the narrow band pulse. ....	31

Figure 2-9	Visualization of the time-varying complex-valued tap at the fading rate of 100 Hz. ....	34
Figure 2-10	The autocorrelation function and the Doppler power spectrum of Rayleigh fading tap. ....	35
Figure 2-11	The transceiver operation in baseband representation, frequency-domain representation, and the equivalent fractionally sampled system. ....	37
Figure 2-12	L independent diversity antenna channel model .....	41
Figure 2-13	The square-root raised cosine filter: continuous wave form and the half-symbol spaced filter coefficients. (Shown truncated at 10 symbol-periods). ....	42
Figure 2-14	Visualization of the time-varying channel, fading at 100 Hz is shown over 80 symbol periods. ....	45
Figure 3-2	Baseband system description for $q$ -QAM transmission over the dispersive channel and the receiver structure of fractionally-spaced decision feedback equalizer .....	49
Figure 3-1	The passband channel impulse response of $c_0$ , $c_2$ and $c_4$ . The sampling rate is 8229 Hz. Total number of samples for each channel is 256 samples. ....	50
Figure 3-3	The channel-filter rate conversion process. ....	52
Figure 3-7	Baseband system description for $q$ -QAM transmission over the dis-	

	persive channel and the structure of fractionally-spaced decision feedback equalizer .....	54
Figure 3-4	Time and frequency domain responses of the channel c0 at different combination of the baud rates and the carrier frequencies. ....	55
Figure 3-5	Time and frequency domain responses of the channel c2 at different combination of the baud rates and the carrier frequencies. ....	56
Figure 3-6	Time and frequency domain responses of the channel c4 at different combination of the baud rates and the carrier frequencies. ....	57
Figure 3-8	Step-by-step illustration of DFE transceiver operation .....	63
Figure 3-9	The baseband equivalent system description for the Tomlinson-Harashima precoder and equalizer. ....	65
Figure 3-10	16- and 32-QAM symbol error rate simulation results on the telephone channel. ....	66
Figure 3-11	64-QAM symbol error rate simulation results on the telephone channel. ....	67
Figure 3-12	The eigenvalues of the system matrix for $(N_f, N_b) = (40, 40)$ . Top figure shows the eigenvalues in linear scale and the bottom figure shows them in the log-scale. ....	70
Figure 3-13	The eigenvalues of the system matrix for $(N_f, N_b) = (30, 10)$ . Top figure shows the eigenvalues in linear scale and the bottom figure shows them in the log-scale. ....	71

Figure 3-14	The LMS training of the fractionally-spaced DFE filter coefficients. 73
Figure 3-15	The standard RLS training of the fractionally-spaced DFE filter coefficients. ....74
Figure 3-16	The regularized RLS training of the fractionally-spaced DFE filter coefficients. ....76
Figure 4-1	The recursive algorithms applied for tracking of time-varying channels .....81
Figure 4-2	The RLS and LMS tracking of fast time-varying channel .....84
Figure 4-3	Channel estimation and interpolation tracking on a TDMA frame. 86
Figure 4-4	Snap-shot channel parameter estimation .....89
Figure 4-5	Theoretical and simulation mean square channel estimation errors (MSCEEs) for $(N_t, N_c) = (7,4)$ and $(11, 6)$ . ....101
Figure 4-6	(a). Simulation of MAP estimators using the estimated powers of the multipath components. (b). Analytical results of correlated multipath channel, the numbers in the parentheses indicate the mutual correlation coefficients of the three paths. ....102
Figure 5-1	The baseband model for multiple diversity antenna channels where each channel introduce the multipath delay dispersion. ....110
Figure 5-2	The receiver architecture of straightforward diversity-combining

	DFE .....	111
Figure 5-3	The receiver structure of the matched filtered diversity combining DFE. ....	118
Figure 5-4	The equivalent symbol-spaced, single channel DFE setting.	123
Figure 5-5	Addition of the symbol-rate sampled matched filter outputs.	124
Figure 5-6	Average QPSK BERs in slow fading: RLS channel tracking T-DFE and LSE NT-DFE compared with theoretical matched filter bounds.	126
Figure 5-7	Average DQPSK BER simulation: Toeplitz DFE with RLS channel tracking. ....	128
Figure 5-8	Average DQPSK BER performance: LSE and MAP NT-DFE with channel tracking by interpolation. Ideal CIR NT-DFE implies NT-DFE with no channel estimation errors at all time. ....	130
Figure 5-9	Sources of BER floors .....	131
Figure 5-10	Average QPSK BER simulations to determine the source of error floor .....	134
Figure 6-1	64-QAM illustration. denotes the instantaneous combined channel gain. ....	143
Figure 6-2	Illustration of upper bound of the square QAM symbol error rate	145
Figure 6-3	Matched filter bound SER for 4-QAM transmission over -flat fading	

	diversity channels. ....	151
Figure 6-4	Matched filter bound SER for 16-QAM transmission over -flat fading diversity channels. ....	152
Figure 6-5	Matched filter bound SER for 64-QAM transmission over -flat fading diversity channels. ....	153
Figure 6-6	Matched filter bounds symbol error probability for 4-QAM, 157	
Figure 6-7	Matched filter bounds symbol error probability for 16-QAM, 158	
Figure 6-8	Matched filter bounds symbol error probability for 64-QAM, 159	
Figure 6-9	Spectral Efficiency for frequency-flat fading channel. ....	167
Figure 6-10	Capacity for the frequency-selective channels, MPDP 1. ....	168
Figure 6-11	Capacity for frequency-selective channels, MPDP 2. ....	169
Figure 6-12	Capacity comparison, flat fading, MPDP1 and MPDP2. ....	170
Figure 7-1	The wireless channel models. ....	181
Figure 7-2	The baseband representation of the diversity channels. ....	185
Figure 7-3	The optimum MLSD pre-processing filters, which is again the matched filtering, diversity combining, and symbol-rate sampling. ....	189
Figure 7-4	The whitening filter (ZF-DFE) example with $N_f = 17$ and zero input noise. ....	200
Figure 7-5	The mean-squares whitening filter example with $N_f = 17$ and 10 dB input SNR. ....	203

Figure 7-6	The results of pre-processing, the matched filter bank, the combiner and symbol rate sampler, and the (mean-square) whitening filter.	204
Figure 7-7	Illustration of channel mismatch .....	209
Figure 7-8	The example of channel mismatch, MS-WF with $N_f = 6$ at the input SNR = 10 dB. ....	211
Figure 7-9	Optimal use of PSP is to feedback the channel mismatch information of the overall channel estimate and recompute the matched filters, the MS-WF and finally recompute the output sequence $\{y_k\}$ at each survivor. ....	212
Figure 7-10	Simulation results for channel-1 .....	221
Figure 7-11	Simulation results for channel-2 .....	222
Figure 7-12	4-QAM simulation results for the fading ISI channel .....	223
Figure 7-13	16-QAM simulation results for the fading ISI channel .....	224
Figure 7-14	64-QAM simulation results for the fading ISI channel .....	225
Figure 7-15	64-QAM simulation results for the fading ISI channel ( $L = 2$ ). .....	226
Figure 8-1	(a) Baseband system description of the system from A to B in Figure 8-2. (b) The symbol-spaced TDL is the model representing the system from A to B for the operation of T-algorithm receiver. ....	235
Figure 8-2	The block diagram of the overall system: the details of the system from A to B are described in Figure 8-1 (a). ....	237

Figure 8-3	$(N_I \times B)$ transmitted symbols. Each row is $B$ symbols, $N_t$ training symbols and $N_J$ unknown symbols. ....	246
Figure 8-4	The signal set and trellis for 8-PSK, eight-state code. This code has time-diversity order of two. ....	246
Figure 8-5	Average BER performance over the fading ISI channels (100 Hz). 4-QAM Gray coding is the signalling format for NT-DFE and 8-states 8-PSK trellis modulation for the other receivers, T-alg. & VA, joint-T-alg and Ideal Joint-T-alg. The Ideal receiver is the same as the joint-T-alg., but the channel is perfectly known to the receiver, which is fading at 200 Hz to implement the ideal interleaving. ....	247
Figure 8-6	Average number of survivors vs. SNR for each receivers. (a) is for $L = 1$ and (b) is for $L = 2$ . ....	248

# List of Tables

Table 1-1 : Basic mitigation techniques for the frequency-selective channel with varying degrees of time-selective distortion and shadowing.....	8
Table 3-1: Output SNR for ideal MMSE-DFE and MMSE-LE .....	60
Table 4-1: The optimal binary training sequences.....	100
Table 5-1: The number of complex multiplications and divisions required..	136
Table 7-1: Factorization theorems for static and time-varying channels.....	194
Table 7-2: Comparison of the metric computation for Ungerboeck and Forney	196
Table 7-3: Simulation parameters and results.....	218

# Acknowledgments

First and foremost, I would like to express my heart-felt gratitude to my advisor, Gregory J. Pottie, for his endless support, direction, and encouragement during my pursuit of M.S. and Ph.D. at UCLA. Without Gregory's unwavering encouragement and patience, I would have never reached this point. Throughout the long journey of my Ph.D. work, he always welcomed my visits with a big smile on his face, answered my questions and listened to my ideas with unlimited enthusiasm and support. It has been a great privilege and rewarding experience to work with him.

I would like to thank Professors Kung Yao, Babak Daneshrad and Kirby Baker for serving on my Ph.D. committee and their valuable comments on the dissertation. I also extend my deepest gratitude to Dr. Cheon-Won Choi, a friend as well as senior colleague of mine during his Ph.D. tenure at UCLA. From the numerous discussions I had with him, I often obtained research insight and was able to start to open my eyes to mathematics of probability and statistics. I also would like to express special thanks to Philsung Ghang, also a friend as well as senior colleague of mine during his Ph.D. tenure at UCLA, for his uninhibited help in my preparing for my Ph.D. exams. I would also like to extend my thanks to some of unforgettable friends I met during my stay at UCLA, including Kyung-Ho Cho, Chu-Dong Lee, Kwang-Yong Kim, Inyup Kang, Jin-Ho Seo, Insoo Jun, Jae-Hyeong Kim, Dong-Su

Koh, Juno Kim, Jong-Eun Chang and Hea-Joong Kim. In addition, I would like to express my thanks to Jeff Putnam, Chris Hansen, Dennis Connors, George Kondylis, Kathy Sohrabi and Jay Gao for their friendship and rewarding comments on my research works.

At the triumph of today, I deeply thank my mother and father for their endless support and encouragement. Specifically, I am truly thankful to my mother for her strong and consistent support to my craving for a higher education, even while an unstable financial condition persisted throughout my school years. Lastly, but by no means least, I would like to thank Chong-Hui Lee, my lovely wife who has always stood beside me throughout this long, long journey. For more than 10 years, from my undergraduate years to this very moment, she has always been there with me whenever I needed her the most. Since I met her, my life became more focused, meaningful and pleasant. Because of her love and smiles of our lovely children, our daughter Hyun-Ji and our son Hyun-Kyu, I was able to accomplish the triumph of today.

## Vita

November 20, 1966	Born, Chung-Nam, Non-San, Korea
1993	B.S., Electrical Engineering University of California, Los Angeles Los Angeles, California
1994	M.S., Electrical Engineering University of California, Los Angeles Los Angeles, California
1994-1999	Research Assistant University of California, Los Angeles Los Angeles, California
1999-1999	Research Staff Member Information Science Laboratory HRL Research Laboartory Malibu, California

## PUBLICATIONS

- Heung-No Lee and G. J. Pottie, "Fast Adaptive Equalization/ Diversity Combining for Time-Varying Dispersive Channels", *IEEE Transactions on Communications*, vol. 46, no. 9, pp 1146 - 62, Sept. 1998.
- Heung-No Lee and G. J. Pottie, "Adaptive sequence detection using T-algorithm for multipath fading ISI channels," in *Proc. Comm. Theory Mini Conf. of IEEE Int. Conf. on Commun.*, p. 125 - 9, Jun. 1999.
- Heung-No Lee and G. J. Pottie, "Adaptive sequence detection of channel-interleaved trellis-coded modulation signals over multipath fading ISI channels," in *Proc. of IEEE Veh. Tech. Conf.*, vol. 3, May. 1999.
- Heung-No Lee and G.J. Pottie, "Channel estimation based adaptive equalization/ diversity combining for time-varying dispersive channels, in *Proc. of IEEE 47th Veh. Tech. Conf.*, vol. 2, p 884-8, May. 1997.

## **Abstract of the Dissertation**

# **Adaptive Diversity Combining, Equalization and Sequence Decoding for Time-Varying Dispersive Channels**

Heung-No Lee

Doctor of Philosophy in Electrical Engineering  
University of California, Los Angeles, 1999  
Professor Gregory J. Pottie, Chair

Next generation wireless networking systems require a robust, flexible and efficient establishment of a communication link over the underlying time-varying wireless channels to be able to support different QoS requirements for various kinds of services such as voice, video and data. In this dissertation, we investigate a robust wireless modem techniques that should provide a reliable, spectrally efficient communication link over rapidly time-varying and severely delay-dispersive wireless channels. We first examine the feedforward channel estimation techniques. Fast time-varying channel is tracked down by two steps. First a set of snap-shot channel impulse estimates is obtained by utilizing the channel training symbols periodically inserted into the stream of unknown data symbols. Then, the fast time-varying channel during the unknown data segments is tracked down by the use of interpolation on the set of snap-shot channel estimates. For this problem, we propose a set of novel channel estimators.

Having obtained the feedforward channel estimates, a robust detection receiver structure, utilizing the diversity receive antennas and the decision feedback equalizer, is investigated for uncoded (or gray-coded) transmissions of a relatively small constellation signals, such as QPSK (or DQPSK). Assuming that a number of independent diversity

signals are available at the receiver by the use of space-diversity antenna systems, we have developed a robust diversity combining DFE (DC-DFE), which is derived under minimum mean square error criterion (MMSE). Advantages of the new receiver include that the complexity of obtaining the optimum coefficients does not increase as the number of diversity channel increases. In addition, the proposed DC-DFE was derived under the assumption of fast-time varying channel, unlike conventional derivations. Thus, the DC-DFE provide a significant performance improvement over the previously proposed diversity combining DFE receivers and also to the RLS channel tracking DC-DFE systems, especially in fast-time varying channel conditions.

If the symbols from a large constellation are used to convey the digital information, the spectral efficiency of the underlying wireless channels can be improved in multiple times. For a large constellation signalling such as 64-QAM, we propose the use of sequence-based detection schemes, derived under maximum likelihood sequence detection (MLSD) criterion. The complexity problem implementing the MLSD is resolved by the use of reduced complexity search algorithms. By comparing a set of several existing tree-or trellis-search algorithms, we propose the use of T-algorithm along with the per-survivor processing. The proposed sequence-based detection receiver using the T-algorithm is extended further to be used in decoding of symbol-interleaved trellis-coded modulation signals. Main research result in this is that the receiver searches a tree and thus is able to perform a joint decoding, deinterleaving and equalization. A joint decoding is optimal since it does not make any early decision on the received symbol sequence and thus achieves the full MLSD performance without doing any iteration. We show with an example of simple trellis-code that the proposed joint, tree-search decoder achieves the full diversity benefit available to the code without increasing the decoding complexity.

# **Chapter 1**

## **Introduction**

### **1.1 Recent Advances in Communications Technologies**

During the last three decades, we have witnessed an exciting and explosive advancement of digital communication technologies, including high speed modems, the cellular telephone systems, satellite networking, high speed local area computer networking and the world wide Internet. We briefly address some of the major achievements that are relevant to the topics of this dissertation. For convenience we begin our discussion on two distinct but highly related areas of development, one in wireline and the other wireless technologies.

#### **1.1.1 The advent of the Internet**

The most salient accomplishment of wireline communications/telecommunications technology we have seen during the last two decades is the area of inter-networking of computers where the information and user applications are shared and knowledge bases are distributed in different parts of the world. The networking technology of today, which

started from a single file transfer from one computer to the other in the mid 60's, has reached up to the level that it is now very common to see that our office computers are connected to high speed local area networks (LAN) with up to a few Gbps connection speed. In addition, we have seen the fast emergence of the world wide internet over the last several years. The wide area network (WAN) known as the Internet interconnects many heterogeneous LANs scattered around the globe. This global networking of computers not only allows sharing of computing resources and data bases amongst the members of a particular local area group but also provides us with the remote access to services and information that may exist and be available anywhere in the wide area network, at any time.

Now, the future of the Internet is believed to be the universal computing, information disseminating and retrieval system, far exceeding the mere role of file transfers and sharing applications amongst clusters of connected computers. In the next decade or less, we will be able to ask the Internet, via a user-device [1] that interfaces us to the Internet, more active service requests such as "Make a flight reservation to New York for tomorrow for me" or "Make a video conference connections with all the members of my group," who may be on travel abroad, at home or at the office [2]. For this to happen, the current Internet which consists mostly of wireline infrastructure of technologies such as public switched telecommunications network (PSTN), last mile xDSL accesses, high speed fiber-optic backbone networks and wired LANs, should be extended to allow tetherless and seamless connections to the some existing and some futuristic wireless networks, including the mobile cellular networks, the satellite networks, and various sizes of local area wireless networks such as wireless office and home networks [5][6][7].

### **1.1.2 The wireless networks**

Transmission of digital information over wireless communication links such as terrestrial land mobile radio channels, indoor LAN channels and satellite channels has also

received much research and development attention, with many accomplishments during the last twenty years. For example, TDMA or CDMA based *cellular* telephone technologies, which were perhaps realized only in a small scale military application about two decades ago, now has become a mass market with a large variety of services available. In cellular networks, the base station located at the center of a cell relays all the telephone calls directed from/to the wireless terminals residing in the cell for the duration of the call. It is a connection oriented networking system, originally developed for the voice transmission but now becoming available for data transmission as well. The current cellular phone system has now tens of millions of subscribers in America [5] and has become almost an essential part of our daily lives in many industrialized countries. Wireless connections also provide a convenient means for indoor networking, removing the need of hard-wiring among office computers and printers. This is in some ways a miniature version of the cellular network. It interconnects computers in the vicinity of the base station, rather than phones, and thus runs in the packet switching mode, as this is more suitable for computer-oriented bursty data traffic.

### **1.1.3 The hybrid networks and emergence of the universal computing systems**

In the next decade, perhaps we will see the emergence of next generation internetworking technology, the so called the next generation Internet, which may be a hybrid of heterogeneous tiers of networks, from pico cells to micro cells, micro cells to macro cells, telephone network to the Internet, low earth orbit (LEO) network to geostationary earth orbit (GEO) network, all of which are to be interconnected. The Internet today provides a convenient means to disseminate and retrieve information over the wireline network. The next generation wireless communications technology will allow us to have wireless access to the Internet in a much faster and ubiquitous manner. The goal is

to realize a global system that operates without regards to many limitations of today's system. It will provide seamless wireless connections regardless of any particular air-interface technology, a broadband access with multimedia applications, remote access to the computing resources and knowledge data base available in the network, without regard to whether one is at home, at the office, in the street, in a fast moving vehicle, or in travel abroad.

#### **1.1.4 Need for spectrally efficient, robust wireless modem technologies**

In order to bring such a universal communication and computing network into reality, we need a wireless networking solution that ubiquitously and seamlessly interconnects us to the existing wireline/wireless infrastructure and finally to the other part of the communication entity. Since the goal is that the networking service is to be established anywhere, at any time and for any kinds of services, the wireless networking solution must perform well with a wide variety of networking scenarios, system requirements and channel conditions. This has inspired new design concepts and fundamental technological breakthroughs in almost every aspect of communication research, including the investigation of wireless channel capacity, joint source and channel coding/decoding, robust modulation and demodulation, the use of diversity transmit and receive antennas, design of power control algorithms, design of new medium access control (MAC) algorithms and development of new networking protocols.

In this dissertation, we focus on the design of a wireless modem which enables a robust, reliable and spectrally efficient communication link to the higher MAC and network layers. It is very difficult to realize such a wireless modem technology because of the uncertain nature of the wireless channel, which may include high mobility, variation of signal to noise ratio (SNR) and multipath signal propagation. In addition, the spectrum is a very scarce resource and thus the design should be optimized for bandwidth efficiency.

## 1.2 Overview of Dissertation

The scope of this dissertation is the wireless transceiver design and optimization in the physical layer, which primarily deals with the combined problems of robust transmission and detection of digital information over the wireless channels. Specifically, we investigated a novel optimal performance solution for wireless channel estimation problems, optimal receive antenna diversity combining techniques, minimum mean square error decision feedback equalization (MMSE-DFE), a sequential detection technique for large constellation signaling using maximum likelihood sequence detection (MLSD), and the optimal/suboptimal joint sequential detection of channel-interleaved trellis-codes transmitted over multipath fading inter-symbol interference (ISI) channels.

The objective of our research was to develop transceiver technologies to facilitate the implementation of a reliable and spectrally highly efficient communication link over a fast time-varying, severe delay-dispersive channel. The proposed transceiver should have the capability to incorporate channel coding, adaptive bit rate transmission, adaptive equalization, adaptive channel estimation, and explicit diversity combining through space diversity antenna systems.

The channel studied was adopted from the perspective of outdoor mobile cellular environments. There are three main distortion mechanisms: delay-spreading (frequency-selective distortion) due to multipath propagation, channel variation (time-selective or Doppler spread) due to motion of the mobile, and the large scale variation of SNR due to shadowing. The distortion model employed follows the typical examples provided for IS-54 [9] or GSM [34] systems where the use of an equalizer is mandatory.

For convenience of explanation, we categorize the channel environment into four different regions as shown in Table 1-1. According to a particular channel distortion region, the optimum technique may vary. For instance, differential phase shift keying

(DPSK) detection may be sufficient to provide a robust receiver performance for slowly time-varying flat-fading channels, with low system complexity. However, the DPSK system would eventually fail, producing an irreducible bit error rate (BER) floor due to intersymbol interference once the ratio of the root mean square (rms) delay dispersion to the symbol period exceeds a certain threshold, say about 1/10 the symbol period [49]. On the other hand, the channel may start to exhibit fast fading when either one of the transmit or receiving terminals begin to move at a high speed. This fast fading channel requires a highly optimized fast channel tracking technique. In other circumstances, the transceiver might be situated in a very low signal to noise ratio (SNR) environment, perhaps due to a large scattering object along the signal path from the transmitter to receiver that obstructs signal propagation. Then, the transceiver system may need a larger number of diversity antennas or lower rate channel coding to account for the SNR loss of the link.

Table 1-1 : provides a tabular summary of all the basic channel-mitigation techniques that can be utilized for each of these different channel situations. In all regions, we assume frequency-selective channels and thus adaptive equalization. Figure 1-1 provides an overview of the system functions of the adaptive transceiver developed in the dissertation. For example, at the transmitter a fixed sequence of training symbols are periodically inserted into the unknown data streams for the purpose of channel estimation at the receiver. For the channel situation A. in Table 1-1 :, a trellis-code can be used. For adaptive rate transmission, frequency-division duplex (FDD) and time-division duplex (TDD) systems can be assumed. The functions of the receiver include channel estimation, diversity combining, symbol or sequential detection and sequential detection.

The adaptive transceivers are assumed to operate in the general framework of time division multiple access (TDMA) systems. For this, we take as examples well-known wireless cellular radio standards such as IS-54, IS-136 and GSM to obtain some of the system parameters. These systems use TDMA as an efficient method of providing more

users in an assigned channel bandwidth, and employ training sequences, inserted into each TDMA frame, for the purpose of tracking the time-varying channel during the burst. We also use wireless channel parameters, such as delay spread and Doppler spread, that are indicative of the channel environment where the system is expected to operate.

### 1.3 Roadmap of Dissertation

Figure 1-2 provides the road map of the dissertation. We describe the wireless channel model in Chapter 2. This channel model was developed for the system specifications of IS-54 such as the signal bandwidth (30 kHz) and the carrier frequency of 900 MHz. It uses the representative multipath delay profile GSM recommends. Here, it was used to simulate the channel situations described in Table 1-1 :

Chapter 3 discusses some of the basic issues of digital communications system

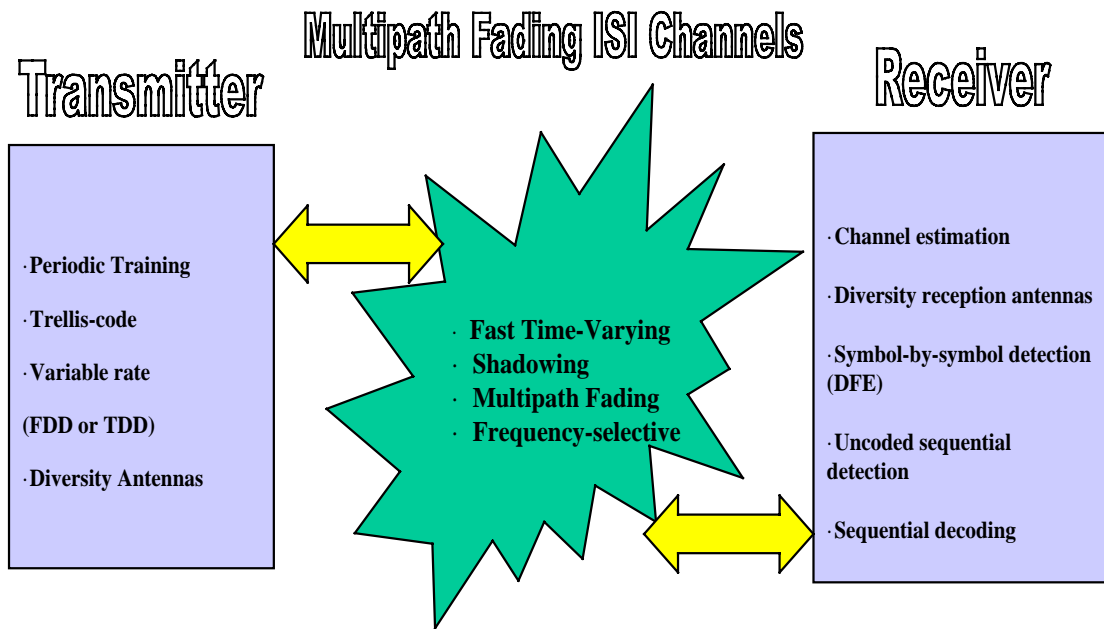


Figure 1-1 Overview of the transceiver techniques over the multipath fading ISI channels

		Time-selective distortion	
		Slow fading	Fast fading
Large scale shadow-fading	Low avg. SNR	A. <ul style="list-style-type: none"> <li>• Explicit diversity combining</li> <li>• Low-rate trellis-code</li> <li>• Sequential Joint-Decoding</li> </ul>	B. <ul style="list-style-type: none"> <li>• Explicit diversity combining</li> <li>• Frequent update of the receiver parameters</li> <li>• Low-rate trellis-code</li> <li>• Sequential Joint-Decoding</li> </ul>
	High avg. SNR	C. <ul style="list-style-type: none"> <li>• Uncoded Larger constellations</li> <li>• Symbol-by-symbol detection transceiver</li> <li>• Decision directed channel tracking</li> </ul>	D. <ul style="list-style-type: none"> <li>• Larger constellations</li> <li>• Frequent update of the receiver parameters</li> <li>• Sequential detection (MLSE)</li> </ul>

**Table 1-1 : Basic mitigation techniques for the frequency-selective channel with varying degrees of time-selective distortion and shadowing.**

simulation and discusses some equalizer design problems with examples of telephone channels. In particular, minimum mean square error decision feedback equalizer (DFE), linear equalizer (LE) and Tomlinson-Harashima precoder are compared as the mitigation techniques for the dispersive telephone channels. In addition, the least mean squares (LMS) and recursive least squares (RMS) adaptive algorithms are considered for the purpose of training the DFE filter coefficients, and the simulation results are discussed.

Chapter 4 discusses the feedforward channel estimation and tracking problems. The

channel estimation is feedforward, in that explicitly known training symbols are periodically inserted into the streams of unknown data for the purpose of the receiver's estimation of the channel. The *snapshot* estimates of the channel are interpolated to track the channel variation of the time-segment inbetween the two adjacent channel training segments. Novel channel estimators that utilize the *a priori* information of the transmit shaping filter's impulse response at the receiver are proposed. Least squares, maximum likelihood and maximum *a posteriori* estimators are derived. Closed form, theoretical mean square errors for each estimator were derived and compared with the simulation results.

Chapter 5 discusses the diversity combining decision feedback equalizer (DFE) for uncoded symbol transmission (gray coded or differentially encoded). We have proposed an optimal receiver architecture based on the minimum mean square error criterion and also based on the performance obtained in the presence of channel estimation error. That is, we have shown the equivalence of the two systems, the straightforward architecture and the matched filtered diversity combining version, by deriving the latter from the former. We have identified the eigenvalue spread problem of the former and proposed the use of the latter architecture which provides much more stable performance than the former in the presence of severe ISI and of channel estimation errors. Previous derivations of the MMSE DFE were all done with the assumption of a time-invariant channel. Our new solution takes into account the channel variation even during the duration of the decision delay of the diversity combining receiver. The improved performance of the new solution particularly stands out in the case of fast time-varying channels.

Chapter 6 deals with calculation of the theoretical matched filter bounds (MFB) and the channel capacity (spectral efficiency). From MFB analyses, we will be able to see the exact relationship between the order of diversity in terms of detection probability, and the number of diversity channel or the delay-dispersion characteristics of the wireless channel.

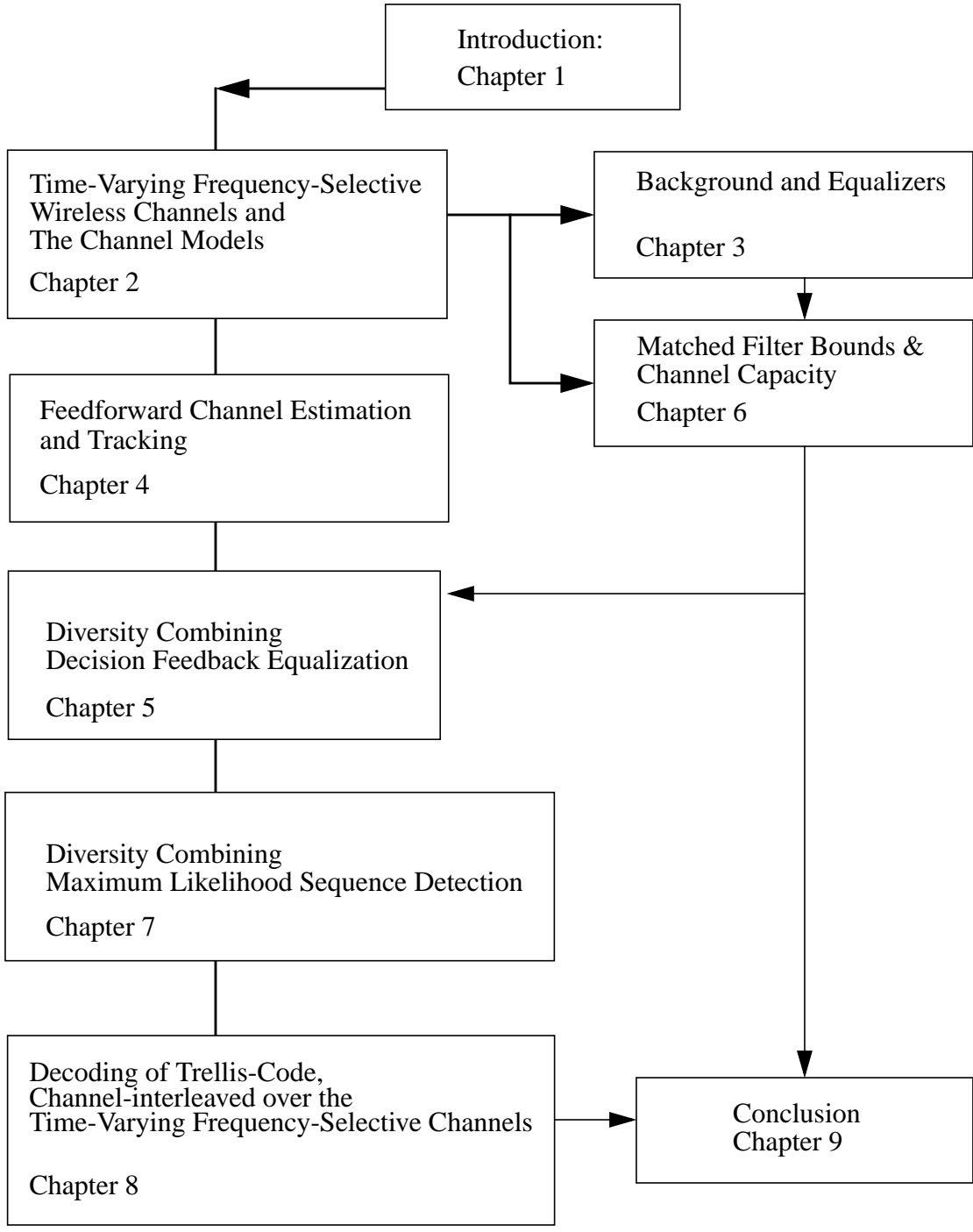


Figure 1-2 Roadmap of the dissertation

We will observe that the order of diversity is increased as the number of diversity antennas are added, and also as the delay-dispersion of the wireless channel increase. In addition, as the order of the diversity increases the detection performance converges to the results of AWGN channel. These theoretical MFB bounds are compared with the relevant simulation results in each Chapter of the dissertation.

In Chapter 7 we move into the area of sequence based detection using the maximum likelihood sequence detection (MLSD) criterion. We also deal with larger signal constellations, such as 64 QAM, to be used in the case of variable rate QAM transmission where the number of bits can be varied from 1 bit to 6 bits according to the varying conditions of the channel. Large size constellations and the use of a DFE is a potentially problematic combination, because of the error propagation problem of a DFE. The complexity problem of using the MLSD receiver is resolved by using a suboptimal tree-search T-algorithm, instead of using the Viterbi algorithm. A comparison is made with other sequential search algorithms. The T-algorithm is shown to give the best performance with the lowest increase in the average complexity. Moreover, we have proposed the use of per-survivor processing to estimate the channel mismatch at each path, to achieve a substantial additional SNR advantage while reducing almost in half the number of survivor paths. The reason is that the per-survivor processing of the channel estimate promotes early elimination of bad paths from the survivor list.

Chapter 8 discusses the decoding of trellis-codes transmitted over the multipath fading ISI channel. Since the channel has correlated fading, the code must be interleaved before being transmitted to obtain the diversity benefit of the code. The use of the interleaver makes it impossible to perform a joint decoding, based on the traditional approach of constructing and searching a joint-trellis. However, since the T-algorithm is a tree-search version of the sequential search algorithm, we were able to devise a way to perform a joint tree-search on the combined state machines of encoder trellis, the de-

interleaver and the minimum phase ISI channel. The minimum phase ISI channel is the result of preprocessing of the wireless channel, where the preprocessing consists of matched filtering (using the interpolated channel estimation results of Chapter 4) and the mean square whitening filter (described in Chapter 7). The simulation results shows that the receiver achieves the available time-diversity benefit of the trellis-code with only a modest increase in the decoding complexity compared to the uncoded system.

In Chapter 9, we provide the conclusion of the dissertation and presents topics for future inquiry.

# Chapter 2

## Wireless Channels and Simulation Models

The focus of this Chapter is to introduce the major signal distortion mechanisms and impairments of the wireless channel to be addressed in the body of the dissertation, explain the physics behind them, and develop the simulation model for the frequency-selective diversity channel to be used in the performance evaluation of the transceivers. The channel impairments will be discussed include the signal fading due to multipath signal propagation, intersymbol interference (ISI) due to multipath delay spread, frequency-selective and non-selective channels, and the time-varying channels due to Doppler broadening.

### 2.1 Characterization of Multipath Channels

When a signal is transmitted in a wireless environment, the propagation path of the signal to the receiver is affected by the geometry of the environment. When an extremely short pulse is transmitted in a wireless environment, for instance, the received signal might appear as a dispersed train of pulses instead of a single pulse, as shown in Figure 2-2. The

geometry of the environment at that moment determines the channel impulse response, the dispersion of the pulse train. Each individual pulse at the receiver is the uniquely determined end-product of the particular propagation environment at the moment the transmitted signal pulse went through. The transmitted pulse may hit into buildings, trees, streets and other scatterers in the environment. The more scatterers in the environment, the more pulses might appear at the receiver and each might arrive at a different time. When the geometry of the propagation medium changes--as the transmitter, the receiver or both might be in motion, for example a mobile receiver in a moving vehicle or a transmitter in an airplane--the shape of the multipath varies over time. This chapter attempts to characterize such random channel behavior using some mathematical expressions, especially to model the dispersion and the time-variant nature of the channel.

In the equivalent lowpass description the wireless channel can be expressed as a train of impulses, i.e.,

$$c(\tau ;t) = \sum_i \alpha_i(t) e^{-j2\pi f_c \tau_i(t)} \delta(\tau - \tau_i(t)), \quad (2.1)$$

where  $\alpha_i(t)$  is the attenuation factor of the  $i$ -th path,  $\tau_i(t)$  is the propagation delay and  $f_c$  is the carrier frequency [65]. The sample impulse responses, shown in Figure 2-2, Figure 2-3 and Figure 2-4, indicate the multipath propagation paths with the phase information of (2.1) ignored.

### **2.1.1 Multipath fading: the small-scale variation of the signal strength**

Consider a case in which the multipath delay dispersion is much smaller than the duration of the signal pulse. Specifically, suppose that there are  $K$  multipaths with propagation delay  $\tau_i(t)$ ,  $0 \leq i \leq K - 1$  and a transmit pulse of unit amplitude whose signal duration is much greater than the maximum delay dispersion  $T_0 \gg \tau_{K-1}(t)$ , then the

received signal can be written for the interval  $0 \leq t \leq T + \tau_{K-1}(t)$  as,

$$\begin{aligned}
 r(t) &= \sum_{i=0}^{K-1} \alpha_i(t) e^{-j2\pi f_c \tau_i(t)} \\
 &= \sum_{i=0}^{K-1} \alpha_i e^{-j\theta_i} \\
 &= a \text{ complex-valued Gaussian random number}
 \end{aligned}$$

Now, note that the attenuation factor and the dispersion delay associated with an individual path does not change too fast, i.e.  $\alpha_i(t) \approx \alpha_i$  and  $\tau_i(t) \approx \tau_i$  compared to the duration of the pulse. However, the phase factor  $\theta_i = 2\pi f_c \tau_i$  might vary significantly for a different path- $i$  since it changes by  $2\pi$  rad as  $\tau_i$  changes by  $\frac{1}{f_c}$ , which is typically very small for a radio frequency. The set of dispersion-delays and the attenuation factors is determined randomly by the propagation medium surrounding the receiver for each instant. If the receiver does not move and there is no change in the environment, the summed number does not change. However, as the receiver makes a movement or the environment changes--for example the presence of a large moving scattering object in the vicinity--the number will take a different value as there will be a change in the set of dispersion delays and attenuation factors. Thus, the received signal can be modeled as a random process. In fact, with the assumption of a large number of multipath components, i.e. a large  $K$ , the central limit theorem can be applied and thus the received signal can be modeled as a complex-valued Gaussian random variable--hence the absolute value is Rayleigh distributed. As there will be changes in the surrounding environment and movement of the receiver (or the transmitter) over time, the received signal can be modeled as the complex-valued Gaussian random process, parameterized with the time variable. The time-correlation behavior of this random process over time will be studied in 2.1.4.

### 2.1.2 Shadow fading: the large-scale variation of the signal strength

Multipath propagation of the signal produces small-scale signal fading when a number of unresolved randomly phased pulses are added. The Rayleigh fading models provide a good approximation to the amplitude variation of the signal in a small-scale local region, such as the signal strength variation for a car moving along a short patch of a local street. Shadow fading refers to the variation of a “local mean” over a large-scale space due to terrain and large-scale obstacles such as buildings, while the local statistics may be Rayleigh.

The path loss, the ratio of received power over transmitted power, at a local region is widely modeled as a random variable having a log-normal distribution, i.e.

$$L_p(d)(dB) = L_s(d)(dB) + 10n \log\left(\frac{d}{d_0}\right) + \chi_\sigma, \quad (2.2)$$

where

- $d$  is the distance between the transmitter and the receiver
- $d_0$  is the reference distance, corresponding to a point located in the far field of the antenna, typically taken to be 1 km for large cells.
- $n$  is the value of the exponent, depending on the frequency, antenna heights, and propagation environment. For example,  $n = 2$  for free space and higher for large number of obstructions are present.
- $L_s(d) = \left(\frac{4\pi d}{\lambda}\right)^2$  the free space loss, where  $\lambda$  is the wavelength of the propagating signal
- $\chi_\sigma$  denotes a zero-mean Gaussian random variable (in decibels) with standard deviation  $\sigma$  (typically, 6-10 dB).  $\chi_\sigma$  is site- and distance-dependent.

### 2.1.3 Multipath delay spread

The autocorrelation function of  $c(\tau ;t)$  will be useful for the characterization of the channel dispersion and provide a measure of the delay spread. First, we assume that the channel  $c(\tau ;t)$  is wide-sense stationary and characterized as a complex-valued zero mean Gaussian random process in the  $t$  variable. Then, we define the autocorrelation function as

$$\phi_c(\tau_1, \tau_2; \Delta t) := E\{c^*(\tau_1 ;t)c(\tau_2 ;(t + \Delta t))\}. \quad (2.3)$$

Assuming uncorrelated scattering at two different delays such that the phase shift and attenuation of the channel associated with path delay  $\tau_1$  and  $\tau_2$  are uncorrelated, (2.3) becomes

$$E\{c^*(\tau_1 ;t)c(\tau_2 ;(t + \Delta t))\} = \phi_c(\tau_1; \Delta t)\delta(\tau_1 - \tau_2). \quad (2.4)$$

If we let the observation time difference be zero  $\Delta t = 0$ , then the resulting autocorrelation function is simply the average power output of the channel as a function of the delay variable  $\tau$ . We call it the *power-delay* function of the channel, which is defined as

$$\phi_c(\tau) = \phi_c(\tau; \Delta t = 0). \quad (2.5)$$

In the discrete-time channel case, it can be written as

$$\begin{aligned} \phi_c(\tau) &= \sum_i E[|\alpha_i(t)|^2]\delta(\tau - \tau_i(t)) \\ &= \sum_i \phi_{c,i}\delta(\tau - \tau_i(t)) \end{aligned}, \quad (2.6)$$

where we have defined  $\phi_{c,i} = E[|\alpha_i(t)|^2]$  for  $i \geq 0$ . We will call this function as the *multipath power-delay profile* (MPDP) of the channel.

Now, one can model the power-delay profile as a type of probability distribution by normalizing  $\phi_c(\tau)$  by  $\int_0^\infty \phi_c(\tau)d\tau$ . Then, we use the standard deviation of  $\tau$ ,  $\tau_{rms}$ , as the

measure of delay dispersion of the channel with a particular MPDP. That is,  $\tau_{rms}$  is defined as

$$\begin{aligned}\tau_{rms} &= \left( \frac{\int_0^{\infty} \tau^2 \phi_c(\tau) d\tau}{\int_0^{\infty} \phi_c(\tau) d\tau} - \left( \frac{\int_0^{\infty} \tau \phi_c(\tau) d\tau}{\int_0^{\infty} \phi_c(\tau) d\tau} \right)^2 \right)^{\frac{1}{2}} \\ &= \left( \frac{\sum_{i \geq 0} \phi_{c,i} \tau_i^2}{\sum_{i \geq 0} \phi_{c,i}} - \left( \frac{\sum_{i \geq 0} \phi_{c,i} \tau_i}{\sum_{i \geq 0} \phi_{c,i}} \right)^2 \right)^{\frac{1}{2}}.\end{aligned}\tag{2.7}$$

In modeling a wireless channel, one may use a MPDP measured from the field test or may assume a certain MPDP such as exponential power delay profile  $\exp\left(-\frac{\tau}{\tau_{rms}}\right)$ .

#### 2.1.4 Time-variation of a fading component

Due to the movement of the environment, the receiver or the transmitter, the wireless channel should be modeled as time-varying. We use Jake's model which is well-known and widely used model for the generation of the time-varying ensemble path of the fading channel [15]. The time-correlated fading can be explained as follows. First, let  $\mathbf{w}$  be the displacement vector from the transmitter to the receiver at time  $t_0$  and assume the receiver is traveling at a velocity  $\mathbf{v}$  with  $\|\mathbf{v}\| = v$  and the angle  $\varphi$ , which is between  $\mathbf{v}$  and  $\mathbf{w}$ , as illustrated in Figure 2-1. Then, the displacement vector from transmitter to receiver is  $\mathbf{w} + \mathbf{v}\delta t$  at  $t_0 + \delta t$ . The distance for a short time,  $\delta t$ , can be approximated by a linear function of time [16],

$$\|\mathbf{w} + \mathbf{v}\delta t\| \approx w + v\delta t \cos(\varphi).\tag{2.8}$$

Then, the phase of the wave has changed by  $v\delta t \cos(\varphi) f_c / c$ , where  $c$  is the speed of the light. Thus, from the attenuation of the path at time  $t_0 + \delta t$  is

$$r(t_0 + \delta t) = \sum_{i=0}^{K-1} \alpha_i \exp\left(-j2\pi\left(f_c \tau_i + v\delta t \frac{\cos(\varphi)}{c} f_c\right)\right). \quad (2.9)$$

We call the term  $\cos(\varphi)\left(\frac{v}{c}f_c\right)$  the Doppler shift or Doppler frequency. We then define the maximum Doppler frequency,

$$f_{dm} = \frac{v}{c}f_c, \quad (2.10)$$

and this will give a measure of how fast the channel is changing.

Next, in order to find out the time-correlation of the Rayleigh fading path we consider, again assuming uncorrelated scattering of the  $K$  paths,

$$\begin{aligned} E\{r^*(t_0)r(t_0 + \delta t)\} &= E\left\{\sum_{q=0}^{K-1} \alpha_q^* e^{j2\pi f_c \tau_q} \sum_{i=0}^{K-1} \alpha_i e^{-j2\pi\left(f_c \tau_i + v\delta t \frac{\cos(\varphi)}{c} f_c\right)}\right\} \\ &= \sum_{q=0}^{K-1} \phi_{c,q} E\{e^{-j2\pi \cos(\varphi) f_{dm} \delta t}\} \end{aligned} \quad (2.11)$$

By modeling the angle of incident  $\varphi$  to be uniform random variable on  $[0, 2\pi)$ , we have

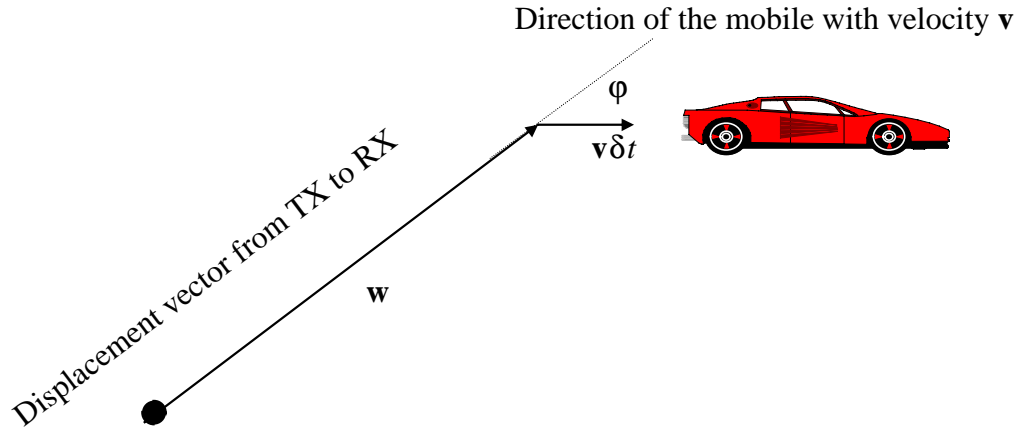


Figure 2-1 Angle of incident of the incoming signal to the direction of mobile.

$$\begin{aligned}
E\{r^*(t_0)r(t_0 + \delta t)\} &= Const \cdot \frac{1}{2\pi} \int_0^{2\pi} e^{-j2\pi \cos(\phi) f_{dm} \delta t} d\phi \\
&= Const \cdot J_0(2\pi f_{dm} \delta t)
\end{aligned} \tag{2.12}$$

where  $J_0(\ )$  denotes the zeroth order Bessel function. Thus, the autocorrelation function is a real-valued function since the cross correlation of real and imaginary parts is zero. In section 2.3, a method of generating Rayleigh fading paths with the time-correlation (2.12) will be discussed.

## 2.2 Wireless Propagation Channels

The propagation channel is the surrounding physical environment which influences the propagation of the radio signal from the transmitter to the receiver antenna. For design of outdoor communications systems, the propagation channel is commonly categorized by its typical impulse response, or a typical response to a wideband transmitted pulse for a certain type of geographical region. From a particular geographic region to another, the statistical behavior of the channel is assumed significantly different. In particular, the outdoor cellular communication channels are usually categorized into three distinct areas such as rural, urban and hilly terrains. To insure satisfactory operability of a radio over these different characteristic regions, a system is tested under a set of channel impulse responses carefully selected from field experiment and thus representing the particular region.

### 2.2.1 Typical multipath delay profiles

The following figures describe the physical propagation environmental settings for the three different regions. Figure 2-2 illustrates the channel environment of a typical rural area, and Figure 2-3 is for an urban area and Figure 2-4 for hilly terrain. Specifically, these figures illustrate the physical propagation medium of typical down-link radio channels for the choice of carrier frequencies and frequency bands relevant to the current cellular

systems such as IS-54, IS-95, GSM and IS-136. Each figure also includes the typical wideband pulse responses, as well as the narrow-band pulse responses. As the bandwidth of the pulse narrows, multipaths of the received signal becomes less distinguishable, leading to the small-scale fading condition explained in Section 2.1.1.

### 2.2.2 Basic mechanism of signal propagation

Much of the observed propagation behavior can be explained in terms of reflection, diffraction and scattering. Reflection occurs when the wave impinges on a smooth surface with a very large dimension compared to the wavelength. Reflection is illustrated by path-2 and 3 in Figure 2-3. Diffraction occurs when the radio wave impinges upon a sharp edge of a dense object with a large dimension compared to the wavelength. The first path of Figure 2-3 shows the result of diffraction. The building obstructs the direct line-of-sight path between the transmitter and the mobile receiver but the secondary wave formed by the

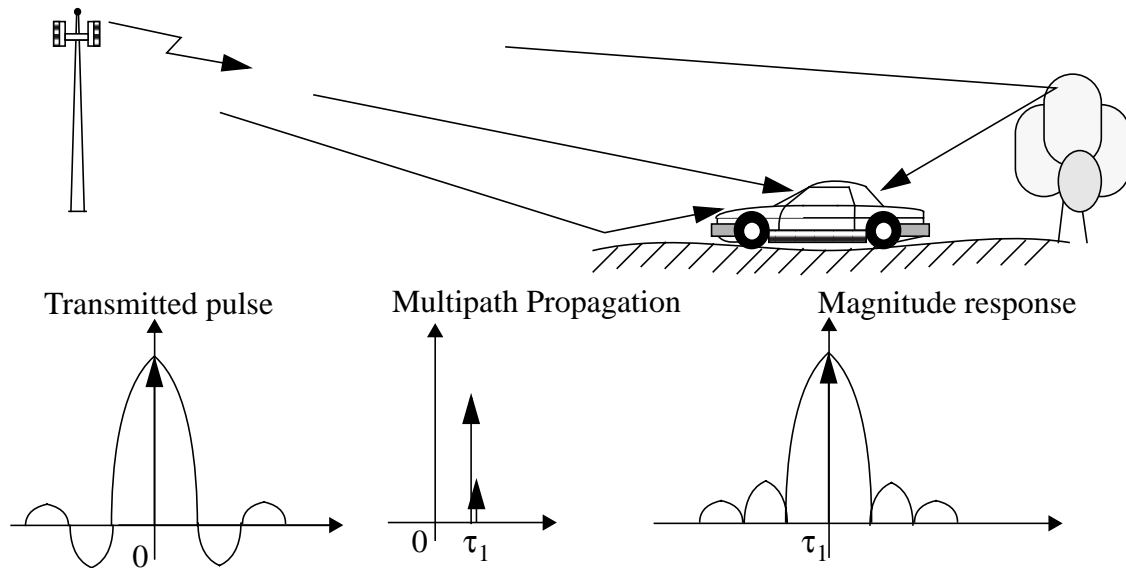


Figure 2-2 Outdoor wireless communication channels in cellular structure for the typical rural area.

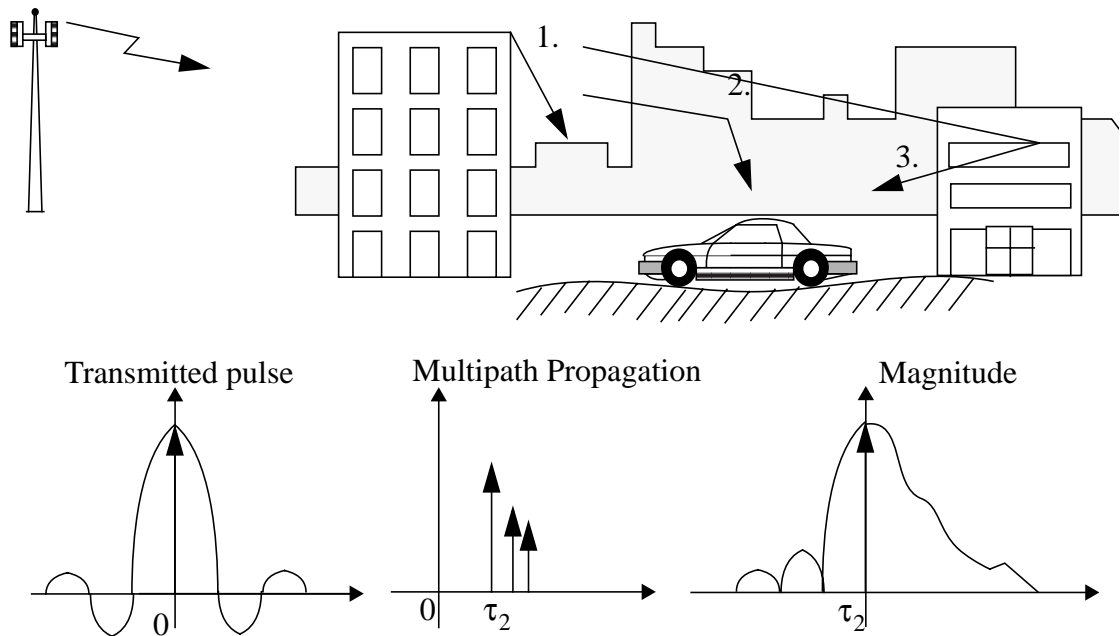


Figure 2-3 Outdoor wireless communication channels in cellular structure for the typical urban area.

sharp edge of the building still reaches the receiver. This is why it is often called shadowing. Scattering occurs when the radio wave impinges on a surface or an object with a dimension on the order of wavelength. The resulting waves are spread out in all directions. Typical scattering objects are lampposts, street signs and foliage. Typical reflection and diffraction objects are buildings and mountains.

The second row in each Figure is the graphical representation of the channel's wideband- or narrow-band pulse responses. The first shows the transmitted pulse, which may be in the form of either an ideal impulse (having an extremely large bandwidth) or a finite bandwidth pulse. The second<sup>1</sup> is the wideband impulse response of the channel for the transmitted pulse shot at time zero. The third is the magnitude impulse response of the wideband channel when the finite bandwidth pulse was transmitted.

<sup>1</sup>Note that magnitude only is shown, neglecting the phase information for now.

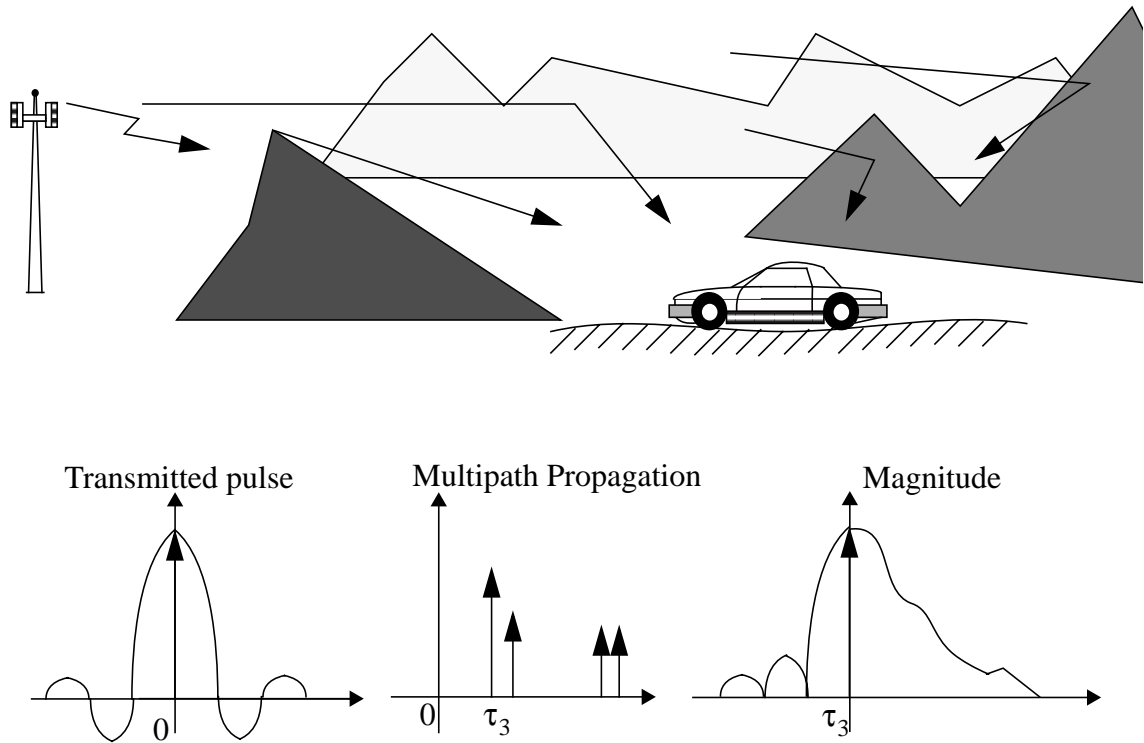


Figure 2-4 Outdoor wireless communication channels in cellular structure for the Hilly Terrain area.

### 2.2.3 Building a suitable channel model for a geographic region

The channel's impulse response represents the multipath propagation behavior of the wireless channel. An extremely wideband pulse, approximately an impulse, can be employed in a channel sounding experiment. That is, an impulse is transmitted at a reference time at the base station and its responses are recorded at the receiver. Usually, a number of distinct delay-spread impulses would reach the receiver. Each path is the result of a different propagation mechanism with varying distance of travel, varying attenuation factors and phases. The associated attenuation factor, phase and time of arrival of the multipath components is determined by the surrounding medium. This is called multipath propagation of the radio waves. The response is time-varying since the receiver is assumed

to be mobile. Therefore, as there are numerous possible setting of the surrounding media and as the receiver will experience many of them while receiving the signal, the channel is usually modeled as a random process, as was given in (2.1).

The multipath profiles provided in Figure 2-5 are the measured impulse responses for the rural, hilly terrain and urban areas. This set of channel responses is recommended by the GSM systems standard [34] for generation of the simulation channel and performance evaluation of a complete system via computer simulation.

Rural channels are often characterized by starting with a strong direct line-of-sight path and quick, exponential decay of responses. It assumes no distant large scatters such as large buildings and mountains. In this class of channels, the multipath is mainly due to scattering objects such as trees and streets which are within the proximity of the mobile receiver, and thus the span of arrival times is short. The typical rural area example shown in Figure 2-5 indicates that there are no more arriving pulses after the first 1  $\mu$  sec. The first impulse in Figure 2-2 is a direct line of sight path, and thus modeled as a deterministic attenuation. The rest of the paths are recommended to be modeled as Rayleigh fading amplitude [34], assuming they are the superposition of a large number of independent paths having uniform phase distribution, as explained in 2.1.1.

In the urban case, shown in Figure 2-3, it is typically assumed that the mobile would be surrounded by many reflective and diffracting objects such as buildings which are a sizable distance away from the receiver which lead to distinguishable multipath arrivals at the receiver, in addition to the small-scale scatterers in its proximity. As a result, the delay spread becomes larger than that of the rural area. Figure 2-5 (c) indicates that most of the multipath rays are arrived within the first 5  $\mu$  sec.

On the other hand, the hilly terrain case indicates that there is a distinct second group of late arriving rays to the receiver, set largely apart from the first group, due to the presence of distant mountains and hills. Thus, the delay spread becomes the largest of all.

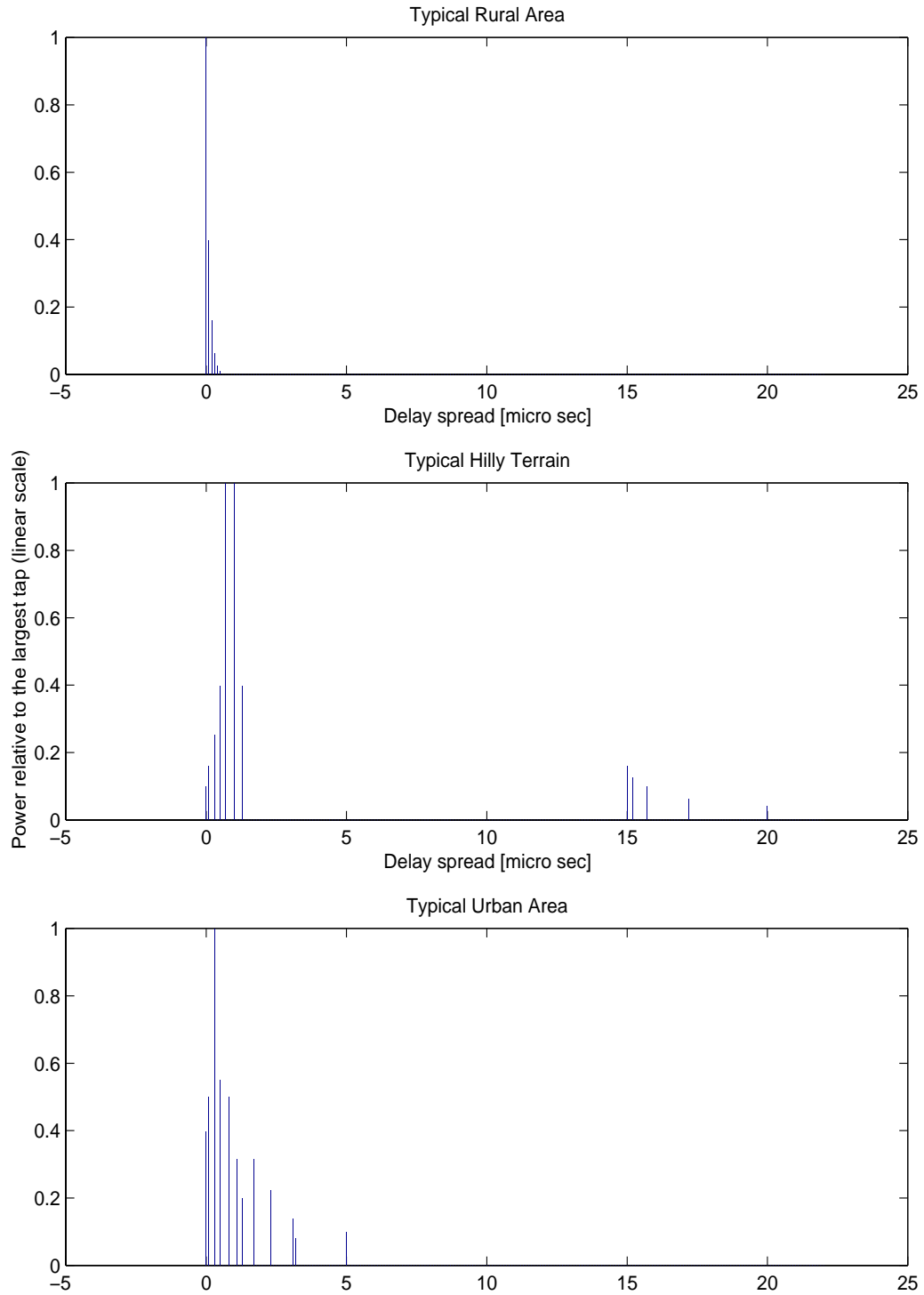


Figure 2-5 Typical propagation models defined in GSM 05.05 version 4.13.0.

In Figure 2-5 (b), it is shown that the second group arrives after the first 15  $\mu$  sec. GSM recommends that all of the paths be modeled as independent and Rayleigh fading.

The rms delay spread of the channels shown in Figure 2-5 are 0.0977  $\mu$  sec, 5.0978  $\mu$  sec and 1.0260  $\mu$  sec, for the rural area, the hilly terrain and the urban area respectively.

#### **2.2.4 Frequency-selective channels due to multipath spread**

The transmission bandwidth is 1.25 MHz for the CDMA systems such as IS-95 whereas in TDMA cellular systems such as IS-54 it is 30 KHz (or the effective bandwidth of 24 KHz). The transmission bandwidth of the CDMA systems is about 42 times that of the TDMA systems. As will be illustrated in this Section, the larger transmission bandwidth provides greater multipath resolution power. That is, the receiver is able to resolve more multipath components. Thus, the channel for CDMA systems is typically designed as multitap filter, and for each tap a RAKE finger may be assigned for signal detection. For IS-54 or IS-136 systems, however, the number of channel taps depends on the region. In a rural area, the channel can be modeled as a single tap fading channel. In the mountainous terrain the channel should be a multitap channel due to the delay spread.

A channel whose magnitude response in the frequency-domain is not uniform across the frequency band of interest is called a frequency-selective channel, where the frequency band of interest is the transmission bandwidth of the signal. More precisely, this implies that in the frequency-domain the folded spectrum of the channel is not flat. In the symbol-rate sampled, discrete-time domain, the impulse response is not a single Kronecker delta function but multiple delta functions, that cause interference among adjacent transmitted symbols. This is called *intersymbol interference* (ISI). Any channel that results in non-flat folded spectrum and thus results in ISI is a frequency-selective channel for the chosen baud rate. Note that the reciprocal of the baud rate should be the effective bandwidth of the transmit shaping pulse. Explained in another way, all radio communication systems

have a finite delay resolution related to the reciprocal of their transmission bandwidth. Two propagation paths separated by less than the system's delay resolution will appear to the receiver as one path. Thus, whether a channel is frequency-selective or non-selective depends not only on the multipath delay itself but also on the transmission bandwidth. In the frequency-domain, the frequency-selective channel is a channel where the coherence bandwidth of the channel is significantly smaller than the transmission bandwidth.

All the channels in Figure 2-5 are frequency-selective channels with respect to the wideband channel sounding pulse. We may note from the figure that the channel has a delay resolution of at least  $0.1 \mu\text{ sec}$  and thus the bandwidth of the transmit and receive filter used should have been more than 10 MHz. The pulse shaping filter of a practical system would be much narrower than 10 MHz, and thus depending on the actual choice of the shaping pulse, the channel can be categorized accordingly, frequency-selective or non-selective. This will be illustrated next.

Take the urban area multipath profile given in Figure 2-5 (c) first. Suppose the pulse has a transmission bandwidth of 1.25 MHz as would be appropriate for IS-95 systems. Figure 2-6 shows the scenario. Figure 2-6 (a) shows the shape of the overall pulse which is the cascade of the transmit and receive filters, the raised cosine filter (i.e., assuming the transmitter and the receiver used the same square-root raised filter). Figure 2-6 (c) is the time-domain response of the cascade of the pulse (a) and the random channel (b), where the random channel is realized with the FIR channel whose tap energy and tap spacings are determined from Figure 2-6 (b) and the phases of the taps are independently selected from the random variable uniform over  $[0, 2\pi)$ . Figure 2-6 (d) is the frequency response of the cascade of the random channel (b) and the pulse (a), sampled at a rate  $\frac{2}{1.25}$  MHz, which is twice the chip-rate. The response exhibits the frequency-selective magnitude response across the frequency-band of interest.

Now, suppose a 30 KHz transmit pulse is used (e.g., IS-54, IS-136) instead of 1.25

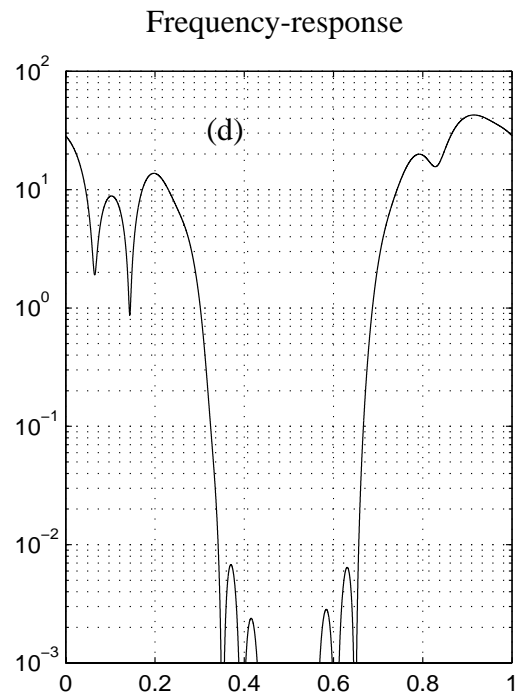
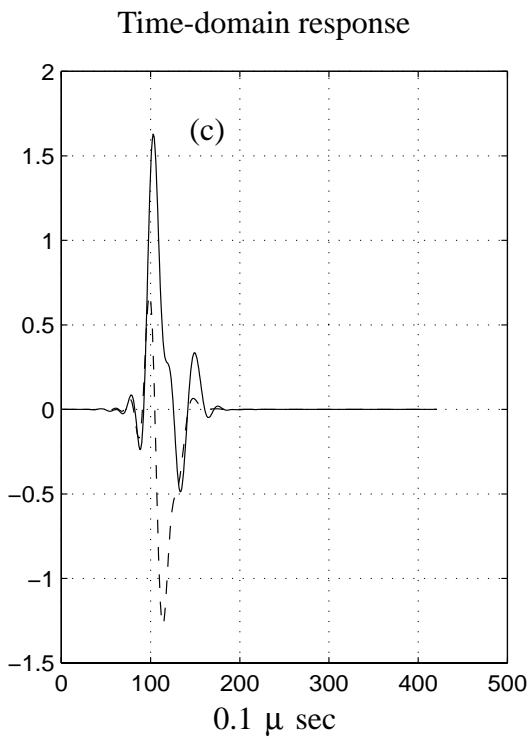
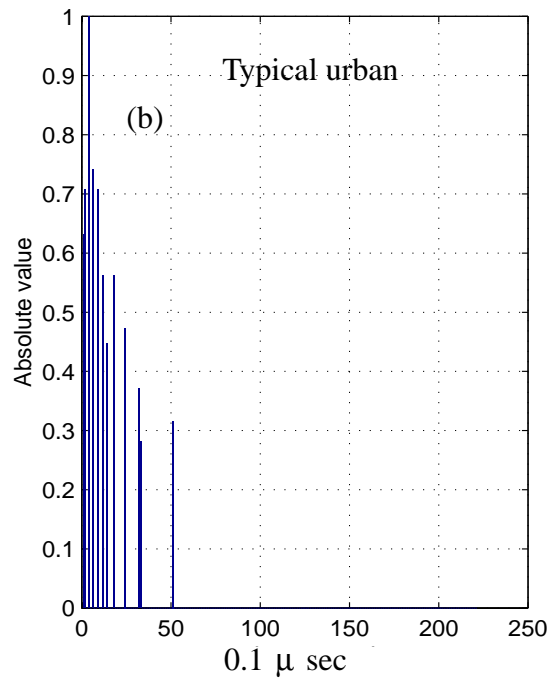
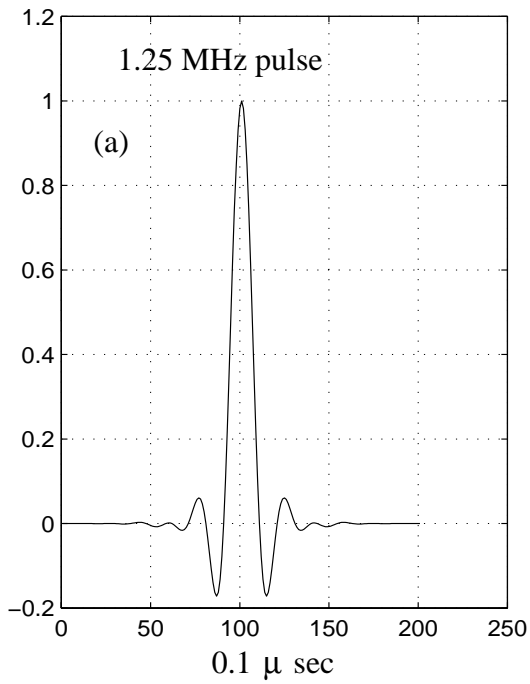


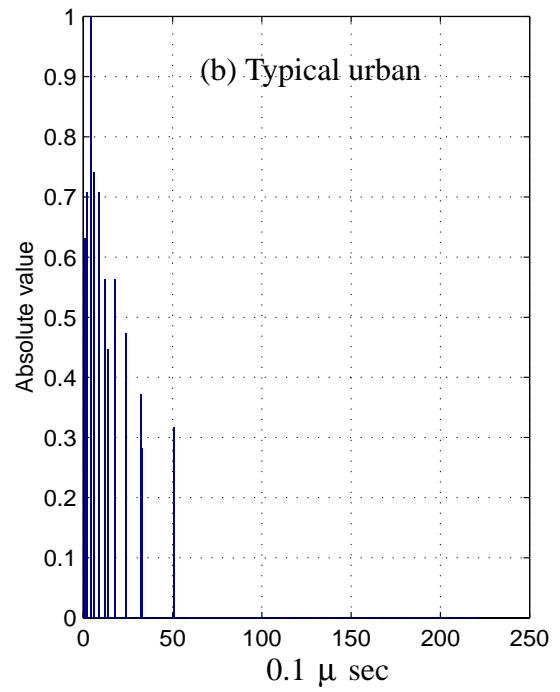
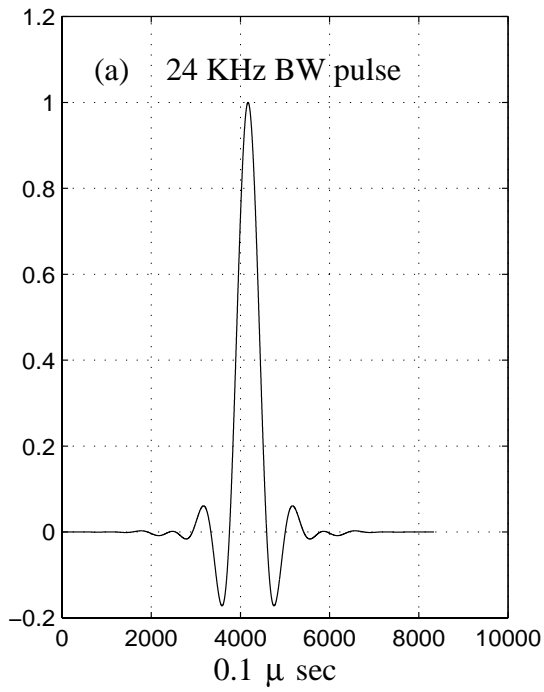
Figure 2-6 Response of the typical urban channel to the 1.25 MHz pulse.

MHz pulse on the typical urban channel. Figure 2-7 (a) shows the cascade of the transmit shaping pulse and the matched filter at the receiver. Note that the overall pulse is much wider in time-domain. Thus, the resolution power in the time-domain is much less than the previous case in Figure 2-6 (a). As a result, the frequency response of the channel and the cascade pulse is almost flat as shown in Figure 2-7 (d). The resulting ISI is insignificant as shown in Figure 2-7 (c). The typical urban channel is thus a flat fading channel for the use of 30 KHz transmit pulse, but a frequency-selective channel for the systems using a 1.25 MHz pulse.

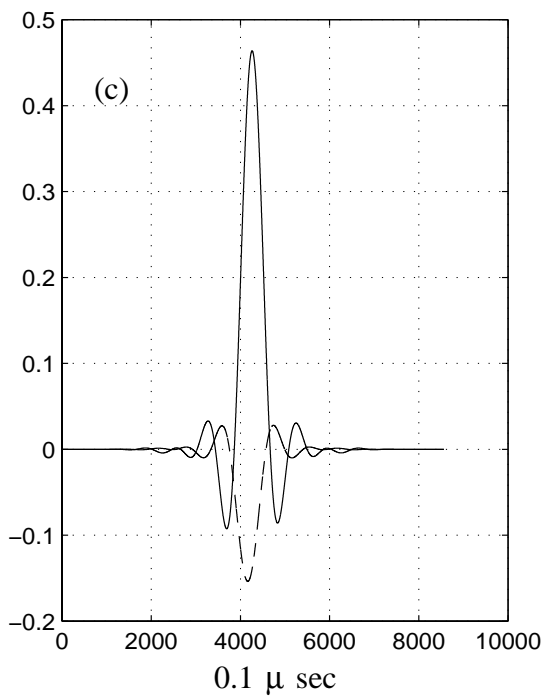
It is now shown in Figure 2-8 that the channel for the hilly terrain area should be modeled as the frequency-selective channel, even when the 30 KHz narrow-band pulse is used. This is due to the second group of pulses around 15 to 20  $\mu$  sec. The frequency-response given in Figure 2-6 (d) shows how one frequency response could be different from the other. In this case, the channel will cause severe intersymbol interference. This hilly terrain or a mountainous terrain model is the basis for the tapped delay line channel model [62] for system simulation and we adopt the model. This frequency-selective channel will be modeled as finite impulse response (FIR) filters in section 2.3.

### **2.2.5 Time-varying channel due to Doppler spreading**

This section addresses the time-varying nature of the wireless channel, and supplements our earlier treatment of Doppler fading in section 2.1.4. Basically, the channel is time-varying because of the change in the environmental configuration surrounding the transceiver or the movement of the mobile. The motion between the transmitter and the receiver results in a changed propagation path. In indoor applications, for instance, the rate of change may be insignificant due to the relatively slow movement (assuming the carrier frequency is the same). In outdoor applications, on the other hand, it may become significant since mobiles are capable of moving at highway speed.



Time-domain response



Frequency-domain

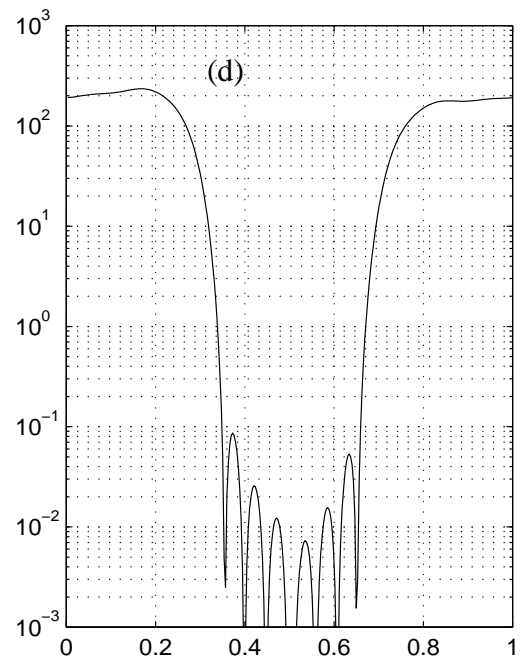
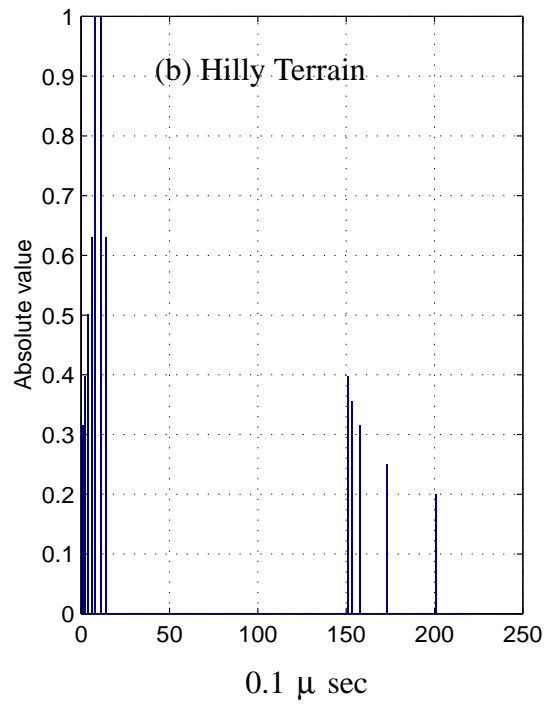
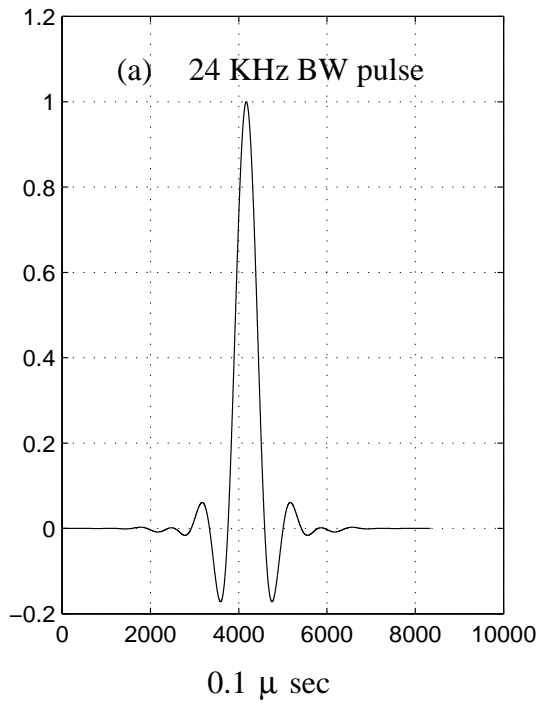
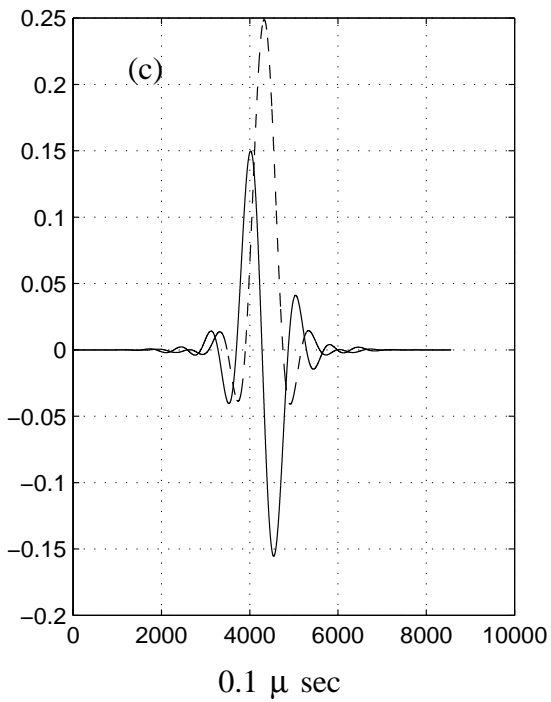


Figure 2-7 Narrowband pulse response of the typical urban area channel.



Time-domain



Frequency-response

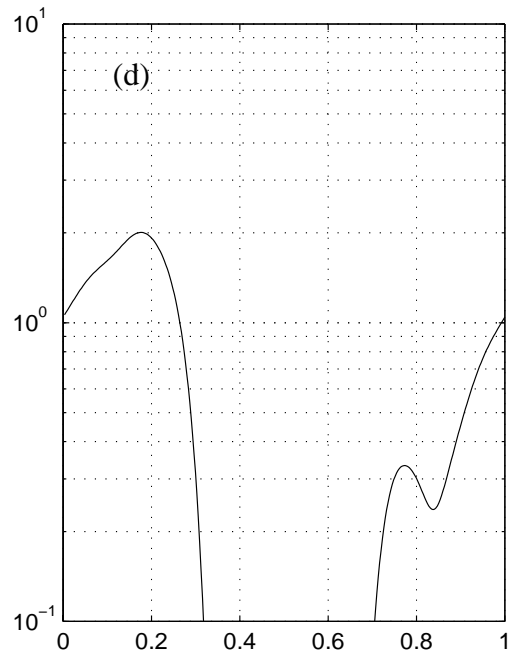


Figure 2-8 Response of the HT channel to the narrow band pulse.

Invoking the wide sense stationary uncorrelated scattering argument, the evolution of the random process corresponding to each tap is uncorrelated to each other. That is, the time-variation of the tap coefficients are mutually uncorrelated while each of them obeys the same time-correlation behavior. Thus, describing the time-varying property of a single component will be sufficient since all the components obey the same law. Now, using the correlation analyses result of 2.1.4, we now define the normalized time-autocorrelation function (2.12) as

$$\begin{aligned}\phi_D(\delta t) &= \frac{1}{Const} E\{r^*(t_0)r(t_0 + \delta t)\}, \\ &= J_o(2\pi f_{dm}\delta t)\end{aligned}\quad (2.13)$$

where  $J_o(\cdot)$  is the zeroth order Bessel function of the first kind and  $f_{dm}$  is the maximum Doppler fading rate. The Fourier transform of (2.13) provides the Doppler power spectrum, which is

$$S(f_d) = \begin{cases} (1 - (f_d/f_{dm})^2)^{-1/2}, & |f_d| \leq f_{dm} \\ 0 & , |f_d| \geq f_{dm} \end{cases} \quad (2.14)$$

This is a model resulting from the dense-scatter model [15] which is reasonable for the outdoor channel model. For the indoor model, a flat spectral density model may be used.

Then, using Jakes' Rayleigh fading model [15], each Rayleigh fading channel tap coefficient  $b_{l,i}(k)$  can be modeled as the sum of nine sinusoids,

$$\rho(t;ST) = N_D \sum_{j=0}^8 d_j \cos(2\pi\delta_j f_{dm}t + ST), \quad (2.15)$$

where

- $N_D$  is a normalization coefficient that makes the second moment of  $\rho(t;ST_{li})$  equal to 1.0,
- $d_j$  is the complex-valued amplitude for the  $(j+1)$ -th Doppler frequency whose in-

phase and quadrature components are

$$Re\{d_j\} = \begin{cases} \sqrt{2} \cos\left(\frac{\pi}{4}\right), j = 0 \\ 2 \cos\left(\frac{\pi}{8}j\right), 1 \leq j \leq 8 \end{cases}, \quad (2.16)$$

and

$$Im\{d_j\} = \begin{cases} \sqrt{2} \sin\left(\frac{\pi}{4}\right), j = 0 \\ 2 \sin\left(\frac{\pi}{8}j\right), 1 \leq j \leq 8 \end{cases}. \quad (2.17)$$

- $\delta_j$  is a relative frequency scaling factor for the  $(j+1)$ -th Doppler shift which is

$$\delta_j = \cos\left(\frac{2\pi}{8}j\right). \quad (2.18)$$

- $ST$  is a randomly chosen real-number to begin the generation of the ensemble at a random starting point. The distribution we have chosen is uniform over  $[-10000, 10000]$ . This can be used to simulate many ensemble of paths of wide-sense stationary uncorrelated scattering taps.

Figure 2-9 illustrates the Doppler fading tap generated using (2.15)  $f_{dm} = 100$  Hz, (a) is the amplitude variation and (b) is the variation of the phase. Figure 2-10 (a) compares the autocorrelation functions. One is a sample autocorrelation function calculated from the generated ensemble (the dashed line curve), i.e.,

$$\hat{\phi}_D(k) = \frac{1}{N_{samples}} \sum_i \rho^*(t = iT) \rho(t = (i+k)T) \quad (2.19)$$

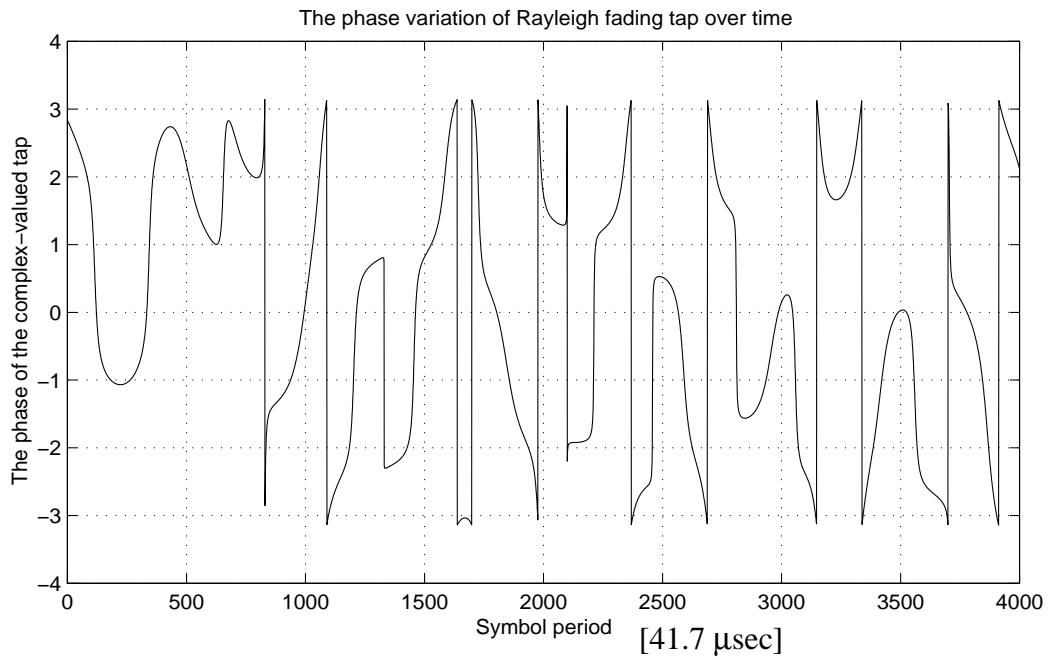
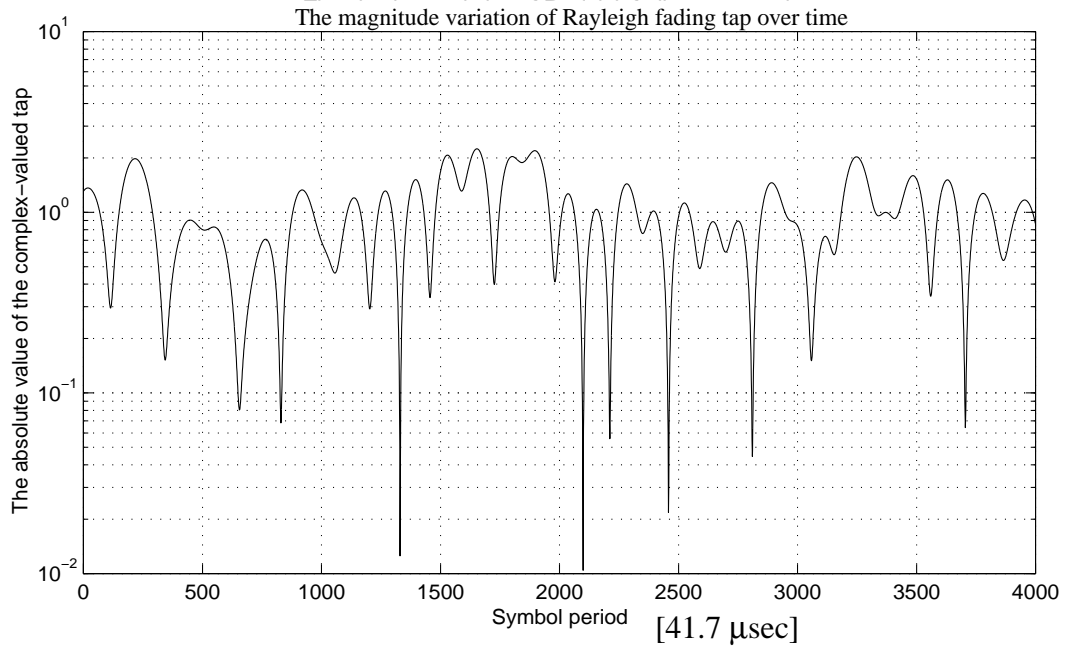


Figure 2-9 Visualization of the time-varying complex-valued tap at the fading rate of 100 Hz.

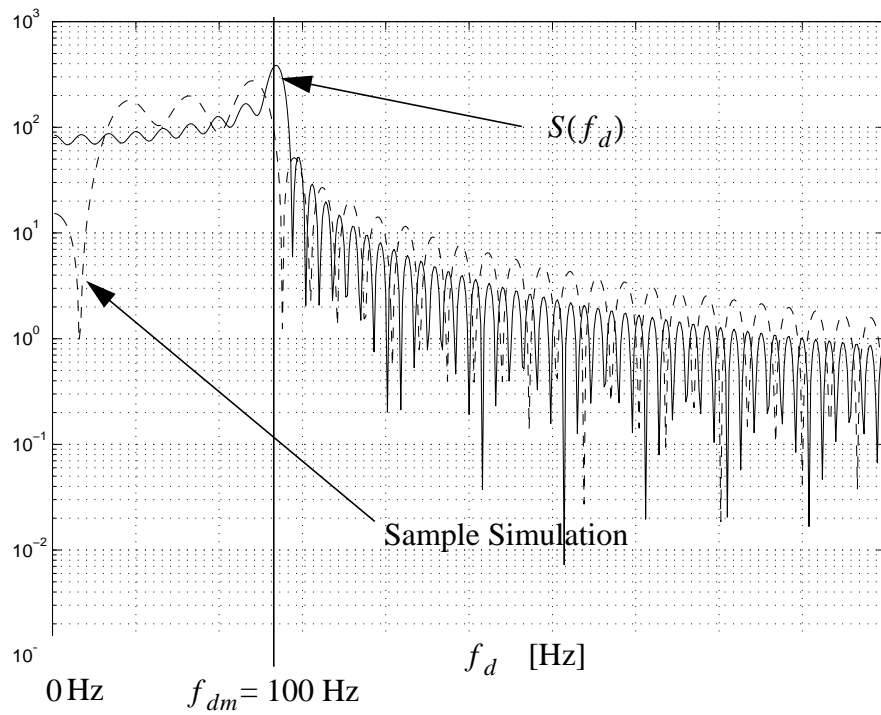
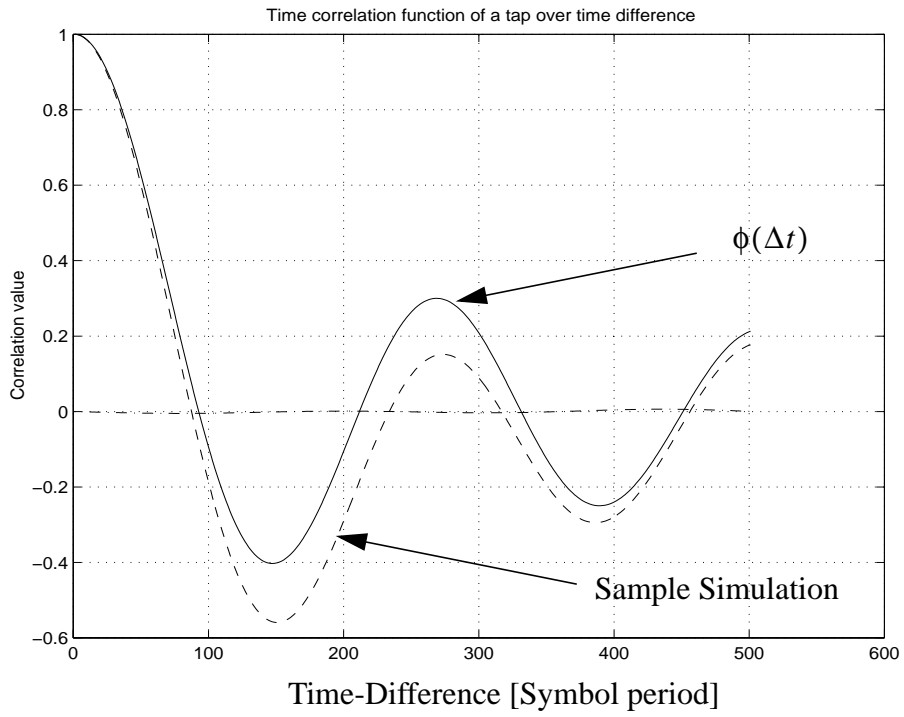


Figure 2-10 The autocorrelation function and the Doppler power spectrum of Rayleigh fading tap.

and the other is the exact autocorrelation function of Eq. (2.13).

## **2.3 The Diversity FIR Channel Model**

We now describe the frequency-selective channel model that will be used throughout the dissertation. As an effective counter-measure to the fading, the receiver diversity technique is frequently suggested for the future generation of transceiver technology. Thus, we develop the diversity channel model for the simulation of our system.

### **2.3.1 FIR representation of the channel, transmit and receive filters**

In practice, the transmission bandwidth always exceeds the baud rate. This is to allow a smooth transition from a passband to stopband of the transmit and receive shaping filters since sharp transitions are hard to realize and expensive. In wireless channel applications, the channel is unknown and the receive filter cannot perform the matched filtering until the channel is estimated. As a result, the discrete-time sampled channel should be modeled as a fractionally sampled filter. For example, IS-54 and IS-136 systems use 35% excess bandwidth of the baud rate, i.e. the baud rate is 24 kbps but the total bandwidth of the shaping filter is 30 KHz. For such systems, a fractional sampling must be employed in order not to lose any information until a matched filtering for the unknown channel is performed. We use the half symbol-rate sampling system and the channel, transmit and receive filters are modeled as finite impulse response filters (FIR). As will be described in more detail, the wireless channel will be modeled as three-tap fading finite impulse response (FIR) filter with tap-spacing of half the symbol period.

Figure 2-11 (a) illustrates the baseband representation of the system in continuous-time domain. The symbol sequence is modulated with the transmit shaping filter and transmitted to the wireless channel. The received signals are processed with the ideal brick-

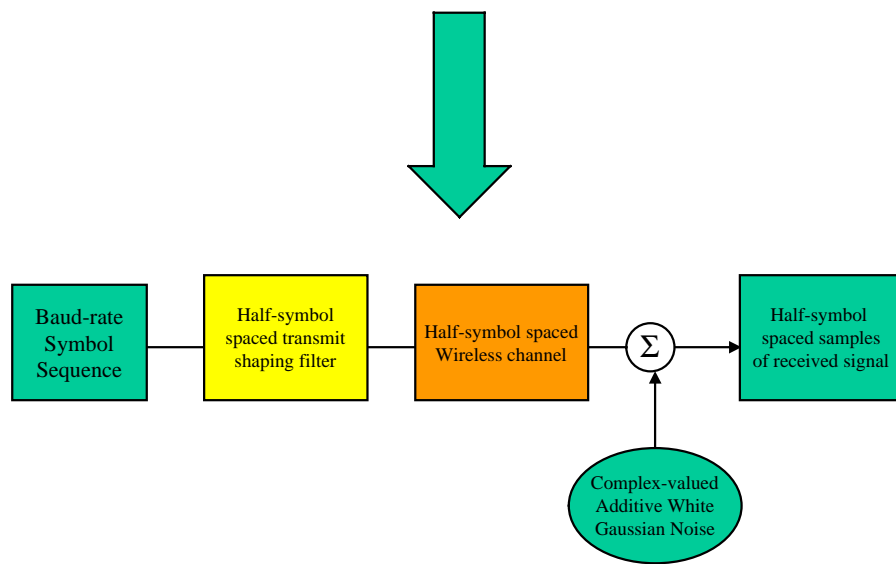
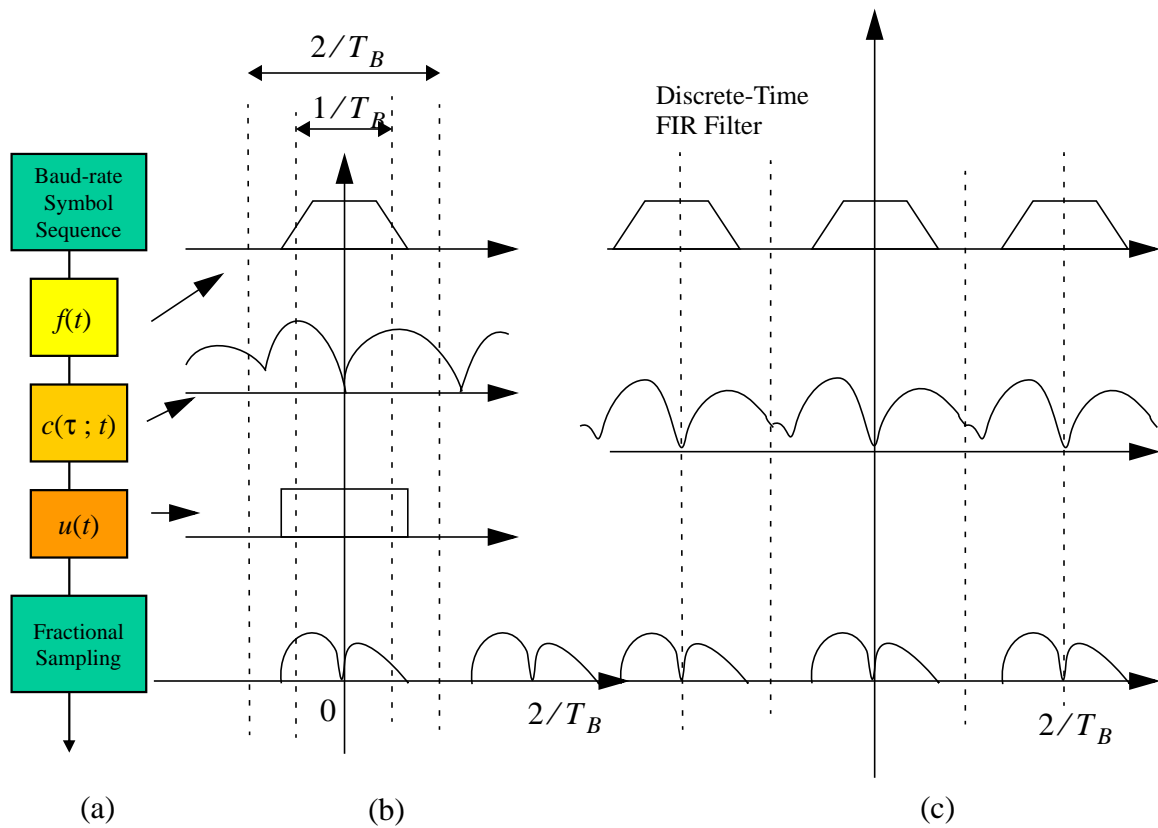


Figure 2-11 The transceiver operation in baseband representation, frequency-domain representation, and the equivalent fractionally sampled system.

wall anti-aliasing filter  $u_W(t)$ ,  $W = \frac{2}{T_B} + \text{Excess Bandwidth}$ , before getting sampled with a fractional rate, e.g. two samples per symbol period. This can be represented in the frequency domain as illustrated in Figure 2-11 (b). The bandlimited  $T_B/2$ -sampled received signal can be represented in the  $T_B/2$ -sampled discrete time system, illustrated in Figure 2-11 (c). In fact, the frequency-response of the  $T_B/2$ -sampled discrete-time filter is just a scaled version of the continuous response, repeating at every multiple of  $2/T_B$  frequency. It is obvious that the transmit shaping filter can be represented as a  $T_B/2$ -spaced discrete-time sampled FIR filter because it is a bandlimited filter. The wideband filter can also be represented as the  $T_B/2$ -spaced discrete-time sampled FIR filter, because of the use of anti-aliasing filter  $u_W(t)$ . That is, the combined response,  $c(\tau;t) \otimes u_W(\tau)$ , is bandlimited and thus can be represented in  $T_B/2$ -spaced sampled system. Note the following,

$$f(\tau) \otimes c(\tau;t) = f(\tau) \otimes c(\tau;t) \otimes u_W(\tau) = f(\tau) \otimes (c(\tau;t) \otimes u_{2/T_B}(\tau)),$$

where  $u_{2/T_B}(\tau)$  is the brick-wall filter with bandwidth  $2/T_B$  whose Fourier transform is

$$F\{u_{2/T_B}(\tau)\} = \begin{cases} T_B/2, & |f| \leq \frac{1}{T_B} \\ 0, & |f| > \frac{1}{T_B} \end{cases}. \quad (2.20)$$

Thus, we can use  $c_{2/T_B}(\tau;t) = c(\tau;t) \otimes u_{2/T_B}(\tau)$  as a discrete-time FIR filter with tap-spacing of  $T_B/2$ .

Now, we need to obtain the multipath profile suitable for the fractionally-spaced system. The multipath delay profile for the  $T_B/2$ -spaced sampled system is just the filtered / sampled version of the wideband result (2.6) such that the autocorrelation function of the low-pass filtered channel response

$$\phi_{c, T_B/2}(\tau_1, \tau_2; \delta t = 0) = E \left\{ c_{2/T_B}^*(\tau_1; t) c_{2/T_B}(\tau_2; t) \right\} \quad (2.21)$$

$$\begin{aligned} &= E \left\{ \int_{-\infty}^{\infty} c^*(\alpha; t) u_{2/T_B}(\tau_1 - \alpha) d\alpha \int_{-\infty}^{\infty} c(\beta; t) u_{2/T_B}(\tau_2 - \beta) d\beta \right\} \\ &= \int_{-\infty}^{\infty} \int_{-\infty}^{\infty} E \{ c^*(\alpha; t) c(\beta; t) \} u_{2/T_B}(\tau_1 - \alpha) u_{2/T_B}(\tau_2 - \beta) d\alpha d\beta. \end{aligned}$$

From (2.4),

$$\begin{aligned} &= \int_{-\infty}^{\infty} \int_{-\infty}^{\infty} \phi_c(\alpha; \delta t = 0) \delta(\alpha - \beta) u_{2/T_B}(\tau_1 - \alpha) u_{2/T_B}(\tau_2 - \beta) d\alpha d\beta \\ &= \int_{-\infty}^{\infty} \phi_c(\alpha) u_{2/T_B}(\tau_1 - \alpha) u_{2/T_B}(\tau_2 - \alpha) d\alpha. \end{aligned} \quad (2.22)$$

It is observable from (2.22) that the multipath profile for the fractionally-spaced system can be obtained from sampling the results of convolution of the wideband MPDP to the autocorrelation function of the low-pass filter. Assuming the ideal brick wall, low-pass filter with bandwidth  $2/T_B$  such as (2.20), the sampled multipath components can be assumed mutually uncorrelated. We now denote the low-pass filtered and  $T_B/2$ -sampled version of the MPDP as

$$\phi_{c, T_B/2}(i) = \phi_{c, T_B/2}(iT_B/2; \delta t = 0), \quad (2.23)$$

for  $i = 0, 1, \dots, N_R$ . We note that each  $\phi_{c, T_B/2}(i)$  denotes the average power of the multipath component of the  $i$ -path.

In this paper, we use the following two classes of the low-pass filtered/sampled version of MPDPs. One is adopted from [62] where three  $T_B/2$ -spaced taps were used for the simulation of mountainous MPDP. Each tap's power is distributed as

$[0 \ -5 \ -15 \ -\infty] \text{ dB}$ ,

$$[\phi_{c,T_B/2}(0) \ \phi_{c,T_B/2}(1) \ \phi_{c,T_B/2}(2)] = [0.7419 \ 0.2436 \ 0.0234]. \quad (2.24)$$

(2.24) is the MPDP used for the analyses results given in Chapter 4 and Chapter 5. For those given in Chapter 6, 7 and 8, we use the exponential distribution to obtain the average powers of the three fading taps, i.e., for  $i = 0, 1, 2$

$$\phi_{c,T_B/2}(i) = \frac{\exp(-i\tau_0)}{\sum_i \exp(-i\tau_0)}. \quad (2.25)$$

The evolution of the channel filter tap can now be generated by multiplying the square-root value of the MPDP to the Rayleigh fading coefficient (2.15).

### 2.3.2 Diversity receive antennas

We assume diversity antennae at the receiver. The use of multiple receive antennae provides rather large diversity benefit against signal fading and thus are a very desirable receiver scheme. For this, we assume  $L$  independent receive signals are available at the receiver. There are many diversity techniques using a number of antenna to provide independent fading signals. Among them are spatial-diversity and polarization antenna techniques. In the former the receiving antennas are separated on the order of a few wavelengths apart from each other to obtain independent fading. The latter approach is to use different polarization antennae. We assume that independent receive signals are available at our disposals by one of these techniques.

### 2.3.3 Diversity antenna channel model

Figure 2-12 illustrates the equivalent complex-baseband  $L$ -diversity channel model. For the transmit shaping filter  $f(t)$ , we use a square root raised cosine (SRRC) filter with a roll-off  $\beta = 0.35$ . The time-domain response of the square-root raised cosine filter is

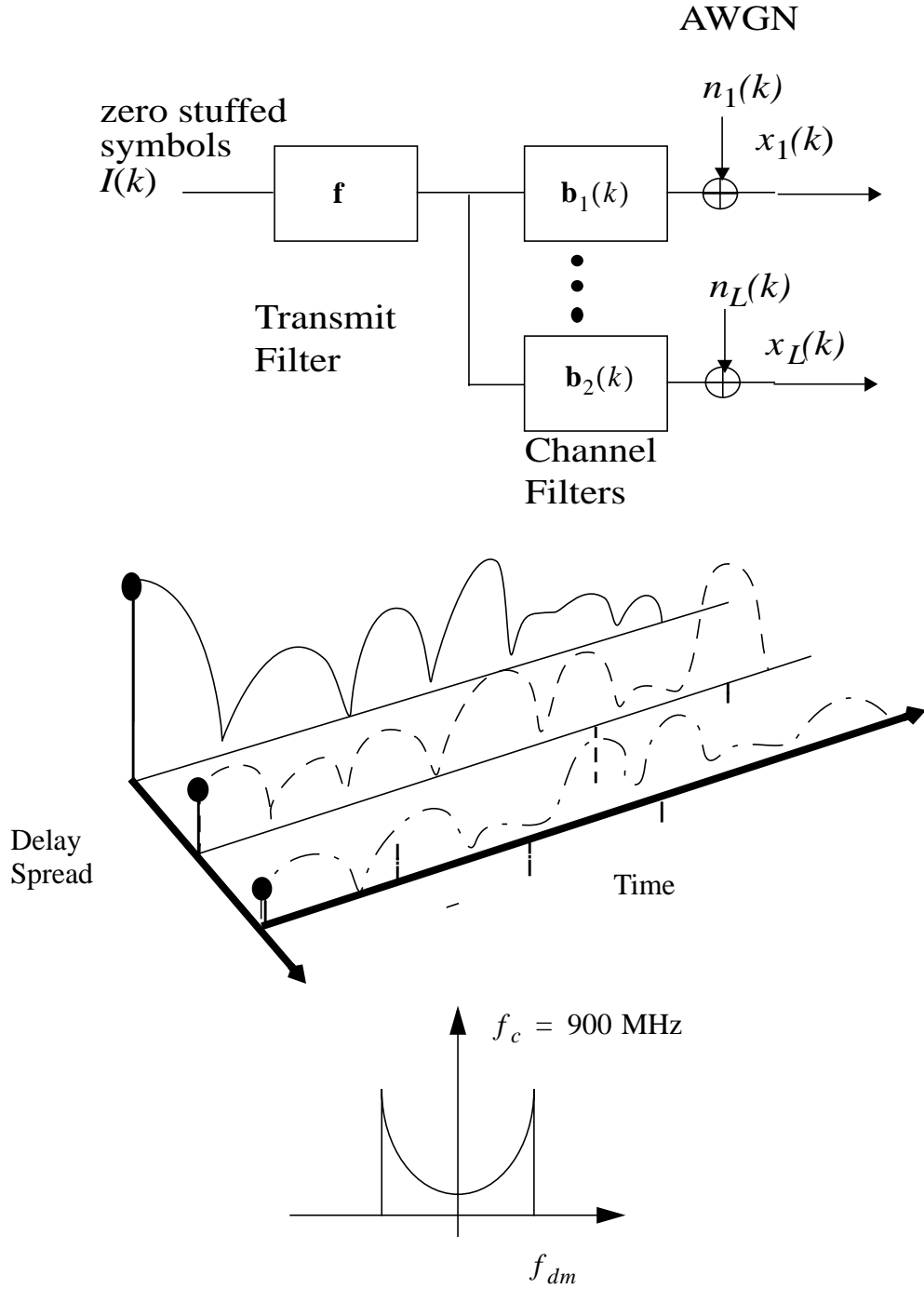


Figure 2-12 L independent diversity antenna channel model

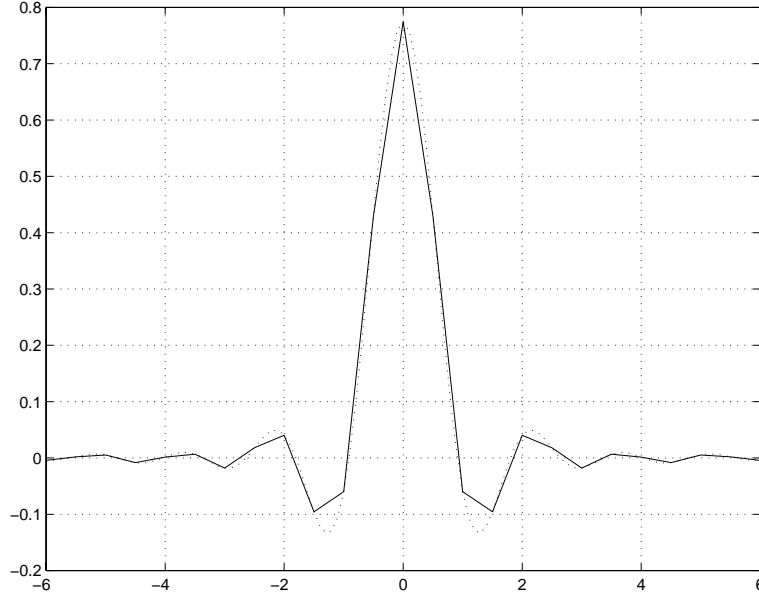


Figure 2-13 The square-root raised cosine filter: continuous wave form and the half-symbol spaced filter coefficients. (Shown truncated at 10 symbol-periods).

given by

$$f(t) = \frac{4\alpha}{\pi\sqrt{T_B}} \cdot \frac{\cos((1+\beta)\pi t/T_B) + T_B \sin((1-\beta)\pi t/T_B)/(4\beta t)}{1 - ((4\beta t)/T_B)^2}, \quad (2.26)$$

where  $\beta$  is the rolloff factor,  $0.0 \leq \beta \leq 1.0$ . The half-symbol spaced sampled filter is used for the simulation, see Figure 2-13 for an example.

Now, the symbols in Figure 2-12 are summarized here as

- The  $T_B/2$ -spaced sampled transmit filter  $f(t)$  is represented by a unit energy  $[31 \times 1]$  column vector  $\mathbf{f}$  which corresponds to a 15 symbol truncation.
- $x_l(t)$  the received signal at each diversity branch, which is bandlimited with the excess bandwidth of  $(1+\beta)(1/T_B)$ .  $T_B/2$ -spaced sampling is considered, i.e.,  $x_l(t) :=$

$x_l(t = kT_B/2)$ , where  $k$  denotes the  $T_B/2$ -spaced epoch index.

- $\{I(k)\}$  represents the symbol sequence at the half-symbol sampling rate. That is, it is a zero stuffed sequence such that  $I(k)$  at even  $k$  represents the symbol transmitted at the baud rate and  $I(k)$  at every odd  $k$  is zero-valued. Later in Chapter 7, we develop a more efficient convention using the polyphase representation of the filters. For now up to Chapter 5, we will use this zero-stuffed convention.
- The noise  $n_l(t)$  is also assumed to be  $T_B/2$ -spaced sampled and the sampled noise sequence  $n_l(k)$  is assumed to be a complex-valued additive white Gaussian with zero mean and variance  $\sigma_n^2$ . The noise sequences for different branches are assumed to be mutually uncorrelated and also independent with the wireless channel.
- $\mathbf{b}_l(k) = [b_{l,0}(k) \dots b_{l,N_R-1}(k)]^T$ , represents the time-varying impulse response of the  $l$ -th channel, where  $N_R$  is the number of the time-varying channel taps ( $N_R = 3$  in this dissertation).
- Each  $T_B/2$ -spaced overall channel impulse response  $\mathbf{h}_l(k)$  is defined as  $\mathbf{h}_l(k) := \underline{f} \otimes \mathbf{b}_l(k)$ , where  $\otimes$  denotes the convolution operation.

### 2.3.4 Generation of independent diversity channels

In this section, we illustrate the generation of the diversity wireless channel in a step-by-step manner.

1. Choose the MPDP, either from (2.24) or (2.25). Each diversity branch should have the same MPDP profile because MPDP is dependent only upon a large geographic region such that it is not dependent upon a diversity antenna. For example, get the average power delay profile for the three taps,  $\{\phi_{c,T_B/2}(i), i = 0, 1, 2\}$  with  $\sum_i \phi_{c,T_B/2}(i) = 1.0$ .
2. The  $L$  diversity channels are assumed to be mutually independent. In addition, all channel taps are also assumed to be mutually uncorrelated by the wide-sense

stationary uncorrelated scattering argument. Thus, in effect we need to generate  $L \cdot N_R$  uncorrelated scattering taps. For this select  $L \cdot N_R$  starting phases  $\{ST_{li}, l = 1, \dots, L, i = 0, 1, 2\}$  independently from a uniform distribution for example uniform of  $[-10000, 10000]$ . This method of generating the WSSUS tap is adopted from [61].

3. Choose the maximum Doppler frequency using (2.10)  $f_{dm} = \frac{v}{c}f_c$ . For example, with a carrier frequency of 900 MHz and assuming a mobile moves at a maximum highway speed of 120 km/hr,

$$f_{dm} = \frac{120 \text{ km/hr}}{3.0 \times 10^8 \text{ m/sec}} 900 \times 10^6 \text{ Hz} = 100 \text{ Hz}, \quad (2.27)$$

or for 12 km/hr,  $f_{dm} = 10 \text{ Hz}$ . Usually, we use a normalized fading rate, such that the normalized maximum Doppler fading rate  $f_{dm}T_B$  is 0.00417 for 100 Hz since the symbol rate is 24 ksps. In this dissertation we imply fast fading by  $f_{dm} = 100 \text{ Hz}$  ( $f_{dm}T_B = 0.00417$ ) and the slow fading by  $f_{dm} = 10 \text{ Hz}$  ( $f_{dm}T_B = 0.000417$ ).

4. Using 1, 2, and 3, each channel tap coefficient  $b_{l,i}(k)$  can be obtained by

$$b_{l,i}(k) = \sqrt{\phi_{c,T_{B/2}(i)}} \rho\left(t = k\frac{T}{2}; ST_{li}\right), \quad (2.28)$$

where  $\rho(t; ST_{li}) = N_D \sum_{j=0}^8 d_j \cos(2\pi\delta_j f_{dm}t + ST_{li})$  is the sum of nine sinusoids defined in (2.15).

Figure 2-14 illustrates the time-variation of the twelve-tap truncated, combined response of  $\mathbf{h}_l(k) = \mathbf{f} \otimes \mathbf{b}_l(k)$  over 80 symbol periods at the fading rate of 100 Hz.

## 2.4 Concluding Remarks

In this section, we have reviewed some of basic assumptions and simulation models on the wireless radio channel, especially, for digital cellular radio channels. In particular,

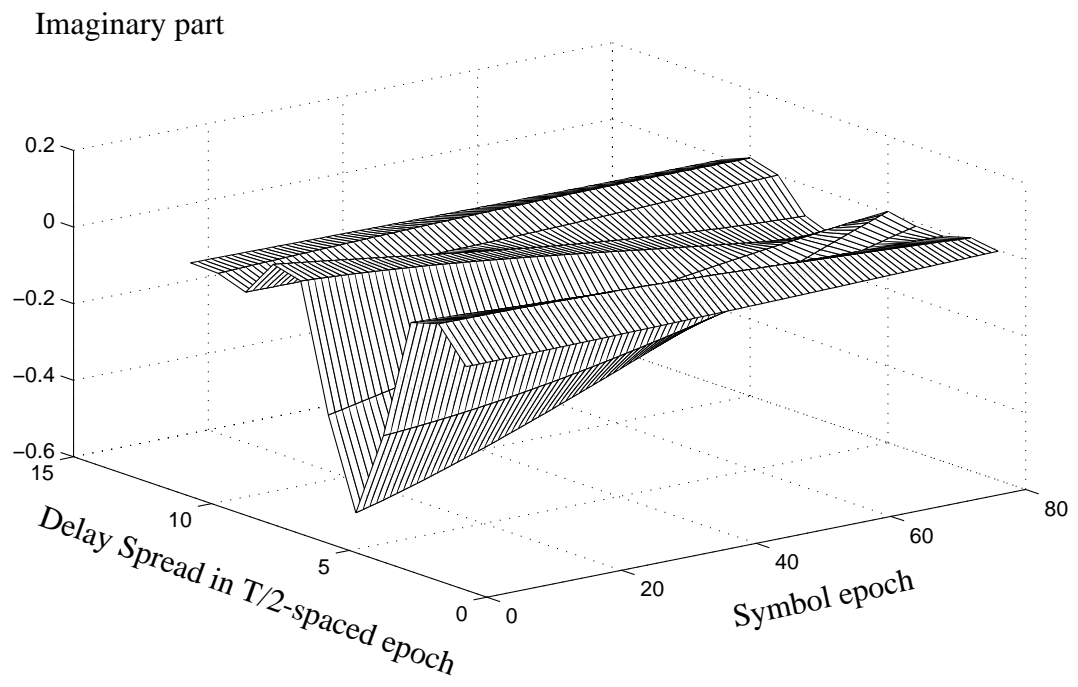
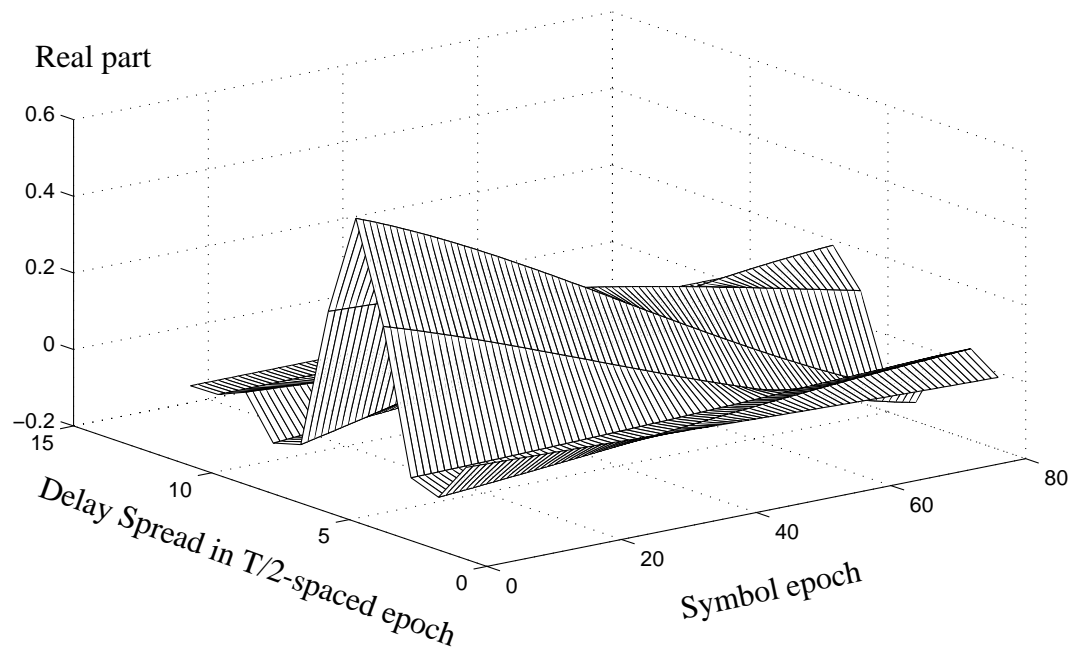


Figure 2-14 Visualization of the time-varying channel, fading at 100 Hz is shown over 80 symbol periods.

the delay dispersion and the time-varying nature of the channel are studied in reasonable detail. In addition, the simulation model for independent diversity antennas has been developed. In-depth characterization of the mobile radio communications channel are available in many resources, including Sklar [35], chapter 13 of Proakis [65] and chapter 1 and 2 of Steele [17]. For example, the article by Sklar provides a good summary of fading land mobile radio channels and the basic mitigation techniques for fading. Steele with more rigorous mathematical treatment of the subject, provides more complete characterization of digital cellular radio (DCR) channels, ranging from physical description of the propagation channel to the mathematically rigorous channel models of Bello, and covers diverse topics such as Rayleigh and Ricean fading channels, wideband or narrow band channels, propagation loss in micro-cellular areas and indoor propagation media. The readers are referred to the above references for in-depth coverage of the subject.

# Chapter 3

## Background and Equalizers

In this Chapter, we want to qualitatively reviews some of the well-known equalization structures for single carrier transmission systems, such as the linear equalizer, decision feedback equalizer (DFE), Tomlinson-Harashima precoder [44] and maximum likelihood sequence detection (MLSD) equalizer. Among them, the DFE and MLSD will be developed rigorously in the upcoming Chapters as the proposed mitigation methods against the rapidly time-varying multipath fading ISI channels. Other ISI mitigation methods not discussed in this dissertation may include the use of spread-spectrum modulation with orthogonal codes and RAKE receiver [65], and the use of multitone carrier modulation [39][40]. While we discuss equalization methods, we also describe the baseband communication systems and the simulation methodology. The voiceband telephone modem [36] is taken as an example to show the baseband representation, need for equalization and computer simulation results for some equalizers. We show that the telephone channel is bandlimited and becomes highly delay-dispersive when the symbol rate is increased up to the point comparable to the bandwidth of the telephone channel. As

the symbol rate is increased, the transmission frequency band starts to contain the nulls at the band edges<sup>1</sup>, and thus severe intersymbol interference (ISI) occurs. Thus a sophisticated equalizer is needed which handles the nulls gracefully. For this type of channel, an equalizer which linearly inverts the channel would perform very poor. They are the channels with a severe ISI, such that channels contain in-band nulls, for which a significant difference in detection performance occurs between a good and a bad equalizer. For example, the use of a non-linear equalization method, such as decision feedback equalizer (DFE) significantly outperforms the linear equalizers. Furthermore, the use of MLSD receiver via Viterbi Algorithm [88] makes another significant improvement over the use of the DFE. On the other hand, when there is no null(s) in the transmission band, the performance differences will be insignificant, and basically many equalization methods perform well.

With the telephone channel example, we will illustrate in terms of an ideal output SNR calculation that the difference between the linear equalizer (LE) and the DFE widens as the symbol rate increases. The DFE, however, may suffer from a significant SNR loss due to the inherent problem of error-propagation since the decided symbols are fed back and used to cancel the post-cursor ISI. The use of a T-H precoder brings back most of the SNR loss due to decision feedback by moving the feedback filter of the DFE into the transmitter. Finally, we then discuss the training of the DFE filter using LMS and RLS adaptation algorithms, and investigate their convergence properties.

### **3.1 Simulation of Digital Communication Systems**

The performance of continuous-time passband communications system can be simulated in the baseband by using the procedure described in this section. We take the

---

1. In fact, anywhere in the transmission bandwidth if there is a null, severe ISI occurs. For the case of telephone modems, the nulls are included at the band-edges as the symbol rate is increased.

voice-band telephone modem [36] as an example to illustrate the simulation methodology. The voice-band modems are tested against a set of pre-specified passband channel impulse responses. Figure 3-1 illustrates the three different channel impulse responses  $c_0$ ,  $c_2$  and  $c_4$ . The values in the ordinate represents the voltage (or the current) samples of impulse response of the real telephone channels. The sampling rate was 8229 Hz.

### 3.1.1 Baseband Representation of the Bandpass Systems

Figure 3-2 describes the complex baseband equivalent system model for a carrier modulation system. The real communication channel over which the signal is transmitted are usually a shared medium, and thus the use of the channel almost always has to be limited in bandwidth to an interval of frequencies centered about the carrier. For the voiceband telephone channel, the channel is already limited in the transmittable region by a band limit-filtering done *a priori* to the telephone line. For the wireless channel, a fixed amount of frequency spectrum is assigned for the establishment of a communication link, and the transmit shaping filter is used to limit the spectrum use of the link. Thus, by distribution of carrier frequencies among different users, the channel can be shared by

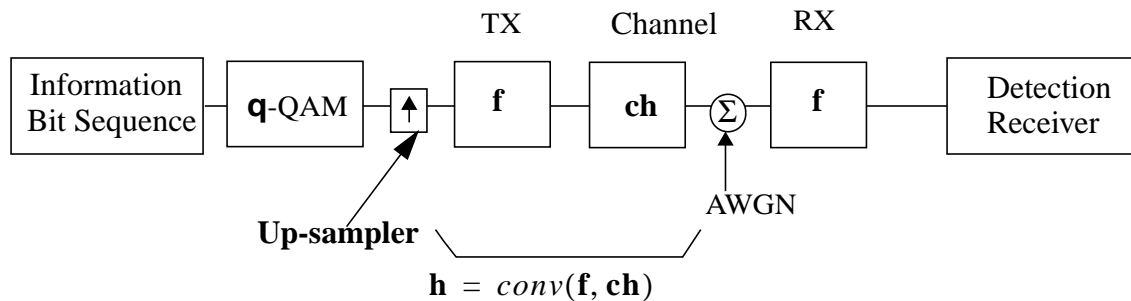


Figure 3-2 Baseband system description for  $q$ -QAM transmission over the dispersive channel and the receiver structure of fractionally-spaced decision feedback equalizer

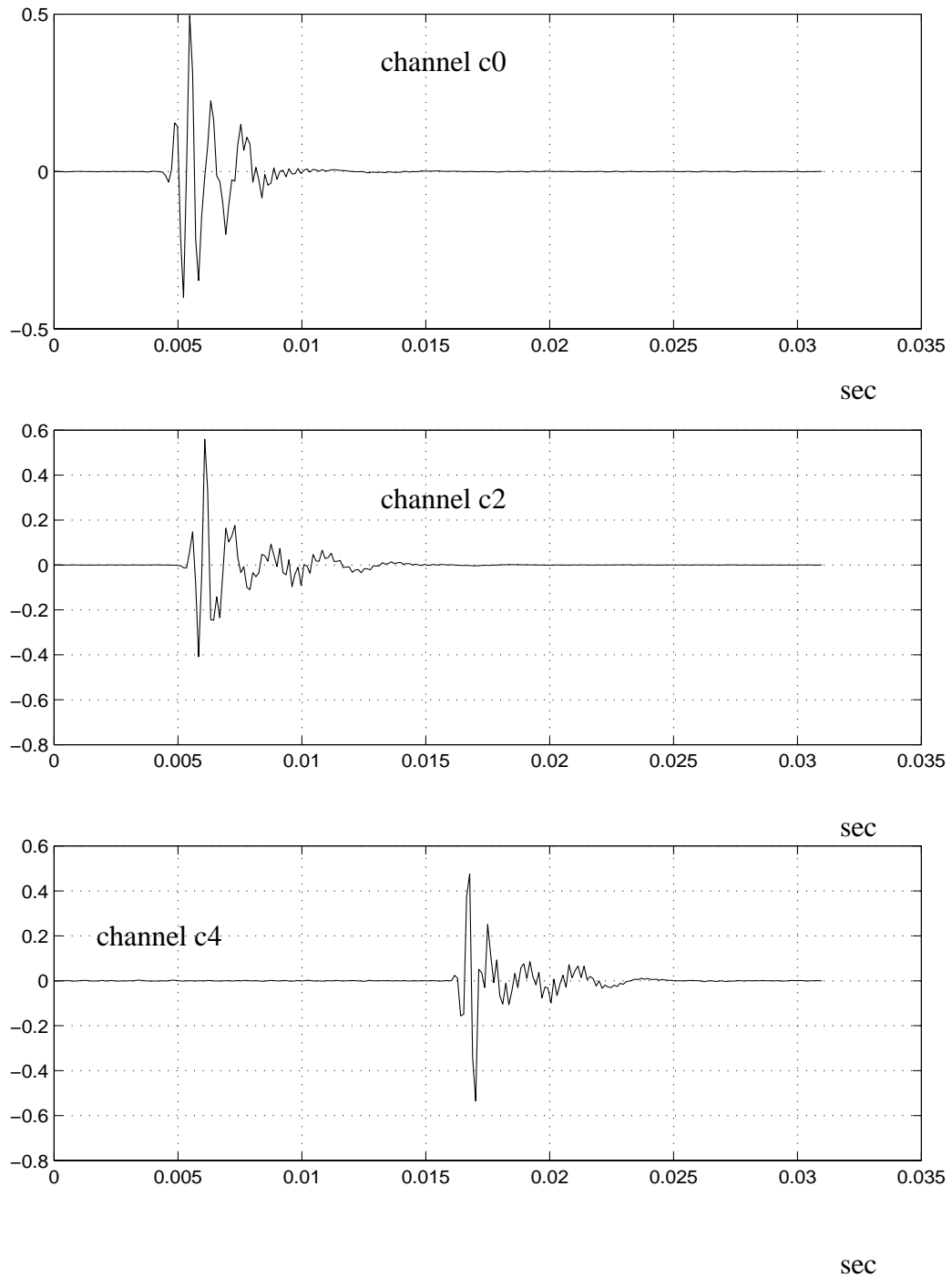


Figure 3-1 The passband channel impulse response of c0, c2 and c4. The sampling rate is 8229 Hz. Total number of samples for each channel is 256 samples.

multiple users. For telephone modems, the carrier frequency can be varied to find the best frequency band to transmit the information. This passband operation of communication can be equivalently represented in the baseband. The carrier modulation is performed on the baseband signal at the transmitter to generate the bandpass signal and the carrier-demodulation is performed at the receiver to recover the baseband signal. These upward and downward modulation steps can be omitted without loss of generality. For this to happen, however, we need to have the information symbols, the transmit/receive filters, and the passband channel represented in the baseband.

For the quadrature modulation using the cosine and sine carriers, the baseband information symbols can be represented as complex-valued symbols, such that the real parts of the information symbols are transmitted on the cosine-carrier and the imaginary part on the sine-carrier.

The transmit and receiver filter have the same impulse response of square-root raised cosine filter (SRRC). This combination of transmit and receive filters is desirable since it is a matched filter when we have a flat channel response. In addition, the cascade of SRRC in series results in a Nyquist overall pulse, the raised cosine pulse, and thus no ISI occurs. The time-domain expression of the SRRC was given in (2.26). By the use of excess bandwidth and assumption of frequency-selective channel response, we need to consider a fractional sampling of the received signal (see Chapter 2 for more details on why).

In order to simulate the telephone-modem at different baud rates or at different carrier frequencies, we first need to obtain the baseband equivalent channel for each of passband channels for different combinations of the baud rate and the carrier frequency. The passband channel should be interpolated first, resampled at the desired sampling frequency, and then down modulated by the amount of the carrier frequency. Figure 3-3 illustrates the steps taken to generate the baseband equivalent channel for the channel c0 with the baud rate of 2400 sps and the carrier frequency 1829 Hz, where

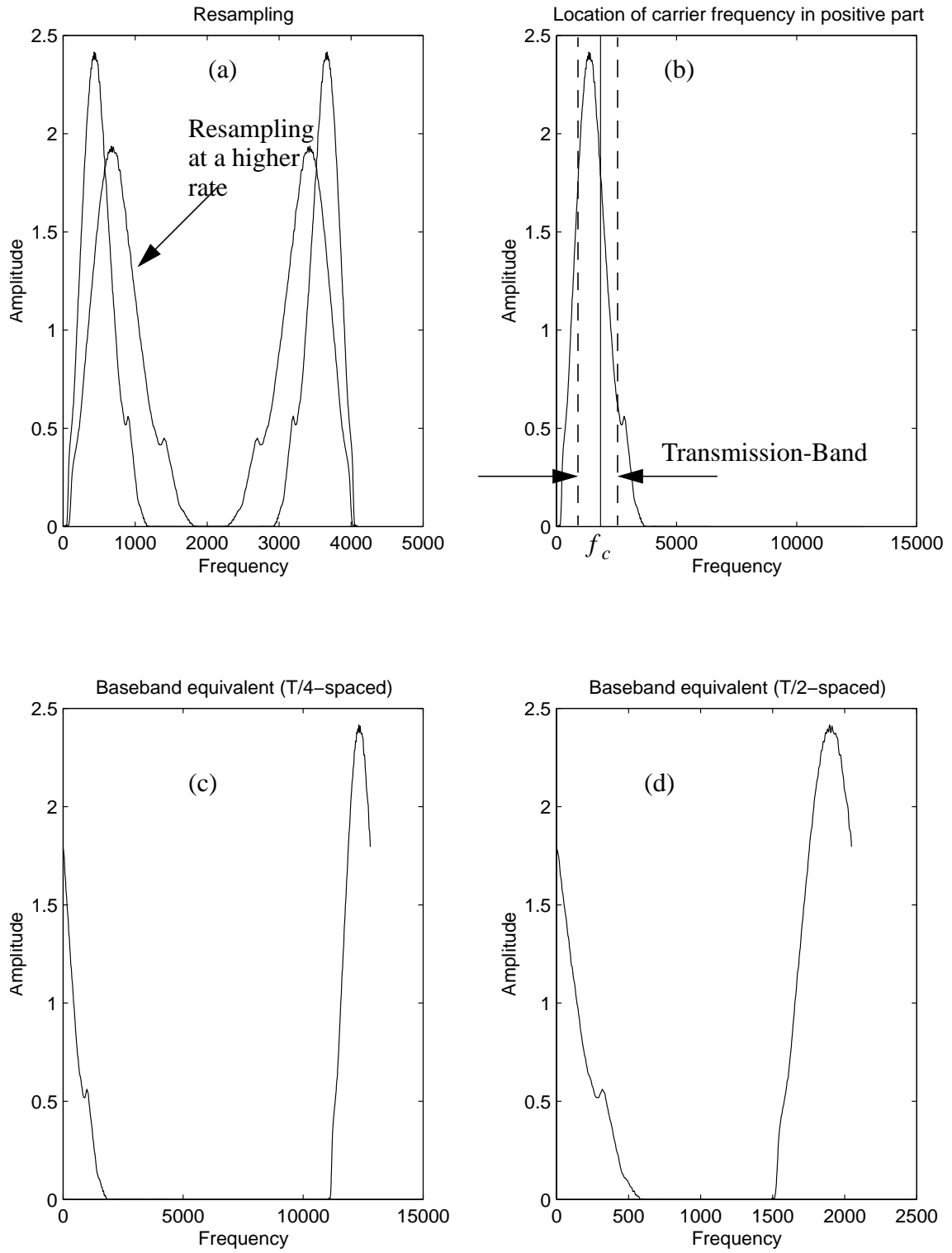


Figure 3-3 The channel-filter rate conversion process.

- (a) represents the interpolation and resampling at a higher rate (4 times the baud rate)
- (b) shows the location of carrier frequency ( $f_c = 1829$  Hz), which is at the center of the transmission band that is equal to the baud rate. Thus, as baud rate increase the transmission band start to include the null at the band-edge.
- (c) shows the baseband channel at the sampling rate, four times the baud rate
- (d) finally represents the complex-baseband channel at the sampling rate, i.e. twice the baud rate.

The baseband simulation of the system shown in Figure 3-2 can now be described. The information bits are mapped to  $q$ -ary QAM symbols. Assuming fractional sampling by two, the symbol sequence is upsampled by two (zero-stuffed at every other symbol) and passed to a  $T_B/2$ -spaced square-root raised cosine filter of 15% rolloff before transmitted through the  $T_B/2$ -spaced sampled channel. The received signal is corrupted by the additive white Gaussian noise (AWGN) of variance  $\sigma_n^2$ . It is finally matched filtered (matched TX filter). We normalize the  $T_B/2$ -spaced combined response of transmit and channel filters, to be denoted as a column vector  $\mathbf{h}$ , i.e.,

$$\sum_i |h_i|^2 = 1.0.$$

Then, the input SNR can be simplified as follows

$$SNR = \frac{E_{avg} \cdot \sum_i |h_i|^2}{\sigma_n^2} = \frac{E_{avg}}{\sigma_n^2}, \quad (3.1)$$

where  $E_{avg}$  is the average energy of the input symbols and  $\sigma_n^2$  is the variance of the complex-valued noise. Thus, the  $T_B/2$ -spaced noise  $n(k)$  can be generated by

$$n(k) = \sqrt{\frac{\sigma_n^2}{2}}(n_1(k) + j n_2(k)), \quad (3.2)$$

where  $n_1(k)$  and  $n_2(k)$  are mutually independent Gaussian random variables having zero

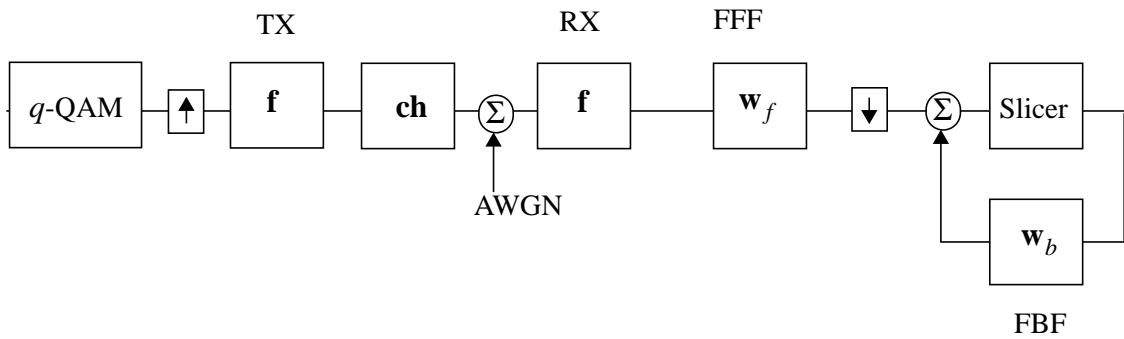


Figure 3-7 Baseband system description for  $q$ -QAM transmission over the dispersive channel and the structure of fractionally-spaced decision feedback equalizer

mean and unit variance.

Figure 3-4, Figure 3-5 and Figure 3-6 are graphical illustrations of channel filter rate conversion results for different combinations<sup>1</sup> of baud rates and carrier frequencies, for each channel  $c_0$ ,  $c_2$  and  $c_4$ . The results are represented in amplitude responses in time- and frequency-domain. We should note that as the baud rate increases, the null in the folded spectrum (see next Section for definition) gets deeper. For example, the channel for  $c_0$  at 3200 baud rate and 1829 carrier frequency Figure 3-4, has an in-band null which is about  $10^{-3}$ .

## 3.2 LE, DFE and TH-precoder

We now compare performances of the minimum mean square error (MMSE) linear equalizer (LE), the MMSE-DFE and the Tomlinson-Harashima (TH) Precoder. LE and DFE are compared in terms of the ideal output SNR. DFE and T-H precoder are compared with the symbol error rate evaluated from C++ system simulation.

1. See Table 3-1: for the combinations.

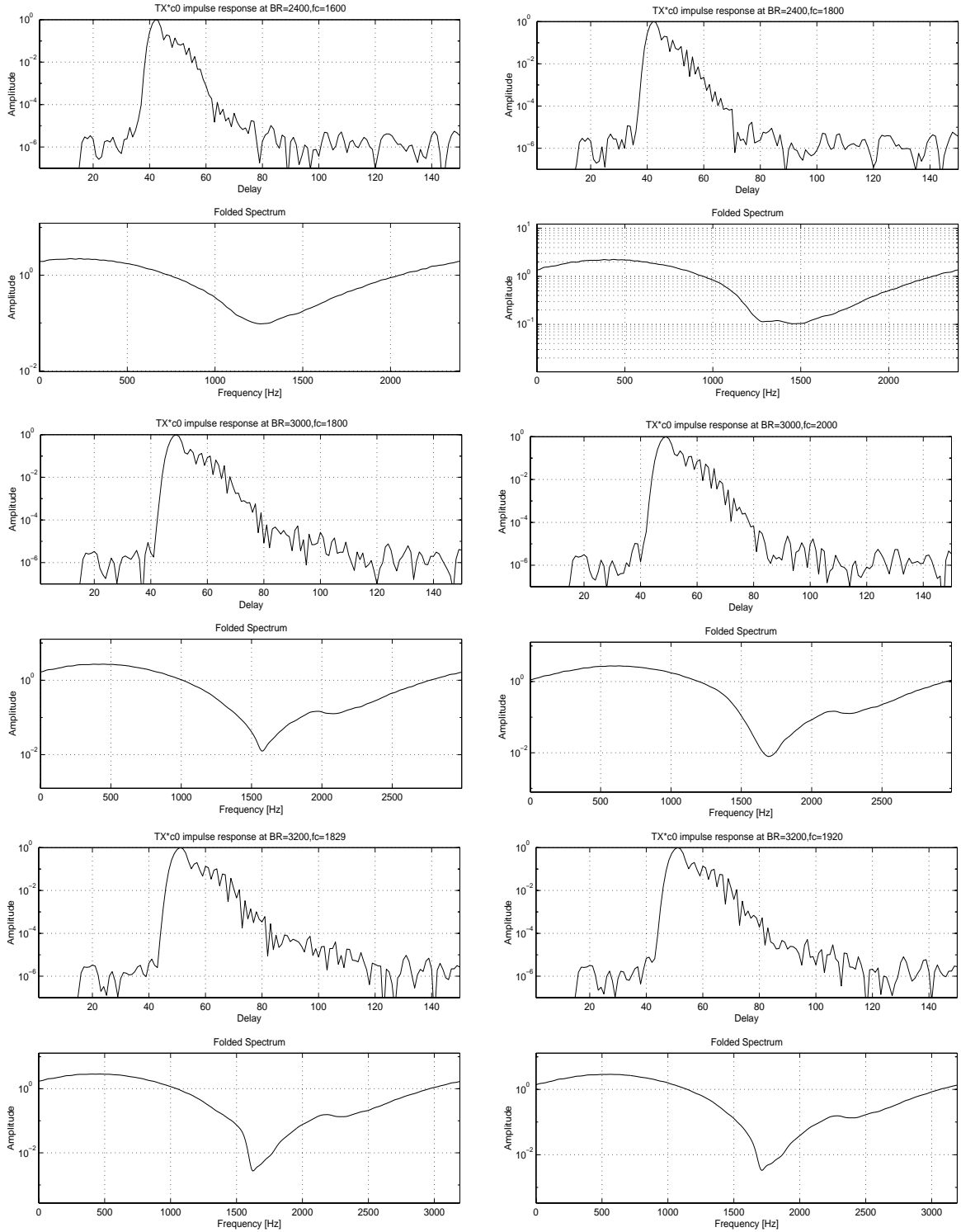


Figure 3-4 Time and frequency domain responses of the channel c0 at different combination of the baud rates and the carrier frequencies.

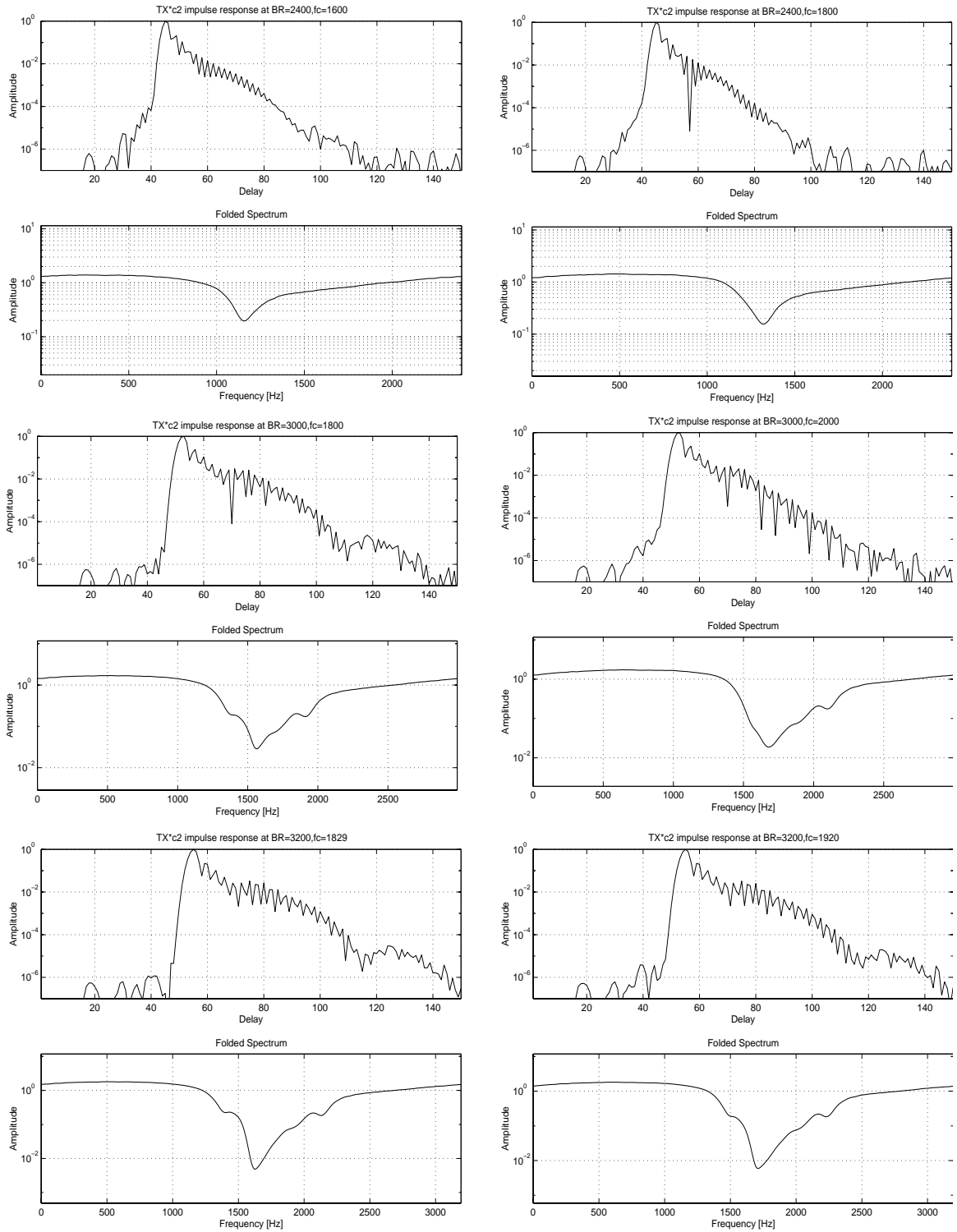


Figure 3-5 Time and frequency domain responses of the channel c2 at different combination of the baud rates and the carrier frequencies.

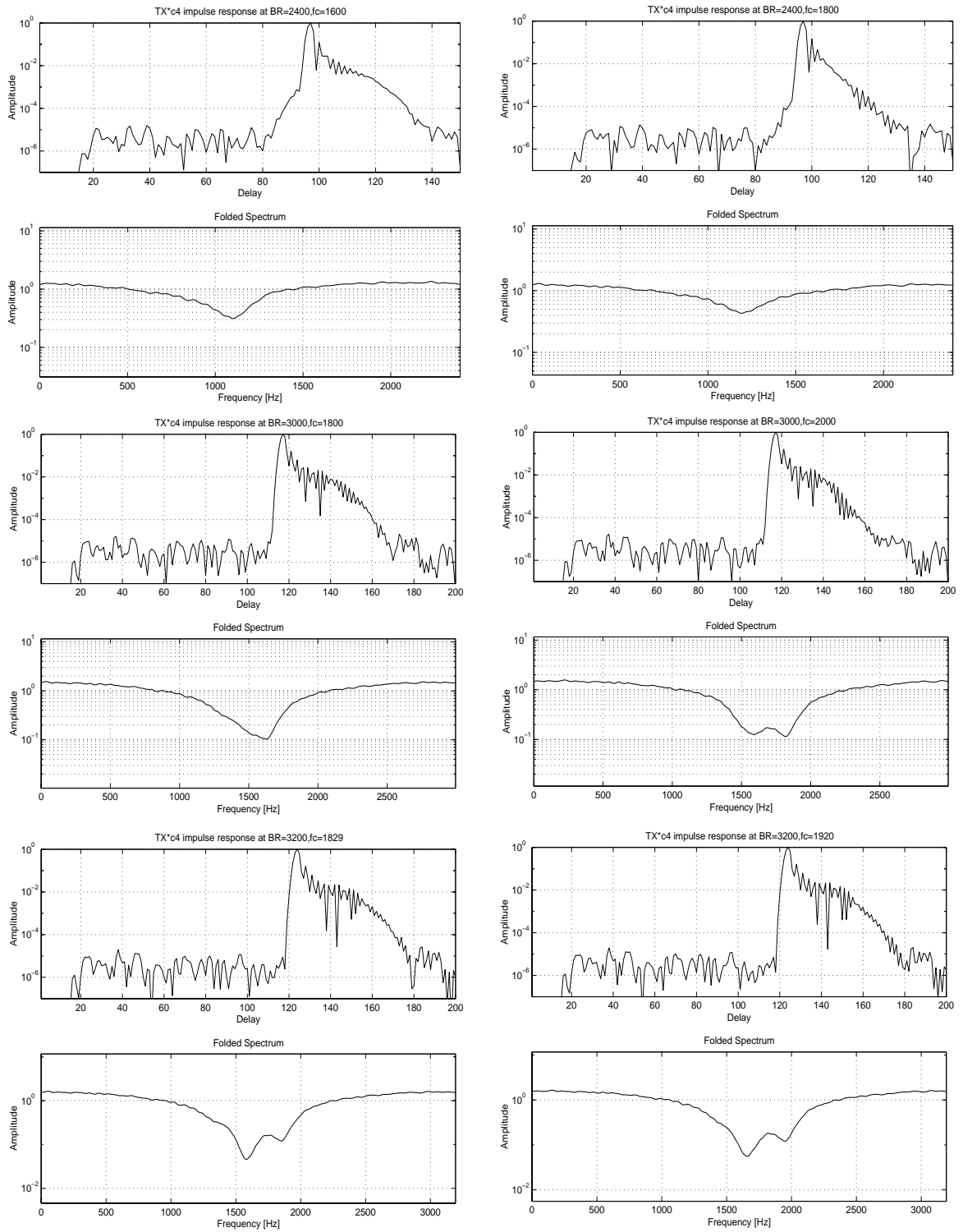


Figure 3-6 Time and frequency domain responses of the channel c4 at different combination of the baud rates and the carrier frequencies.

### 3.2.1 Ideal output SNR comparison of LE and DFE

Figure 3-7 shows the receiver structure of a fractionally-spaced DFE. It has a feedforward transversal filter part and a symbol-spaced feedback filter part. With the use of feedforward filter alone, the receiver is called a linear equalizer. We may define the error signal to be the difference between the equalized pre-decision sample and the input symbol (or decided symbol). The optimum criterion is to minimize the mean square of the error signal. From this, the well known MMSE-LE and MMSE-DFE are derived [65].

The minimum mean square error of ideal MMSE-DFE is expressed as

$$J_{min}^{DFE} = \exp \left\{ \frac{T_B}{2\pi} \int_{-\pi/T_B}^{\pi/T_B} \ln \left( \frac{N_o}{X(e^{j\omega T_B}) + N_o} \right) d\omega \right\}, \quad (3.3)$$

and that of the ideal MMSE-linear equalizer (MMSE-LE) is

$$J_{min}^{LE} = \frac{T_B}{2\pi} \int_{-\pi/T_B}^{\pi/T_B} \frac{N_o}{X(e^{j\omega T_B}) + N_o} d\omega, \quad (3.4)$$

where we denote  $X(e^{j\omega T_B})$  to be the folded spectrum, i.e.,

$$X(e^{j\omega T_B}) = \frac{1}{T_B} \sum_{n=-\infty}^{\infty} \left| H \left( \omega + 2\pi \frac{n}{T_B} \right) \right|^2, \quad (3.5)$$

where  $H(\omega)$  denotes the frequency response of the combined channel, the transmit and the channel filters. Then, the output SNR  $\gamma_\infty$  is given by

$$\gamma_\infty = \frac{1 - J_{min}}{J_{min}}. \quad (3.6)$$

In our simulation, the integrals are numerically evaluated as follows:

- Obtain the  $T_B$ -spaced autocorrelation function by correlating the  $T_B/2$ -spaced sam-

pled overall channel by itself

$$x(k) = \sum_i h_i^* \cdot h_{i+2k}. \quad (3.7)$$

- Take a  $N_{fft}$  point-DFT of the obtained sequence  $\{x(k)\}$  and take the absolute values of the result to get the folded spectrum. Denote the result as  $X(n)$ . Note that in the sequence  $\{x(k)\}$  the value corresponding to the origin  $x(k=0) = 1.0$  is located at the center of the sequence, instead of at the first place of the sequence, thus we need to take the absolute value to get the folded spectrum  $X(n)$ . If we had cyclically shifted the sequence  $\{x(k)\}$  to locate  $x(k=0)$  at the first place of the sequence, then a real-valued  $X(n)$  would have been obtained.
- Then, the integral can be evaluated by

$$\exp\left\{\frac{1}{N_{fft}} \sum_{n=1}^{N_{fft}} \ln\left[\frac{\sigma_n^2}{\sigma_n^2 + X(n)}\right]\right\}. \quad (3.8)$$

The folded spectrum of a channel provides the most critical information about how to design an equalizer and how well the equalizer would perform. For example, when a relatively flat folded spectrum is obtained for a given channel, an inversion filter as a zero-forcing equalizer may provide us with simple but satisfactory results. On the other hand, when there is (are) deep null(s) in the folded spectrum, an inversion filter implies the amplification of received noise at the frequency components where the null(s) are located. Thus, a more sophisticated equalizer is required to achieve symbol detection without noise enhancement.

The folded spectrum of the telephone channels not only depend on the channel characteristics, but also on the choice of the baud rate and the carrier frequency since the channel is bandlimited. As the baud rate is increased, the transmission bandwidth starts to include the band edges of the channel. Then, the folded spectrum starts to contain deep

nulls at the band edges. For the time-varying wireless channel, we don't know whether or not the folded-spectrum will contain any null at any given time instance. The null (s) in the folded-spectrum will appear and disappear as the channel is evolving over time. The frequency of appearance, the degree and the number of nulls completely depend on the rms delay spread (2.7) of the wireless channel and the transmission bandwidth.

We now compare the performance of MMSE-DFE and MMSE-LE in terms of the output SNR evaluated from (3.3) and (3.4). The results are tabulated in Table 3-1:. The input SNR is 28.0 dB.

**Table 3-1: Output SNR for ideal MMSE-DFE and MMSE-LE**

channel	Baud Rate	$f_c$	DFE	LE
c0	2400	1600	26.24	23.90
		1800	26.10	23.62
	3000	1800	24.84	20.05
		2000	24.89	18.18
	3200	1829	24.01	16.28
		1920	23.92	16.29
c2	2400	1600	27.63	27.05
		1800	27.54	26.77
	3000	1800	26.47	23.02
		2000	26.08	21.37
	3200	1829	25.68	18.70
		1920	25.60	18.78
c4	2400	1600	27.75	27.40
		1800	27.84	27.63
	3000	1800	27.17	25.57
		2000	27.08	25.36

**Table 3-1: Output SNR for ideal MMSE-DFE and MMSE-LE**

channel	Baud Rate	$f_c$	DFE	LE
	3200	1829	26.80	24.27
1920		26.80	24.40	

Figure 3-4 ~ Figure 3-6 shows the folded spectrum of each combination. Note that as the baud rate is increased, the folded spectrum contains a deeper null and the output SNR degrades. Also note that the SNR difference for DFE and LE is larger when the null gets deeper. From evaluation of output SNRs, a maximum constellation size for each combination which satisfies a certain symbol error rate (for example,  $SER = 10^{-4}$ ) can be calculated, and then a maximum achievable transmission rate can be calculated by multiplying the baud rate with the number of bits/symbol.

### 3.2.2 Output SNR for finite length DFE

For the illustration of a finite length DFE, we pick the channel c0 with  $f_c = 1829$  Hz and the baud rate of 3200 sps. The output SNR from Table 3-1: is 24.01 dB. The DFE equation to obtain the  $T_B/2$ -spaced feedforward and  $T_B$ -spaced feedback filter coefficients from the channel impulse response are described in [43]. Once the filter coefficients are obtained, the output SNR for finite DFE can be readily computed using the expression given in [43]. We found out that the use of  $(N_f, N_b) = (40, 40)$  achieves the output SNR of 23.0 dB, where  $N_f$  denotes the feedforward filter length and  $N_b$  the feedback filter length.

Figure 3-8 describes the operation of the receiver step by step:

- (a) shows the amplitude response of the overall channel, the transmit shaping filter, the channel c0 and the receive filter
- (b) shows the  $T_B/2$ -spaced overall response including the feedforward filter
- (c) indicates the symbol-spaced overall response including the feedforward filter, RX,

ch, and TX. Note that the mean square error can be expressed as

$$J_{min}^{Finite} = 1.0 - \text{Overall Response at the optimum delay}, \quad (3.9)$$

and thus the output SNR can be calculated from

$$\gamma_{Finite} = \frac{1.0 - J_{min}^{Finite}}{J_{min}^{Finite}} \quad (3.10)$$

- (d) represents the symbol-spaced overall response including the feedforward filter and the feedback filter, assuming perfect previous decision
- (e) shows the magnitude of the feedforward filter coefficients
- (f) shows the magnitude of feedback filter coefficients.

In the following section, we evaluate the symbol error performance of QAM signals using the finite length DFE with  $(N_f, N_b) = (40, 40)$  and compare the results with those obtained from using the T-H precoder.

### 3.2.3 TH-Precoder

The DFE was derived under the assumption that the feedback decisions are correct. In practice, this assumption is not valid, and for severe ISI channels the DFE suffers from error propagation. Tomlinson-Harashima-precoder get rid of the feedback part of the DFE at the receiver, replacing it with the modulo-inverse filter at the transmitter. Figure 3-9 describes the baseband equivalent system description of TH-precoder and equalizer. The inverse filter at the transmitter uses exactly the same filter coefficients as the decision feedback filter of the DFE. In fact, postcursor removal is performed even before transmission using the input symbols, instead of at the receiver using symbol decisions. Thus, the error propagation problem of DFE is resolved. The precursor removal is still performed by the feedforward filter which stays exactly the same as that of DFE.

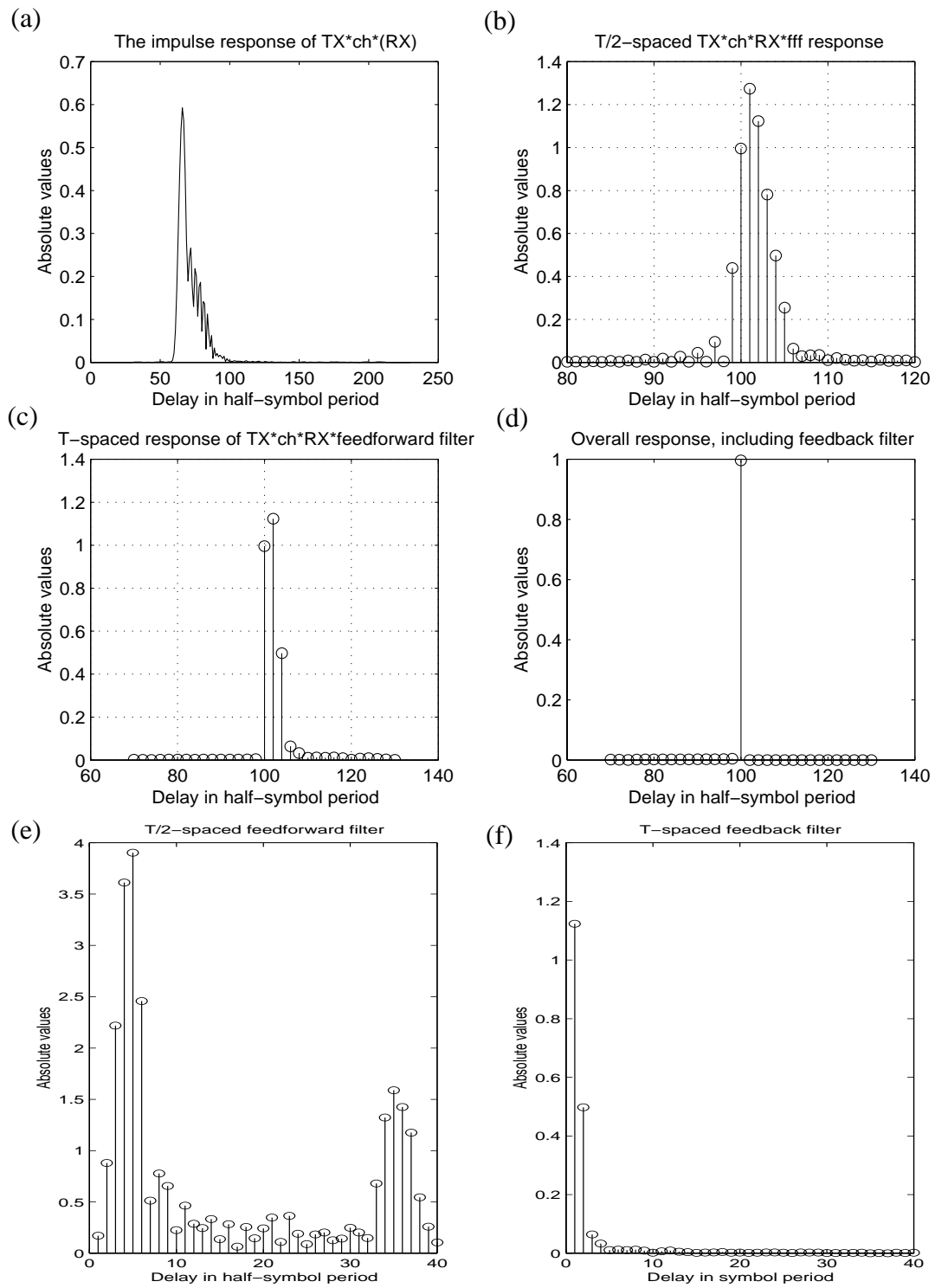


Figure 3-8 Step-by-step illustration of DFE transceiver operation

TH-precoder requires the modulo- $\tau$  operation at the transmitter and the receiver [44]. The following illustrate the modulo operation and the TH-precoder depicted in Figure 3-9:

- the range of the modulo- $\tau$  is  $(-\tau/2, \tau/2]$ ,
  - if the input is greater than  $\tau/2$ ,  $\tau$  is subtracted an integral number of times until the result is in the range,
  - if the input is less than  $-\tau/2$ ,  $\tau$  is added an integral number of times until the result is in the range.
- The modulo- $\tau$  operation is applied to each of the real and imaginary part individually, i.e.,

$$\text{modulo}(\text{complex number}) = \text{modulo}(\text{real part}) + j \cdot \text{modulo}(\text{imag part}).$$

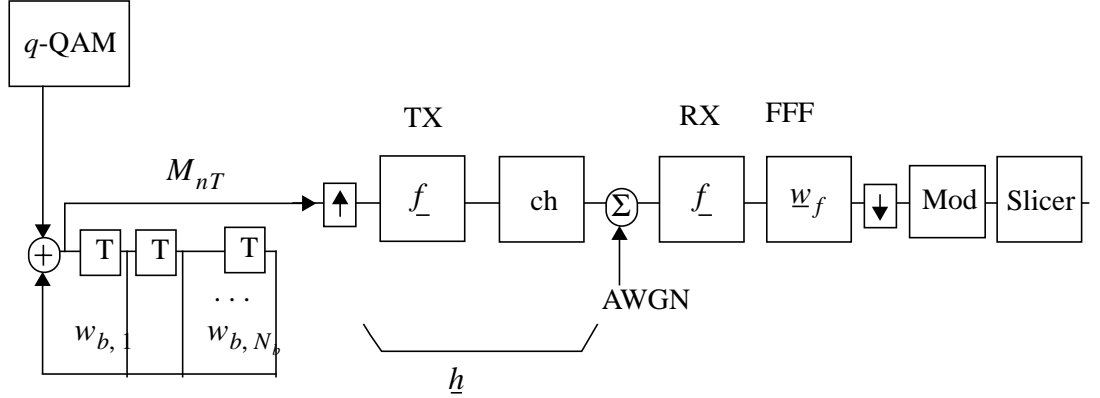
- Choose  $\tau = 2 \cdot \lceil \sqrt{q} \rceil$  for  $q$ -QAM, to insure that both real and imaginary parts of input symbols are within the range.
- The modulo operation removes the correlation and the possibility of instability introduced by the inverse filter.
- For the input SNR defined in (3.1), the average power should be rescaled by

$$E_{avg} = \frac{1}{\tau^2} \int_{-\tau/2}^{\tau/2} \int_{-\tau/2}^{\tau/2} (x^2 + y^2) dx dy = \frac{\tau^2}{6}. \quad (3.11)$$

- With a careful choice of the threshold value  $\tau$ , the modulo addition output  $M_{nT}$  can be assumed to be uniformly distributed over the range--so  $E_{avg}$  re-scaling of (3.11) is valid.

### 3.2.4 Simulation comparison of DFE and TH-Precoder

The DFE, correct decision feedback DFE and TH-precoder are simulated using



$\oplus$  denotes the modulo addition

Figure 3-9 The baseband equivalent system description for the Tomlinson-Harashima precoder and equalizer.

Monte-Carlo simulation. In Figure 3-11 symbol error rate of the receivers are compared for  $q = 16, 32$  and  $64$ . The results indicate that the TH-precoder indeed achieves the symbol error rate very close to that of correct decision feedback DFE. For 16 and 64-QAM, the SNR difference of the two are within 1.0 dB. For non-square 32-QAM constellation, the  $E_{avg}$  calculation of (3.11) is less accurate, and thus a higher SNR penalty is observed.

### 3.3 LMS and RLS training of DFE filter

In this Section we describe LMS and RLS training of DFE coefficients using training symbols. The baseband channel used is the channel c0 with the 2400 sps Baud rate and 1829 Hz carrier. The DFE filter lengths are  $(N_f, N_b) = (40, 40)$ . More in-depth coverage of the LMS and RLS algorithms discussed in this Section can be found in [42][33].

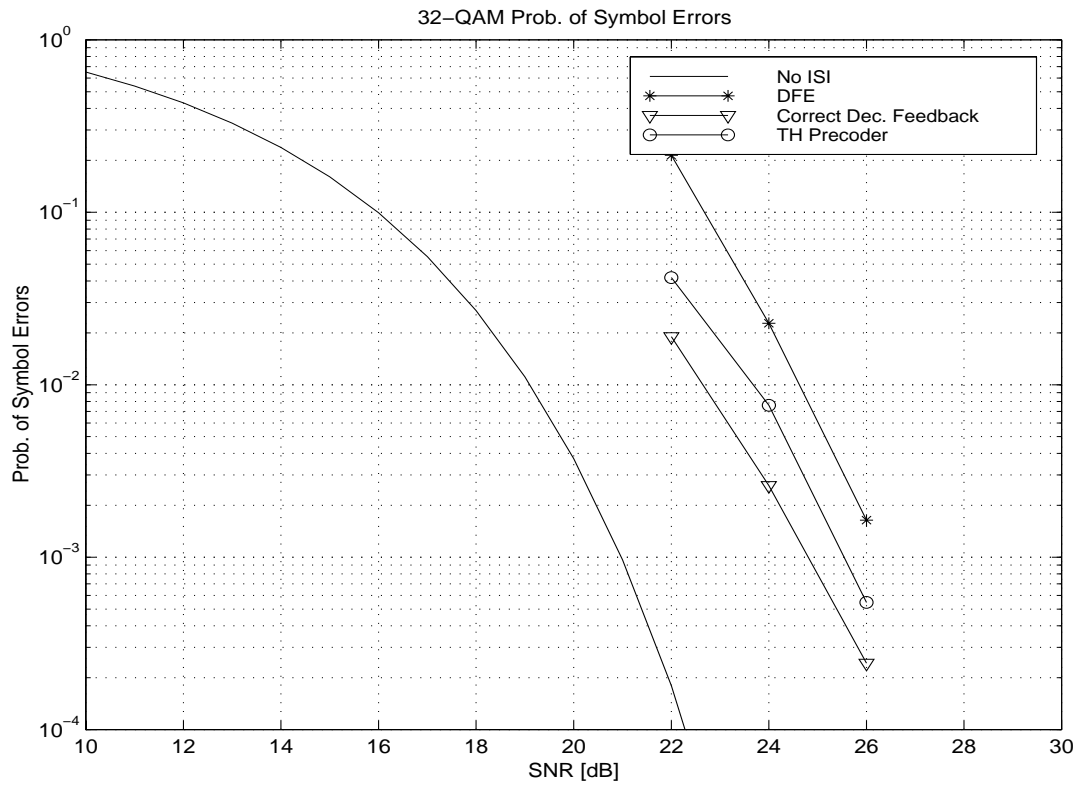
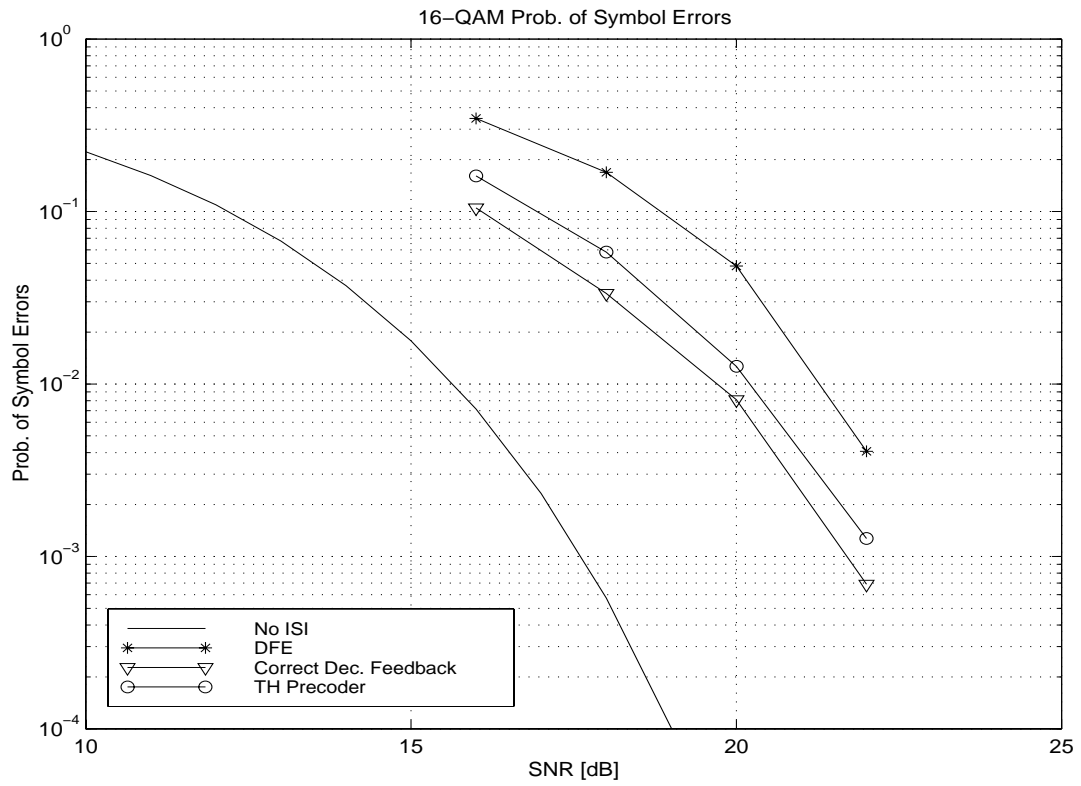


Figure 3-10 16- and 32-QAM symbol error rate simulation results on the telephone

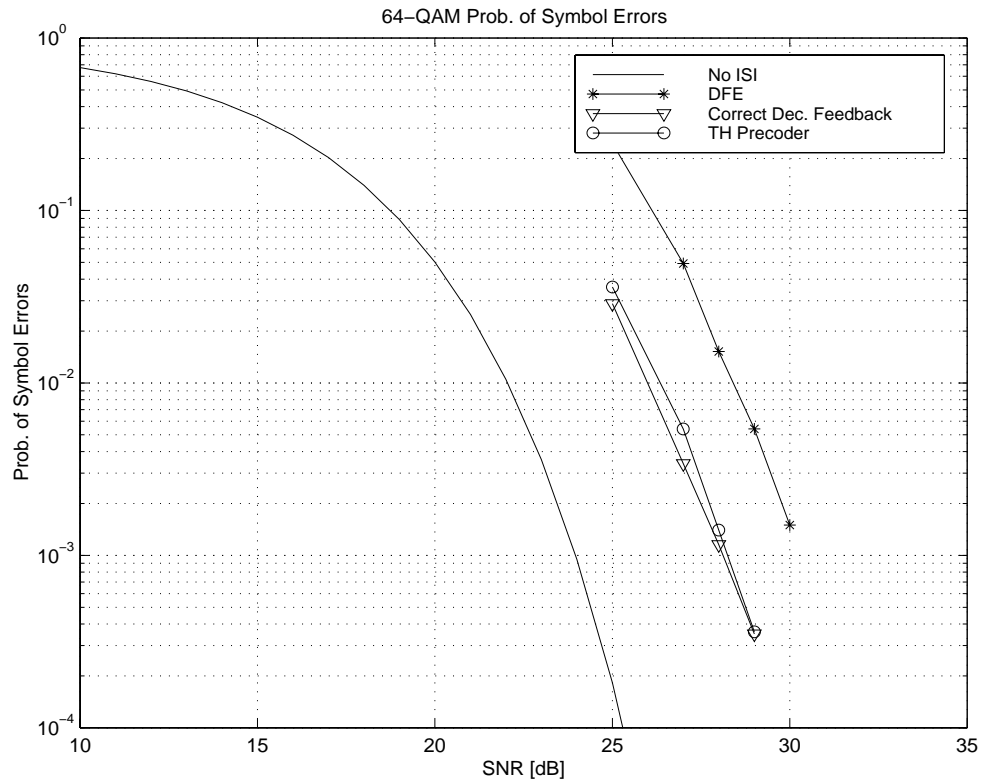


Figure 3-11 64-QAM symbol error rate simulation results on the telephone channel.

### 3.3.1 LMS training of DFE filters

We now provide the LMS training of DFE filter coefficients:

- BEGIN
- Pick the stepsize  $\Delta \in \mathfrak{R}^+$ , a small positive real value.
- Initialize  $\hat{\mathbf{w}}_k = (0 \dots 0)^t$  at  $k = 0$ .
- For  $k = 0, 1, 2, \dots$  until the end of the training sequence, Compute

$$\hat{\mathbf{w}}_{k+1} = \hat{\mathbf{w}}_k + \Delta \cdot \mathbf{v}_k \cdot \xi_k. \quad (3.12)$$

- END

where we have defined

- $\mathbf{w}_k = [w_{f,0} \cdots w_{f,N_f-1} \ w_{b,0} \cdots w_{b,N_f-1}]^t$ ,
- $\mathbf{v}_k = [r_{2k+D_m} \ r_{2k+D_m-1} \ \cdots \ r_{k+D_m-N_f+1} \ I_{k-1} \ \cdots \ I_{k-N_f}]^t$ ,
- $r_n$  denotes the  $T_B/2$ -spaced sampled received signal, the output of the SRRC receive filter
- $\xi_k = I_k - \hat{I}_k$ , where  $\hat{I}_k = \mathbf{v}_k^H \hat{\mathbf{w}}_k$
- $\Delta$  is the stepsize.

It is helpful to examine the eigenvalues of the system matrix, a  $N \times N$  correlation matrix  $\mathbf{R}_{\mathbf{v}} = E(\mathbf{v}\mathbf{v}^H)$ . It provides critical information about the recursive algorithm, on the selection criterion of the step size to ensure convergence, the speed of convergence and the stability.

The convergence behavior of the algorithm can be given in statistical terms. We now consider the mean value of the weight vector,

$$\begin{aligned}
 E(\hat{\mathbf{w}}_{k+1}) &= E(\hat{\mathbf{w}}_k + \Delta \cdot \mathbf{v}_k \cdot (I_k - \mathbf{v}_k^H \hat{\mathbf{w}}_k)) \\
 &= E(\hat{\mathbf{w}}_k - \Delta \mathbf{v}_k \mathbf{v}_k^H \hat{\mathbf{w}}_k + \Delta \mathbf{v}_k I_k) \\
 &= (\Xi_{N \times N} - \Delta \mathbf{R}_{\mathbf{v}}) \hat{\mathbf{w}}_k + \Delta E(\mathbf{v}_k I_k)
 \end{aligned} \tag{3.13}$$

where  $\Xi_{N \times N}$  denotes the identity matrix. By orthogonal transformation,  $\mathbf{R}_{\mathbf{v}}$  can be diagonalized, i.e.

$$\mathbf{R}_{\mathbf{v}} = \mathbf{Q} \mathbf{D}_{\mathbf{v}} \mathbf{Q}^H, \quad \mathbf{D}_{\mathbf{v}} = \text{diag}(\lambda_1, \dots, \lambda_N), \tag{3.14}$$

where  $\mathbf{Q}$  is a  $N \times N$  orthogonal matrix. Denoting  $\tilde{\mathbf{w}}_k = \mathbf{Q}^H \hat{\mathbf{w}}_k$ , (3.13) can be rewritten

$$E(\tilde{\mathbf{w}}_{k+1}) = (\Xi_{N \times N} - \Delta \mathbf{D}_{\mathbf{v}}) \tilde{\mathbf{w}}_k + \Delta E(\mathbf{Q}^H \mathbf{v}_k I_k) \tag{3.15}$$

Note that (3.15) is a set of  $N$  decoupled first-order difference equations. Considering the  $i$ -

th equation, the convergence of the  $i$ -th subspace weight vector can be shown to be proportional to

$$(1 - \Delta \cdot \lambda_i)^k . \quad (3.16)$$

Exponential convergence is ensured for all the subspace weight vectors for  $i = 1, 2, \dots, N$ , provided that

$$|1 - \Delta \cdot \lambda_i| < 1, \text{ or } 0.0 < \Delta < \frac{2.0}{\lambda_i} . \quad (3.17)$$

This implies that the convergence speed of LMS algorithm is determined by the subspace weight vector associated with the smallest eigenvalue  $\lambda_{min}$ . If we pick a stepsize  $\Delta = 1/\lambda_{max}$ , it is given by from (3.16)

$$(1 - \lambda_{min}/\lambda_{max})^k . \quad (3.18)$$

Figure 3-12 and Figure 3-13 shows the sorted distribution of eigenvalues of  $\mathbf{R}_v$  from smallest to largest, for two choices of filter lengths  $(N_f, N_b) = (40, 40)$  and  $(30, 10)$ . They indicate that the ratio of the largest to the lowest eigenvalue is  $O(10^8)$ . Thus, we expect that the LMS algorithm would converge extremely slowly. For example, even after  $k = 10^7$  iterations, the expected value is still significant

$$(1 - 10^{-8})^{10^7} = 0.9048 .$$

This implies that it would take more than  $10^7$  training symbols to converge to the optimal DFE filter coefficients with the use of the LMS algorithm.

For the simulation of training of DFE coefficients using the LMS algorithm, we use the stepsize of 0.01 for  $(N_f, N_b) = (40, 40)$ . The stepsize chosen is a little smaller than  $\frac{1}{\text{trace}\mathbf{R}_v} = \frac{1}{80.04} = 0.0125$  and thus satisfies the convergence requirement of (3.17). In Section 3.2.2, the output SNR for this setting was obtained to be 23.84 dB ( $J_{min} = 0.0052$ ). Figure 3-14 shows the convergence speed of LMS training algorithm

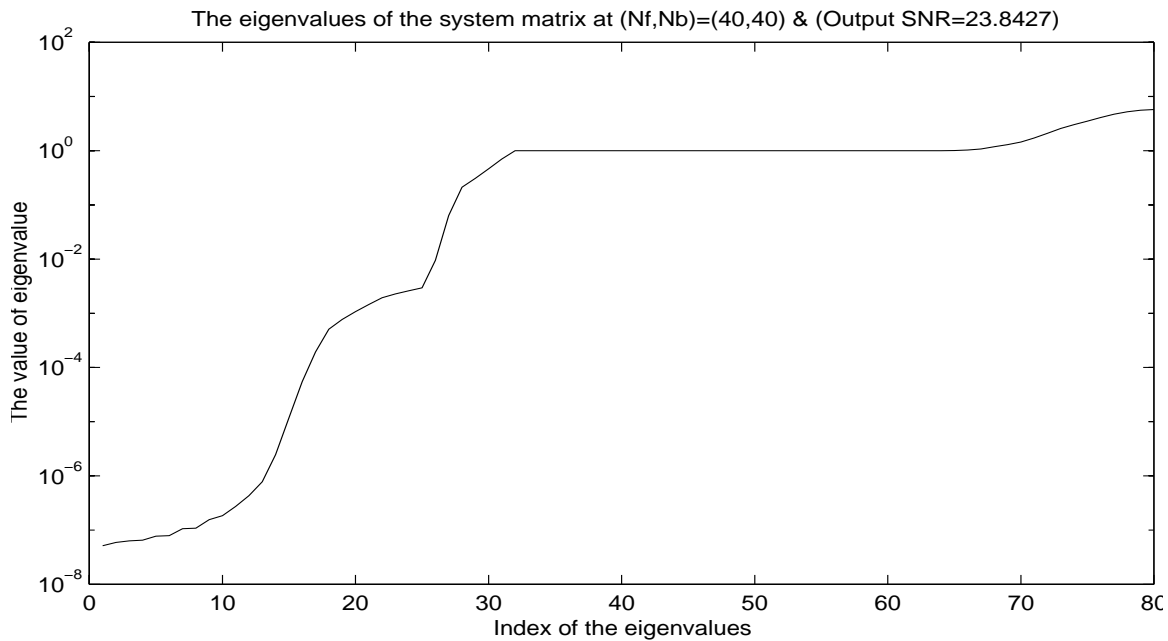
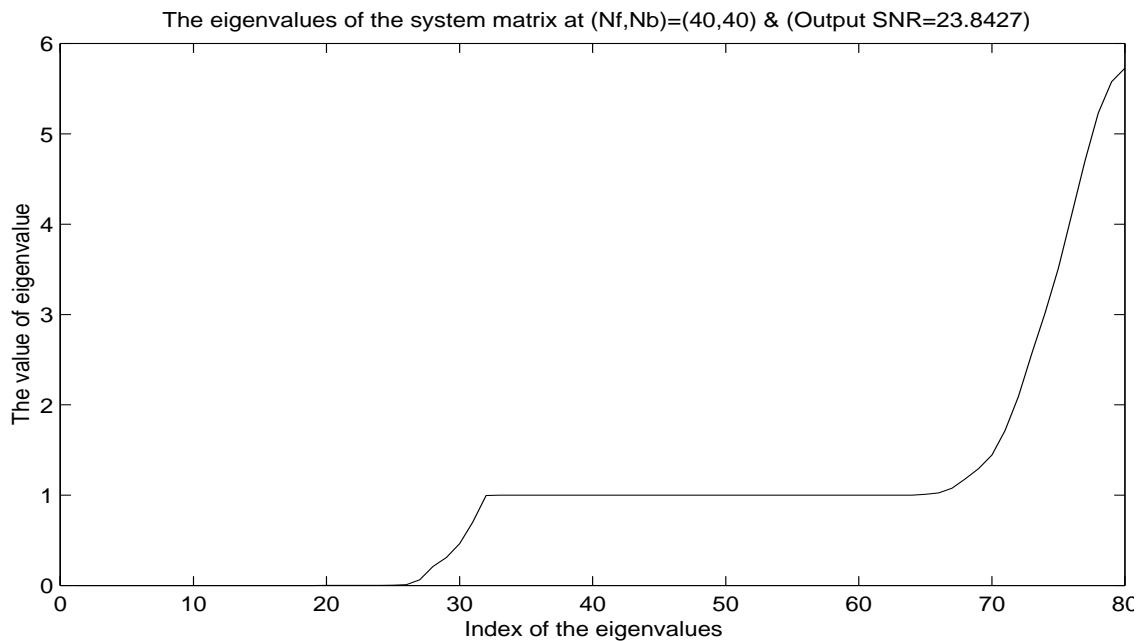


Figure 3-12 The eigenvalues of the system matrix for  $(N_f, N_b) = (40, 40)$ . Top figure shows the eigenvalues in linear scale and the bottom figure shows them in the log-scale.

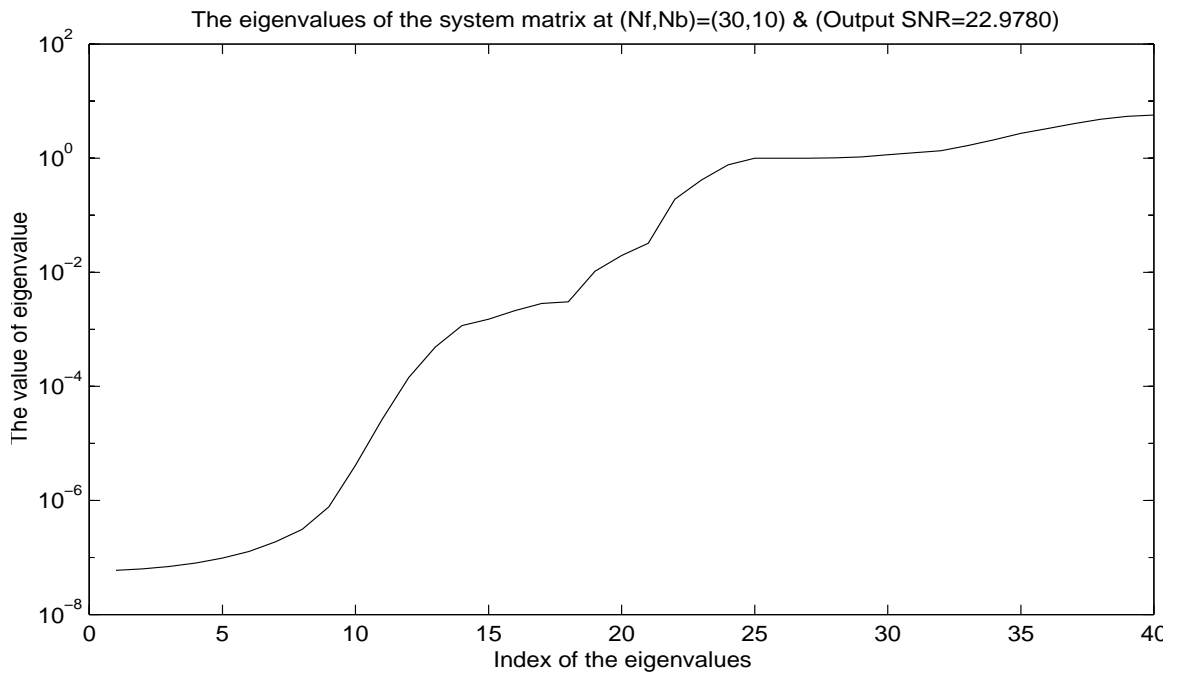
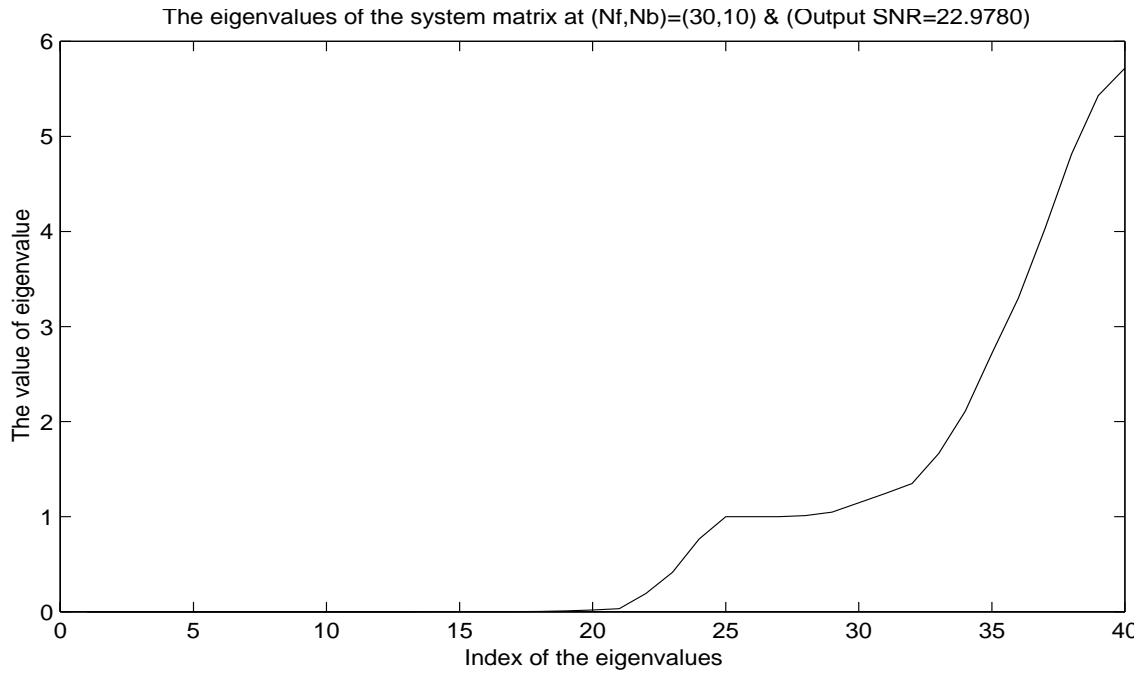


Figure 3-13 The eigenvalues of the system matrix for  $(N_f, N_b) = (30, 10)$ . Top figure shows the eigenvalues in linear scale and the bottom figure shows them in the log-scale.

using 5000 known 4-QAM symbols. It indicates that the average square error is still 0.0534 after 5000 iterations, where the last 100 squared errors are averaged. It can be concluded from the simulation results that LMS algorithm is not suitable to be used in training of DFE filter coefficients for channels which contain deep in-band null(s).

### 3.3.2 RLS training of DFE filters

The recursive least squares (RLS) algorithm may be considered to obtain rapid convergence. The convergence speed of RLS does not depend on the eigenvalue spread of the system. We have tried the standard RLS algorithm provided in Proakis [65] (or refer to Chapter 4 of this dissertation) to train the equalizer, where we picked the forgetting factor  $\beta$  of 0.99 and initial diagonal matrix of gain 0.1. Figure 3-15 shows that the average square error has been lowered as much as to 0.01 (20 dB output SNR) only after training with a few hundred 4-QAM symbols.

The standard RLS algorithm is not a regularized algorithm, and thus may incur numerical instabilities in presence of ill-conditioned system matrix. As indicated in Figure 3-13 the eigenvalue spread of the system matrix is enormous. From the simulation we notice that the feedforward filter trained by the standard RLS algorithm sometimes become unstable--the energy of the feedforward filter diverges. To prevent this, we have also tested a regularized RLS algorithm. The simplest form of regularized RLS [42] has been selected, i.e.,

$$\mathbf{w}_{k+1} = \hat{\mathbf{R}}_{k+1}^{-1} \mathbf{c}_{k+1}, \quad (3.19)$$

where

- $\hat{\mathbf{R}}_{k+1} = \beta \hat{\mathbf{R}}_k + (1 - \beta) \mathbf{R}^o + \mathbf{v}_k \mathbf{v}_k^*$ ,
- $\mathbf{c}_{k+1} = \beta \mathbf{c}_k + (1 - \beta) \mathbf{c}_k^o + I_k \mathbf{v}_k^*$ ,

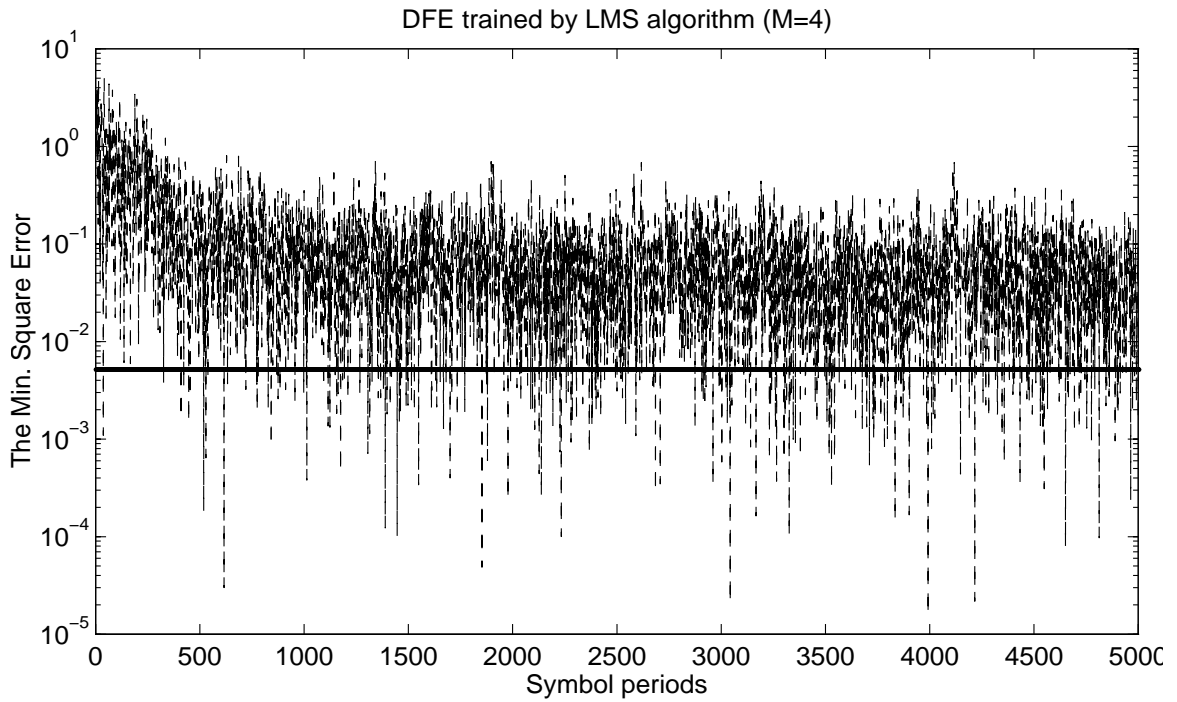
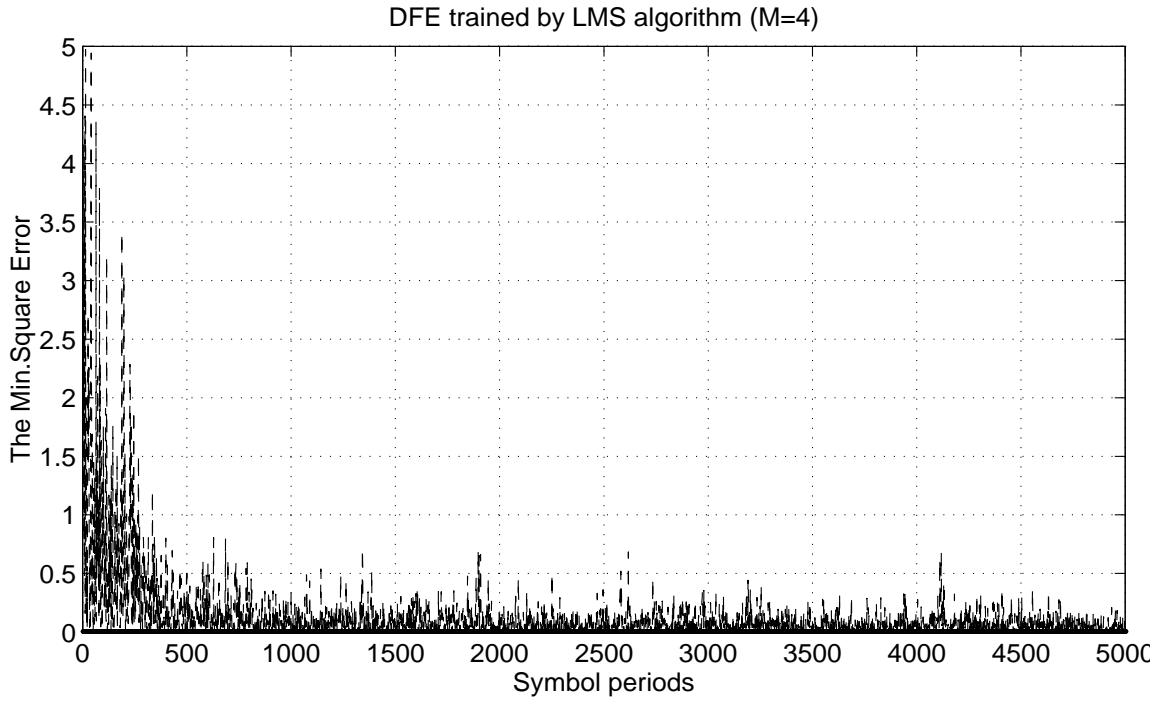


Figure 3-14 The LMS training of the fractionally-spaced DFE filter coefficients.

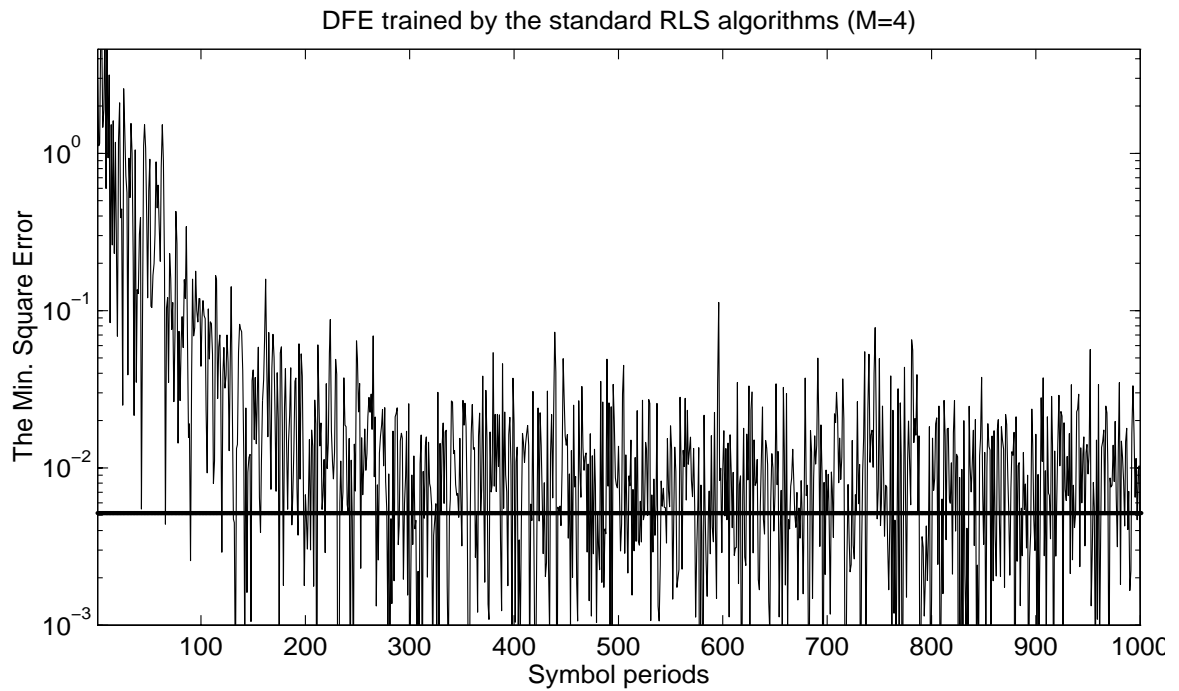
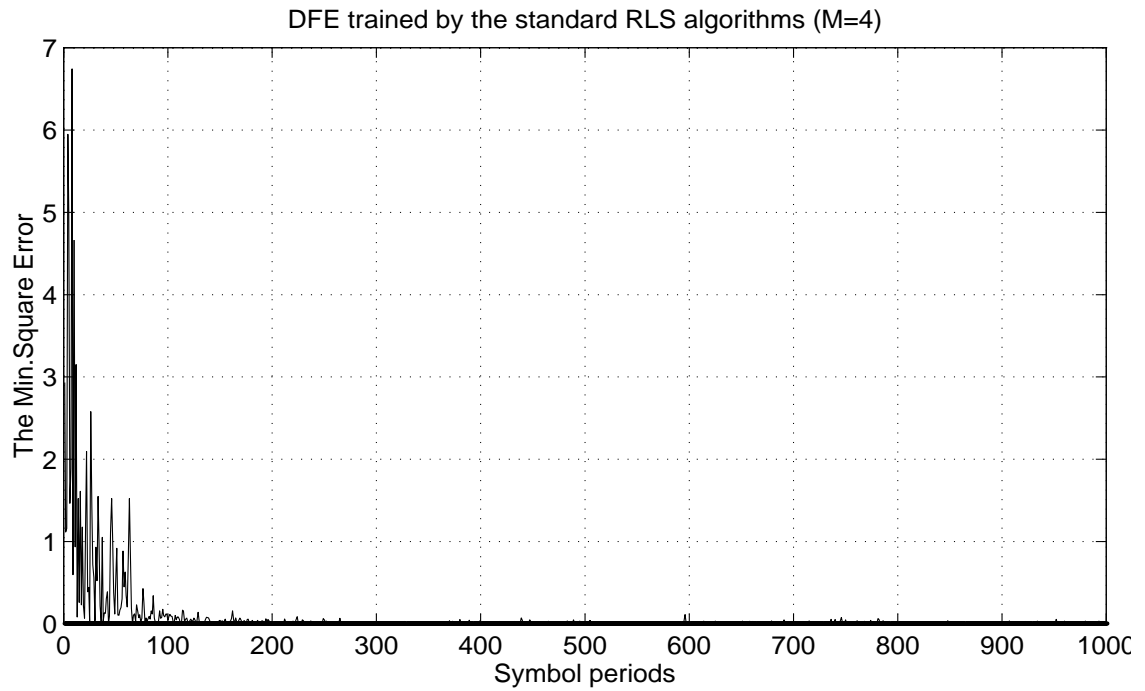


Figure 3-15 The standard RLS training of the fractionally-spaced DFE filter coefficients.

- $\mathbf{c}_k^o = \mathbf{R}^o \mathbf{w}_k$ , and
- $\mathbf{R}^o = \kappa \mathbf{\Xi}_{N \times N}$ ,  $\kappa$  is a small positive value.

Note that smallest eigenvalue of the correlation matrix  $\mathbf{R}$  is lower bounded to be greater than or equal to  $\kappa$ . Figure 3-16 is the simulation result of the regularized RLS simulation results with  $\beta=0.99$  and  $\kappa=0.01$ . The MSE results are similar to the standard RLS, but this result is obtained without the possibility of an unstable feedforward filter.

### 3.4 Concluding Remarks

We have compared different equalizers for a set of telephone channels. For channels with no deep null in folded spectrum, we expect no significant performance degradation from the ideal AWGN results and no significant difference among different forms of equalizations. For instance, if the 2400 sps baud rate would have been chosen, the detection performance of MMSE-LE performance would also be acceptable. On the other hand, as the baud rate is increased, the folded spectrum starts to contain nulls at the band edges and thus more sophisticated equalizer is needed to maintain a satisfactory detection performance.

We have picked a baseband channel which has about a  $10^{-3}$  null in the folded spectrum to test different equalizers. In Table-I we observe the output SNR difference of 7.7 dB between LE and DFE. We also compared the symbol error rates of DFE, correct decision feedback DFE, and TH-precoder in section 3.2.4. We note that the performance of the TH-precoder is very close to the correct decision feedback DFE. We also note that SNR penalty of the correct decision feedback DFE is about 4.0 dB, which is very close to the difference of input SNR and output SNR calculated in section 3.2.1. In addition, DFE and correct feed back DFE curves shows about 2.0 dB difference.

Equalizer training is also very difficult for the channel with deep in-band nulls. For the channel chosen to be simulated, the system matrix has a large eigenvalue spread and thus the use of LMS training is almost impractical due to slow convergence. RLS algorithm can be used instead at the cost of increased computational complexity. In general, these

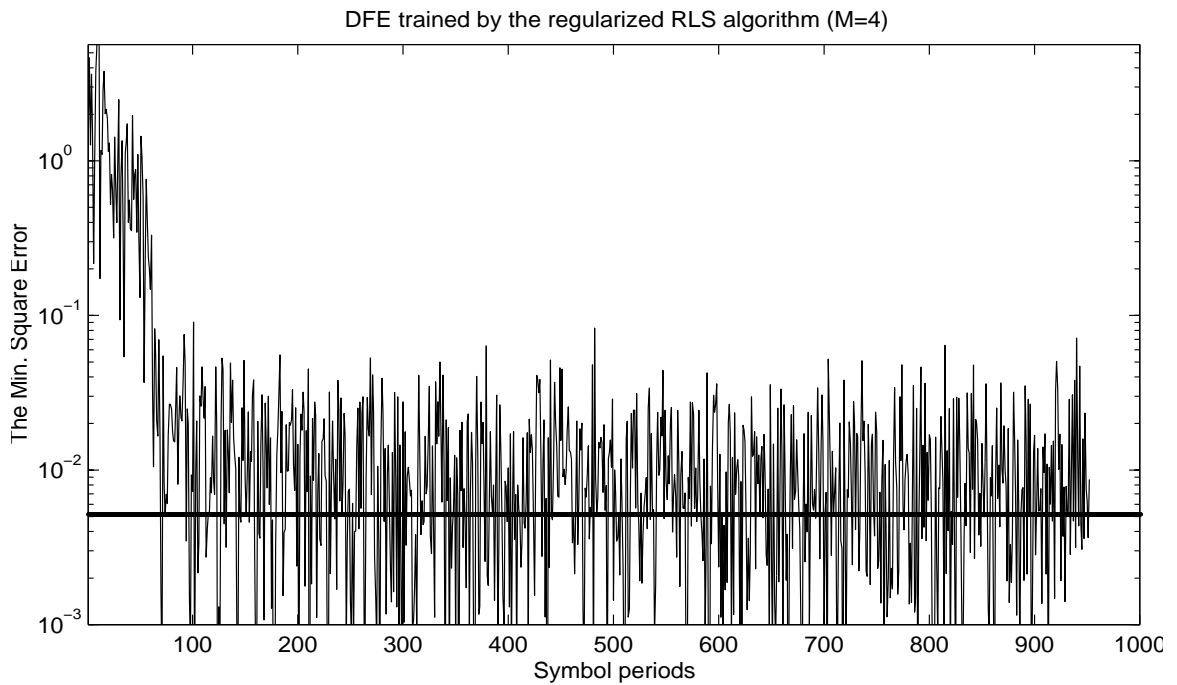
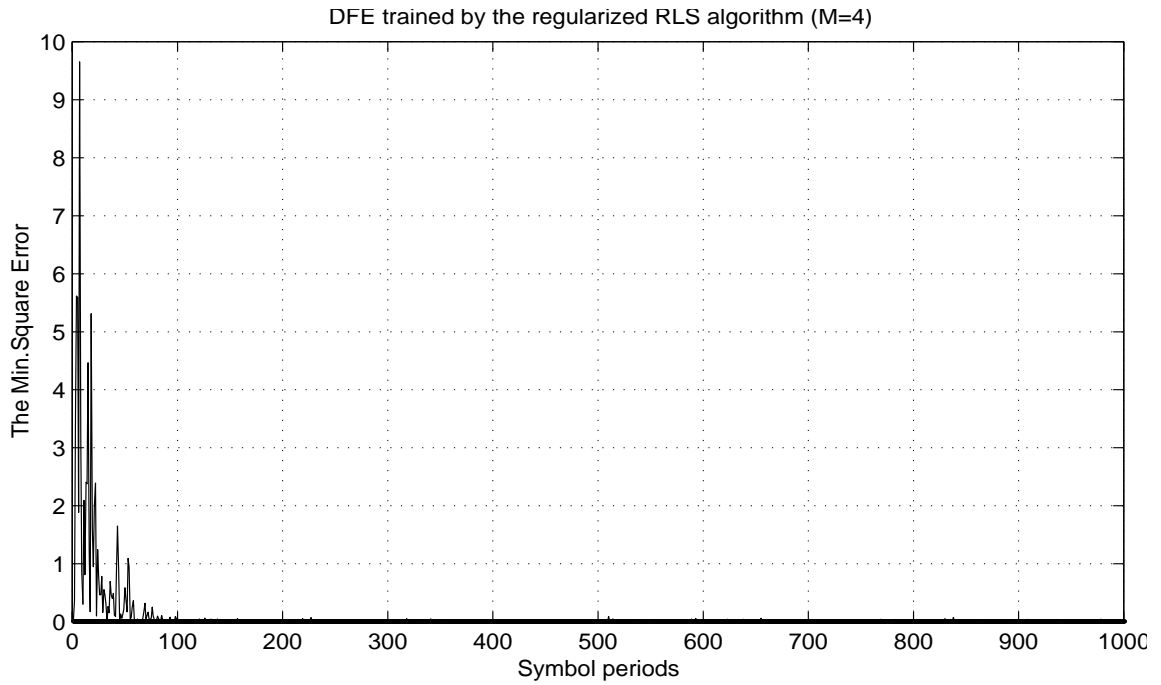


Figure 3-16 The regularized RLS training of the fractionally-spaced DFE filter coefficients.

standard adaptation techniques have been successfully applied to the telephone modem systems; some of this is of use in mobile radio applications as well, adopted to track the time-varying channel. However, as the simulations in Chapter 5 will show, these standard adaptive algorithms have shown limited capability to track the fast time-varying channel we are considering in the dissertation. Thus, further development of an adaptive transceiver scheme was required, as will be discussed in the following Chapters.

## Chapter 4

# Feedforward Channel Estimation and Tracking

In Chapter 2, we showed how fast the channel impulse response (CIR) may vary over time due to the possibility of the mobile terminal in a fast moving vehicle. From (2.10), we note that the fading rate of the channel is directly proportional to the speed of the mobile and also to the carrier frequency. This implies that the fading rate of 100 Hz for 900 MHz carrier frequency will become doubled to 200 Hz for the signal transmission with 1.8 GHz carrier frequency. Thus, in out-door mobile communications, we need faster channel estimation techniques to accommodate the high mobility of the terminal. In this chapter, we discuss the general framework of the channel estimation scheme we propose in this dissertation as well as some of the novel channel estimators developed. The channel impulse response estimation techniques developed in this chapter form the essential part of the detection receivers discussed in the upcoming chapters such as diversity combining decision feedback equalizer (Chapter 5), as well as the sequential detection (Chapter 7) and joint decoding receivers (Chapter 8) using the maximum likelihood sequence criterion.

## **4.1 Why Not Symbol-By-Symbol Recursive Adaptation?**

The standard symbol-by-symbol adaptive algorithms such as least mean squares (LMS) or recursive least squares (RLS) algorithms that were introduced in Chapter 3 are the classical, standard techniques in the area of equalizer training as well as channel identification. These algorithms can be applied to adaptive update of equalizer coefficient or to directly estimate the channel response.

### **4.1.1 Recursive adaptation of DFE filters using LMS and RLS**

We have already investigated this subject when we use LMS and RLS to train the DFE filter coefficients in Chapter 3. Recalling the results we had in chapter 3: LMS and RLS were applied to find out the decision feedback equalizer taps in the training mode such that known symbol sequences were transmitted over the channel. The LMS algorithm took thousands of symbols, vs. a couple hundreds symbols for RLS before it converges. The channel was a non-time varying channel. Why did it take so many symbols to converge? It was because the channel contains deep in-band nulls (two deep in-band nulls along the band edges for the worst case) in the folded spectrum. There was a large eigenvalue spread in the system matrix that actually determines the tracking speed of LMS algorithm and causes a severe instability problem in RLS algorithm. In the case of severe multipath delay spread the mobile channel would also contain a deep null (or possible many nulls) in the folded spectrum. In addition, a training sequence length of thousands or even hundreds cannot be tolerable for the spectrum scarce wireless environment. Therefore, the use of the LMS and the RLS adaptation of DFE filter coefficients is not recommended for the fast time-varying channel we are considering here.

## 4.1.2 Recursive channel estimation using LMS and RLS

Training of the DFE equalizer taps using the LMS or RLS algorithms is an indirect way of channel estimation. In fact, an improved tracking performance could be obtained if these algorithms are applied directly to track the channel parameters. That is, the LMS or RLS algorithms can be applied to estimate the channel impulse response, instead of the equalizer taps. Once the channel estimates are available, the equalizer coefficients can be obtained from the channel estimates. Previous research in this direction include Eleftheriou, et. al. [55] or Shuklar [67] where they compared the performance of RLS and LMS algorithms in tracking the time-varying channel and computed the DFE coefficient from the channel estimate. We apply the fast tracking RLS algorithm to the DC-DFE receiver developed in Chapter 5, where the estimation of the Rayleigh fading channels is performed by the RLS algorithm and the diversity combining DFE coefficients are computed from the channel estimates. Figure 4-1 illustrates a simple model system for the purpose of introducing the algorithms, where we have made following definitions and assumptions:

- For now let's assume a symbol-spaced sampled system for simplicity and let  $k$  be the symbol period epoch index.
- $I(k)$  denotes the input symbols
- $\mathbf{h}(k)$  denotes the unknown time-varying channel vector with size  $N_h$
- $\mathbf{w}(k)$  denotes the equalizer tap vector, that can be computed from the channel estimate vector  $\mathbf{h}(k)$ .
- $x(k)$  denotes the received signal
- The symbol ' $\hat{\cdot}$ ' implies it is an estimate.
- The error signal is defined  $\xi(k) = x(k) - \hat{x}(k)$ .

- The input vector is defined  $\mathbf{I}(k) = (I(k) \dots I(k - N_h + 1))^T$  with  $I(k) = 0$  for  $k < 0$ .

Now, we describe the two algorithms, applied to track the time-varying channel vector. First, we start with the LMS update of the channel vector.

### LMS update of the channel vector:

- BEGIN
- Pick the stepsize  $\Delta \in \mathfrak{R}^+$ , a small positive real value<sup>1</sup>.

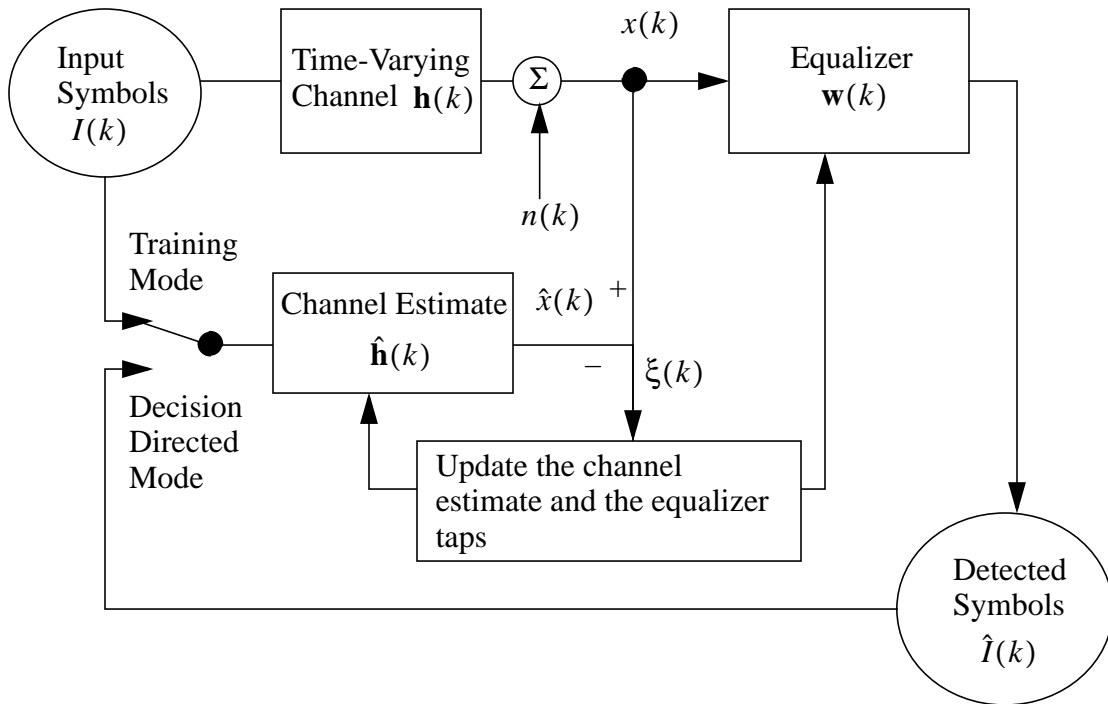


Figure 4-1 The recursive algorithms applied for tracking of time-varying channels

1. See Section 3.3 for selection criterion.

- Initialize  $\hat{\mathbf{h}}(k) = (0 \dots 0)^T$  at  $k = 0$ .
- For  $k = 0, 1, 2, \dots$  until the end of the training sequence, Compute

$$\hat{\mathbf{h}}(k+1) = \hat{\mathbf{h}}(k) + \Delta \cdot \xi(k) \cdot \mathbf{I}(k). \quad (4.1)$$

- END

Now, we describe the RLS update of the channel vector.

### RLS update of the channel vector:

- BEGIN
- Pick a small positive number  $\delta \in \mathfrak{R}^+$ .
- Pick the exponential weighting factor  $\omega \in (0, 1)$ .
- Initialize  $\mathbf{h}(k) = (0 \dots 0)^T$  at  $k = 0$ .
- Initialize  $\mathbf{P}(k) = \delta \cdot \mathbf{e}_{N_h}$ , where  $\mathbf{e}_{N_h}$  is  $(N_h \times N_h)$  identity matrix.
- For  $k = 0, 1, 2, \dots$  until the end of training sequence, compute

$$\mathbf{K} = \frac{\mathbf{P}(k) \cdot \mathbf{I}^*(k)}{\omega + \mathbf{I}^T(k) \cdot \mathbf{P}(k) \cdot \mathbf{I}^*(k)}, \quad (4.2)$$

$$\mathbf{P}(k+1) = \frac{1}{\omega}(\mathbf{P}(k) - \mathbf{K} \cdot \mathbf{I}^T(k) \cdot \mathbf{P}(k)), \text{ and} \quad (4.3)$$

$$\hat{\mathbf{h}}(k+1) = \hat{\mathbf{h}}(k) + \mathbf{K} \cdot \xi(k). \quad (4.4)$$

- END

As discussed in Section 3.3, the convergence speed of the LMS algorithm and the stability condition of the RLS algorithm can be studied when we examine the system

matrix. Following Lemma will help in this regard.

**Lemma 1:** For a well designed training sequence, the system matrix of the channel adaptive algorithm is a weighted identity matrix.

**Proof:** The system matrix for the channel identification problem of Figure 4-1 is  $E\{\mathbf{I}(k)\mathbf{I}^H(k)\}$ . The property of a good training sequence is the pseudo-noise with a white power spectral density such that the matrix becomes a weighted identity matrix, i.e.

$$E\{\mathbf{I}(k)\mathbf{I}^H(k)\} = E\{I^*(k)I(k)\} \cdot \Xi_{N_h}, \quad (4.5)$$

where  $\Xi_N$  is the identity matrix. QED.

Thus, there is no eigenvalue spread of the system matrix. Compare it with the system matrix for the equalizer tap adaptive example of section 3.3.1. The part of the matrix contains the channel correlation matrix which becomes a large eigenvalue spread system whenever a significant null occurs in the folded spectrum of the channel. Eq. (4.5) suggests that the convergence speed of the LMS algorithm will now be much faster once the convergence requirement of Eq. (3.17) is met such that the stepsize is smaller than 2.0. In addition, this implies that for the RLS case, the operation of RLS algorithm will also become much more stable. From this observation, we can conclude.

**Theorem 1:** Recursive adaptation applied directly to the channel estimation problem always converges faster than the same algorithm applied to the equalizer adaptation. **Proof:** follows from Lemma 1.

In addition, this led to the following remark.

**Remark:** The LMS and RLS algorithms have the same channel tracking capability when they are applied to track the time-varying channel directly with a white input sequence.

In fact, there are a few observations in this regards reported in the literature that the

two algorithms would not make any significant performance difference in terms of tracking speed when applied to a fast time-varying channel. If one fails at a certain point of tracking speed, the other follows. We have performed some simulations to verify the claims. Figure 4-2 is the channel tracking results of the two algorithms when the fading rate of the channel was 200 Hz. The channel was initially known from the start and both algorithms are in training mode. The results show that both algorithms are capable of tracking the fast fading channel in the training mode. There were four fading taps.

However, as we have also found out from our own simulation results (to be discussed in Chapter 5) the symbol-by-symbol recursive algorithm could still not meet the

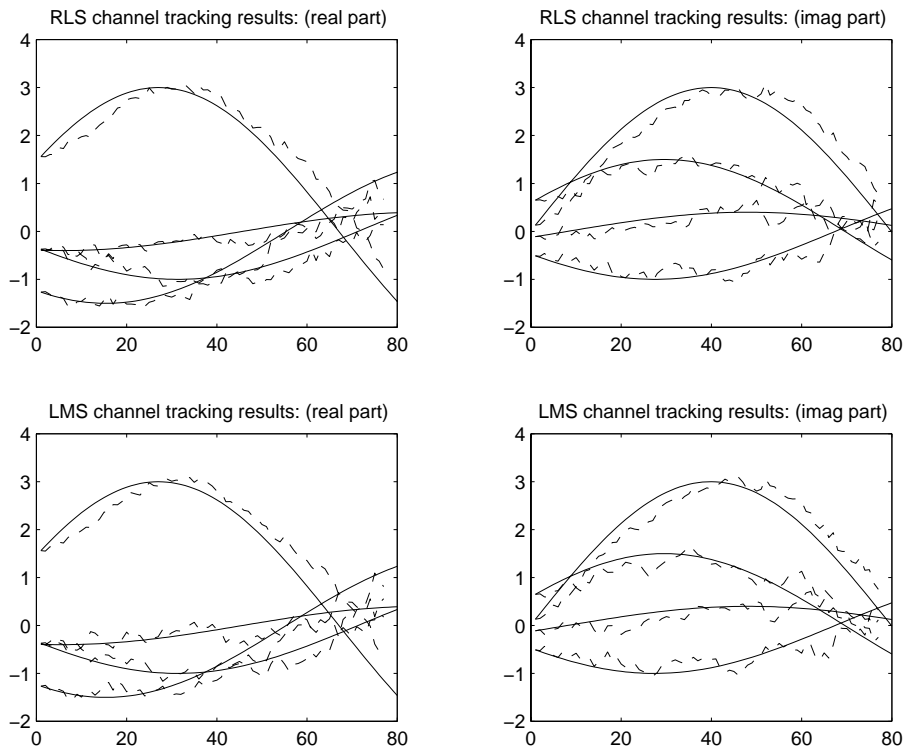


Figure 4-2 The RLS and LMS tracking of fast time-varying channel

tracking speed requirement of the digital cellular system even at the fading rate of 100 Hz.

The reasons can be found from the following statements:

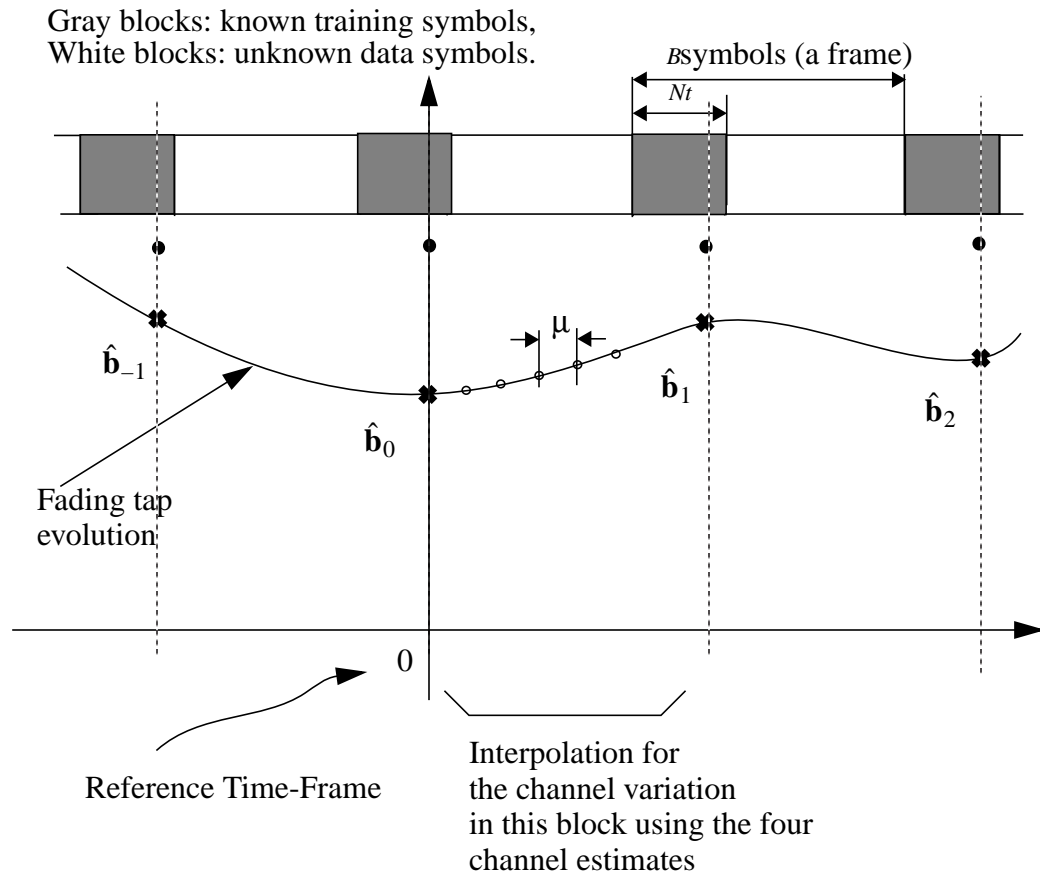
- Error propagation in the decision directed mode: The algorithm needs to be in a decision directed mode in order to increase the throughput of the link in the realistic scenario of operation. There will be a possibility of decision error propagation, especially after a deep fade
- Lag in the channel estimate due to decision delay: The channel is updated when a new decision symbol becomes available. The received signal must pass through the transversal equalizer filters to reach the decision device. Thus, there is always a significant decision delay, and this delay must be a significantly large whenever the ISI of the channel is severe since the length of the filter has to be long enough to suppress the ISI.

In order to avoid the specified problems of the recursive adaptation, feedforward channel estimation techniques [53][54][57][58][59][8][71] have been proposed in which known training symbols inserted into the stream of data are used for the channel estimation and the decided symbols are not used in channel estimation. Following Section will discuss the proposed feedforward channel estimation techniques.

## **4.2 The Structure of Feedforward Channel Estimation**

We use the term *feedforward* to imply that we do not make use of the detected symbols to estimate the channel or update the channel estimates. The channel estimation is solely based on the knowledge forwarded from the transmitter, the known training symbols periodically sent to sound the channel. The continuous transmitted data frames are structured as illustrated in Figure 4-3.

The feedforward channel estimation method to be described in this chapter involves two steps: The first step is to estimate the fractionally-spaced channel impulse response by



- ✱ Channel estimates from the periodic training.  
Interpolation on a  $Q (= 4)$  set of channel estimates
- Computes the interpolated estimates of the channel at every  $\mu$  symbol epoch.

Figure 4-3 Channel estimation and interpolation tracking on a TDMA frame.

observing the training segment of the received signal. The second is to obtain a finer time-scale channel estimate for the channel responses in-between any two training segments, by interpolating a set of obtained channel estimates.

The first step starts with an important assumption. That is, during the reception of training segments, the channel parameters are assumed to be fixed (time-invariant). Without

this assumption we run into the problem of an infinite number of solutions by having more unknowns than the number of observation equations. This is called a “*snap-shot*” channel estimation. Specifically, the fractionally-spaced impulse response of the channel assumed to be fixed during the observation period. Solving the set of observation equations provides the estimate of the channel impulse response, which will be discussed in more detail in Section 4.3.

The second step involves tracking the channel variation during the data segment in the middle block as shown in Figure 4-3, by interpolating a set of the snap-shot channel impulse response (CIR) estimates. Specifically, two parameters are required to be defined for interpolation. One parameter is the frequency of periodic channel estimation, i.e., the length of a frame  $B$ , where a frame consists of a training block of length  $N_t$  and a data block of length  $N_d$ , i.e.,  $B = N_t + N_d$ . According to the sampling theorem,  $B$  should at most satisfy  $B \leq 1/(2f_{dm}T)$ . For instance, if  $f_{dm}T = 0.0042$ , the shortest expected period of a fading tap is about 240 symbols. Thus,  $B$  should be less than 120 symbols. The other parameter is  $Q$ , the number of channel estimates used in each interpolation. In this paper, only  $Q = 4$  will be considered. Thus, an interpolation over 4 consecutive channel estimates, 2 past and 2 future, is performed to obtain an interpolate of  $\mathbf{b}$  at an epoch during the middle data segment. The maximum interpolation delay for  $Q = 4$  is 3  $B$  symbol periods. We use a sinc function ( $\sin x/x$ ) interpolator for the simulation results for DFE receivers in chapter 5 or a square-root raised cosine interpolator for simulation results for chapter 7 and chapter 8. For an example of interpolation using the sinc function; first define

$$\text{sinc}\left(\frac{t}{T_{est}}\right) = \frac{\sin(\pi t/T_{est})}{\pi t/T_{est}}, \quad (4.6)$$

where  $T_{est} = T_B \cdot B$  such that it is the sampling period of the estimated CIR samples. Then, the interpolated channel vector can be represented in the following equation for any

of the channel estimate vector for  $t = 0, \frac{T_B}{2}, T_B, \frac{3T_B}{2}, \dots$  of the reference time-frame indicated in Figure 4-3,

$$\mathbf{b}(t) = \sum_{i=-1}^2 \mathbf{b}_i \operatorname{sinc}\left(\frac{t - iT_{est}}{T_{est}}\right). \quad (4.7)$$

At the expense of the interpolation delay, channel tracking technique by interpolation resolves a few problems inherent in the recursive symbol-by-symbol adaptation techniques. First, it uses only the channel estimate from the known training symbols. Thus there is no decision error propagation problem. Second, there will be no more decision delay problem which was the limiting factor of recursive channel tracking techniques that must rely on the detected symbols to update the channel states.

The decision delay in the case of diversity combining decision feedback equalizer in chapter 5 is the addition of all the anticausal delays in the receiver, i.e., the overall length of the anticausal matched filter and anticausal feedforward filter, which will add up to quite significant number. This advantage of having a channel estimate even during the decision delay, however, has not been fully utilized in the framework of DFE symbol detection schemes in previous research; for example see [10, 20]. In Chapter 5, a new DFE computation algorithm that fully exploits this advantage will be developed.

### 4.3 Parametric Channel Estimation

The use of a bandwidth efficient square-root raised cosine (SRRC) transmit filter  $\mathbf{f}$  increases the effective span of the overall channel impulse response (CIR) perceived at the receiver. For the *flat* fading channel, a receive filter matched to the SRRC filter can be used to recover an isolated source pulse with zero crossing at every  $T$  seconds. In the presence of frequency-selective channel  $\mathbf{b}$ , however, matched filtering with the SRRC filter alone could not provide a Nyquist pulse: The composite pulse,  $\mathbf{f} \otimes \mathbf{b} \otimes \mathbf{f}$ , is no longer a Nyquist

pulse. Thus we need an estimate of the overall channel response for optimum symbol detection.

For the description of the channel estimation procedure in this chapter we focus on a single channel branch Figure 4-4 among the number of diversity channel branches described in Figure 2-12 since each diversity channel branch has the identical structure. Briefly reviewing the notation we have for Figure 4-4:

The  $T_B/2$ -spaced sampled transmit filter  $\mathbf{f}$  is a unit energy  $[31 \times 1]$  column vector which corresponds to a 15 symbol truncation.

- $x(t)$  the received signal at each diversity branch, which is bandlimited with the excess bandwidth of  $(1+\beta)(1/T_B)$ .  $T_B/2$ -spaced sampling is considered, i.e.,

$$x(k) := x(t = kT_B/2), \quad (4.8)$$

where  $k$  denotes the  $T_B/2$ -spaced epoch index.

- $\{I(k)\}$  represents the symbol sequence at the half-symbol sampling rate. That is, it is

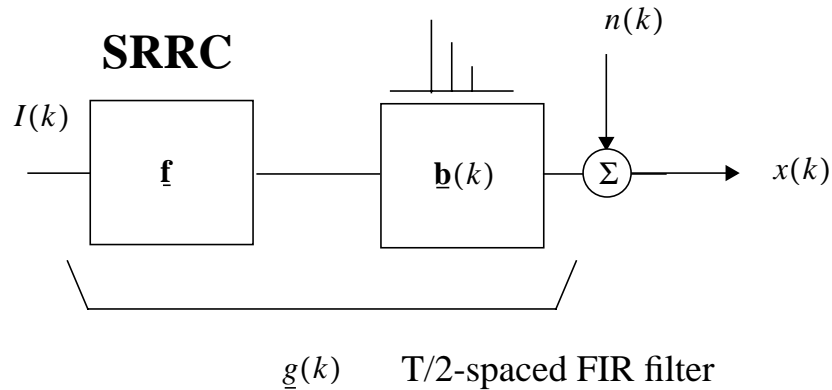


Figure 4-4 Snapshot channel parameter estimation

a zero stuffed sequence such that  $I(k)$  at even  $k$  represents the symbol transmitted at the baud rate and  $I(k)$  at every odd  $k$  is zero-valued.

- The  $T_B/2$ -spaced sampled noise sequence  $\{n(k)\}$  is assumed to be complex-valued additive white Gaussian with zero mean and variance  $\sigma_n^2$ .
- $\mathbf{b}(k) = [b_0(k) \dots b_{(N_R-1)}(k)]^T$ , represents the Rayleigh fading time-varying impulse response of the  $l$ -th channel, where  $N_R$  is the number of the time-varying channel taps ( $N_R = 3$  in this dissertation).
- Each  $T_B/2$ -spaced overall channel impulse response  $\mathbf{h}(k)$  is defined as  $\mathbf{h}_l(k) := \underline{f} \otimes \mathbf{b}_l(k)$ , where  $\otimes$  denotes the convolution operation.

### 4.3.1 Construction of channel estimation equation

The following two assumptions were made for the construction of the channel estimation equation, so that a tractable solution could be obtained.

- **Assumption 1:** The channel vector is truncated to be  $N_c$  symbol periods:

To reduce the length of the training sequence required, a truncated channel is used in the channel estimation equation. That is, the estimation accuracy is traded off for a shorter training since longer CIR requires longer training sequences. We represent the truncated overall CIR with a  $[2N_c \times 1]$  vector  $\mathbf{h}$ , where  $N_c < 15$ .

- **Assumption 2:** The channel is assumed to be a fixed vector, non-time varying during the training observation period.

We make the snap-shot assumption that during the observation interval,  $mT$ , the channel is effectively fixed. Consequently, we drop the epoch index of the channel vector, denoting  $\mathbf{b}(k)$  as  $\mathbf{b}$ . Similarly, the cascade channel  $\mathbf{h}(k) = \underline{\mathbf{f}} \otimes \mathbf{b}(k)$  during  $k = 0, 1, \dots, 2m - 1$

For the half symbol-spaced system the received signal over an observation period is

described by,

$$x(k) \cong \sum_{i=0}^{2N_c-1} h_i I(k-i) + n(k), \quad (4.9)$$

where  $\{I(k)\}$  is the zero stuffed input symbol sequence, i.e., it includes known training symbols for even  $k$  and 0.0 for odd  $k$ . That is,  $k$  is the half symbol-spaced epoch index, the zero stuffed input sequence  $\{I(k)\}$  represents the input symbols at the baud rate.

Note that there are  $2N_c$  unknown parameters in (4.9). Previous channel estimation methods (e.g. see [9,10,20] for double sampling and [30, 33] for  $T$ -spaced sampling) estimate these parameters without exploiting the fact that the overall CIR is a convolution of the transmit shaping filter and the time-varying channel filter. In fact, the impulse response of the shaping filter is *a priori* known to the receiver and thus the true unknown parameters are only the time-varying channel filter taps.

### **Key equation:**

Using the *a priori* knowledge of the transmit filter, the number of unknown parameters can be reduced. The truncated CIR  $\mathbf{h}$ , the convolution of a truncated transmit filter and the channel filter, can be represented by  $\mathbf{h} = \mathbf{F} \mathbf{b}$ , where  $\mathbf{F}$  is a  $[2N_c \times N_R]$  matrix whose elements  $F_{(i,j)}$  can be determined for the SRRC filter (an example of constructing the matrix is given at the end of the section). Then, (4.9) can be rewritten as

$$x(k) \cong \sum_{i=0}^{2N_c-1} \sum_{j=0}^{N_R-1} F_{(i,j)} b_j I(k-i) + n(k). \quad (4.10)$$

Note that the number of unknown parameters in (4.10) is now  $N_R$ . This brings about a number of benefits. First, with fewer unknown parameters, a shorter observation window is needed. Second, with a shorter observation period the snap-shot channel estimation performs robustly in fast fading. Since a snap-shot channel estimation problem relies on a fixed channel during the observation period, a long observation may become counterproductive [10, 20]. Finally, the estimates will be more accurate when there are

fewer parameters to be estimated. Having obtained the estimates of the channel, the overall channel can be computed from the convolution of the estimate  $\mathbf{b}$  and the SRRC filter.

The training observation vector  $\mathbf{x} = (x(0)x(1) \dots x(2m-1))^T$  is a  $(2m \times 1)$  vector. We can divide the observation vector into two  $(m \times 1)$  vectors, collecting only even elements of  $\mathbf{x}$  into even-observation vector and the rest to the odd-one. Each decomposed observation vector poses a symbol-spaced channel estimation problem of

$$\mathbf{x} = \mathbf{X}\mathbf{F}\mathbf{b} + \mathbf{n}, \quad (4.11)$$

where

- $\mathbf{x} = (x(0)x(2) \dots x(2m-2))^T$  when we refer to the vector of even elements and  $\mathbf{x} = (x(1)x(3) \dots x(2m-1))^T$  when we refer to the vector of odd elements,
- $\mathbf{X}$  is a  $[m \times N_c]$  Toeplitz matrix whose elements are determined from the training sequence of length  $N_t$  such that

$$\mathbf{X} = \begin{bmatrix} I(0) & I(-2) & \dots & I(-2(N_c-1)) \\ I(2) & I(0) & \dots & I(-2(N_c-2)) \\ \dots & \dots & \dots & \dots \\ I(2(m-1)) & I(2(m-2)) & \dots & I(2(m-N_c)) \end{bmatrix}, \quad (4.12)$$

- There is a relationship between  $N_t$  the length of training sequence,  $m$  the observation period in symbol-epoch and  $N_c$  the number of channel coefficients, which is

$$m = N_t - N_c + 1. \quad (4.13)$$

- $\mathbf{F}$  is a  $[N_c \times N_R]$  SRRC matrix, an *a priori* SRRC matrix that can be determined for the even and odd parts.
- The  $[m \times 1]$  noise vector  $\mathbf{n}$  is a multivariate Gaussian with a zero mean vector and a covariance matrix of

$$\mathbf{R}_n = \sigma_n^2 \mathbf{e}_m, \quad (4.14)$$

where  $\mathbf{e}_m$  denotes the  $(m \times m)$  identity matrix.

#### 4.3.1.1 Constructing the SRRC matrix $\mathbf{F}$

An example with  $N_c = 6$  and  $N_R = 3$  is sufficient to describe the procedure of obtaining the square root raised cosine filter matrix.  $\mathbf{f}$  denotes the 31 tap square root raised cosine filter, i.e.  $\underline{f} := [f_0 f_1 \dots f_{30}]^T$ , where  $f_{15}$  is the main tap of the SRRC vector. Then, a  $[12 \times 1]$  truncated overall CIR  $\mathbf{h}$  can be described by a matrix and a vector multiplication as  $\mathbf{h} = \mathbf{F} \mathbf{b}$ , where  $\mathbf{F}$  is a  $[2N_c \times N_R]$  Toeplitz matrix which can be described by the first row and the first column. The first row is  $[f_{10} f_9 f_8]^T$  and the first column is  $[f_{10} f_{11} \dots f_{21}]^T$ . Thus,  $\mathbf{F}$  is

$$\mathbf{F} := \begin{bmatrix} f_{10} & f_9 & f_8 \\ f_{11} & f_{10} & f_9 \\ \dots & \dots & \dots \\ f_{21} & f_{20} & f_{19} \end{bmatrix}. \quad (4.15)$$

Finally, a  $N_c \times N_R$  matrix  $\mathbf{F}$  in (4.11) for even  $\mathbf{x}$  is obtained from taking all the even-indexed rows of  $\mathbf{F}$ . Similarly, taking all odd rows is  $\mathbf{F}$  for odd  $\mathbf{x}$ .

## 4.4 Novel Channel Estimators

Based on the new observation equation (4.11), we apply three classical parameter estimation techniques. They are least squares, maximum likelihood and maximum a posteriori estimation. From the two observation equations representing odd and even symbols, two estimators of  $\mathbf{b}$  can be obtained. We will choose the one that yields a smaller theoretical mean square estimation error for a given training sequence. In the derivations of the estimator, the training matrix  $\mathbf{X}$  and the *a priori* matrix  $\mathbf{F}$  are assumed to be fixed both in the contents and in the dimension such that they are not subject of optimization in this section. In addition we only considered cases with  $m \geq N_R$ . Moreover, the inverse matrices

to be derived are assumed to be well defined with an optimal or sub-optimal choice of the training sequence matrix  $\mathbf{X}$ . The optimal training sequences will be discussed in section 4.6.

#### 4.4.1 The Least Squares Estimator

If there is no *a priori* statistical knowledge about the noise and the channel, the LSE of  $\mathbf{b}$  can be considered and computed by

$$\hat{\mathbf{b}}_{LSE} := \arg \min_{\mathbf{b}} |\mathbf{x} - \mathbf{X}\mathbf{F}\mathbf{b}|^2 = (\mathbf{F}^H \mathbf{X}^H \mathbf{X} \mathbf{F})^{-1} (\mathbf{X} \mathbf{F})^H \mathbf{x}, \quad (4.16)$$

where the superscript ' $H$ ' implies the conjugate transpose operation of a matrix and *arg* denotes the argument. This results in the lowest complexity estimator among the three. The  $[N_R \times m]$  matrix  $(\mathbf{F}^H \mathbf{X}^H \mathbf{X} \mathbf{F})^{-1} (\mathbf{X} \mathbf{F})^H$  can be precomputed and stored, and then an estimate can be obtained by simply multiplying it with the observation vector.

#### 4.4.2 The Maximum Likelihood Estimator

The MLE of  $\mathbf{b}$  can be obtained as follows,

$$\hat{\mathbf{b}}_{ML} := \arg \max_{\mathbf{b}} (p(\mathbf{x}|\mathbf{b})) = \arg \max_{\mathbf{b}} [-(\mathbf{x} - \mathbf{X}\mathbf{F}\mathbf{b})^H \mathbf{R}_n^{-1} (\mathbf{x} - \mathbf{X}\mathbf{F}\mathbf{b})], \quad (4.17)$$

where  $\mathbf{R}_n$  is the covariance matrix of the noise. Setting the gradient of the quadratic term equal to zero, we obtain

$$\hat{\mathbf{b}}_{ML} = (\mathbf{F}^H \mathbf{X}^H \mathbf{R}_n^{-1} \mathbf{X} \mathbf{F})^{-1} (\mathbf{X}^H \mathbf{F}^H \mathbf{R}_n^{-1}) \cdot \mathbf{x}. \quad (4.18)$$

Thus, the MLE requires the second order statistics of the noise, such as the noise covariance matrix  $R_n$ . Thus, MLE would perform better than LSE provided that the noise is correlated and that the autocorrelation function of the noise is acquired. In our estimation model of (4.11), however, we have assumed white noise, i.e.,  $\mathbf{R}_n = \sigma_n^2 \mathbf{e}_m$ , and thus the LSE is identical to the MLE. Note that interpreting the  $\mathbf{R}_n^{-1}$  as a weighting matrix, the MLE of  $\mathbf{b}$

can be interpreted as an optimally weighted LSE of  $\mathbf{b}$ . Thus, the MLE also minimizes weighted square residual errors,  $|\mathbf{x} - \mathbf{X}\mathbf{F}\hat{\mathbf{b}}|$ , but not the estimation errors,  $|\hat{\mathbf{b}} - \mathbf{b}|$ .

#### 4.4.3 The Maximum A Posteriori Estimator

An estimator which directly minimizes the mean square estimation errors of  $\mathbf{b}$  requires *a priori* distribution of  $\mathbf{b}$ . The MAP estimator is in this category. In particular, the MAP estimator can be obtained from

$$\hat{\mathbf{b}}_{MAP} := \arg \max_{\mathbf{b}} (p(\mathbf{b}|\mathbf{x})) = \arg \max_{\mathbf{b}} \left( \frac{p(\mathbf{b}, \mathbf{x})}{p(\mathbf{x})} \right). \quad (4.19)$$

In our case, the noise vector is a multivariate Gaussian, and thus the posterior density  $p(\mathbf{b}|\mathbf{x})$  is also a Gaussian distribution where the mode and the mean coincide. Thus, with some algebraic manipulations of the posterior density we can obtain the MAP estimator as

$$\hat{\mathbf{b}}_{MAP} = E\{\mathbf{b}|\mathbf{x}\} = \mathbf{R}_b(\mathbf{F}^H\mathbf{X}^H)(\mathbf{X}\mathbf{F}\mathbf{R}_b\mathbf{F}^H\mathbf{X}^H + \mathbf{R}_n)^{-1}\mathbf{x}, \quad (4.20)$$

where  $\mathbf{R}_b := E\{\mathbf{b}\mathbf{b}^H\}$ . This MAP estimator of  $\mathbf{b}$  amounts to the minimum mean square estimator of  $\mathbf{b}$ .

Note that MAP not only requires  $\mathbf{R}_n$  but also  $\mathbf{R}_b$ . Thus, in practice it can be employed only after enough information about the noise variance and multipath has been obtained. While collecting the information we can employ the LSE. In this dissertation we assume they are estimated. In particular, diagonal elements of the channel correlation matrix  $\mathbf{R}_b$  are the average powers of multipath components such as defined in (2.24) and (2.25). They are assumed to be estimated; off-diagonal elements are all zero valued assuming wide-sense stationary uncorrelated scattering of the multipath components. We consider more practical cases when these assumptions fail in Section 4.7.

## 4.5 The Mean Squares Channel Estimation Errors

It is useful to compare the estimators in terms of their theoretical mean square channel estimation error (MSCEE) performance. We first derive the mean square estimation error matrix for each criterion. Then, a MSCEE is obtained from the *trace* of the mean square estimation error matrix. These theoretical results will be compared with simulation MSCEEs in section 4.7.

The MLE (or LSE with similar steps) can easily be verified to be an unbiased estimator by taking the *expectation* of the following equation which is obtained by substituting (4.11) into (4.18), i.e.,

$$\hat{\mathbf{b}}_{ML} = \mathbf{b} + (\mathbf{F}^H \mathbf{X}^H \mathbf{R}_n^{-1} \mathbf{X} \mathbf{F})^{-1} (\mathbf{F}^H \mathbf{X}^H \mathbf{R}_n^{-1}) \mathbf{n}, \quad (4.21)$$

and by using  $E\{\mathbf{n}\} = \mathbf{0}_m$ , where  $\mathbf{0}_m$  defines a  $[m \times 1]$  vector of element of zeros. Thus, for the MLE and the LSE the error covariance matrix of the estimator is equal to the mean square channel estimation error matrix. The mean square estimation error matrix of the MLE is

$$\Theta_{ML} := E\{(\hat{\mathbf{b}}_{ML} - E(\hat{\mathbf{b}}_{ML}))((\hat{\mathbf{b}}_{ML}' - E(\hat{\mathbf{b}}_{ML})))^H\} = (\mathbf{F}^H \mathbf{X}^H \mathbf{R}_n^{-1} \mathbf{X} \mathbf{F})^{-1}. \quad (4.22)$$

This error covariance matrix of (4.22) meets the Cramer-Rao lower bound (unbiased class). Thus,  $\hat{\mathbf{b}}_{ML}$  is the best linear unbiased estimator for the estimation problem of (4.11).

In our problem, however,  $\mathbf{R}_n = \sigma_n^2 \mathbf{e}_m$  is assumed, thus LSE and MLE produce identical results, i.e.,

$$\Theta_{ML} = \sigma_n^2 (\mathbf{F}^H \mathbf{X}^H \mathbf{X} \mathbf{F})^{-1} = \Theta_{LSE}, \quad (4.23)$$

and  $\hat{\mathbf{b}}_{ML} = \hat{\mathbf{b}}_{LSE}$ .

**Theorem 3:** The maximum likelihood estimator achieves the Cramer-Rao lower bound for

unbiased estimators.

**Proof:** Stating the Cramer-Rao lower bound for unbiased estimators as,

$$\text{Cov}(\hat{\mathbf{b}}) \geq \mathbf{M}^{-1}, \quad (4.24)$$

where  $M$  is the Fisher information matrix defined as

$$M := E \left[ \left( \frac{\partial}{\partial \mathbf{b}} \ln(p(\mathbf{x}|\mathbf{b})) \right) \left( \frac{\partial}{\partial \mathbf{b}} \ln(p(\mathbf{x}|\mathbf{b})) \right)^H \right]. \quad (4.25)$$

We will prove the equality, i.e.,  $\text{Cov}(\hat{\mathbf{b}}_{ML}) = M^{-1}$ .

Note,

$$\frac{\partial}{\partial \mathbf{b}} \ln(p(\mathbf{x}|\mathbf{b})) = -\frac{1}{2}(-2(\mathbf{X}\mathbf{F})^H \mathbf{R}_n^{-1} \mathbf{x} + 2((\mathbf{X}\mathbf{F})^H \mathbf{R}_n^{-1} (\mathbf{X}\mathbf{F})) \mathbf{b}), \quad (4.26)$$

then,

$$\mathbf{M} = [(\mathbf{X}\mathbf{F})^H \mathbf{R}_n^{-1} (\mathbf{X}\mathbf{F})] \text{Cov}(\hat{\mathbf{b}}_{ML}) [(\mathbf{X}\mathbf{F})^H \mathbf{R}_n^{-1} (\mathbf{X}\mathbf{F})] = [(\mathbf{X}\mathbf{F})^H \mathbf{R}_n^{-1} (\mathbf{X}\mathbf{F})], \quad (4.27)$$

since we already know  $\text{Cov}(\hat{\mathbf{b}}_{ML}) = [(\mathbf{X}\mathbf{F})^H \mathbf{R}_n^{-1} (\mathbf{X}\mathbf{F})]^{-1}$  from (4.22). Thus the equality in (4.24) holds.

MAP estimator achieves the minimum mean square error. Since the MAP estimator is a biased estimator, we directly obtain the mean square error matrix using  $\hat{\mathbf{b}}_{MAP} = \mathbf{B}^+ \mathbf{x}$ , where  $\mathbf{B}^+ := \mathbf{R}_b (\mathbf{F}^H \mathbf{X}^H) (\mathbf{X} \mathbf{F} \mathbf{R}_b \mathbf{F}^H \mathbf{X}^H + \mathbf{R}_n)^{-1}$ , i.e.,

$$\begin{aligned} \Theta_{MAP} &:= E\{(\hat{\mathbf{b}}_{MAP} - \mathbf{b})(\hat{\mathbf{b}}_{MAP} - \mathbf{b})^H\} \\ &= \mathbf{B}^+ E\{\mathbf{x}\mathbf{x}^H\} \mathbf{B}^{+H} - E\{\mathbf{b}\mathbf{x}^H\} \mathbf{B}^{+H} - \mathbf{B}^+ E\{\mathbf{x}\mathbf{b}^H\} + E\{\mathbf{b}\mathbf{b}^H\}. \end{aligned} \quad (4.28)$$

Then, we find

$$\Theta_{MAP} = E\{\mathbf{b}\mathbf{b}^H\} - \mathbf{B}^+ E\{\mathbf{x}\mathbf{b}^H\} = (\mathbf{R}_b - \mathbf{B}^+ \mathbf{X} \mathbf{F} \mathbf{R}_b). \quad (4.29)$$

**Theorem:** The MAP estimator achieves the minimum mean square estimation of  $\mathbf{b}$ .

**Proof:** Define  $\mathbf{B}^+$  to be the best linear estimation operator, and then the linear

estimator that achieves the MMSE of  $\mathbf{b}$  is defined to be  $\hat{\mathbf{b}} = \mathbf{B}^+ \mathbf{x}$ . Then,  $\hat{\mathbf{b}}$  will satisfy the following equality,

$$\hat{\mathbf{b}} = \arg \min_{\mathbf{b}} (E\{(\hat{\mathbf{b}} - \mathbf{b})^H(\hat{\mathbf{b}} - \mathbf{b})\}). \quad (4.30)$$

The orthogonality relation,  $E\{(\hat{\mathbf{b}} - \mathbf{b})\mathbf{x}^H\} = \underline{0}$ , leads to  $\mathbf{B}^+ E\{\mathbf{x}\mathbf{x}^H\} = E\{\mathbf{b}\mathbf{r}^H\}$ , and finally

$$\mathbf{B}^+ = E\{\mathbf{b}\mathbf{r}^H\}E\{\mathbf{x}\mathbf{x}^H\}^{-1}, \quad (4.31)$$

where  $E\{\mathbf{x}\mathbf{x}^H\} = E\{(\mathbf{X}\mathbf{F}\mathbf{b} + \mathbf{n})(\mathbf{X}\mathbf{F}\mathbf{b} + \mathbf{n})^H\} = (\mathbf{X}\mathbf{F}\mathbf{R}_b\mathbf{F}^H\mathbf{X}^H + \mathbf{R}_n)$ ,

and  $E\{\mathbf{b}\mathbf{r}^H\} = E\{\mathbf{b}(\mathbf{X}\mathbf{F}\mathbf{b} + \mathbf{n})^H\} = \mathbf{R}_b\mathbf{F}^H\mathbf{X}^H$ . We note that  $\mathbf{B}^+$  is identical to the MAP operator in (4.20).

As defined in (4.11) there are two *a priori* matrices,  $\mathbf{F}$  for the even and odd observation vectors, and thus two estimators of  $\mathbf{b}$  can be obtained for each estimation criterion. In this paper, for an estimation criterion we select the  $\mathbf{F}$  that produces a smaller MSCEE for a given training sequence. Then, the estimator  $\mathbf{b}$  with the selected  $\mathbf{F}$  will represent the estimator for the criterion.

## 4.6 The Optimal Training Sequences

Crozier [4] tabulates binary training sequences (BTS, binary sequences of 1 and -1) for different channel lengths  $N_c$  and observation lengths  $m$ . The design criterion of the sequence is to minimize the *trace* of the error covariance matrix of a LSE of  $\mathbf{h}$  and thus they are optimal in the least squares error sense. They are found either from exhaustive computer search or using the ‘‘m-sequences.’’ The same design concept can be applied to the LSE of  $\mathbf{b}$ , and new training sequences which minimize the *trace* of the error covariance matrix of the LSE of  $\mathbf{b}$  can be obtained by the procedure.

The LSE criterion applied to a  $[m \times 1]$  observation vector  $\mathbf{x} = \mathbf{X}\mathbf{h} + \mathbf{n}$  produces

the LSE of  $\mathbf{h}$ , i.e.,

$$\hat{\mathbf{h}} = \mathbf{X}^\dagger \mathbf{x}, \quad (4.32)$$

where  $\mathbf{X}^\dagger = (\mathbf{X}^H \mathbf{X})^{-1} \mathbf{X}^H$  and  $\mathbf{h}$  is a  $[N_c \times 1]$  vector. Then, the covariance matrix of the estimator is

$$\Theta := E\{(\hat{\mathbf{h}} - E(\hat{\mathbf{h}}))(\hat{\mathbf{h}} - E(\hat{\mathbf{h}}))^H\} = \sigma_n^2 (\mathbf{X}^H \mathbf{X})^{-1}. \quad (4.33)$$

Therefore, the optimum sequences (stored in matrix  $\mathbf{X}$ ) are the sequences that satisfy,

$$\mathbf{X} = \underset{\mathbf{X}}{\arg \min} \{tr(\Theta)\}. \quad (4.34)$$

Given  $N_c$  and  $m$ , the optimum binary training sequence (OBTS) satisfies (4.34) and makes the matrix  $\mathbf{X}^H \mathbf{X}$  as close as possible to diagonal.

From (4.23), the covariance matrix of  $\hat{\mathbf{b}}_{LSE}$  is

$$\Theta_{LSE} := E\{(\hat{\mathbf{b}}_{LSE} - E(\hat{\mathbf{b}}_{LSE}))(\hat{\mathbf{b}}_{LSE} - E(\hat{\mathbf{b}}_{LSE}))^H\} = \sigma_n^2 (\mathbf{F}^H \mathbf{X}^H \mathbf{X} \mathbf{F})^{-1}. \quad (4.35)$$

Now, the optimal training sequence is the sequence that makes  $\mathbf{F}^H \mathbf{X}^H \mathbf{X} \mathbf{F}$  to be as close as possible to diagonal. This optimization problem can be approached by representing the convolution operation  $\mathbf{X} \mathbf{F}$  in a matrix and vector multiplication form as  $\mathbf{F}_1 \mathbf{X} = \mathbf{c}$ , where  $\mathbf{x} = [I_0 \ I_1 \ I_2 \dots \ I_{N_t-1}]$  is a  $[N_t \times 1]$  vector, is now a  $[N_c \times N_t]$  matrix, and  $\mathbf{c}$  is the  $[N_c \times 1]$  OBTS vector. Then, the new optimal sequence  $\mathbf{x}$  that minimizes the  $trace\{\Theta_{LSE}\}$  can be obtained as

$$\mathbf{x} = \mathbf{F}_1^\dagger \mathbf{c}, \quad (\text{A.1})$$

where  $\mathbf{F}_1^\dagger$  is the generalized inverse of  $\mathbf{F}_1$  [34]. The vector  $\mathbf{x}$  should be scaled so that the energy of the scaled vector  $\mathbf{x}$  is  $N_t$ .

However, for two reasons Crozier's BTS will be used for our system simulations. First, an improvement of the new sequence is typically less than a 1 dB SNR saving compared to the BTS, while the exact SNR saving depends on the value of  $N_c$  and  $m$ . For

a short training sequence, the difference narrows. This indicates that the BTS achieves a near optimum performance also for the estimation of  $\mathbf{b}$ . Second, the elements of the new sequence are real valued and not usually members of a digital modulation constellation.

The following table summarizes the training symbols used in this dissertation.

**Table 4-1: The optimal binary training sequences**

$(N_t, N_c)$	The Sequence
(15, 6)	1 1 1 1 -1 1 1 1 -1 1 -1 -1 -1 -1 1
(11, 6)	1 1 -1 -1 -1 1 -1 1 1 1 1
(7, 4)	1 1 1 -1 1 1 1

## 4.7 Simulation Results and Discussion

In Figure 4-5, the performance of two channel estimators, LSE and MAP, in terms of the mean square channel estimation errors (MSCEE) are assessed both in theory and in simulation. The training sequence of length  $N_t$ , and the truncation length  $N_c$  are 11 and 6 respectively. We first note the effect of truncation at high SNR. Recall the channel estimation of (4.10) where we truncate the length of the overall channel to be  $N_c$  symbol intervals. The slow fading curves stay very close to theory out up to 30 dB, whereas the slow fading curves for  $(N_t, N_c) = (7, 4)$  deviate significantly from theory at high SNR due to the truncation errors. This suggests that truncation at  $N_c = 6$  is sufficient for the purpose of channel estimation. Next, we note that the fast fading curves show deviations from the slow fading curves at 30 dB. These degradations are due to the snap-shot assumption that during the observation periods  $m (= N_t - N_c + 1)$  the channel is fixed. Finally, we note that the marked advantage of MAP estimation over LSE at low SNRs.

In Figure 4-6, we evaluate the MAP estimator performance in two practical

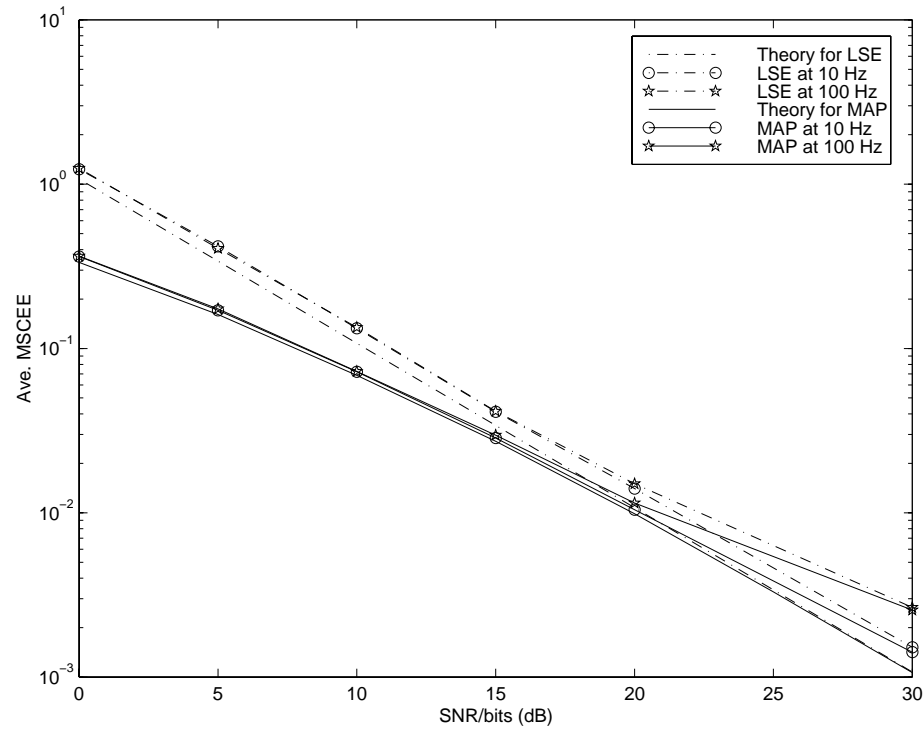
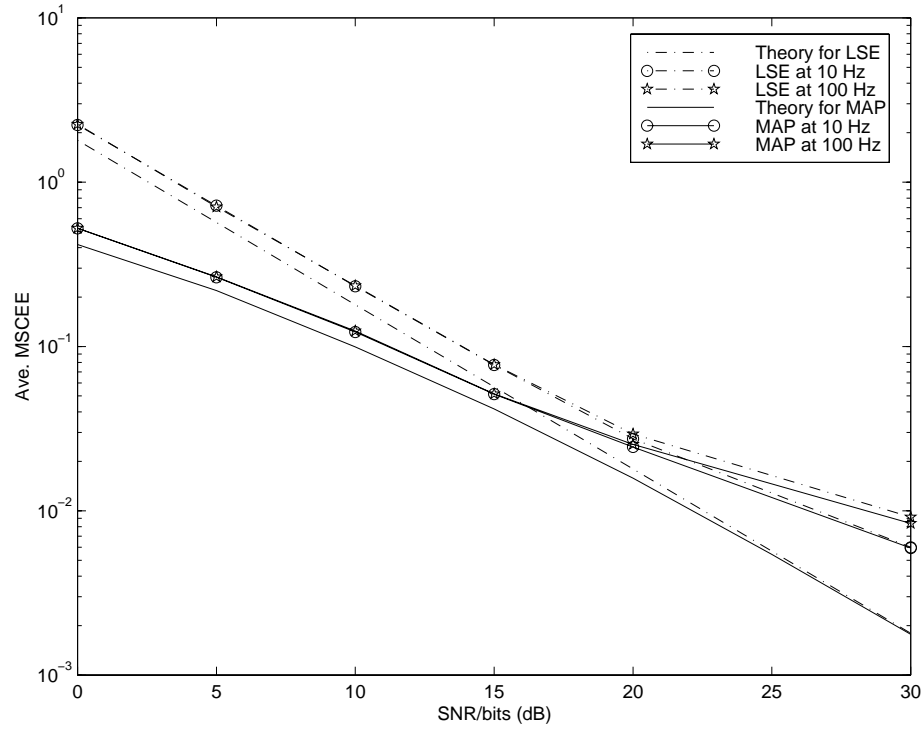


Figure 4-5 Theoretical and simulation mean square channel estimation errors (MSCEEs) for  $(N_p, N_c) = (7, 4)$  and  $(11, 6)$ .

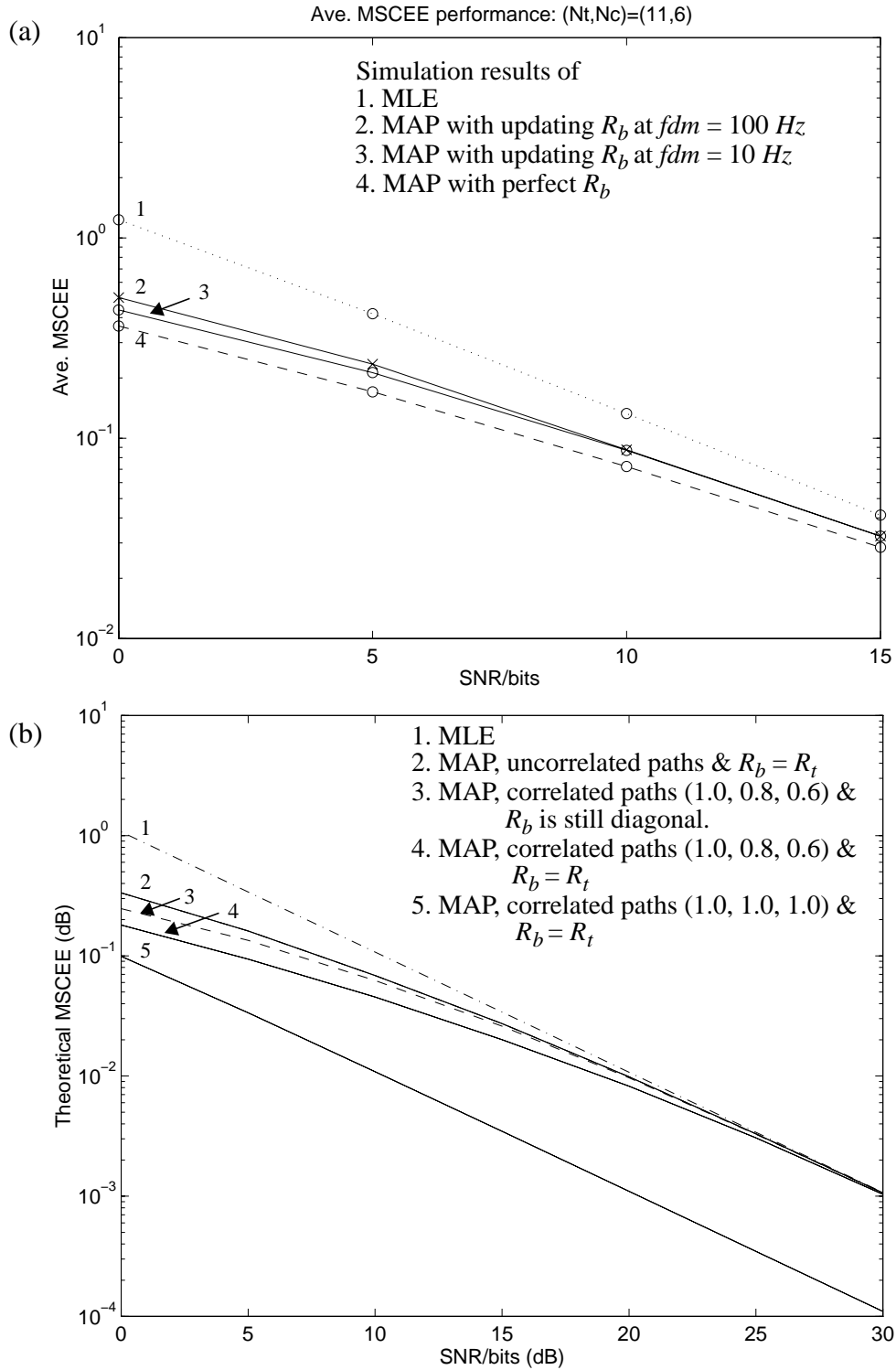


Figure 4-6 (a). Simulation of MAP estimators using the estimated powers of the multipath components. (b). Analytical results of correlated multipath channel, the numbers in the parentheses indicate the mutual correlation coefficients of the three paths.

situations; (1) when the multipath power profile is not available; (2) when the multipath undergoes a correlated scattering but we assume the paths are uncorrelated. For (1), we estimate the power profile from the estimates of  $\mathbf{b}$ . That is, for the first frame in a 16 frames long trial we use the MLE; for the rest 15 frames we switch to the MAP. The diagonal matrix of  $\mathbf{R}_b$  at each frame is obtained by simply averaging the powers of each estimated taps from previous frames. We plot the simulation result in Figure 4-6 (a). The results are averaged over 500-1000 independent trials. We observe that the MAP with noisy estimates still performs better than the MLE.

In order to evaluate the sensitivity of MAP against the correlation of the path, we revisit Eq. (4.28). In particular, two separate channel correlation matrices can be employed in the calculation of the mean square error matrix such that one is the diagonal matrix  $\mathbf{R}_b$  to denote the uncorrelated scattering channel correlation matrix for the MAP operator  $\mathbf{B}^+$  and the other  $\mathbf{R}_t$  to denote the expression  $E\{\mathbf{b}\mathbf{b}^H\}$  in Eq. (4.28).  $\mathbf{R}_t$  is non-diagonal matrix and each off-diagonal term indicates the correlation value of the two corresponding fading taps. That is, for the MAP estimator operator we use

$$\hat{\mathbf{b}}_{MAP} = \mathbf{B}^+ \mathbf{x}, \quad (4.36)$$

where  $\mathbf{B}^+ := \mathbf{R}_b (\mathbf{F}^H \mathbf{X}^H) (\mathbf{X} \mathbf{F} \mathbf{R}_b \mathbf{F}^H \mathbf{X}^H + \mathbf{R}_n)^{-1}$  and for the calculation of the mean square error we use

$$\begin{aligned} \Theta_{MAP} &:= E\{(\hat{\mathbf{b}}_{MAP} - \mathbf{b})(\hat{\mathbf{b}}_{MAP} - \mathbf{b})^H\} \\ &= \mathbf{B}^+ E\{\mathbf{x}\mathbf{x}^H\} \mathbf{B}^{+H} - E\{\mathbf{b}\mathbf{x}^H\} \mathbf{B}^{+H} - \mathbf{B}^+ E\{\mathbf{x}\mathbf{b}^H\} + \mathbf{R}_t \end{aligned}$$

Figure 4-6 (a) Curve #1 is the results for the MLE. Curve #2 is the results of usual MAP estimator. That is, both correlation matrices are uncorrelated ones, i.e.,  $\mathbf{R}_b = \mathbf{R}_t = \text{diag-matrix}$ . Curve #4 is the case where  $\mathbf{R}_t$  is not diagonal reflecting the correlation of the paths and also  $\mathbf{R}_b = \mathbf{R}_t$ . Comparing #2 and #4 we see that the MAP exploits the path correlation and achieves a better MSCEE. The extreme case of this is

described in curve #5, when all three paths are perfectly correlated in which case the MAP estimator practically becomes a MLE having only one unknown to be estimated. Curve #3 shows how much we will lose by assuming uncorrelated scattering of the taps, i.e., a diagonal  $\mathbf{R}_b$ . We note that curve #3 is still better than #2 which implies the MAP with the assumption of uncorrelated paths still benefits from the correlated paths.

In this experiment, we observe: (1) the MAP takes advantage of the path correlation, (2) when assuming uncorrelated scattering the receiver still achieves SNR advantage over the MLE but not as much as knowing the correlations. Thus, our conclusion is as follows: Provided that the path correlation among the fading taps in a real operation scenarios of the transceiver would not be as large as our examples (i.e., the mutual correlation coefficients of (1.0, 0.8, 0.6) and (1.0, 1.0, 1.0)), we can conclude that the path correlation is not a big concern at least from the channel estimation point of view.

## 4.8 Concluding Remarks

In this chapter, we provided the feedforward channel estimation techniques. We have pointed out some of problems with the recursive adaptation schemes such as LMS and RLS. Whether the recursive algorithm is applied to equalizer taps directly or to track the channel tap, the tracking speed could not deal with a fast Rayleigh fading channel. The channel estimation technique proposed in this section uses the training symbols to estimate the snap-shot channel impulse response and interpolate a set of them to capture finer time-scale channel variation. This scheme avoids the problem of error propagation of recursive algorithms running in a decision directed mode. We have proposed also a novel channel estimators which utilize the *a priori* channel information of transmit shaping filter in the estimation equation. The number of unknown coefficients were significantly reduced while the performance became much more robust against fast fading channel. This performance

advantage of the new channel estimation technique will dramatically improve the detection performance of the receivers in the upcoming chapters. Future work in the channel estimation may include the tracking of the maximum Doppler frequency so as for us to be able to reduce/increase the training overhead. Others include the design of combined estimation problem in the channel parameter estimation problem. We have used only one term (even or odd) of the observation vector in estimating the channel vector. If we were able to somehow combine the two estimates into a final estimate, we would expect a further improvement in the estimation performance.

# Chapter 5

## Diversity Combining DFE

We consider the use of decision feedback equalizer (DFE) as the proposed non-linear symbol detection receiver for uncoded, single level constellation symbol transmission. As shown in chapter 3, the use of DFE provides a significant advantage in detection performance over that of linear transversal equalizers for severe ISI channels at a very small increase in complexity--the increase in complexity is due to the calculation of the feedback filter coefficients. Thus, the DFE has been successfully applied in practice, for equalization of telephone channels as well as the time-varying wireless channels. In this chapter, we want to investigate the design issues of DFE when we have available multiple independently received signals from the diversity receiving antennas and the feedforward channel estimates. Specifically, based on the assumption that the given channel estimates are perfect, we derive a jointly optimum receiver in which the DFE and the multiple received signals from the diversity antennas are optimally combined. In addition, unlike previous assumptions that the channel is a fixed or quasi-static vector for the duration of a burst, in our derivation of the DC-DFE the assumption is generalized to include the time-

varying channel. As a result, a novel diversity combining DFE equation is obtained to cope with the fast time-varying channel.

## 5.1 Robust Signal Detection over Fast Multipath Fading, ISI Channels

Wireless digital communications systems such as IS-54, GSM, and PCS suffer from many channel impairments such as discussed in Chapter 2, including low detection SNR due to signal fading, intersymbol interference (ISI) due to multipath spread, and the time-varying channel due to Doppler spread. For each of these channel impairments, a counter-measure must be considered and should be optimally combined in a successful transceiver design.

Let's discuss individual counter-measure techniques to deal with the stated problems. To deal with a very low instantaneous channel SNR due to signal fading, use of multiple independent receiving antennas are desired as they provide higher order of signal diversity. To deal with the ISI problems, caused by multipath propagation of the signal as well as a stringent shaping requirement of transmit filter, the use of an equalizer is highly recommended for the land mobile systems. For a low complexity, simple transceiver system, no equalizers are used and in this case the channel can be blindly assumed to be *flat-fading*. In such systems the transceiver may employ the differential encoded symbol transmission and differential detection at the receiver. Such a system would not provide a robust performance due to intersymbol interference when the transceiver is to operate in a high delay-spread region such as Urban areas as well as hilly terrains where a distant-scatters are present. The ISI-induced irreducible bit error floors become significantly high and persistent once the rms delay spread of the multipath power delay profile (MPDP) of the region exceeds about 1/10 the symbol period  $T_B$  [1, 3, 8, 32]. This holds true regardless

of the fading rate.

In addition, the transceiver design must also take care of the channel mobility since the *frequency-selective* fading channels is also capable of being rapidly time-varying channel due to the highway speed mobile movement. For example, in IS-54, with a carrier frequency of 900 MHz and assuming a mobile moving at a maximum highway speed of 120 km/hr, the maximum normalized Doppler fading rate  $f_{dm}T_B$  (the product of the maximum Doppler fading rate and the symbol period) reaches up to 0.0042 [8]. This implies that the minimum time between the two fading nulls is 5 ms ( $1/2f_{dm}$ ) which is even shorter than the proposed burst length of 6.7 ms.

To deal with such rapidly time-varying, fading and dispersive channels, we are considering the use of decision feedback equalizers, diversity receiving antennas and the feedforward channel estimation developed in chapter 4.

For tracking of fast time-varying dispersive channels, a block adaptive decision feedback equalizer (DFE) based on feedforward channel estimation [4, 10, 20] has been shown to be more effective than the conventional symbol-by-symbol adaptation methods, such as least mean squares (LMS) or even recursive least squares (RLS) [5, 26] as discussed in Chapter 4. Other block adaptive schemes, based on the feedforward channel estimation but using the maximum likelihood sequence estimator (detector), can be found in [6, 9, 11], and the chapter 7 and 8 of this dissertation.

In this chapter, we follow the block transmission scheme and the feedforward channel estimation and tracking methods in chapter 4. That is, the receiver is assumed to operate on continuous transmitted frames, where each frame consists of training and unknown data segments. A “snap-shot” channel estimate is obtained from training segment. Channel tracking during the data segments is performed by interpolating a set of the snap-shot channel estimates. With the interpolated channel estimates, the receiver filter coefficients are computed.

The contributions of this chapter is that our results significantly extends the previous published results [10, 20] in the areas of block adaptive strategy using the channel estimate-based DFE. First, we compare two possible diversity combining DFE implementations and propose the structure that is more robust and less computationally complex for the block adaptive strategy. Second, we propose a new DFE coefficient computation algorithm to deal with very fast time-varying channels. Third, we illustrate the improved performance of the derived diversity combining DFE receiver and the feedforward channel estimation through Monte-Carlo computer simulations. Finally, we suggest a low computational complexity but very feasible suboptimal solution.

## 5.2 Baseband Equivalent Channel Model

In section 2.3, we have developed the diversity channel model and generation methods for simulation. Here, we briefly review the channel model and notations. The channel model is again illustrated in Figure 5-1.

Now, the symbols in Figure 5-1 are summarized here as

- $\mathbf{f}$  is a unit energy  $[31 \times 1]$  column vector. It represents the transmit shaping filter, obtained from truncating the square root raised cosine filter (with roll-off factor  $\beta$ ) for the duration of seven symbol periods each side and sampling at the rate  $2/T_B$ .
- $x_l(t)$  represents the received signal at each diversity branch, which is bandlimited with the excess bandwidth of  $(1+\beta)(1/T_B)$ .  $T_B/2$ -spaced sampling is considered, i.e.,  $x_l(k) := x_l(t = kT_B/2)$ , where  $k$  denotes the  $T_B/2$ -spaced epoch index.
- $\{I(k)\}$  represents the symbol sequence at the half-symbol sampling rate. That is, it is a zero stuffed sequence such that  $I(k)$  at even  $k$  represents the symbol transmitted at the baud rate and  $I(k)$  at every odd  $k$  is zero-valued.
- The noise  $n_l(t)$  is also assumed to be  $T_B/2$ -spaced sampled and the sampled noise

sequence  $n_l(k)$  is assumed to be complex-valued additive white Gaussian with zero mean and variance  $\sigma_n^2$ . The noise sequences for different branches are assumed to be mutually uncorrelated and also independent with the wireless channel.

- $\mathbf{b}_l(k) = [b_{l,0}(k) \dots b_{l,N_R-1}(k)]^T$ , represents the time-varying impulse response of the  $l$ -th channel, where  $N_R$  is the number of the time-varying channel taps ( $N_R = 3$  in this dissertation).
- Each  $T_B/2$ -spaced overall channel impulse response  $\mathbf{h}_l(k)$  is defined as  $\mathbf{h}_l(k) := \underline{f} \otimes \mathbf{b}_l(k)$ , where  $\otimes$  denotes the convolution operation.

In this chapter, we adopt the feedforward channel estimation and tracking scheme developed in Chapter 4. That is, we use the interpolated channel estimate vectors for  $\mathbf{b}_l(k)$  and thus  $\mathbf{h}_l(k)$  in computing the receiver coefficients.

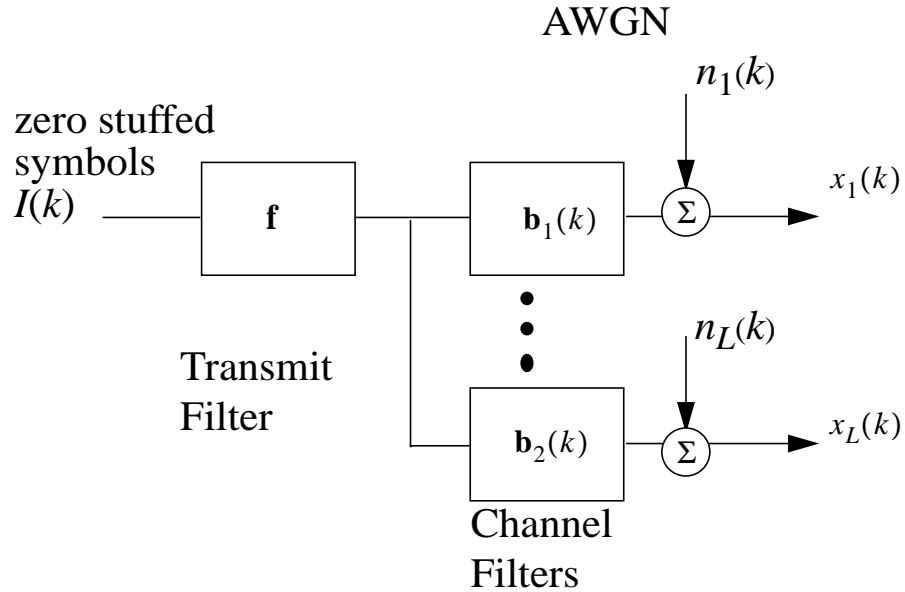


Figure 5-1 The baseband model for multiple diversity antenna channels where each channel introduce the multipath delay dispersion.

### 5.3 Diversity-Combining DFE

In this section we illustrate how to obtain diversity combining DFE coefficients using the interpolated channel estimates. For the channel-estimate based receiver, the coefficients of diversity combining DFE are computed from the channel estimates, which involves some form of matrix inversion. Thus, a stable method of computing the DC-DFE coefficients or the receiver architecture resulting in more stable solution would be desirable. In Section 5.3.1, we apply the minimum mean square error (MMSE) criterion to the receiver structure depicted in Figure 5-3, and obtain the basic *straightforward* solution. The straightforward DC-DFE turns out to be disadvantageous, due to high tendency to developing severe eigenvalue spread in the correlation matrix of the Wiener-Hopf equation. The eigenvalue spread will be large for a severe ISI channel. In addition, the straightforward

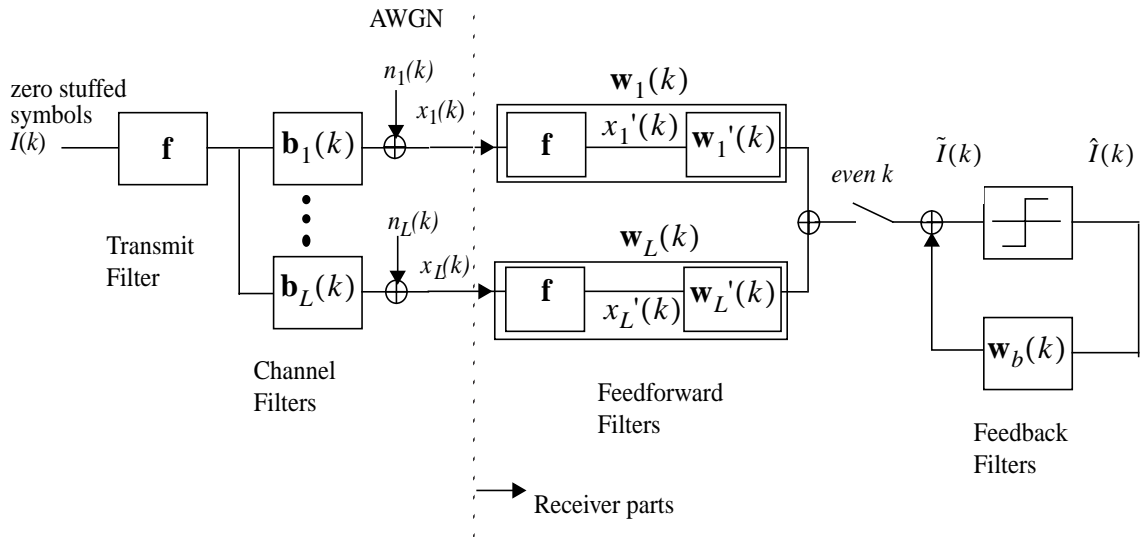


Figure 5-2 The receiver architecture of straightforward diversity-combining DFE

DC-DFE increases the degree of eigenvalue spreads as the diversity order increases. Advancing a few critical steps from the straightforward Wiener-Hopf equation, however, we derive the proposed, matched filtered form of the DC-DFE which solves the problem of eigenvalue spreads. Thus we explicitly prove that the two structures are exactly the same. This provide us good insights into how the two are related. The first DFE realization will be termed the *straightforward* realization, and the other as a *matched filtered* realization.

On the other hand, the decision feedback equalizer solutions were traditionally derived under the assumption of non time-varying impulse response during the decision-delay of the receiver. These conventional solutions had been applied without any modification of the solution according to the time-varying channel. As the results, even in a genie-aided mode where the channel variation is perfectly known to the receiver the DFE receiver using the static coefficient computation method develops high irreducible detection error floors such that no matter how large the input SNR may be the symbol error rate does not decrease. To correct this problem, when deriving the MMSE DC-DFE derivation we explicitly take into account of the channel variation during the decision delay. Thus, the derived solution will fully utilize all the channel variation during the decision delay. Specifically, the channel variations during the decision delay are available from interpolation method described in Chapter 4. These were obtained at the expense of interpolation delay, thus all should be utilized in finding the optimum receiver coefficients.

Main goal in the following sections is to obtain the matched filtered diversity combining DFE that takes into account the channel variation over the decision delay. Main purpose of the straightforward solution is to illustrate the eigenvalue spread problem and the relationship with the matched filtered DC-DFE.

### **5.3.1 The Wiener-Hopf normal equation**

The receiver side of Figure 5-2 depicts the straightforward diversity combining

DFE (DC-DFE). We apply the minimum mean square error (MMSE) criterion to this structure and obtain the straightforward solution. Briefly reminding the notation and our assumption, the index  $k$  denotes the  $T_B/2$ -spaced epoch and thus even  $k$  corresponds to symbol rate sampling.  $n_l(k)$  denotes the complex valued AWGN at  $l$ -th branch with zero mean and variance of  $\sigma_n^2$ . We assume that the noises at each diversity branches are mutually independent, and also independent to the channel and the transmitted symbols, and that a transmitted symbol is an independent, identically distributed (*i.i.d.*) complex-valued random variable with zero mean and unit variance.

For the convenience of deriving the matched filtered diversity combining DFE, we choose the received signal  $x_l(k)$  to be the input signal into the adaptive parts  $\{\mathbf{w}_l(k), \mathbf{w}_b(k)\}$ . We might have also chosen  $x_l'(k)$  as the input signal to the adaptive parts  $\{\mathbf{w}_l(k), \mathbf{w}_b(k)\}$ , which is the approach we have taken in section 5.3.2.

Each  $T/2$ -spaced feedforward filter is represented by  $\mathbf{w}_l(k)$  and the  $T_B$ -spaced feedback filter by a  $[N_b \times 1]$  vector  $\mathbf{w}_b(k)$ . We denote  $\mathbf{w}(k) := [\mathbf{w}_1^T(k) \dots \mathbf{w}_L^T(k) \mathbf{w}_b^T(k)]^T$ . Each  $T_B/2$ -spaced interpolated overall channel is assumed perfectly estimated and represented by a  $[\tilde{N}_g \times 1]$  vector  $\mathbf{h}_l(k)$ . We assume  $\tilde{N}_g$  is even, and  $N_g = \tilde{N}_g/2$ .

We now want to find the optimal vector  $\mathbf{w}_b(k)$  that minimizes the mean square error at each decision instant ( $k = 0, 2, 4, \dots$ ), i.e.,

$$\mathbf{w}_o(k) = \underset{\mathbf{w}(k)}{\arg \min} E \left\{ \left| \tilde{I}(k) - I(k - \tilde{\Delta}) \right|^2 \left| \mathbf{h}_l(q), q = k, k-1, \dots, k-\tilde{\Delta}, l = 1, \dots, L \right. \right\}, \quad (5.1)$$

where  $\tilde{\Delta}$  is the required decision delay in units of  $T/2$ . We also assume that  $\tilde{\Delta}$  is even, and  $\Delta = \tilde{\Delta}/2$ . The predecision value  $\tilde{I}(k)$  is now described by,

$$\tilde{I}(k) = \sum_{l=1}^L \mathbf{x}_l^T(k) \mathbf{w}_l(k) + \mathbf{I}_b^T \mathbf{w}_b(k), \quad (5.2)$$

where  $\mathbf{I}_b(k) = [I(k-2-\tilde{\Delta}) \dots I(k-2N_b-\tilde{\Delta})]^T$  (assuming the past decisions were

correct), and where  $\mathbf{x}_l(k) := [x_l(k) \ x_l(k-1) \ \dots \ x_l(k-\tilde{\Delta})]^T$ . By defining  $\mathbf{s}(k) := [\mathbf{x}_1^T(k) \ \dots \ \mathbf{x}_L^T(k) \ \mathbf{I}_b^T(k)]^T$ ,  $\tilde{I}(k)$  can be written compactly as  $\tilde{I}(k) = \mathbf{s}^T(k)\mathbf{w}(k)$ . Note that the length of  $\mathbf{x}_l(k)$  is  $\tilde{\Delta} + 1$  and thus the length of the feedforward  $\mathbf{w}_l(k)$  is also  $\tilde{\Delta} + 1$ . At this point, we are simply assuming a very large feedforward filter length for the derivation of the matched filtered solution. The desired relationship between the feedforward filters of a finite length and the decision delay can be established later for each solution.

Now each input vector  $\mathbf{x}_l(k)$  to the feedforward filter  $\mathbf{w}_l(k)$  can be written as

$$\mathbf{x}_l(k) = \mathbf{H}_l(k)\mathbf{I}(k) + \mathbf{n}_l(k), \quad (5.3)$$

where we have defined

$$\mathbf{H}_l(k) := \begin{bmatrix} h_{l,0}(k) & h_{l,2}(k) & \dots & h_{l,\tilde{N}_g-2}(k) & 0 & 0 & \dots \\ 0 & h_{l,1}(k-1) & h_{l,3}(k-1) & \dots & h_{l,\tilde{N}_g-1}(k-1) & 0 & \dots \\ 0 & h_{l,0}(k-2) & h_{l,2}(k-2) & \dots & h_{l,\tilde{N}_g-2}(k-2) & 0 & \dots \\ \dots & \dots & \dots & \dots & \dots & \dots & \dots \\ \cdot & \dots & 0 & h_{l,1}(k-\tilde{\Delta}-1) & h_{l,3}(k-\tilde{\Delta}-1) & \dots & h_{l,\tilde{N}_g-1}(k-\tilde{\Delta}-1) \\ \dots & \dots & 0 & h_{l,0}(k-\tilde{\Delta}) & h_{l,2}(k-\tilde{\Delta}) & \dots & h_{l,\tilde{N}_g-2}(k-\tilde{\Delta}) \end{bmatrix}$$

$\mathbf{I}(k) := [I(k)I(k-2)\dots I(k-2(\Delta + N_g - 1))]^T$ , and  $\mathbf{n}_l(k) := [n_l(k)n_l(k-1)\dots n_l(k-\tilde{\Delta})]^T$ .

In what follows, assuming a decision at  $k = 0$ , we omit the notation of epoch (the parenthesis) from the matrices for brevity and retrieve it after the solution is derived. We also omit the notation for the mathematical *conditioning* operation in (5.1) but it is understood that the mathematical *expectation* is meant to apply only to the noise and the symbol sequences. Then the mean square measure of (5.1) can be compactly written as  $E\{|\mathbf{s}^T\mathbf{w} - I(-\tilde{\Delta})|^2\}$ . Invocation of the orthogonality principle gives

$E\{\mathbf{s}(\mathbf{s}^H \mathbf{w}^* - I^*(-\tilde{\Delta}))\} = 0$ , which results in the Wiener-Hopf normal equation

$$E\{\mathbf{s}\mathbf{s}^H\}\mathbf{w}^* = E\{\mathbf{s}I^*(-\tilde{\Delta})\}. \quad (5.4)$$

Now we denote  $\mathbf{x} := [\mathbf{x}_1^T \dots \mathbf{x}_L^T]^T$ ,  $\mathbf{R}_{\mathbf{xx}} := E\{\mathbf{xx}^H\}$ ,  $\mathbf{R}_{\mathbf{xI}} := E\{\mathbf{x}\mathbf{I}_b^H\}$ ,  $\mathbf{w}_f := (\mathbf{w}_1^T \dots \mathbf{w}_L^T)^T$ , and  $\mathbf{c} := E\{\mathbf{x}I^*(-\Delta)\}$ . Then, (5.4) can be rewritten as,

$$\begin{bmatrix} \mathbf{R}_{\mathbf{xx}} & \mathbf{R}_{\mathbf{xI}} \\ \mathbf{R}_{\mathbf{xI}}^H & E(\mathbf{I}_b \mathbf{I}_b^H) \end{bmatrix} \begin{bmatrix} \mathbf{w}_f \\ \mathbf{w}_b \end{bmatrix}^* = \begin{bmatrix} E(\mathbf{xx}^H) & E(\mathbf{x}\mathbf{I}_b^H) \\ E(\mathbf{I}_b \mathbf{x}^H) & \Xi_{N_b \times N_b} \end{bmatrix} \begin{bmatrix} \mathbf{w}_f \\ \mathbf{w}_b \end{bmatrix}^* = \begin{bmatrix} \mathbf{c} \\ \mathbf{0}_{N_b} \end{bmatrix}, \quad (5.5)$$

and in a detailed form as,

$$\begin{bmatrix} E(\mathbf{x}_1 \mathbf{x}_1^H) & E(\mathbf{x}_1 \mathbf{x}_2^H) & \dots & E(\mathbf{x}_1 \mathbf{I}_b^H) \\ E(\mathbf{x}_2 \mathbf{x}_1^H) & E(\mathbf{x}_2 \mathbf{x}_2^H) & \dots & E(\mathbf{x}_2 \mathbf{I}_b^H) \\ \dots & \dots & \dots & \dots \\ E(\mathbf{I}_b \mathbf{x}_1^H) & E(\mathbf{I}_b \mathbf{x}_2^H) & \dots & \Xi_{N_b \times N_b} \end{bmatrix} \begin{bmatrix} \mathbf{w}_1 \\ \mathbf{w}_2 \\ \dots \\ \mathbf{w}_b \end{bmatrix}^* = \begin{bmatrix} \mathbf{c}_1 \\ \mathbf{c}_2 \\ \dots \\ \mathbf{0}_{N_b} \end{bmatrix}, \quad (5.6)$$

where we have used  $E\{\mathbf{I}_b I^*(-\tilde{\Delta})\} = \mathbf{0}_{N_b}$  and  $E(\mathbf{I}_b \mathbf{I}_b^H) = \Xi_{N_b \times N_b}$ . Recall our assumption that the noise at each diversity branch are mutually independent, and also independent with the *i.i.d.* input symbols. Next, each  $[(\tilde{\Delta} + 1) \times 1]$  cross correlation vector can be shown to be the  $(\Delta + 1)$ th column of  $\mathbf{H}_l$ , i.e.,

$$\mathbf{c}_l = E\{(\mathbf{H}_l \mathbf{I} + \mathbf{n}_l)I^*(-\Delta)\} = \mathbf{H}_{l,(:, \Delta)}, l = 1, \dots, L. \quad (5.7)$$

The individual sub-matrices of (5.6) can be identified,  $i, j = 1, \dots, L$ , as

$$E\{\mathbf{x}_i \mathbf{x}_j^H\} = E\{(\mathbf{H}_i \mathbf{I} + \mathbf{n}_i)(\mathbf{H}_j \mathbf{I} + \mathbf{n}_j)^H\} = \mathbf{H}_i \mathbf{H}_j^H + \sigma_n^2 \delta(i - j) \Phi, \quad (5.8)$$

where  $\delta(\bullet)$  is the Kronecker delta function and  $\Phi$ , a  $[(\tilde{\Delta} + 1) \times (\tilde{\Delta} + 1)]$  autocorrelation matrix of the noise, is equal to  $\Xi_{(\tilde{\Delta} + 1) \times (\tilde{\Delta} + 1)}$ . The other  $[(\tilde{\Delta} + 1) \times N_b]$  submatrices of (5.6) are for  $i = 1, \dots, L$ ,

$$E\{\mathbf{x}_i \mathbf{I}_b^H\} = E\{(\mathbf{H}_i \mathbf{I} + \mathbf{n}_i) \mathbf{I}_b^H\} = \mathbf{H}_i E\{\mathbf{I} \mathbf{I}_b^H\} = \mathbf{H}_{i,(:, \Delta + 1: \Delta + N_b)}, \quad (5.9)$$

and  $j = 1, \dots, L$   $E\{\mathbf{I}_b \mathbf{x}_j^H\} = E\{\mathbf{x}_j \mathbf{I}_b^H\}^H$ .

The derivation of the matched filtered solution will be continued from the results obtained so far. In this dissertation, the optimal solution  $\mathbf{w}$  obtained from (5.6) will be categorized as a “straightforward solution.”

### 5.3.2 A straightforward solution

For the straightforward solution with finite filter lengths, we may want to use  $x_l'(k)$ , the received signal after the receive-SRRC filter as depicted in Figure-1, to be the input signal to the adaptive parts,  $\mathbf{w}_l'(k)$  and  $\mathbf{w}_b(k)$ . The benefit of this approach is that the required adaptive filter length  $\tilde{N}_f'$  of the  $T_B/2$ -spaced feedforward filter  $\mathbf{w}_l'(k)$  can be shorter than that of  $\mathbf{w}_l(k)$ . From the standard procedure of Section 5.3.1, (5.3) - (5.9), a matrix equation isomorphic to the straightforward solution of (5.6) can be obtained. The differences are that  $x_l'(k)$  replaces  $x_l(k)$ , and that only the  $[\tilde{N}_f' \times 1]$  sub-vector  $x'_{l, \tilde{\Delta} - \tilde{N}_f' + 2 : \tilde{\Delta} + 1}$ , instead of the  $[(\tilde{\Delta} + 1) \times 1]$  vector, represents the input vector in (5.3). This leads to the following modifications to (5.3) - (5.9):

- $\mathbf{h}_l(k)$  with length  $\tilde{N}_g$  represents the convolution of the channel  $\mathbf{b}_l(k)$  and the raised cosine function.
- $\mathbf{H}_l$  represents the  $[\tilde{N}_f' \times (N_g + \Delta)]$  sub-matrix  $\mathbf{H}_{l, (\tilde{\Delta} - \tilde{N}_f' + 2 : \tilde{\Delta} + 1, :)}$ .
- The cross-correlation vectors  $\mathbf{c}_l$ , each individual sub-matrix of  $E\{\mathbf{x}_l \mathbf{x}_j^H\}$ , and that of  $E\{\mathbf{x}_l \mathbf{I}_b^H\}$  are appropriately truncated to have the correct dimension of  $[\tilde{N}_f' \times 1]$ ,  $[\tilde{N}_f' \times \tilde{N}_f']$ , and  $[\tilde{N}_f' \times N_b]$  respectively.
- The  $ij$  th element of the noise autocorrelation matrix in (5.8) is now  $\Phi_{(i, j)} = f_{rc}((i - j)T_B/2)$ , where  $f_{rc}(t)$  is the raised cosine function with a roll-off  $\beta = 0.35$ .

The decision delay of this solution takes the form,  $\tilde{\Delta} \leq \tilde{N}_f' - 1 + \Delta_g$  (equality with a sufficient number of feedback filter taps), where  $\Delta_g$  is the main tap location of the channel  $\mathbf{h}(k)$ . Furthermore, ignoring the channel variation over  $\tilde{N}_f'$  the straightforward solution of

$\{\mathbf{w}_l'(k), \mathbf{w}_b(k)\}$  reduces to the one of [20].

In fact, the  $L N_f' T_B/2$ -spaced coefficients of the feedforward filters can be obtained from solving

$$[\mathbf{R}_{\mathbf{xx}} - \mathbf{R}_{\mathbf{xI}}\mathbf{R}_{\mathbf{xI}}^H]\mathbf{w}_f^* = \mathbf{c}, \quad (5.10)$$

and the  $N_b T$ -spaced feedback filter coefficients from

$$\mathbf{w}_b^* = -\mathbf{R}_{\mathbf{xI}}^H\mathbf{w}_f^*. \quad (5.11)$$

We now illustrate two major drawbacks of the straightforward methods. First, the computational complexity increases exponentially with diversity order. The complexity is order  $(LN_f')^3$  provided we use a Cholesky factorization to solve (5.10). Second, a more serious problem, is that the matrix  $\mathbf{R}_{\mathbf{xx}} - \mathbf{R}_{\mathbf{xI}}\mathbf{R}_{\mathbf{xI}}^H$  becomes extremely unstable as we increase the number of diversity order  $L > 1$ ; a huge condition number (the ratio of the largest and the smallest eigenvalues) occurs.

A large eigenvalue spread occurs when the cross-correlation submatrices of  $\mathbf{R}_{\mathbf{xx}}$  of (5.6) have large values. Recalling that since the *expectation* does not apply to the channels  $\mathbf{h}_i(k)$  from (5.1), the cross-correlation between any two diversity channel at any given time is not zero valued in general. These non-zero off-diagonal matrices in  $\mathbf{R}_{\mathbf{xx}}$  are the main cause of the large eigenvalue spreads of the matrix  $\mathbf{R}_{\mathbf{xx}}$ . For a simple illustration, consider a two-by-two correlation matrix, i.e.,

$$\mathbf{A} := \begin{bmatrix} E(X_1X_1) & E(X_1X_2) \\ E(X_2X_1) & E(X_2X_2) \end{bmatrix} = \begin{bmatrix} a & c \\ c & b \end{bmatrix}, \text{ for which a diagonalization reduces to} \quad (5.12)$$

$$\begin{bmatrix} a - \xi & 0 \\ 0 & b + \xi \end{bmatrix},$$

where  $c^2 \leq a \cdot b$  from the Schwartz inequality and where  $\xi$  is denoted as

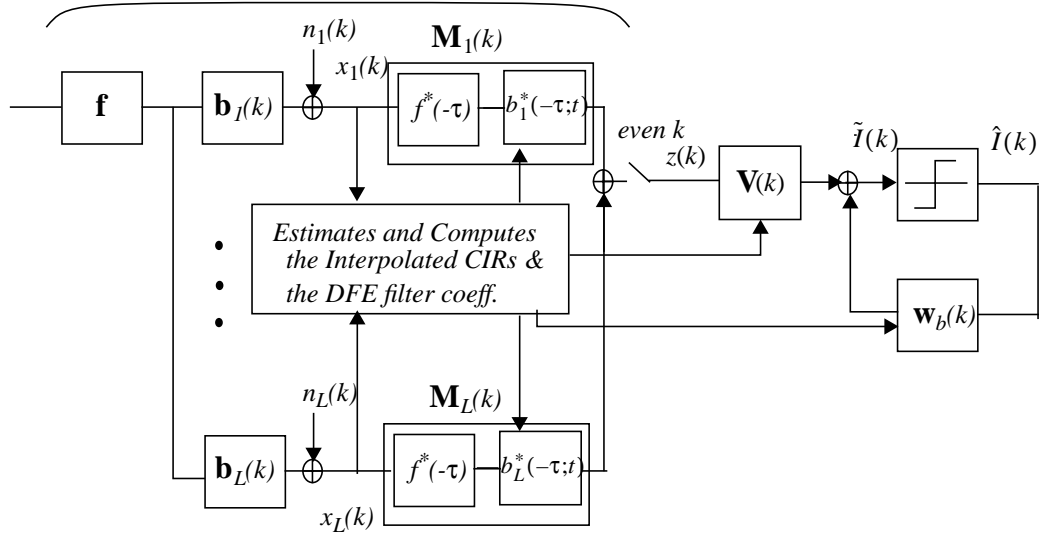


Figure 5-3 The receiver structure of the matched filtered diversity combining DFE.

$\xi := \frac{1}{2}(\sqrt{(a-b)^2 + 4c^2} - |a-b|)$ . It is evident from this example that there will be only one significant eigenvalue when the cross-correlation  $c$  tends to its maximum. By the same analogy, the condition number of  $\mathbf{R}_{\mathbf{xx}}$  may become very large whenever the cross-correlation submatrices have large values. In our simulation, at high SNR (more than 15 dB), the order of the condition number of matrix  $R_{\mathbf{xx}}$  for a relatively small  $N_f'$  ( $= 4$ ) often reaches up to  $10^5$  for  $L = 2$  or  $10^8$  for  $L=4$ . Therefore, without a regularization technique to relieve the eigenvalue spreads, the DFE coefficients obtained at high SNR often become unreliable due to magnification of the channel estimation errors.

### 5.3.3 A matched filtered diversity combining DFE solution

We now discuss the matched filtered diversity combining DFE, depicted in Figure-2. Since channels are estimated, at each diversity branch the received signals can be

matched filtered by  $\mathbf{M}_l(k)$ . The matched filtered signals are then combined and can be sampled at the symbol rate without loss of information. The  $T_B$ -spaced sampled combined signal is then fed to the  $T_B$ -spaced feedforward filter  $\mathbf{V}(k)$ . The correlation matrix of this structure does not suffer from large eigenvalue spreads.

From the results in [52] it can be observed that, although not explicitly stated, the  $L$  channel diversity combining DFE problem can be treated as an equivalent single channel DFE problem when using the matched filtered solution. This implies that for a finite length DFE solution the dimension of the correlation matrix becomes independent of diversity order  $L$ . Thus, there will be no cross-correlation submatrices to spread the eigenvalues.

The derivations in [52], however, are performed using a quasi-static channel assumption and focus on obtaining mean square errors of an infinite order DFE from which the Chernoff upper bounds on bit error probability can be related. What we need, however, is a solution (with finite filter lengths) that takes into account the rapid channel variation over a decision delay. This can be accomplished relatively easily with a matrix representation of the signals and filters as we have developed in V.1.

In this section, we continue the derivation of the NT-DFE solution from the straightforward solution (5.6).

The  $L$  simultaneous matrix equations of (5.6) can now be rewritten as

$$(\mathbf{H}_1 \mathbf{H}_1^H + \sigma_n^2 \Xi_{N_f \times N_f}) \mathbf{w}_1^* + \mathbf{H}_1 \mathbf{H}_2^H \mathbf{w}_2^* + \dots + \mathbf{H}_1 E\{\mathbf{I} \mathbf{I}_b^H\} \mathbf{w}_b^* = \mathbf{c}_1, \text{ for } l = 1, \quad (5.13)$$

$$\mathbf{H}_2 \mathbf{H}_1^H \mathbf{w}_1^* + (\mathbf{H}_2 \mathbf{H}_2^H + \sigma_n^2 \Xi_{N_f \times N_f}) \mathbf{w}_2^* + \dots + \mathbf{H}_2 E\{\mathbf{I} \mathbf{I}_b^H\} \mathbf{w}_b^* = \mathbf{c}_2, \text{ for } l = 2, \quad (5.14)$$

similarly for up to  $l = L$ , and the last matrix equation for the feedback part is

$$E\{\mathbf{I}_b \mathbf{I}^H\} \mathbf{H}_1^H \mathbf{w}_1^* + E\{\mathbf{I}_b \mathbf{I}^H\} \mathbf{H}_2^H \mathbf{w}_2^* + \dots + \mathbf{w}_b^* = \mathbf{0}_{N_b}. \quad (5.15)$$

Arranging the  $L$  matrix equations in terms of  $\mathbf{w}_b^*$  and substituting them into (5.15)(5.14), each of the  $L$  matrix becomes

$$\mathbf{H}_l \sum_{r=1}^L \mathbf{H}_r^H \mathbf{w}_r^* + \sigma_n^2 \mathbf{w}_l^* - \mathbf{H}_l E\{\mathbf{I}\mathbf{I}_b^H\} E\{\mathbf{I}_b \mathbf{I}^H\} \sum_{r=1}^L \mathbf{H}_r^H \mathbf{w}_r^* = \mathbf{c}_l. \quad (5.16)$$

Now, by defining  $\tilde{\mathbf{M}}_l := \mathbf{H}_l - \mathbf{H}_l E\{\mathbf{I}\mathbf{I}_b^H\} E\{\mathbf{I}_b \mathbf{I}^H\}$  and  $\tilde{\mathbf{V}}^* := \sum_{r=1}^L \mathbf{H}_r^H \mathbf{w}_r^*$ , and rearranging with respect to  $\mathbf{w}_l^*$ , (5.16) produces

$$\mathbf{w}_l^* = \frac{1}{\sigma_n^2} (-\tilde{\mathbf{M}}_l \cdot \tilde{\mathbf{V}}^* + \mathbf{c}_l) = \mathbf{M}_l \tilde{\mathbf{V}}^*, \text{ for each } l, \quad (5.17)$$

where the  $[(\tilde{\Delta} + 1) \times (\Delta + 1)]$  matrix  $\mathbf{M}_l$  is equal to the sub-matrix of  $\mathbf{H}_l$ ,

$$\mathbf{M}_l = \mathbf{H}_{l,(:, 0:\Delta)}, \quad (5.18)$$

and the elements of the  $[(\Delta + 1) \times 1]$  vector  $\underline{V}$  are defined as

$$V_i := \begin{cases} (1 - \tilde{V}_i) / \sigma_n^2 & , i = \Delta \\ (-\tilde{V}_i) / \sigma_n^2 & , i = 0, \dots, \Delta - 1 \end{cases}. \quad (5.19)$$

We note from (5.17) that each feedforward filter  $\mathbf{w}_l$  can be decomposed into a matched filter at each diversity branch and a  $T_B$ -spaced feedforward filter which is common to all the diversity branches.

Next, pre-multiplying  $\mathbf{M}_l^H$  and substituting  $\mathbf{w}_l^*$  of (5.17) into the corresponding  $l$ -th equation of (5.16), and then summing over all the  $L$  equations produces

$$\left[ \sum_{l=1}^L \mathbf{M}_l^H \mathbf{M}_l \cdot \sum_{r=1}^L \mathbf{M}_r^H \mathbf{M}_r + \sigma_n^2 \sum_{l=1}^L \mathbf{M}_l^H \mathbf{M}_l \right] \mathbf{v}^* = \sum_{l=1}^L \mathbf{M}_l^H \mathbf{c}_l. \quad (5.20)$$

Now define a  $[(\Delta + 1) \times (\Delta + 1)]$  matrix  $\Psi_l := \mathbf{M}_l^H \mathbf{M}_l$ , and note  $\Psi_l = \mathbf{M}_l^H \mathbf{M}_l = \Psi_l^H$ , and similarly for  $\Psi := \sum_{l=1}^L \Psi_l = \Psi^H$ . Also note that  $\sum_{l=1}^L \mathbf{M}_l^H \mathbf{c}_l$  of (5.20) is just the  $(\Delta + 1)$ -th column of  $\Psi$ , i.e.,  $\sum_{l=1}^L \mathbf{M}_l^H \mathbf{c}_l = \Psi_{(:, \Delta)}$ . Finally, substituting (5.17) into (5.15), we have the feedback coefficients,

$$\mathbf{w}_b^* = - \left( \sum_{l=1}^L E\{\mathbf{I}_b \mathbf{I}^H\} \mathbf{H}_l^H \mathbf{M}_l \right) \mathbf{v}^* = \left( \sum_{l=1}^L (\mathbf{H}_{l, (\Delta+1:\Delta+N_{gs}, :)})^H \mathbf{M}_l \right) \mathbf{v}^*. \quad (5.21)$$

From inspection of (5.17) and (5.20) all the necessary information on the matched filtered diversity combining structure can be obtained. Specifically, the matched filter coefficients of (5.24) can be determined from  $M_f^H$ , the combined signal of the diversity matched filter outputs is the input signal to the  $T_B$ -spaced feedforward filter  $\mathbf{V}$ , and the decision delay should be  $\tilde{\Delta} = \tilde{N}_g + 2(N_f - 1)$  for a  $T_B$ -spaced feedforward filter length with  $N_f$ .

In particular, considering  $\mathbf{V}_{\Delta-N_f+1:\Delta}$  for a feedforward filter with length  $N_f$ , (5.20) can be reduced to

$$\mathbf{R}\mathbf{V}_{\Delta-N_f+1:\Delta}^* = \Psi_{(\Delta-N_f+1:\Delta, \Delta)}, \quad (5.22)$$

where  $\mathbf{R} := (\Psi\Psi^H + \sigma_n^2\Psi)_{(\Delta-N_f+1:\Delta, \Delta-N_f+1:\Delta)}$ . And the  $[N_b \times 1]$  feedback filter can be obtained from

$$\mathbf{w}_b^* = -\mathbf{B}\mathbf{V}_{\Delta-N_f+1:\Delta}^*, \quad (5.23)$$

where the  $[N_b \times N_f]$  matrix  $\mathbf{B} := \left( \sum_{l=1}^L (\mathbf{H}_{l, (\Delta+1:\Delta+N_g, :)})^H \mathbf{M}_l \right)_{(0:N_b-1, \Delta-N_f+1:\Delta)}$ .

For the matched filtered diversity combining DFE, the decision delay is the summation of the matched filter and feedforward filter lengths. It is defined in units of  $T_B/2$ -spaced epochs as  $\tilde{\Delta} = \tilde{N}_g + 2(N_f - 1)$ , or in units of  $T$ -spaced epochs as  $\Delta = N_g + N_f - 1$ , where  $N_f$  is the length of  $T_B$ -spaced feedforward filter  $\mathbf{V}(k)$ .

The  $[\tilde{N}_g \times 1]$  matched filter can be identified as, assuming  $k = 0$  is the current epoch,

$$\mathbf{M}_l = [h_{l, \tilde{N}_g-1}^*(-1) \ h_{l, \tilde{N}_g-2}^*(-2) \ \dots \ h_{l, 0}^*(-\tilde{N}_g)]^T. \quad (5.24)$$

Note the decreasing epoch index of the vector elements. Thus each matched filter at an epoch  $k$  needs  $\tilde{N}_g$  previous snap-shot channel estimates.

To describe the DFE filters, it is convenient to first define a  $T_B$ -spaced sampled summed channel autocorrelation function (SCAF), i.e.,

$$\Psi_a(r) := \sum_{l=1}^L \Psi_{l,a}(r), \quad (5.25)$$

where each diversity channel autocorrelation function, for  $l = 1, \dots, L$  and for  $r = 0, -1, \dots, -N_f+1$ , is defined as

$$\Psi_{l,a}(r) = \sum_{q=|a|}^{\tilde{N}_g-1-|a|} h_{l,q-a}^*(q - \tilde{N}_g - a + 2r) \cdot h_{l,q+a}(q - \tilde{N}_g - a + 2r),$$

for  $a = -N_g + 1, \dots, 0, \dots, N_g - 1$  and  $\Psi_{l,a}(r) = 0$  for  $a \geq |N_g|$ . Note that the phases of the main terms  $\Psi_{l,0}(\bullet)$  are equalized. Thus the main term  $\Psi_0(\bullet)$  is the result of  $L$  constructive additions while non-main terms  $\{\Psi_a(\bullet)\}_{a \neq 0}$  are not.

Now, the  $ij$  th element of a  $[N_f \times N_f]$  correlation matrix  $\mathbf{R}$  can be described as

$$\mathbf{R}_{(i,j)} = \sum_{q=-N_g+1}^{N_f-1-i} \Psi_q(-i) \cdot \Psi_{q+i-j}^*(-j) + \sigma_n^2 \Psi_{j-i}(-j), \quad (5.26)$$

for  $i, j = 0, 1, \dots, N_f - 1$ .

A  $[N_f \times 1]$  cross-correlation vector  $\mathbf{P}$  can be identified as, for  $i = 0, 1, \dots, N_f - 1$ ,

$$P_i = \Psi_{N_f-1-i}(-i). \quad (5.27)$$

Finally, a  $[N_b \times N_f]$  matrix  $\mathbf{B}$  is, for  $i = 0, 1, \dots, N_b - 1$ , and  $j = 0, 1, \dots, N_f - 1$ ,

$$\mathbf{B}_{(i,j)} = \Psi_{N_f+i-j}^*(-j). \quad (5.28)$$

Then, the  $T$ -spaced feedforward filter  $\underline{\mathbf{V}}$  can be obtained from solving  $\mathbf{R}\mathbf{V}^* = \mathbf{P}$ , and the feedback filter  $\mathbf{w}_b$  from  $\mathbf{w}_b^* = -\mathbf{B}\mathbf{V}^*$ . We refer this as a matched filtered non-Toeplitz DFE (NT-DFE). Note that this solution utilizes all the channel state information during the last  $\tilde{\Delta}(T/2)$  period. When time invariance of the channel over the decision delay is assumed, the channel matrix  $\mathbf{H}_l(k)$  of (5.3) becomes block Toeplitz, and all the epoch terms inside the parenthesis of (5.26) - (5.28) can be ignored. We refer this as a matched filtered Toeplitz DFE (T-DFE).

In fact, we have shown that the matched filtering  $L$ -diversity combining DFE

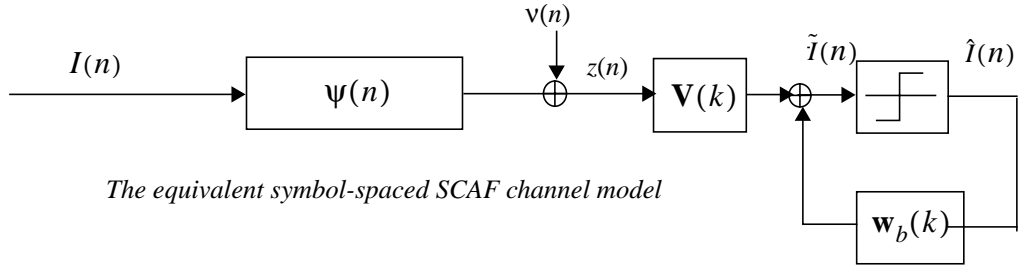
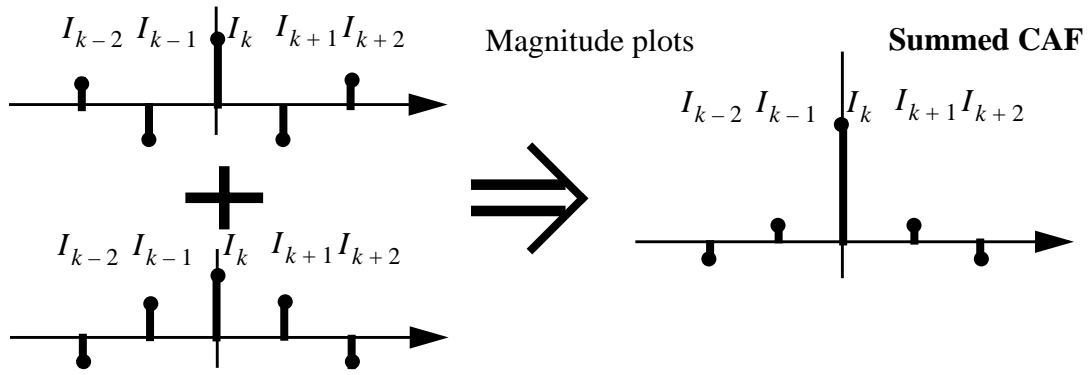


Figure 5-4 The equivalent symbol-spaced, single channel DFE setting.

problem can be treated as an equivalent single channel  $T_B$ -spaced DFE problem, as depicted in Figure-2. Let  $n$  denote the symbol spaced epoch. The equivalent  $T$ -spaced channel is a  $[(2N_g - 1) \times 1]$  vector  $\boldsymbol{\psi}(n)$  whose elements are the  $\{\psi_a(n)\}_{a < |N_g|}$  of (5.25), i.e.,  $\psi_{-N_g+1}(n)$  is the first element of  $\boldsymbol{\psi}(n)$ ; and the equivalent  $T$ -spaced noise is  $v(n)$  with  $\sigma_n^2 \cdot \psi_i(n)$  as its autocorrelation function. Then, the  $T$ -spaced sampled  $z(n)$  is  $z(n) = \boldsymbol{\psi}(n)^T \mathbf{I}(n) + v(n)$ , where  $\mathbf{I}(n) := [I(n) \ I(n-1) \ \dots \ I(n-2N_g+1)]^T$ . Now, for a  $[N_f \times 1]$  input vector  $\mathbf{z}(n) = [z(n) \ \dots \ z(n-N_f+1)]^T$ , the predecision value  $\tilde{I}(n)$  analogous to (5.2) can be defined as  $\tilde{I}(n) = \mathbf{z}^T(n) \mathbf{V}(n) + \mathbf{I}_b^T(n) \mathbf{w}_b(n)$ . Then, following the standard procedure analogous to (5.3)-(5.9) the matched filtered solution of (5.26) - (5.28) can be reproduced.

### 5.3.4 The equivalent single channel

The matched filtered diversity combining DFE has lower complexity than the straightforward approach and does not suffer from the large eigenvalue spread that is observed in the straightforward solution. Note that the dimension of the correlation matrix  $\mathbf{R}$ ,  $[N_f \times N_f]$ , stays the same for any diversity order. Thus, there are no cross-correlation



As  $L \rightarrow \infty$ , the SCAF channel becomes ISI-free, a AWGN channel.

Figure 5-5 Addition of the symbol-rate sampled matched filter outputs.

submatrices to spread the eigenvalues. Thus, the eigenvalue spread of the correlation matrix is now fully determined by the SCAF vector  $\psi(n)$ . Also note that SCAF values  $\{\psi_a(n)\}_{a \neq 0}$  in (5.25) correspond to ISI terms relative to the phase equalized main term  $\psi_0(n)$ , and that their energies relative to the main term decrease for increasing  $L$ . Thus, the correlation matrix tends to be more stable for increasing  $L$ . This indicates that the explicit diversity reduces the intersymbol interference problem. In fact, if  $L \rightarrow \infty$ , the equivalent single channel becomes AWGN. For our block adaptive strategy, the use of matched filtered diversity combining also helps stabilize the DFE computation algorithm; it is obvious since the ISI is reduced as  $L$  is increased. Thus, the DFE coefficients obtained from the channel estimates become less susceptible to channel estimation noise enhancement.

Comparing the matched filtered NT-DFE and T-DFE, the NT-DFE is optimal because it uses all the channel state information during the decision delay which are provided by the channel interpolation. The T-DFE uses only partial information and is thus suboptimal but has lower complexity than the NT-DFE. The NT-DFE provides a

performance advantage over the T-DFE only when the channel is in fast fading and tracked with a reasonable accuracy. The NT-DFE used in an ideal channel reference mode (the use of perfect channel) can serve as a benchmark to identify the source of irreducible symbol detection errors in fast fading. In the next Section, the above comparisons will be made through computer simulations.

## 5.4 Simulation Results and Discussion

We now discuss the simulation results. For computer simulation of the developed systems for wireless channels, we developed the custom-made C++ routines. The wireless channel virtually has an infinite set of possible impulse responses for each channel with a given multipath power delay profile. Therefore, the performance evaluation of communications systems for wireless channels may take a large amount of CPU time until properly averaged simulation results are obtained. For this reason, a system simulation code that can be compiled is highly recommended.

### 5.4.1 BER performance in slow fading

In Figure 5-6, the BER performances of two receivers are compared with the theoretical matched filter bounds<sup>1</sup> (MFB) developed in Chapter 6. The MFB is the lowest attainable bound since it is obtained assuming the transmitted pulses are far enough apart so that no ISI occurs. *Flat* fading indicates the matched filter bound for the single tap Rayleigh fading channel, and was given as a reference.

In Figure 5-6, “LSE and interpolation NT-DFE” refers to the use of least squares channel estimation, channel tracking by interpolation, and non-Toeplitz DFE. “RLS channel tracking T-DFE” refers to the use of a recursive least squares algorithm to track the

---

1. Symbol error rate probabilities developed in Chapter 6 can be translated into the bit error rate results with a minor modification.

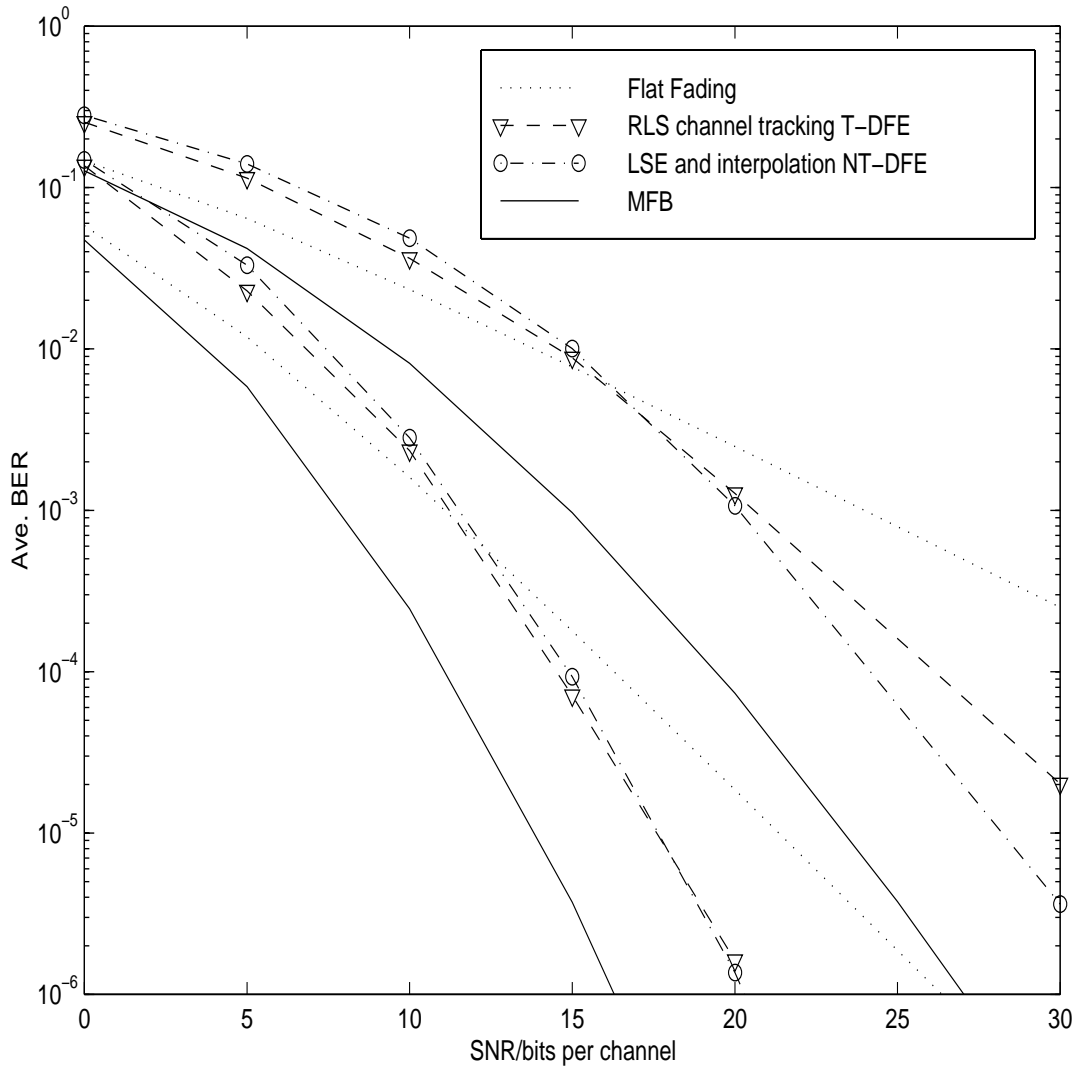


Figure 5-6 Average QPSK BERs in slow fading: RLS channel tracking T-DFE and LSE NT-DFE compared with theoretical matched filter bounds.

time-varying channel (i.e., without channel interpolation), and the Toeplitz DFE for symbol detection. The T-DFE is used since the channel states during the decision delay are not available with the recursive adaptation. With regard to the use of RLS algorithm, the channel-estimate approach, instead of a conventional direct adaptation on the DFE coefficients without channel estimation, is selected since the channel-estimate based DFE (without diversity) has been shown to be more effective than the direct DFE adaptation [54][67]. Specifically, we use the exponential windowing RLS algorithm from [67]. To be a fair comparison the same known training blocks are inserted in the data stream. Thus, during the training segment the RLS algorithm and DFE filters are refreshed at the same rate. Furthermore, the exponential weighting factor  $\omega$  of the RLS algorithm is optimized at various SNRs, fade rates, and channel lengths. For this, the following equation is adopted from [67],

$$SNR = \frac{(N_c + 1) (1 - \omega)^3}{(2f_{dm}\pi T)^2 (1 + \omega)^2}. \quad (5.29)$$

The filter orders used in the simulation are  $(\tilde{N}_g, N_f, N_b) = (20, 5, 5)$ . The channel is in slow fading at  $f_{dm} = 10$  Hz ( $f_{dm}T = 0.00042$ ). We note that the slopes of BER curves for both methods (e.g. about  $10^{-2}$  per 10 dB SNR for  $L = 1$ ) are close to those of their MFBs and steeper than those (e.g.  $10^{-1}$  per 10 dB for  $L = 1$ ) of the theoretical flat fading channel. This indicates that both receivers take advantage of the implicit diversity gain, which is inherent in the frequency selective channel. The RLS T-DFE and LSE NT-DFE show comparable performance in slow fading.

## 5.4.2 BER performance in fast fading

In Figure 5-7, BER performance of RLS T-DFE with DQPSK signaling is evaluated for  $f_{dm} = \{10, 50, 100\}$ . Since T-DFE ignores the channel variation over the feedforward

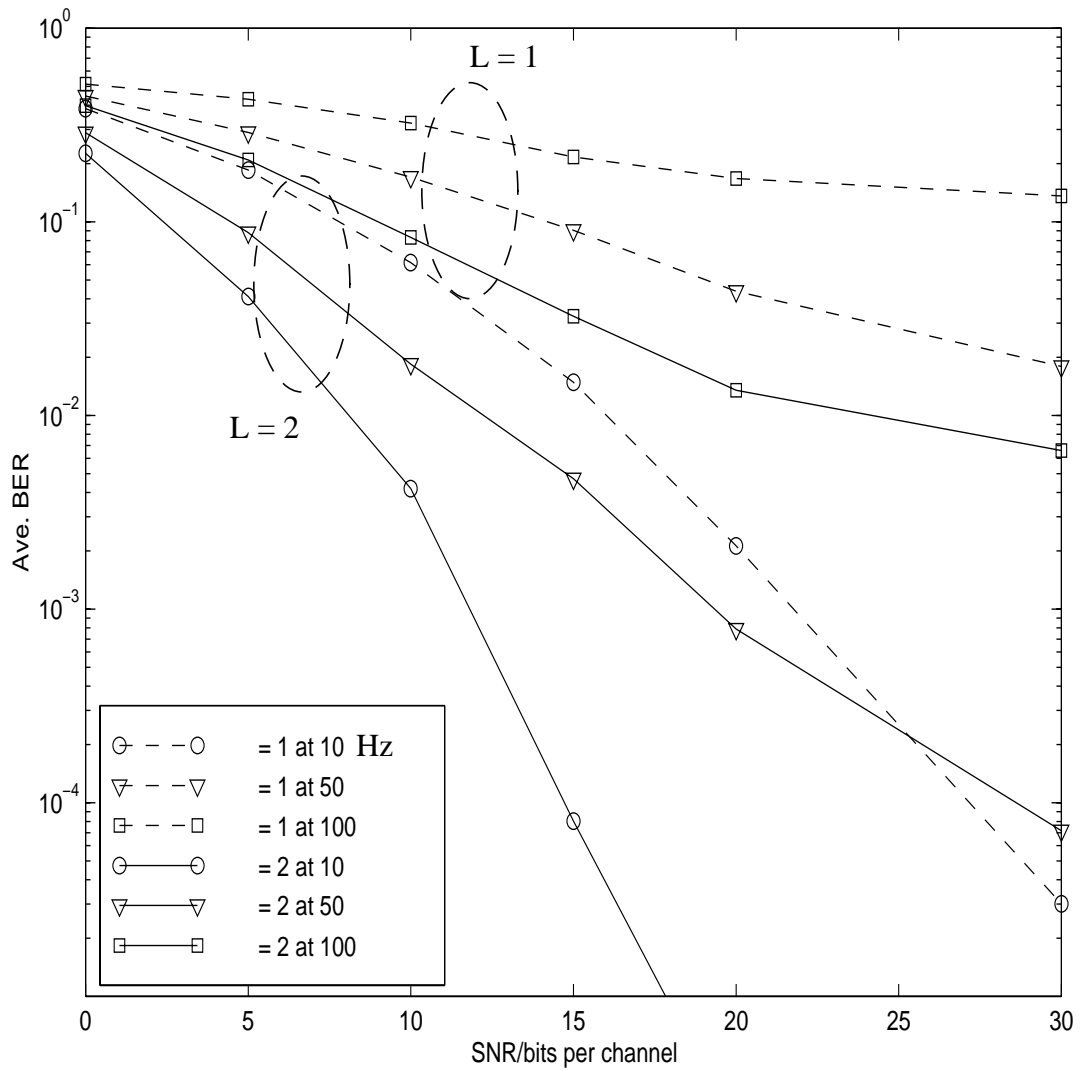


Figure 5-7 Average DQPSK BER simulation: Toeplitz DFE with RLS channel tracking.

filter length, longer filters might become counter productive in fast fading (this behavior is also observed in [58] without diversity). Thus, at  $f_{dm} = 100$  Hz we use shorter filters of  $(\tilde{N}_g, N_f, N_b) = (12, 4, 4)$  which have been determined to be optimal from our simulations.

We observe that at  $f_{dm} = 100$  Hz the irreducible BERs are too high (0.1 for  $L = 1$  and 0.01 for  $L = 2$ ) to be of any practical use. Therefore, we confirm that RLS actually fails to track the three-tap fast Rayleigh fading channel.

In Figure 5-8, the BER performance of LSE and MAP NT-DFE receivers with DQPSK signaling is evaluated at  $f_{dm} = 100$  Hz. “MAP NT-DFE” refers to the use of maximum *a posteriori* channel estimation, channel tracking by interpolation, and non-Toeplitz symbol detection. We note that both receivers show a superior and robust BER performance against the fast fading. LSE and MAP NT-DFE curves are not even flat out up to 30 dB. Moreover, we note the significance of NT-DFE, which is illustrated by “the ideal CIR NT-DFE curves” (the use of perfect channel at all epochs) since the NT-DFE exhibits no sign of irreducible error floors. T-DFE would display irreducible error floors even with the ideal CIR supplied. An example of this can be found in [58] where a DFE receiver, using T-DFE without diversity, shows relatively high irreducible BER floors even in the ideal channel reference mode (the use of perfect channel estimates at all epochs).

We observe that LSE and MAP NT-DFE curves show less than 1 dB difference below a BER of  $10^{-3}$ . This suggests that the use of LSE is a reasonable design choice, at least for an uncoded system. In addition, we note that the throughput rate at this BER is  $\frac{B - N_t}{B} = \frac{80 - 11}{80} = 0.8625$ .

### 5.4.3 The sources of BER floor

In Figure 5-9, the causes of the BER floor at the fastest fading rate can be distinguished. In particular, the non-Toeplitz-DFE and the Toeplitz-DFE are compared, and three modes of obtaining channel impulse responses are also compared. The three modes

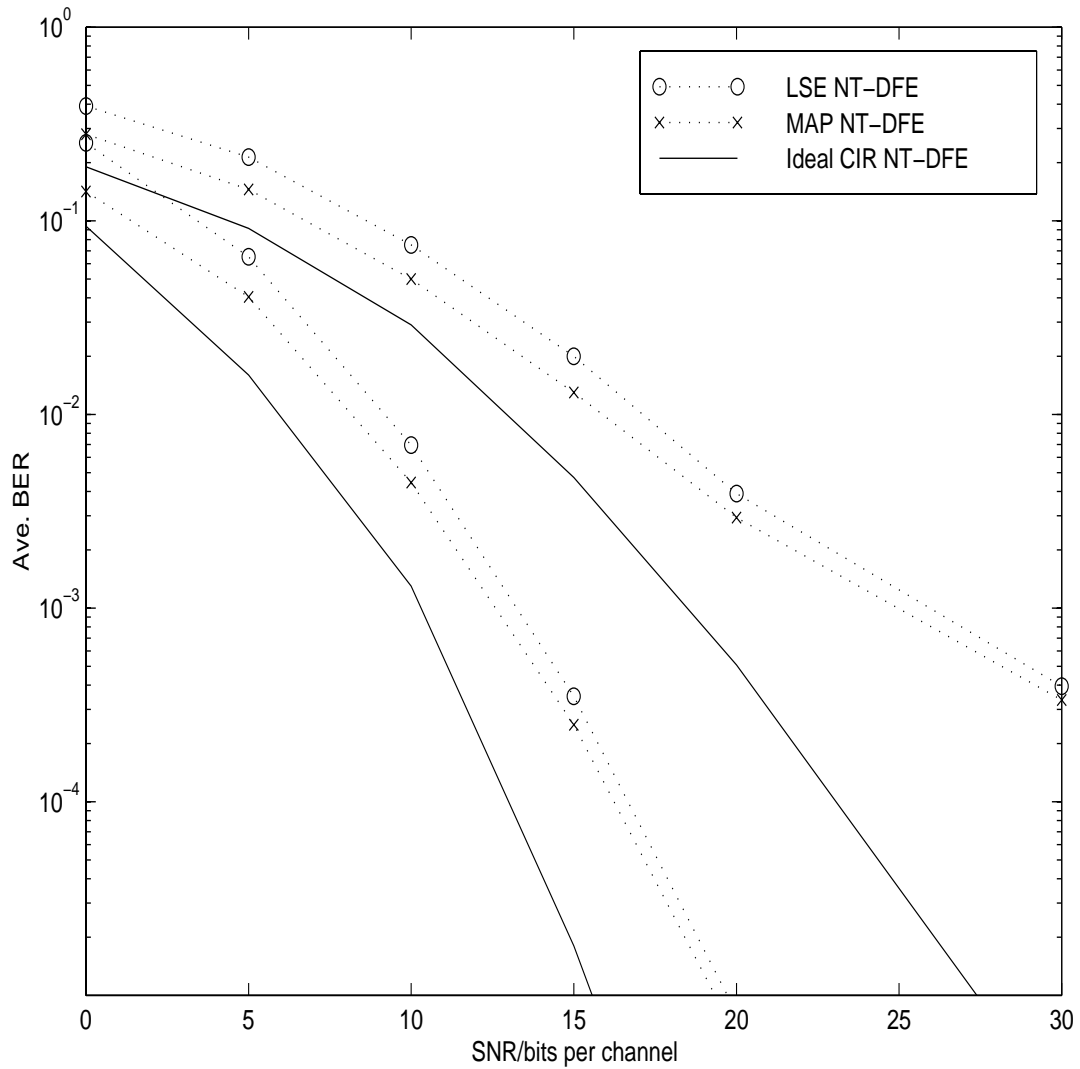


Figure 5-8 Average DQPSK BER performance: LSE and MAP NT-DFE with channel tracking by interpolation. Ideal CIR NT-DFE implies NT-DFE with no channel estimation errors at all time.

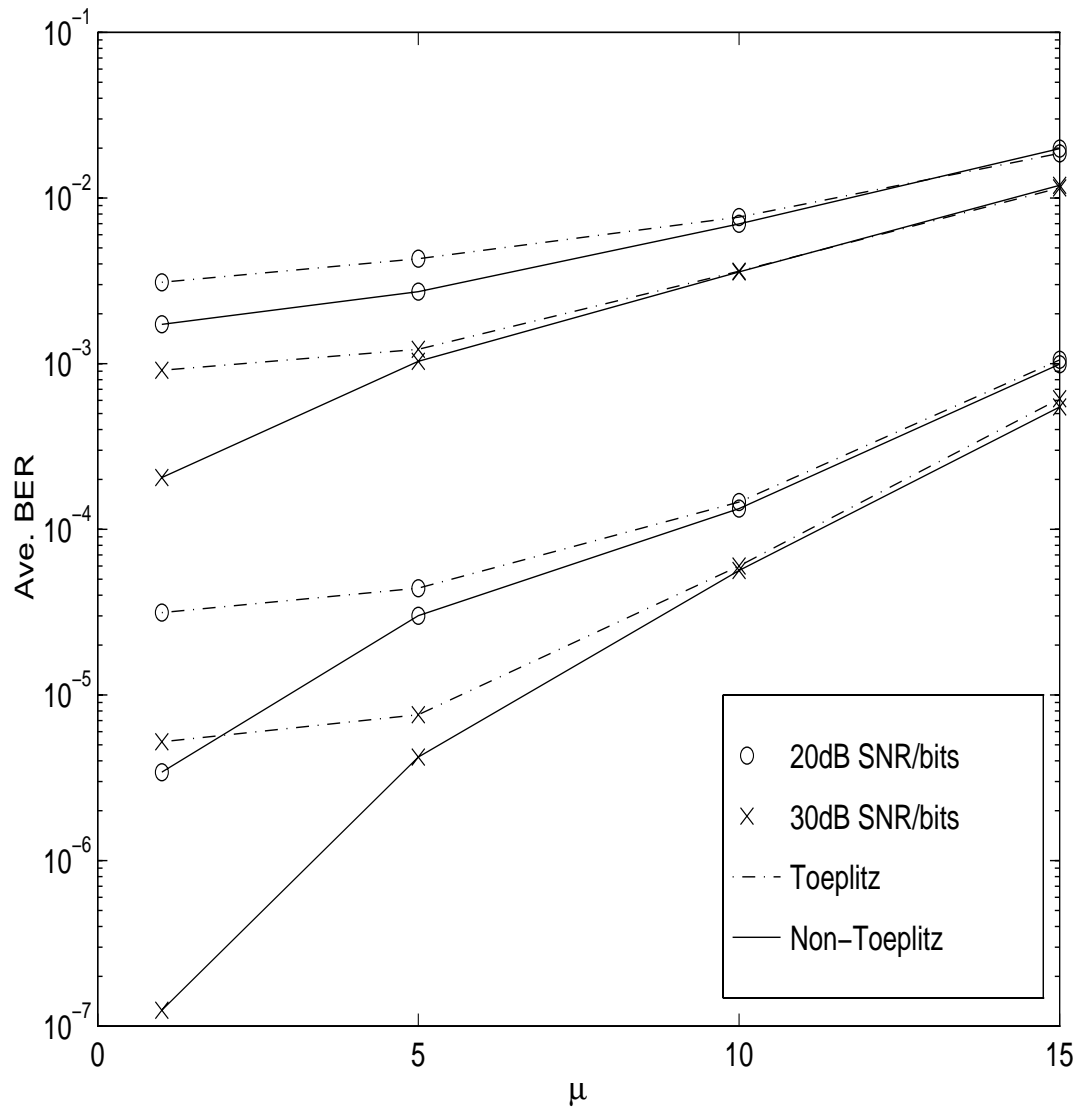


Figure 5-9 Sources of BER floors

are the MAP channel estimation and interpolation tracking, interpolation on perfect channel estimates, and the ideal channel reference. Comparison of these curves should identify the main cause of the symbol detection errors at the high SNRs. The optimal filter orders for the T-DFE are again  $(\tilde{N}_g, N_f, N_b) = (12, 4, 4)$ . The filter orders used for the NT-DFE are  $(20, 5, 5)$ .

Not much difference is observed for low SNR. Thus, we pay attention to BERs at 30 dB. First, note that the T-DFE curves entail higher BER floors. Even the ideal CIR T-DFE produces a higher BER floor than the MAP NT-DFE does. This illustrates the detrimental consequence of ignoring the channel variation during the decision delay in the DFE coefficient computation. Second, by comparing the NT-DFE curves it is demonstrated that the irreducible BER floors are mainly due to the interpolation errors. As it seems natural that the interpolator performs poorly in the middle of the data segment, thus, the decision errors occur predominantly during the middle of the data frame. This problem persists even at  $B = 40$  for which the BER at 30 dB is about  $3 \times 10^{-5}$  (not shown in the figures). Thus, there is still room for improvement.

#### **5.4.4 The suboptimal T-DFE and the DFE update periods.**

In Figure 5-10, the impact on BER from increasing the DFE update periods  $\mu$  is investigated at  $f_{dm}=100$  Hz, where  $\mu$  is the number of symbol periods between any two DFE coefficients updates. Again, the BER performances of the Toeplitz and non-Toeplitz DFE are compared. We use the optimal filter orders,  $(\tilde{N}_g, N_f, N_b) = (12, 4, 4)$ , for the Toeplitz case. For the non-Toeplitz case  $(20, 5, 5)$  are used for  $\mu = 1$ , while shorter filter orders  $(16, 4, 4)$  are used for other values of  $\mu$ . The MAP estimator is used for both. First, note that the performance difference of the two deepens for a higher diversity order and for a higher SNR, whereas it becomes almost negligible for  $L = 1$  and for low SNR. Second, the non-Toeplitz method maintains its superiority to the Toeplitz only for  $\mu = 1$ , as the BER gain

quickly disappears for  $\mu > 1$ . Thus, if a large  $\mu$  has to be chosen for a lower computational complexity, then the use of T-DFE is suitable.

### 5.4.5 Computational complexities

In Table 5-1: we summarize the number of complex multiplications and divisions required for the RLS T-DFE, LSE T-DFE, and LSE NT-DFE. The first and second rows indicate the required number of operations for the channel tracking techniques. For the channel tracking by interpolation, we assume that the  $T/2$ -sampled sinc function is stored. Then, the interpolated channel  $\mathbf{b}$  can be obtained from  $N_R Q$  complex multiplications and the convolution of  $\underline{b}$  and  $\underline{f}$  requires another  $N_R \tilde{N}_g$ . The matched filter coefficient vector  $\mathbf{M}_l$  can be obtained without any computation since it is a pure mapping from the interpolated overall channel. The third row indicates the summation of the number of operations required to form the summed channel autocorrelation function, the correlation matrix, the cross-correlation vector, and the feedback filter matrix. The fourth row is the required computations to solve for the feedforward filter with length  $N_f$  provided the Cholesky factorization [24] is used. The last row are example calculations for  $L = 1, 2$ ,  $\mu = 1$ , with a typical set of filter lengths and channel estimation parameters,  $(\tilde{N}_g, N_f, N_b, B, Nt, Nc) = (12, 6, 4, 4, 80, 11, 6)$ . For the T-DFE receivers, required numbers of operations for a larger DFE update period of  $\mu = 5$  are also calculated and presented inside the parenthesis.

## 5.5 Concluding Remarks

We have presented robust channel estimation methods which require little training overhead over the fast Rayleigh fading dispersive channel. It has been shown through simulations that channel tracking by interpolation along with our proposed channel

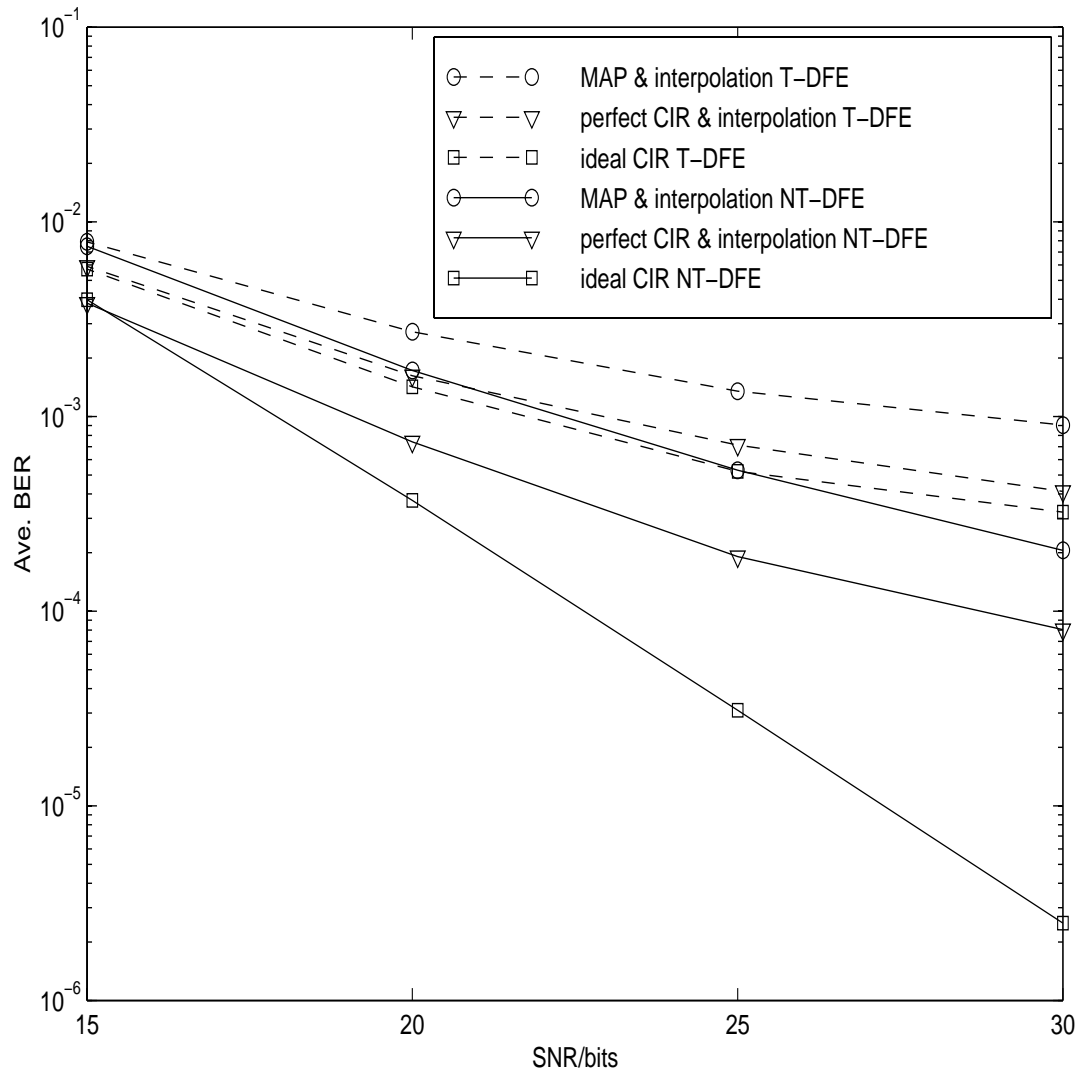


Figure 5-10 Average QPSK BER simulations to determine the source of error floor

estimation method is significantly better than the RLS channel tracking method and previously published feedforward channel estimation methods in terms of both the throughput and the BER performance.

For the block adaptive diversity combining DFE scheme we have proposed the matched filtered approach because of its stable performance in the presence of channel estimation errors. The matched filtered DFE simplifies the  $L$ -diversity combining decision feedback equalizer into an equivalent single-channel DFE problem. This provides a reduced computational burden in tracking the optimum coefficients of the receiver and leads to a well-conditioned correlation matrix.

We have derived a matched filtered diversity combining NT-DFE which takes into account the channel variation over the decision delay. This NT-DFE can obtain the full benefit of the channel interpolation and thus provides a benchmark for performance. While optimal, the NT-DFE incurs relatively high computational complexity, and thus for a suboptimal but low complexity solution we propose the use of the T-DFE which still provides better performance than the RLS algorithm.

**Table 5-1: The number of complex multiplications and divisions required**

	RLS channel tracking T-DFE	LSE T-DFE	LSE NT-DFE
Channel estimation	$9L\tilde{N}_g + 6$	$\frac{(LmN_R)}{(B - Nt)}$	$\frac{(LmN_R)}{(B - Nt)}$
Channel tracking by the interpolation	N/A	$2LN_R(Q + \tilde{N}_g)$	$2LN_R(Q + \tilde{N}_g)$
Forming the SCAF, the corr. matrix, the cross-corr. vector, and the feedback matrix	$\frac{L}{2}(\tilde{N}_g^2 + \tilde{N}_g) + N_f(N_g + N_f - 1)$	$\frac{L}{2}(\tilde{N}_g^2 + \tilde{N}_g) + N_f(N_g + N_f - 1)$	$L(\tilde{N}_g^2 + \tilde{N}_g - 1) + N_f^2(N_g + N_f) - \frac{1}{6}(4N_f^3 + 9N_f^2 - N_f)$
Feedforward filters	$\frac{1}{6}(N_f^3 + 9N_f^2 - 4N_f) + N_f$	$\frac{1}{6}(N_f^3 + 9N_f^2 - 4N_f) + N_f$	$\frac{1}{6}(N_f^3 + 9N_f^2 - 4N_f) + N_f$
Feedback filter	$N_f N_b$	$N_f N_b$	$N_f N_b$
$L = 1, 2$ and $\mu = 1$ ( $\mu = 5$ )	279 (147) 465 (271)	263 (53) 436 (88)	464 714

The last row of table show example calculations for  $(\tilde{N}_g, N_f, N_b, B, Nt, Nc) = (12, 6, 4, 4, 80, 11, 6)$ ,  $N_g = \tilde{N}_g/2$  and  $m = Nt - Nc + 1 = 6$ . The shaded region implies that the numbers of multiplication can be divided by  $\mu$ , where  $\mu$  is the DFE filter update periods in units of symbol period.

## Chapter 6

# Matched Filter Bounds and Spectral Efficiency

This Chapter provides theoretical bounds on the detection probability of the transceiver schemes discussed in the dissertation. They are matched filter bounds which provide the best attainable detection performances in terms of bit error probability or symbol error probability as a function of SNR. The detection probability curves obtained from the matched filter analyses for any given modulation scheme indicate the benchmark performance, which may or may not be obtainable in reality with the use of any particular detection scheme. These matched filter bounds, therefore, will provide meaningful information, when compared with the bit error rate (BER) or symbol error rate (SER) curves obtained from extensive computer simulations.

The spectral efficiency of a channel indicates the capacity (bits/sec/Hz) of the given channel. In this Chapter, the spectral efficiency of the multipath fading ISI channels will be computed using the matched filter output SNR. This will provide insights into how to design a power-and rate-adaptation protocol. The protocols which operating between the

transmitter and the receiver, determine at a particular instant of time how many information bits/sec/Hz and how much power should be used to transmit a symbol across the channel while insuring a particular detection probability.

The matched filter bounds and spectral efficiency calculation techniques provided in this Chapter are specific to  $q$ -ary QAM signals and the three-tap Rayleigh fading diversity channel models developed in Chapter 2. However, they should be generally applicable to any frequency-selective (or non-selective) fading channels and for any linear modulation.

## 6.1 Matched Filter Bound

Based on the matched filter theory [73], the detection SNR of any linearly filtered received signal is maximized when the matched filter is applied to the received signal perturbed by additive noises. The matched filter bound analyses are based on the ideal assumptions that the symbol detection SNR is maximized to achieve the input SNR such that the ideal detector uses a perfect channel estimation and is free from intersymbol interference by the assumption of a single-shot transmission. Therefore, it will provide the benchmark detection performance, which may or may not be achievable. Nevertheless, the matched filter bounds provide invaluable information when compared with the simulation results of the proposed transceivers developed in Chapters 4, 5 and 7.

The derivation provided in this section closely follows the eigenvalue decomposition methods provided by Fuyun Ling [74] and Proakis [33]. New results are that the matched filter bounds are obtained for  $q$ -QAM signalling,  $q$  is 4, 16, and 64, and for the three-tap half symbol spaced diversity channels.

Before starting with the derivations, let us review some of the important assumptions we make in the derivation:

- **Assumption 1:** Matched filter bound is based on a single-shot symbol transmission and detection such that it ignores any intersymbol interference.
- **Assumption 2:** The matched filter theory holds with the colored noise; however in this Chapter we assume that the noise is white, following the same channel conditions given in Chapter 2.
- **Assumption 3:** The channel is assumed to be **time-invariant** over the duration of the overall pulse, which include the channel, the transmit shaping and the receive filters.
- **Assumption 4:** The half-spaced fading components are mutually uncorrelated. The uncorrelated scattering assumption of the wide-band multipath components explained in Chapter 2 is the basis for this assumption.

Based on the assumptions, we first obtain the matched filter bounds for a single channel case from which results for multiple diversity receive channels can be evaluated. Recalling the channel model developed in Section 2.3, the received signal for a single-shot transmission of a pulse modulated by the information symbol  $I_0$  can be written as

$$x_s(t) = \sum_{p=0}^{N_R-1} b_p f(t - pT_B) I_0 + n(t) = h(t) I_0 + n(t), \quad (6.1)$$

where

- $h(t)$  denotes the signal part of received signal  $-\infty < t < \infty$  due to the single-shot transmission of the symbol  $I_0$  at  $t = 0$ <sup>1</sup>,
- $I_0$  denotes the transmitted  $q$ -ary QAM symbol

---

1. A non-causal representation of transmission and reception of the signal is used for brevity.

- $b_p$  denotes the  $p$ -th component of the  $T_B/2$ -spaced delay dispersion of the channel, which is non-time-varying following **Assumption 3**; we use  $N_R = 3$ . In addition, from the assumption that the channel is a low-pass filtered version of the wide-band channel, whose low-pass bandwidth is  $2/T_B$  as assumed in Chapter 3, each components  $b_p$  is mutually uncorrelated. Thus, the uncorrelated scattering assumption still holds. Thus, we have **Assumption 4**,

$$\begin{aligned} E\{b_p^* b_q\} &= \phi_{c, T_B/2}(p) \delta(p - q) \\ &= \alpha_p^2 \delta(p - q) \end{aligned} \quad , \quad (6.2)$$

where we denote  $\alpha_p^2 = \phi_{c, T_B/2}(p)$  for the  $T_B/2$ -spaced sampled, average multipath power delay profile of the low-pass MPDP.

- $f(t)$  is a square root raised cosine filter as defined in (2.26), and  $F(w)$  denotes the Fourier transform of  $f(t)$ ,

$$F(w) = \int_{-\infty}^{\infty} f(t) \exp(-j\omega t) dt \quad (6.3)$$

- $n(t)$  denotes the zero-mean, complex-valued additive white noise with double-side power spectral density of  $N_o$ .

Now consider the Fourier transform of  $h(t)$ , which is denoted as

$$H(w) = F\{h(t)\} = F(w) \sum_{p=0}^{N_R-1} b_p \exp\left(-j\omega p \frac{T_B}{2}\right), \quad (6.4)$$

and the complex-conjugate  $H^*(w)$  can be written as

$$H^*(w) = F^*(w) \sum_{p=0}^{N_R-1} b_p^* \exp\left(j\omega p \frac{T_B}{2}\right). \quad (6.5)$$

Based on the matched filter theory [73],  $H^*(w)$  is the optimal filter that maximizes the detection SNR. Now applying the matched filter response  $H^*(w)$  to the received signal  $x(t)$ , we have the matched filtered signal which can be written in the Fourier transform domain as

$$H^*(w)X(w) = H^*(w)H(w)I_0 + H^*(w)N_o. \quad (6.6)$$

The inverse Fourier transform of (6.6) provides the time-domain response of the matched filtered signal. Now notice that the autocorrelation function channel, which is the inverse Fourier transform  $\frac{1}{2\pi} \int_{-\infty}^{\infty} H^*(w)X(w) \exp(jwt) dw$ , is Hermitian symmetric around  $t = 0$ . Thus, by sampling the matched filtered output response at  $t = 0$ , we achieve the optimal matched filter output.

### 6.1.1 Sampled, matched filter output

Now let  $z_s$  denote the received signal, sampled at  $t = 0$ , and then the sufficient statistics for the detection of  $I_0$  is to consider the following simple equation

$$z_s = A_s I_0 + v_s, \quad (6.7)$$

where

- $A_s$  denotes the value of the Hermitian symmetric autocorrelation channel sampled at time  $t = 0$ ; it is a random variable and implies the instantaneous energy of the cascade filter, the channel and transmit-shaping filters, and can be written as

$$\begin{aligned} A_s &= \frac{1}{2\pi} \int_{-\infty}^{\infty} H^*(w)X(w) \exp(jwt) dw \Big|_{t=0} = \frac{1}{2\pi} \int_{-\infty}^{\infty} H^*(w)H(w) dw \\ &= \frac{1}{2\pi} \int_{-\infty}^{\infty} F^*(w)F(w) \sum_{p=0}^{N_R-1} b_p^* \exp\left(jwp \frac{T_B}{2}\right) \sum_{q=0}^{N_R-1} b_q \exp\left(-jwq \frac{T_B}{2}\right) dw \end{aligned} \quad (6.8)$$

From the uncorrelated scattering assumption (**Assumption 4**) above, (6.8) can be

written as

$$\begin{aligned}
 A_s &= \sum_{p=0}^{N_R-1} \sum_{q=0}^{N_R-1} b_p^* b_q \frac{1}{2\pi} \int_{-\infty}^{\infty} |F(w)|^2 \exp\left(-jw(q-p)\frac{T_B}{2}\right) dw \\
 &= \sum_{p=0}^{N_R-1} \sum_{q=0}^{N_R-1} b_p^* b_q f_{rc}\left(t = (q-p)\frac{T_B}{2}\right)
 \end{aligned} \tag{6.9}$$

where  $f_{rc}(t)$  is the raised cosine filter response,

- $I_0$  denotes the transmitted  $q$ -ary QAM symbol,  $E(I_0) = 0.0$  and

$$Var(I_0) = \frac{2(q-1)}{3} \tag{6.10}$$

- $v_s$  denotes the matched filtered noise output sampled at  $t = 0$  which is

$$v_s = \int_{-\infty}^{\infty} n(\tau)h(t-\tau)d\tau \Big|_{t=0}; \tag{6.11}$$

thus  $v_s$  is zero-mean with  $Var(v_s) = N_0 \cdot A_s$ .

(6.7) provides the sufficient information we need to compute the detection performance of the single-shot matched filter receiver. Note that  $A_s$  is the instantaneous energy of the cascade filter and is a random variable since the channel  $\mathbf{b}(k)$  at a particular time  $k$  is a random vector.

### 6.1.2 Square-QAM symbol error probability

In this section, for a particular value  $A_s$  and  $N_0$  the symbol error probability will be evaluated for square  $q$ -ary QAM signaling, i.e.  $q = 2^k$  where  $k$  is even. Then, referring to Figure 6-1 the following relationships are useful:

- The average energy of the square-QAM signaling set can be computed as, using (6.10) and the definition given in Figure 6-1

$$E_s = E(I_0^2) \left( \frac{A_s}{\sqrt{2}} \right)^2 = \frac{2(q-1)}{3} \left( \frac{A_s}{\sqrt{2}} \right)^2 = \frac{q-1}{3} A_s^2. \quad (6.12)$$

- The minimum Euclidean distance of the square-QAM constellation is

$$d_{min} = \sqrt{2} \cdot A_s. \quad (6.13)$$

- The instantaneous signal to noise ratio is

$$\frac{\text{signal power}}{\text{noise power}} = \gamma = k \cdot \gamma_b = \frac{E_s}{A_s \cdot N_o} = \frac{(q-1) A_s}{3 N_o}, \quad (6.14)$$

where  $\gamma$  is the instantaneous SNR,  $k = \log_2(\sqrt{q})$  the number of bits per symbol,  $\gamma_b$  is the instantaneous SNR/bit.

Then, the  $q$ -ary square-QAM symbol error probability at a particular channel gain  $A_s = a$ , can be computed as

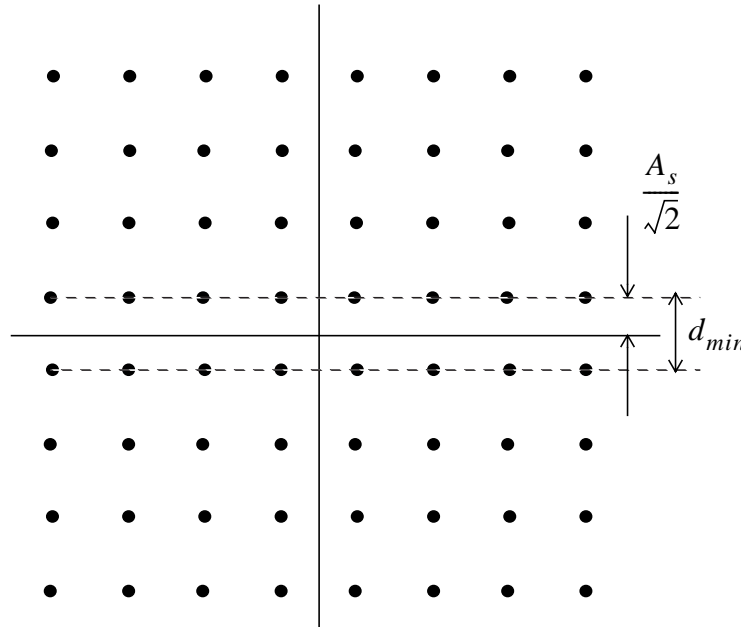


Figure 6-1 64-QAM illustration.  $A_s$  denotes the instantaneous combined channel gain.

$$P_q(A_s = a) = 2\left(1 - \frac{1}{\sqrt{q}}\right) \operatorname{erfc}\left(\frac{d_{\min}(a)}{2\sqrt{\operatorname{Var}(v_s)}}\right) \cdot \left\{1 - \frac{1}{2}\left(1 - \frac{1}{\sqrt{q}}\right) \operatorname{erfc}\left(\frac{d_{\min}(a)}{2\sqrt{\operatorname{Var}(v_s)}}\right)\right\}, \quad (6.15)$$

which can be tightly upper-bounded by the first term as indicated in Figure 6-2. Note in Figure 6-2 the approximation is asymptotically efficient and very tight even at low SNR region. Thus, we have

$$P_q(a) \leq 2\left(1 - \frac{1}{\sqrt{q}}\right) \operatorname{erfc}\left(\frac{d_{\min}(a)}{2\sqrt{aN_o}}\right). \quad (6.16)$$

Now, solving for  $a$  in (6.12), i.e.,  $a^2 = \frac{3}{(q-1)}E_s$  we have

$$d_{\min}(a) = \sqrt{2}a = \sqrt{\frac{2 \cdot 3}{(q-1)}E_s}, \quad (6.17)$$

but using (6.14), (6.17) is

$$d_{\min}(a) = \sqrt{\frac{2 \cdot 3}{(q-1)}ak\gamma_b N_o}, \quad (6.18)$$

Then, the tight upper bound of symbol error probability (6.16) can be written as

$$P_q(a) = 2\left(1 - \frac{1}{\sqrt{q}}\right) \operatorname{erfc}\left(\sqrt{\frac{3}{2(q-1)}k\gamma_b}\right), \quad (6.19)$$

or simply

$$P_q(a) = 2\left(1 - \frac{1}{\sqrt{q}}\right) \operatorname{erfc}\left(\sqrt{\frac{a}{2N_o}}\right). \quad (6.20)$$

### 6.1.3 Average symbol error probability for square-QAM

Now, the symbol error probability, averaged over the ensemble of the channel  $\mathbf{b}(k)$  or equivalently that of  $A_s$ , can be computed from

$$\overline{P}_q(\overline{\gamma}_b) = \int_0^\infty P_q(a) \operatorname{Pr}(A_s = a) da, \quad (6.21)$$

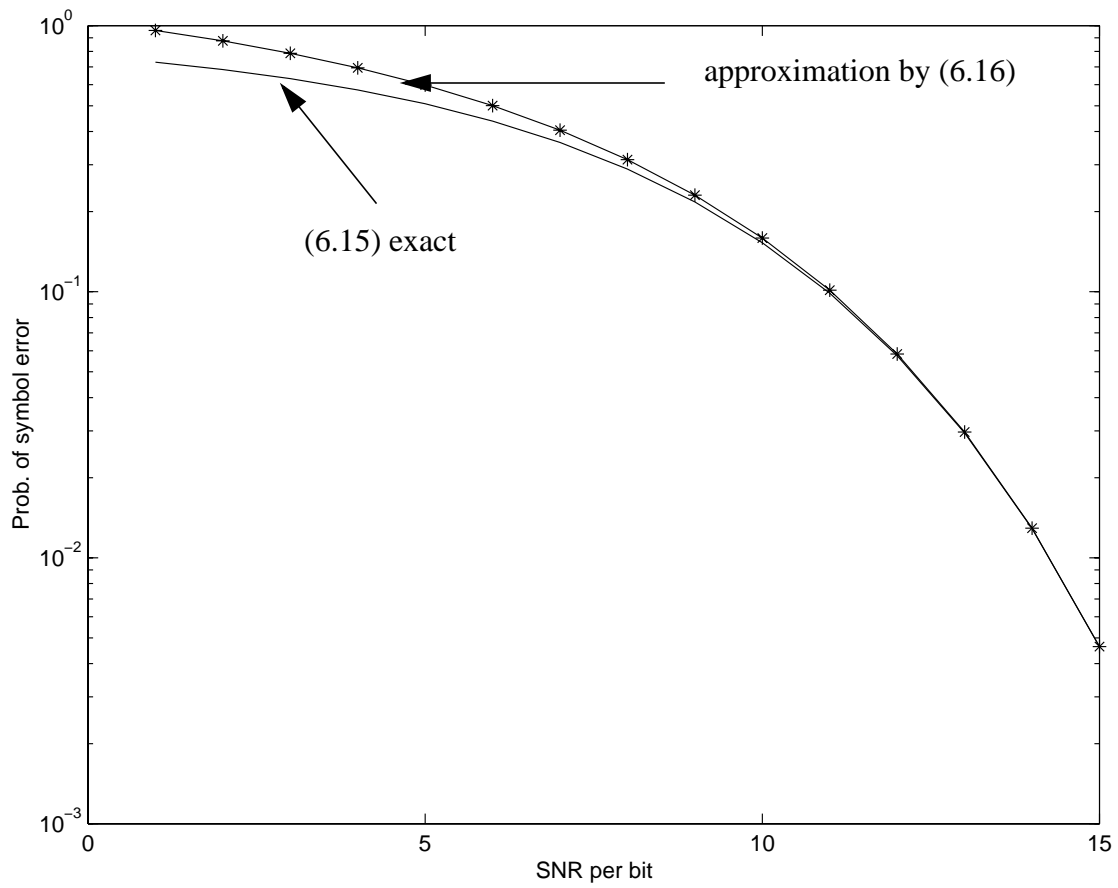


Figure 6-2 Illustration of upper bound of the square QAM symbol error rate

where  $\overline{P}_q(\overline{\gamma}_b)$  denotes the averaged symbol error probability of  $q$ -ary QAM system for average input SNR which is

$$\overline{\gamma}_b = E\{\gamma_b\} = \frac{(q-1)}{3kN_o} E\{A_s\} , \quad (6.22)$$

at a given noise spectral density  $N_0$ . Thus, we need to know the distribution function of the random variable  $A_s$ .

From (6.9), we may note that the random variable can be written as follows:

$$A_s = (b_0^* \ b_1^* \ b_2^*) \begin{bmatrix} f_{rc}(0) & f_{rc}(T_B/2) & f(T_B) \\ f_{rc}(T_B/2) & f_{rc}(0) & f_{rc}(T_B/2) \\ f(T_B) & f_{rc}(T_B/2) & f_{rc}(0) \end{bmatrix} \begin{pmatrix} b_0 \\ b_1 \\ b_2 \end{pmatrix}. \quad (6.23)$$

Denote the matrix in the middle as  $\mathbf{F}_{rc}$ . Now, from (2.15) and (6.2) we know that a fading channel tap can be written as  $b_i = \alpha_i \rho$ , the multiplication of an attenuation and the unit-variance, complex-valued Gaussian random variable  $\rho$ . And, thus, we can write the channel vector  $\mathbf{b}$  as

$$\mathbf{b} = \alpha \rho = \begin{pmatrix} \alpha_0 & 0 \\ \alpha_1 \\ 0 & \alpha_2 \end{pmatrix} \begin{pmatrix} \rho_0 \\ \rho_1 \\ \rho_2 \end{pmatrix}, \quad (6.24)$$

where  $E(\rho \rho^H) = \Xi_{N_R \times N_R}$ , the  $3 \times 3$  identity matrix such that  $\rho_i, i = 0, 1, 2$  are mutually uncorrelated from the uncorrelated assumption (6.2).

(6.23) can now be rewritten using (6.24),

$$\begin{aligned} A_s &= \mathbf{b}^H \mathbf{F}_{rc} \mathbf{b} = \rho^H \alpha^H \mathbf{F}_{rc} \alpha \rho, \\ &= \rho^H \mathbf{G} \rho \end{aligned} \quad (6.25)$$

where in the second line we have defined  $\mathbf{G} = \alpha^H \mathbf{F}_{rc} \alpha$ . Note that for a fixed MPDP,  $\mathbf{G}$  is

fixed. Also note that  $\mathbf{G}$  is Hermitian symmetric, and since  $A_s$  is the energy of the cascade filter (6.8) it is non-negative definite. For any non-negative definite Hermitian symmetric matrix  $\mathbf{G}$ , there exist an orthonormal matrix  $\mathbf{Q}$  such that  $\mathbf{Q}\mathbf{G}\mathbf{Q}^H = \Lambda$ , or

$$\mathbf{G} = \mathbf{Q}^H \Lambda \mathbf{Q} \quad (6.26)$$

where  $\Lambda$  is a diagonals matrix with the diagonal elements,  $\lambda_p \geq 0$ ,  $p = 0, 1, 2$ , being the eigenvalues of the matrix  $\mathbf{G}$ .

Now rewriting (6.25) using (6.26) we have

$$A_s = \rho^H \mathbf{G} \rho = \rho^H \mathbf{Q}^H \Lambda \mathbf{Q} \rho = \dot{\rho}^H \Lambda \dot{\rho} = \sum_{p=0}^2 \lambda_p |\dot{\rho}_p|^2, \quad (6.27)$$

where we have defined  $\dot{\rho} = \mathbf{Q}\rho$ . Note that  $\dot{\rho}_p$ ,  $p = 0, 1, 2$  are again mutually independent, complex-valued Gaussian random number with zero-mean and unit-variance, and thus  $\lambda_p |\dot{\rho}_p|^2$ ,  $p = 0, 1, 2$ , are *iid*  $\chi^2$ -distributed random variables with the characteristic function  $\frac{1}{(1 - jv\lambda_p)}$ . Thus, the characteristic function of  $A_s$  is the product

$$E\{\exp(jvA_s)\} = \prod_{p=0}^2 \frac{1}{(1 - jv\lambda_p)}. \quad (6.28)$$

### 6.1.3.1 Distinct eigenvalues (no eigenvalues in multiplicity)

When all the eigenvalues are distinct, (6.28) can be expressed as

$$E\{\exp(jvA_s)\} = \sum_{p=0}^2 \frac{\pi_p}{1 - jv\lambda_p}, \quad (6.29)$$

where we have defined the weight of an individual random variable to be

$$\pi_p = \prod_{\substack{q=0 \\ q \neq p}}^2 \frac{1}{(1 - \lambda_q/\lambda_p)} \quad (6.30)$$

Finally, we can write the probability density function for  $A_s$  which is the weighted sum of  $N_R (= 3)$   $\chi^2$ -distributed random variables. That is,

$$Pr(A_s = a) = \sum_{p=0}^2 \pi_p \frac{e^{-a/\lambda_p}}{\lambda_p}. \quad (6.31)$$

Now substituting (6.31) and (6.20) into (6.21) we have

$$\begin{aligned} \overline{P}_q(\overline{\gamma}_b) &= \int_0^\infty P_q(a) Pr(A_s = a) da \\ &= 2 \left(1 - \frac{1}{\sqrt{q}}\right) \sum_{p=0}^2 \pi_p \int_0^\infty \text{erfc}\left(\sqrt{\frac{a}{2N_o}}\right) \frac{e^{-a/\lambda_p}}{\lambda_p} da \end{aligned} \quad (6.32)$$

Now define

$$Y = \frac{A_s}{2N_o}, \quad (6.33)$$

then by change of variable (6.32) can be rewritten

$$\overline{P}_q(\overline{\gamma}_b) = 4 \left(1 - \frac{1}{\sqrt{q}}\right) \left\{ \frac{1}{2} \sum_{p=0}^2 \pi_p \int_0^\infty \text{erfc}(\sqrt{y}) \frac{e^{-y/\dot{\lambda}_p}}{\dot{\lambda}_p} dy \right\}, \quad (6.34)$$

where we have defined for  $p = 0, 1, \dots, D-1$ ,  $\dot{\lambda}_p = \frac{\lambda_p}{2N_o}$ . Note that the weight terms  $\pi_p$  stays the same. The expression in the curly-brace of is evaluated in (6.83) in the Appendix of this Chapter. Then, (6.34) becomes

$$\overline{P}_q(\overline{\gamma}_b) = 4 \left(1 - \frac{1}{\sqrt{q}}\right) \left( \frac{1}{2} \sum_{i=0}^{D-1} \pi_i \left(1 - \sqrt{\frac{\dot{\lambda}_i}{1 + \dot{\lambda}_i}}\right) \right), \quad (6.35)$$

where the relationship between the average SNR/bits and the eigenvalues are

$$\overline{\gamma}_b = \frac{2(q-1)E\{A_s\}}{3k \cdot 2N_o} = \frac{2(q-1)}{3k} E\{Y\} = \frac{2(q-1)}{3k} \left(\frac{1}{2N_o}\right) \sum_{i=0}^{D-1} \lambda_i. \quad (6.36)$$

Now, the following steps describe the procedure of how to compute the matched

filter symbol error probability bounds when the input parameters are the average SNR/bits  $\bar{\gamma}_b$ , the constellation size  $q$  and the multipath power delay profile.

- Evaluate the eigenvalues  $\{\lambda_i, i = 0, 1, \dots, N_R\}$  using given MPDP and the transmit shaping filter, which is described in (6.23) to (6.27).
- Now determine the value of  $\left(\frac{1}{2N_o}\right)$  for the given value of  $\bar{\gamma}_b$  and  $q$  by

$$\frac{1}{2N_o} = \frac{3\bar{\gamma}_b \log_2 q}{2(q-1) \sum_{i=0}^{N_R-1} \lambda_i} \quad (6.37)$$

- Calculate  $\{\hat{\lambda}_i, i = 0, 1, \dots, N_R\}$  by evaluating

$$\hat{\lambda}_p = \frac{\lambda_p}{2N_o}. \quad (6.38)$$

- Finally, substitute (6.38) into (6.35) to calculate the average symbol error probability.

### 6.1.3.2 Eigenvalues occurring in multiplicity

We now consider the case of  $D$ -times repeated eigenvalues, i.e.

$$E\{\exp(j\nu A_s)\} = \left(\frac{1}{1 - j\nu\lambda_1}\right)^D. \quad (6.39)$$

This is the case when we have equal gain, independent diversity sources. Then, (6.27) takes the expression

$$A_s = \sum_{p=0}^{D-1} \lambda_1 |\dot{\rho}_p|^2, \quad (6.40)$$

where  $|\dot{\rho}_p|^2$  again are *iid* Chi-square distribution with unit mean. The distribution function for this case is  $Pr(A_s = a) = \frac{1}{(D-1)!\lambda_1^D} a^{D-1} e^{-a/\lambda_1}$ . Then, the average symbol error probability is

$$\begin{aligned}
\bar{P}_q(\bar{\gamma}_b) &= \int_0^\infty P_q(a) Pr(A_s = a) da \\
&= \int_0^\infty 2 \left(1 - \frac{1}{\sqrt{q}}\right) \operatorname{erfc}\left(\sqrt{\frac{a}{2N_o}}\right) \frac{1}{(D-1)! \lambda_1^D} a^{D-1} e^{-a/\lambda_1} da \\
&= 4 \left(1 - \frac{1}{\sqrt{q}}\right) \int_0^\infty \frac{1}{2} \operatorname{erfc}\left(\sqrt{\frac{a}{2N_o}}\right) \frac{1}{(D-1)! \lambda_1^D} a^{D-1} e^{-a/\lambda_1} da.
\end{aligned} \tag{6.41}$$

Then, by defining  $Y = \frac{A_s}{2N_o}$ , we have

$$\bar{P}_q(\bar{\gamma}_b) = 4 \left(1 - \frac{1}{\sqrt{q}}\right) \int_0^\infty \frac{1}{2} \operatorname{erfc}(\sqrt{y}) \frac{1}{(D-1)! \dot{\lambda}_1^D} y^{D-1} e^{-y/\dot{\lambda}_1} dy, \tag{6.42}$$

where we again defined  $\dot{\lambda}_1 = \frac{\lambda_1}{2N_o}$ . From (6.86), we have

$$\bar{P}_q(\bar{\gamma}_b) = 4 \left(1 - \frac{1}{\sqrt{q}}\right) \left(\frac{1-\Omega}{2}\right)^{D-1} \sum_{k=0}^{D-1} \binom{D-1+k}{k} \left(\frac{1+\Omega}{2}\right)^k, \tag{6.43}$$

where we defined  $\Omega = \frac{\dot{\lambda}_1}{\sqrt{1+\dot{\lambda}_1}}$ .

Now, following steps describe the procedure of how to compute the matched filter symbol error probability bounds when the input parameters are the average SNR/bits  $\bar{\gamma}_b$ , the constellation size  $q$  and  $D$  diversity paths of equal gain  $\lambda_1$ .

- Now determine the value of  $\frac{1}{2N_o}$  for the given value of  $\bar{\gamma}_b$  and  $q$  by

$$\frac{1}{2N_o} = \frac{3\bar{\gamma}_b \log_2 q}{2(q-1)D\lambda_1} \tag{6.44}$$

- $\dot{\lambda}_1 = \frac{\lambda_1}{2N_o}$  and thus  $\Omega = \frac{\dot{\lambda}_1}{\sqrt{1+\dot{\lambda}_1}}$ .

- Finally, substitute  $\Omega$  into (6.43) to calculate the average symbol error probability

The considered situation is when each diversity channel is a single Rayleigh fading tap channels. Then, the matched filter combiner simply becomes the maximal ratio combining of the received signal. Figure 6-3 Figure 6-4 Figure 6-5 are the matched filter

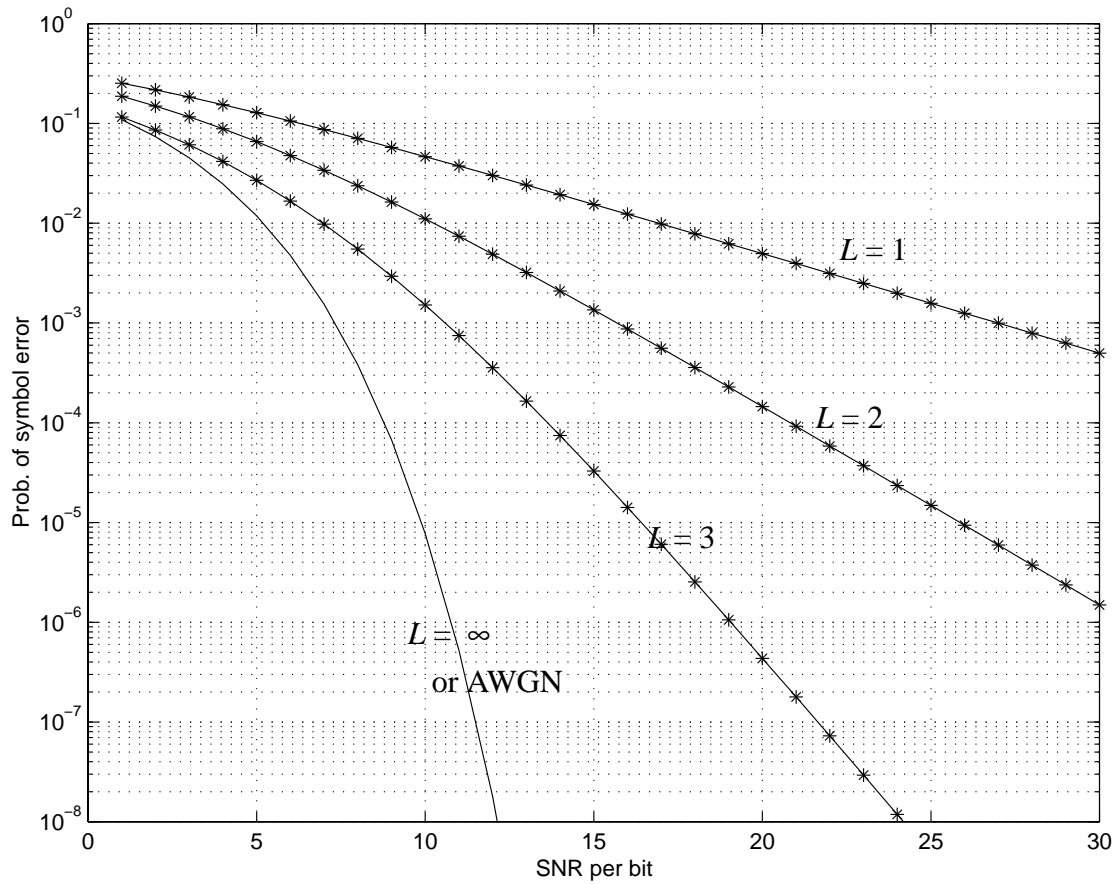


Figure 6-3 Matched filter bound SER for 4-QAM transmission over  $L$ -flat fading diversity channels.

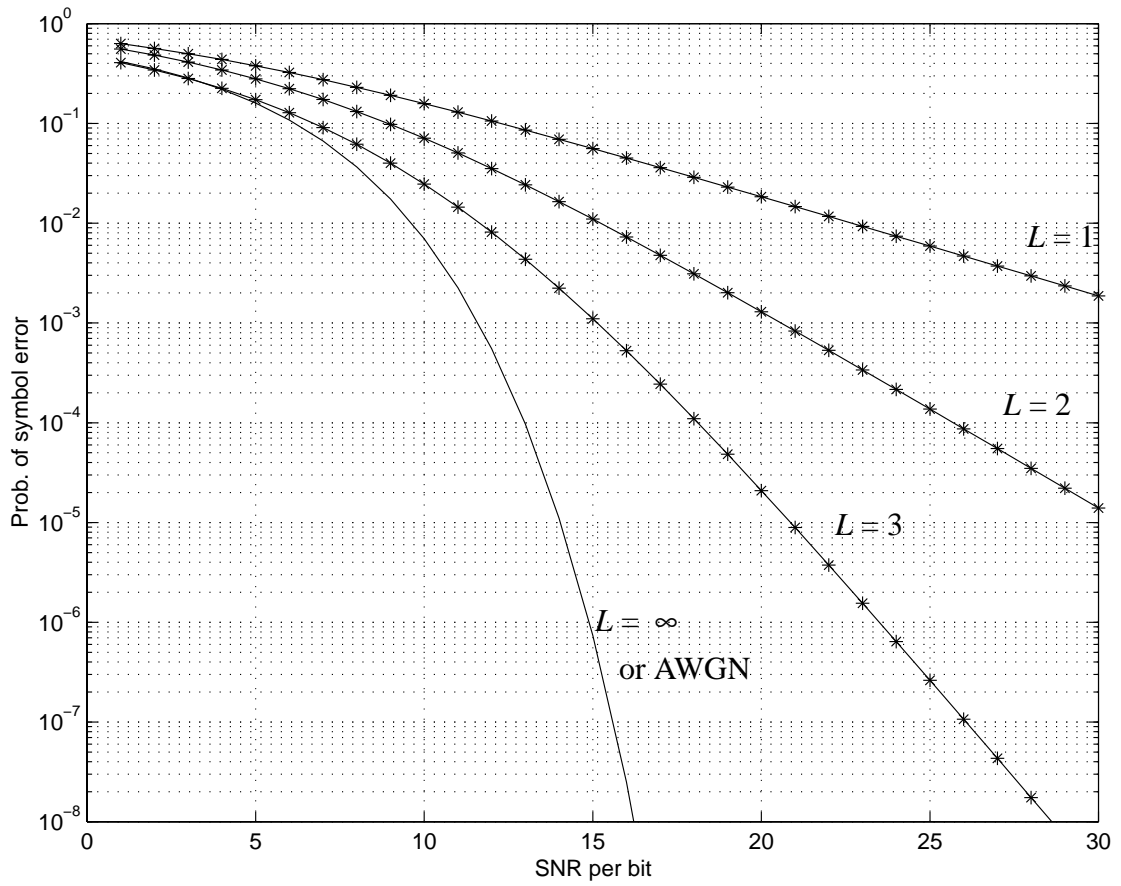


Figure 6-4 Matched filter bound SER for 16-QAM transmission over  $L$ -flat fading diversity channels.

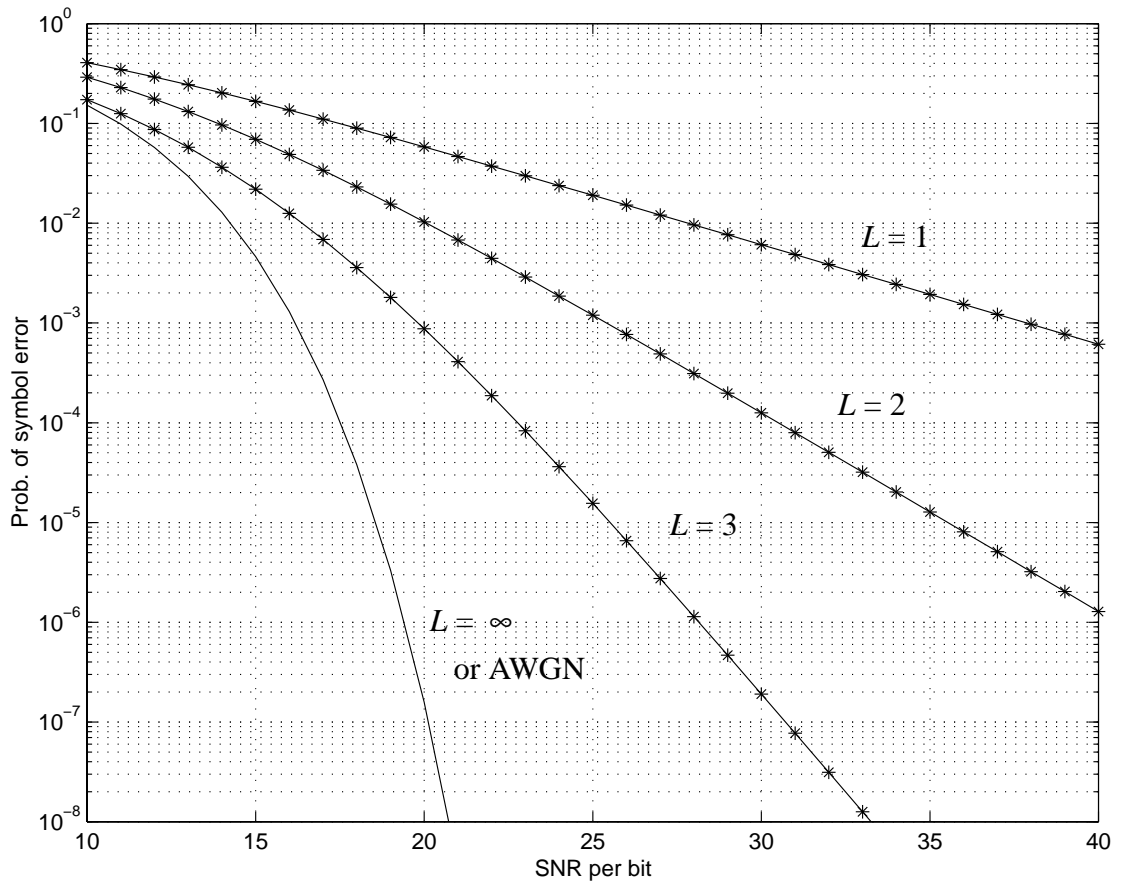


Figure 6-5 Matched filter bound SER for 64-QAM transmission over  $L$ -flat fading diversity channels.

bounds of SER for  $q$ -QAM transmission over the  $L$ -diversity antenna channels, for  $q$  equal to 4, 16 and 64. As the order of diversity increases the matched filter bounds of  $L$ -diversity channels approach the SER performance of the AWGN channel.

### 6.1.3.3 Combination of distinct and multiple poles

We now consider  $L$  diversity antenna cases, where the instantaneous, diversity-combined channel gain  $A_s$  can be shown to be

$$A_s = \sum_{l=0}^{L-1} \sum_{p=0}^{N_R-1} \lambda_p |\rho_{l,p}|^2, \quad (6.45)$$

where  $\rho_{l,p}$ ,  $p = 0, 1, \dots, N_R$  are mutually independent, complex-valued Gaussian random number with zero-mean and unit-variance, and thus  $\lambda_p |\rho_{l,p}|^2$  are *iid*  $\chi^2$ -distributed random variables. Note that the MPDP stays the same for different antennas, and thus the same set of  $N_R$  (distinct) eigenvalues should be repeating  $L$  times. Thus, the characteristic function becomes

$$E\{\exp(j\nu A_s)\} = \prod_{p=0}^{N_R-1} \frac{1}{(1 - j\nu\lambda_p)^L}. \quad (6.46)$$

Now, for the example of  $L = 2$  and  $N_R = 3$ , by the method of partial fraction expansion (6.46) can be decomposed into

$$\prod_{p=0}^2 \frac{1}{(1 - j\nu\lambda_p)^2} = \sum_{p=0}^2 \left( \frac{\Gamma_{2,p}}{(1 - j\nu\lambda_p)^2} + \frac{\Gamma_{1,p}}{1 - j\nu\lambda_p} \right), \quad (6.47)$$

where  $\Gamma$  values are the expansion coefficients. Then, the probability density function is

$$Pr(A_s = a) = \sum_{p=0}^2 \left( \Gamma_{1,p} \frac{e^{-a/\lambda_p}}{\lambda_p} + \Gamma_{2,p} \frac{1}{(L-1)! \lambda_p^L} a^{L-1} e^{-a/\lambda_p} \right). \quad (6.48)$$

Then, the average symbol error probability is

$$\begin{aligned}
\overline{P}_q(\overline{\gamma}_b) &= \int_0^\infty P_q(a) Pr(A_s = a) da \\
&= \int_0^\infty 2 \left(1 - \frac{1}{\sqrt{q}}\right) \operatorname{erfc}\left(\sqrt{\frac{a}{2N_o}}\right) \left( \sum_{p=0}^2 \left( \Gamma_{1,p} \frac{e^{-a/\lambda_p}}{\lambda_p} + \Gamma_{2,p} \frac{1}{(L-1)! \lambda_p^L} a^{L-1} e^{-a/\lambda_p} \right) \right) da \quad (6.49) \\
&= 4 \left(1 - \frac{1}{\sqrt{q}}\right) \sum_{p=0}^2 [\Gamma_{1,p} P_1(\dot{\lambda}_p) + \Gamma_{2,p} P_2(\dot{\lambda}_p)]
\end{aligned}$$

where we have defined

$$\begin{aligned}
\bullet P_1(\dot{\lambda}_p) &= \frac{1}{2} \left(1 - \sqrt{\frac{\dot{\lambda}_p}{1 + \dot{\lambda}_p}}\right), \\
\bullet P_2(\dot{\lambda}_p) &= \left(\frac{1 - \Omega}{2}\right)^L \sum_{i=0}^{L-1} \binom{L-1+i}{i} \left(\frac{1 + \Omega}{2}\right)^i, \\
\bullet \dot{\lambda}_p &= \frac{\lambda_p}{2N_o}.
\end{aligned}$$

Now, the following steps describe how to compute the average probability given the MPDP, the number of diversity channel  $L$ , the average SNR/bits  $\overline{\gamma}_b$  and the constellation size  $q$ :

- Define the average SNR/bits (note, this is not the average SNR/bits/channel),

$$\overline{\gamma}_b = \frac{2(q-1)E\{A_s\}}{3k \cdot 2N_o} = \frac{2(q-1)E\{Y\}}{3k} = \frac{2(q-1)}{3k} \left(\frac{1}{2N_o}\right)^L \sum_{i=0}^{D-1} \lambda_i \quad (6.50)$$

- Evaluate the eigenvalues  $\{\lambda_i, i = 0, 1, \dots, N_R\}$  for given  $L$ , MPDP and the transmit shaping filter, taking the same approach as (6.23) to (6.27).
- Now determine the value of  $\left(\frac{1}{2N_o}\right)$  for the given value of  $\overline{\gamma}_b$ ,  $L$  and  $q$  by

$$\frac{1}{2N_o} = \frac{3\overline{\gamma}_b \log_2 q}{2(q-1) \cdot L \cdot \sum_{i=0}^{N_R-1} \lambda_i} \quad (6.51)$$

- Calculate  $\{\dot{\lambda}_i, i = 0, 1, \dots, N_R\}$  by evaluating

$$\dot{\lambda}_p = \frac{\lambda_p}{2N_o}. \quad (6.52)$$

- Finally, substitute (6.52) into (6.49) to calculate the average symbol error probability

Figure 6-6 Figure 6-7 Figure 6-8 shows the matched filter bounds for  $q$ -QAM transmission,  $q = 4, 16, \text{ and } 64$ , over the multipath fading frequency-selective channels which have MPDP-1 = (0.7413 0.2343 0.0234) and MPDP-2 = (0.6652 0.2447 0.0900) and for the number of diversity channels  $L = 1, 2$ . Note that in this Chapter we use the SNR/bits to draw the matched filter bound curves. When they are compared with the simulation results in Chapter 5 and 7, they are translated to the curves for SNR/bits/Channel, which can be readily done by ignoring  $L$  in (6.51).

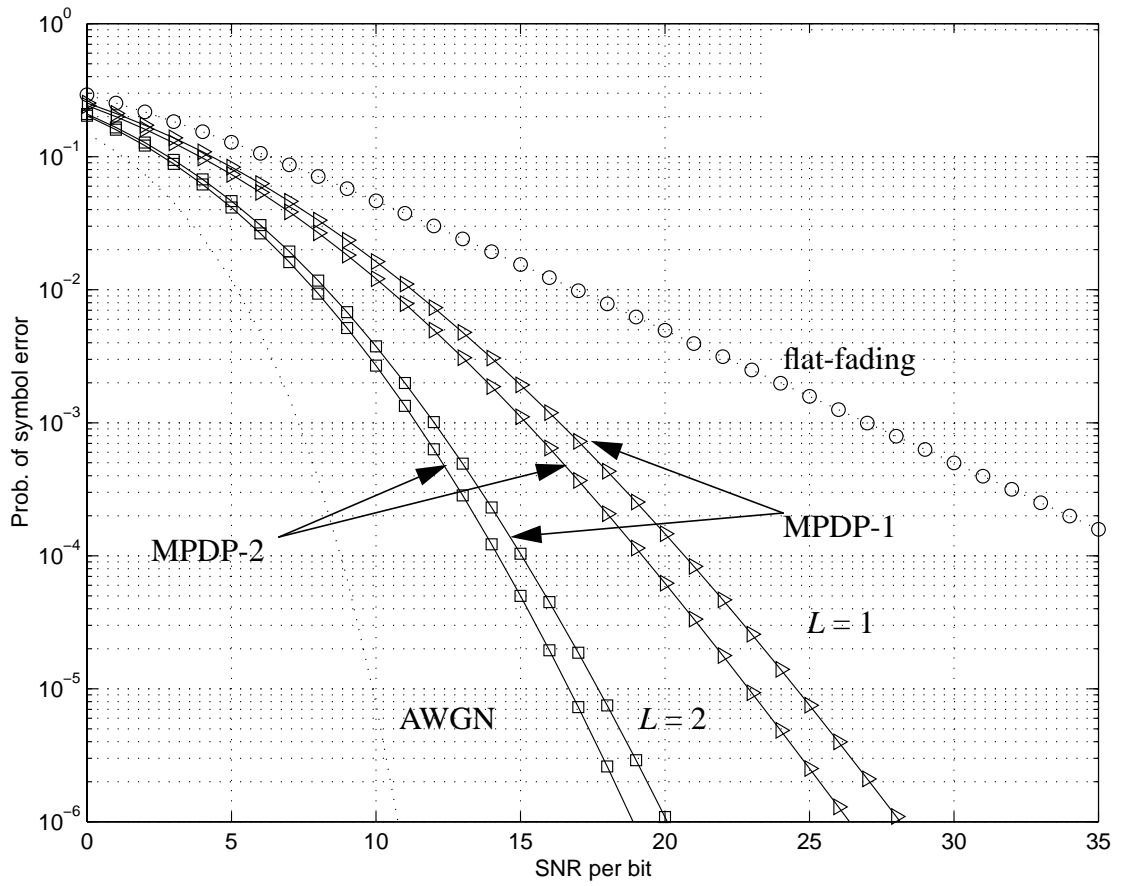


Figure 6-6 Matched filter bounds symbol error probability for 4-QAM,  $L = 1, 2$

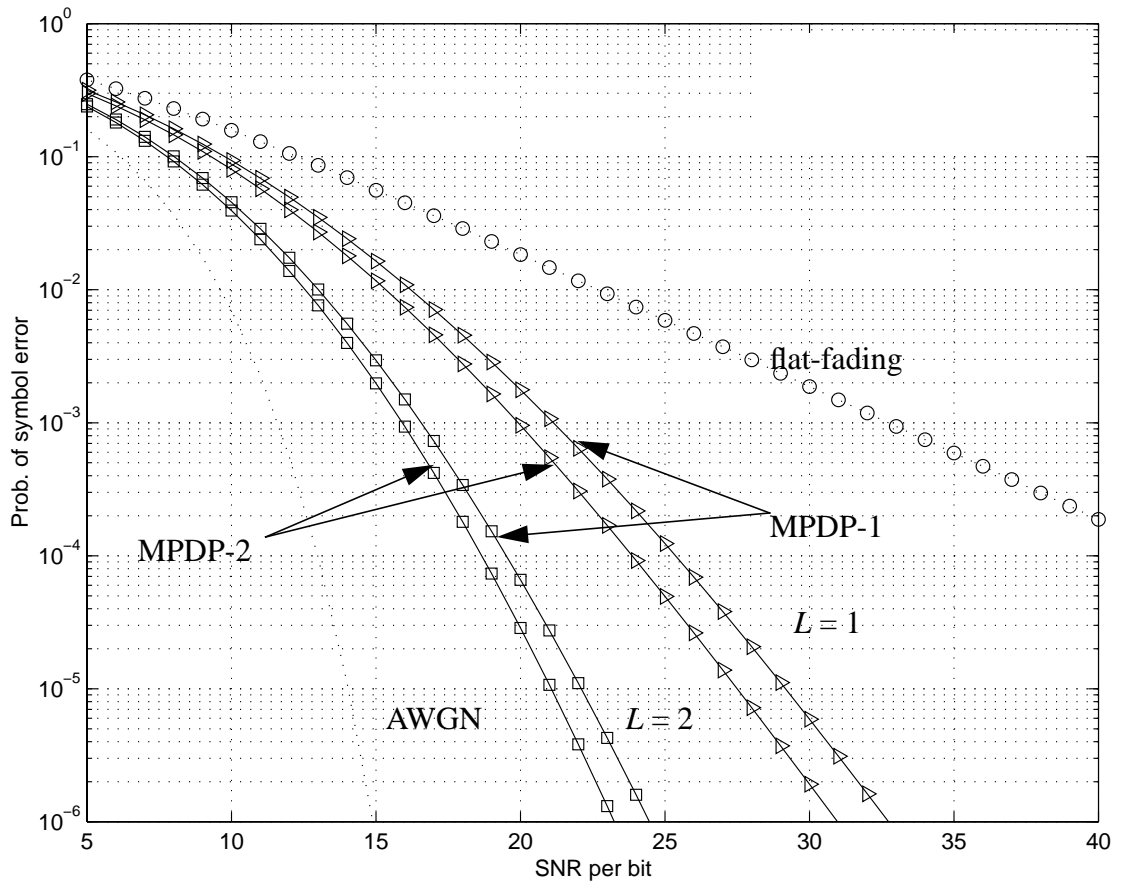


Figure 6-7 Matched filter bounds symbol error probability for 16-QAM,  $L = 1, 2$

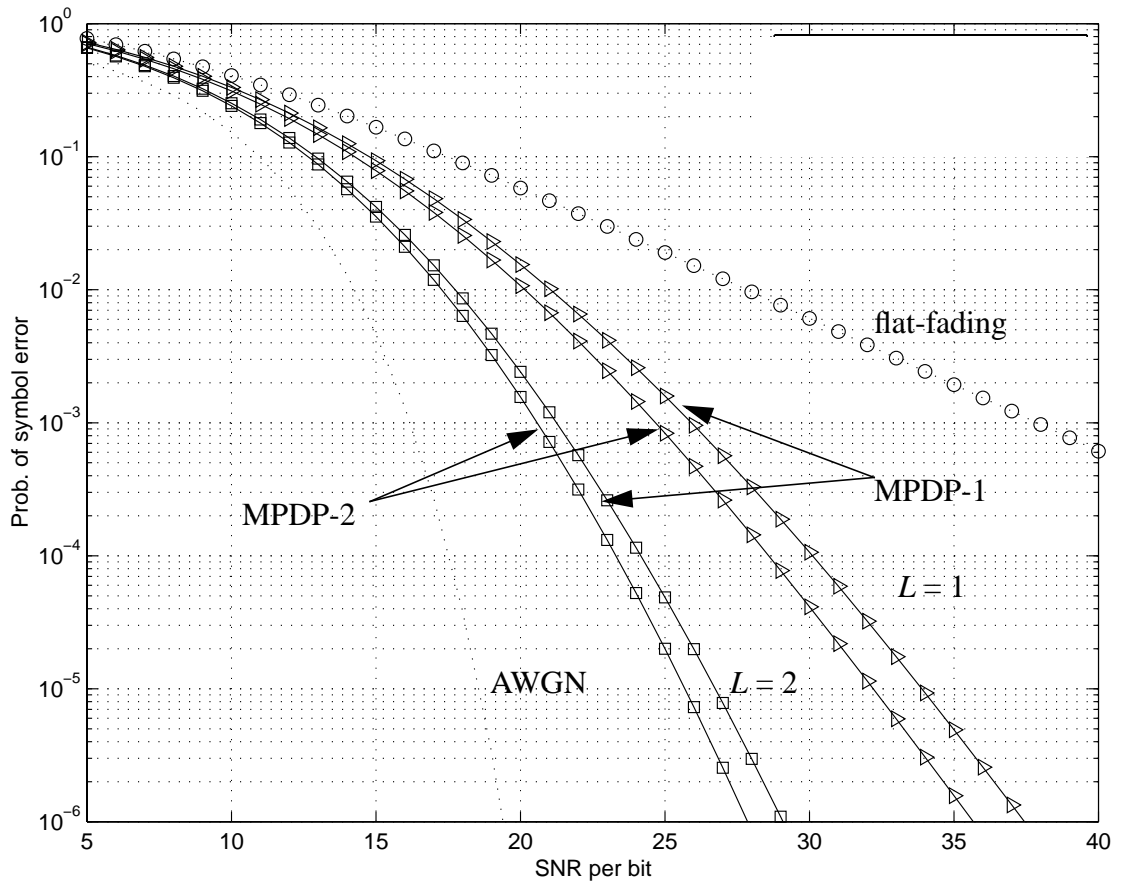


Figure 6-8 Matched filter bounds symbol error probability for 64-QAM,  $L = 1, 2$

## 6.2 Spectral Efficiency of the Fading ISI Channels

The continuous growth in the number of subscribers and traffic volume in mobile telecommunications creates the demand for more radio spectrum. Due to the limited spectrum available, however, spectral efficiency is one of the primary concerns in the design of future wireless communications systems. Spectral efficiency of a wireless communication system can be achieved at various system levels. We focus on the spectral efficiency that can be achieved at the link layer level, and thus we define “spectral efficiency” as the average data rate per unit bandwidth that can be transmitted at a specified average SNR and BER over the time-varying frequency-selective channel.

In recent publications [77 - 81], variable rate transmission systems with multi-level QAM, which is adaptive to the fading envelope of the receiver, were investigated as a means to increase the spectral efficiency of a flat fading channel. Specifically, the transmitter varies the number of modulation levels according to the fade level being experienced at the receiver, such that when the receiver is not in a fade the transmitter uses a large QAM constellation, and as the receiver enters a fade the transmitter decreases the size of the QAM constellation. These scheme assume a duplex system so that the fade level information can be send back to the transmitter. With the feedback information, the transmitter determines the size of the QAM constellation which provides a specified BER and transmit power.

In this section, we investigate the theoretical spectral efficiency bounds for the adaptive  $q$ -QAM modulation scheme in the frequency-selective fading channel. In the open literature this type of capacity calculation has been investigated only for flat fading channels [80], but not for the frequency-selective channel. We take a similar approach [80] for capacity calculation for the frequency-selective fading channels. In addition, we utilize the single-shot matched filter SNR that has been developed in Section 6.1, to calculate the instantaneous BER. Figure-9 is the spectral efficiency limit obtained for the frequency-

selective channel as a function of average SNR at the fixed BER specified.

## 6.2.1 Maximum Spectral Efficiency Calculation

We now consider the maximum spectral efficiency of the frequency-selective channels, using variable rate and variable power  $q$ -QAM transmission. For this we assume the same four **Assumptions** we made in Section 6.1 and modify (6.1) to include the parameter of power-variable. The single-shot received signal is now defined as

$$\begin{aligned} x_s(t) &= \sqrt{P_s} \cdot I_o \cdot \sum_{i=0}^{N_R} \alpha_i \rho_i(t) f\left(t - \frac{T_B i}{2}\right) + n(t) \\ &= \sqrt{P_s} \cdot I_o \cdot \sum_{i=0}^{N_R} b_i f\left(t - \frac{T_B i}{2}\right) + n(t) \end{aligned} \quad , \quad (6.53)$$

where

- $P_s$  denotes the instantaneous transmitter power, assumed fixed for the duration of the pulse
- $I_o$  denotes the transmitted information signal from the  $q$ -QAM constellation, and  $Var(I_o)$  is defined to be unit-variance regardless of the size of constellation
- $N_R$  is the number of multi-path components
- $\alpha_i$  is the average magnitude of  $(i+1)$ -th path, i.e.,  $\alpha_i^2$  is the average power of  $(i+1)$ -th path, and we assume that  $\sum_{i=0}^{N_R} \alpha_i^2 = 1.0$
- $\rho_i(t)$  denotes *iid* complex-valued Gaussian random process
- $f(t)$  denotes the transmit pulse shaping real-valued filter, i.e., it is a Nyquist filter
- $n(t)$  denotes the complex-valued Gaussian noise, independent of signal and channel

fading.

We now assume that the received signal  $x_s(t)$  is passed through the matched filter. The sampled matched filter output, analogous to (6.7),  $z_s$  can be written as

$$z_s = P_s A_s I_o + v_s, \quad (6.54)$$

where the variables in the right side of the equation is defined as

- $P_s$ , the instantaneous transmission and receive power<sup>1</sup>, and the average power  $\overline{P_s}$  is the constraint of the optimization
- $I_o$ , the transmitted information signal from the  $q$ -QAM constellation,  $E(I_o) = 0.0$  and  $Var(I_o) = 1.0$ , regardless of the size of constellation
- $v_s$  a complex-valued Gaussian random variable with zero mean and variance of

$$Var(v_s) = N_o A_s \quad (6.55)$$

- $A_s$ , the fading gain random variable having  $E(A_s) = 1.0$ , which was evaluated in Section 6.1 for various cases. In this Section, we assume  $L = 1$  and  $N_R = 3$ , and thus we discuss the case with distinct eigenvalues. Note that this choice is suitable since for a single antenna channel there will be no eigenvalues with the same values, due to correlation introduced by the use of SRRC filter. Thus, from (6.31) the probability density function is

$$Pr(A_s = a) = \sum_{i=0}^{N_R} \frac{\pi_i}{\lambda_i} \exp\left(-\frac{a}{\lambda_i}\right), \quad (6.56)$$

---

1. absorbing the propagation loss in the channel model and the variance of the noise

$$\text{where } \pi_p = \prod_{\substack{q=0 \\ q \neq p}}^2 \frac{1}{(1 - \lambda_q / \lambda_p)}.$$

Total received energy for the one-shot signal pulse may be defined as  $E_s = P_s \cdot A_s^2 \cdot T_B$ .

Then, the instantaneous received SNR  $\gamma(t)$  is defined as

$$\begin{aligned} \frac{\text{Signal Power}}{\text{Noise Power}} = \gamma &= \log_2(q) \gamma_b = \frac{E_s W_B}{A_s N_o W_B} = \frac{P_s \cdot T_B \cdot A_s^2}{A_s N_o} = \frac{P_s A_s}{N_o W_B}, \\ &= \frac{P_s T_B A_s^2 W_B}{A_s N_o W_B} = \log_2(q) \frac{P_s T_b A_s W_B}{N_o W_B} = \log_2(q) \frac{P_s A_s}{N_o W_B} \left( \frac{W_B}{R_b} \right), \end{aligned} \quad (6.57)$$

where

- $W_B = \frac{1}{T_B}$  denotes the effective transmission duration of a QAM symbol
- $T_b = \frac{T_B}{\log_2(q)}$  denotes the effective transmission duration of a bit
- $R_b = \frac{1}{T_b}$  denotes the bit rate
- $R_s = \frac{R_b}{W_B}$  denotes the spectral efficiency, representing the number of bits for a channel use [bits/sec/Hz]

We find it useful to define the instantaneous channel-SNR, i.e.

$$\gamma_{ch} = \frac{\bar{P}_s A_s}{N_o W_B}, \quad (6.58)$$

thus  $E(\gamma_{ch}) = \frac{\bar{P}_s}{N_o W_B}$  which we defined as the average received SNR. Then, by the change of variable<sup>1</sup> using (6.56) we obtain the probability distribution of  $\gamma_{ch}$  as

$$Pr(\gamma_{ch} = x) dx = \sum_{i=0}^{N_R} \frac{\pi_i}{\lambda_{\gamma, i}} \exp\left(-\frac{x}{\lambda_{\gamma, i}}\right) dx, \quad (6.59)$$

where  $\lambda_{\gamma, i} = \lambda_i \cdot E(\gamma_{ch})$ .

---

1. Substitute  $a = \frac{x}{E(\gamma_{ch})}$  into the expression,  $Pr(A_s = a) da = \sum_{i=0}^{N_R} \frac{\pi_i}{\lambda_i} \exp\left(-\frac{a}{\lambda_i}\right) da$ .

The variable rate and power transmission scheme can now be stated as follows: The receiver, estimate the channel, calculate the instantaneous channel SNR and feedback to the transmitter. The transmitter then adjust the power and constellation size of  $q$ -QAM for  $q = 2, 4, 16$  and  $64$ . Here, it is an ideal assumption that the feedback information is instantaneously available to the transmitter and perfect. Thus, the obtained curves indicate the maximum attainable spectral efficiency of the frequency-selective channel.

For a fixed channel, the instantaneous spectral efficiency can be calculated from,

$$\frac{C}{W_B}(\gamma_{ch}) = \log_2(1 + \gamma) = \log_2 \left( 1 + \frac{P_s(\gamma_{ch})}{P_s} \gamma_{ch} \right). \quad (6.60)$$

Then the spectral efficiency of the multipath ISI channel is obtained by taking the expectation

$$\frac{C}{W_B} = \max \int_0^{\infty} \log_2 \left( 1 + \frac{P_s(x)}{P_s} x \right) Pr(\gamma_{ch} = x) dx, \quad (6.61)$$

subject to the power constraint

$$\int_0^{\infty} P_s(x) Pr(\gamma_{ch} = x) dx. \quad (6.62)$$

The capacity achieving, optimal power control policy is the “water-filling” solution [79],

$$\frac{P_s(x)}{P_s} = \begin{cases} \frac{1}{x_o} - \frac{1}{x} & , x \geq x_o \\ 0 & , x < x_o \end{cases}. \quad (6.63)$$

Thus, substituting (6.63) into (6.61) the maximum attainable spectral efficiency can be calculated

$$\frac{C}{W_B} = \int_{x_o}^{\infty} \log_2 \left( \frac{x}{x_o} \right) Pr(\gamma_{ch} = x) dx, \quad (6.64)$$

where  $x_o$  is determined by

$$\int_{x_o}^{\infty} \left( \frac{1}{x_o} - \frac{1}{x} \right) Pr(\gamma_{ch} = x) dx = 1. \quad (6.65)$$

We obtain  $x_o$  and thus  $\frac{C}{W_B}$  from a numerical solution.

We note that the derived expression (6.64) is the maximum spectral efficiency, regardless of coding or modulation scheme, and holds for many other classes of fading channel: for each class, we just need to switch the density function  $Pr(\gamma_{ch} = x)$ .

We now continue with the derivation of maximum attainable spectral efficiency using uncoded  $q$ -QAM constellation. For this, we may use the upper bound BER formula used in [80], good to within 1 dB for  $q > 2$ . Then, the BER for an instantaneous channel-SNR  $\gamma_{ch} = x$  is expressed as

$$\text{BER} \leq \frac{1}{5} \exp \left( \frac{-1.5x P_s(x)}{q-1 \overline{P}_s} \right), \quad (6.66)$$

and thus the modulation size  $q(x)$  at a particular channel SNR  $x$  is expressed as

$$q(x) = 1 + \frac{1.5x}{-\ln(5\text{BER})} \frac{P_s(x)}{\overline{P}_s}. \quad (6.67)$$

The maximum spectral efficiency is then obtained by maximizing

$$\begin{aligned} E(\log_2 q(\gamma_{ch})) &= \int_0^{\infty} \log_2 q(x) Pr(\gamma_{ch} = x) dx \\ &= \int_0^{\infty} \log_2 \left( 1 + \frac{1.5x}{-\ln(5\text{BER})} \frac{P_s(x)}{\overline{P}_s} \right) Pr(\gamma_{ch} = x) dx \end{aligned}, \quad (6.68)$$

subject to the power constraint

$$\int_0^{\infty} P_s(x) Pr(\gamma_{ch} = x) dx. \quad (6.69)$$

The power control policy that maximize (6.68) is again the “water-filling” solution, i.e.

$$\frac{P_s(x)}{P_s} = \begin{cases} \frac{1}{x_o} - \frac{1}{x \cdot K} & , x \geq \frac{x_o}{K} \\ 0 & , x < \frac{x_o}{K} \end{cases}, \quad (6.70)$$

where  $x_o$  is the cutoff received SNR fading depth, and  $K = \frac{1.5}{\ln(5BER)}$ . Thus, substituting (6.70) into (6.68) and define  $x_K = \frac{x_o}{K}$  we obtain the spectral efficiency

$$\frac{C_{q-QAM}}{W_B} = \int_{x_K}^{\infty} \log_2 \left( \frac{x}{x_K} \right) Pr(\gamma_{ch} = x) dx, \quad (6.71)$$

where  $x_K$  should be obtained from numerically evaluating

$$\int_{x_K}^{\infty} \left( \frac{1}{x_K} - \frac{1}{x} \right) Pr(\gamma_{ch} = x) dx = K. \quad (6.72)$$

Figure 6-9, Figure 6-10, and Figure 6-11 show the maximum spectral efficiency calculation based on (6.71) and (6.72) for a flat fading channel and frequency-selective channels with MPDP-1 and MPDP-2, at a particular BER. Figure 6-12 compares the spectral efficiencies of the three channels at  $BER = 10^{-4}$ . We observed from Figure 6-6, Figure 6-7 and Figure 6-8, that MPDP-2 achieves the highest diversity benefit. In this section, we have shown that the channel with MPDP-2 also achieves the highest capacity among the three. However, one thing that should be noticed is that in spite of the hugh SNR difference shown in Figure 6-6, Figure 6-7 and Figure 6-8, the differences in terms of channel capacity are not much as shown in Figure 6-12.

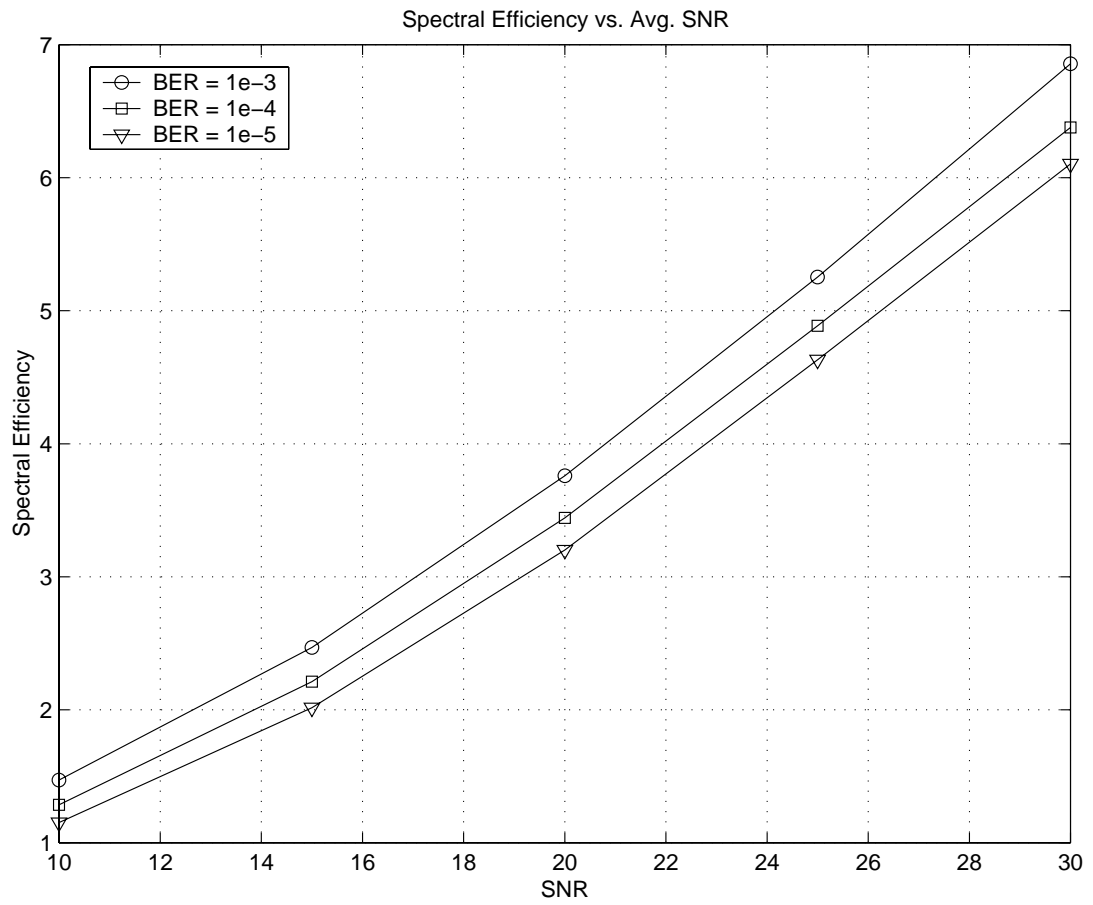


Figure 6-9 Spectral Efficiency for frequency-flat fading channel.

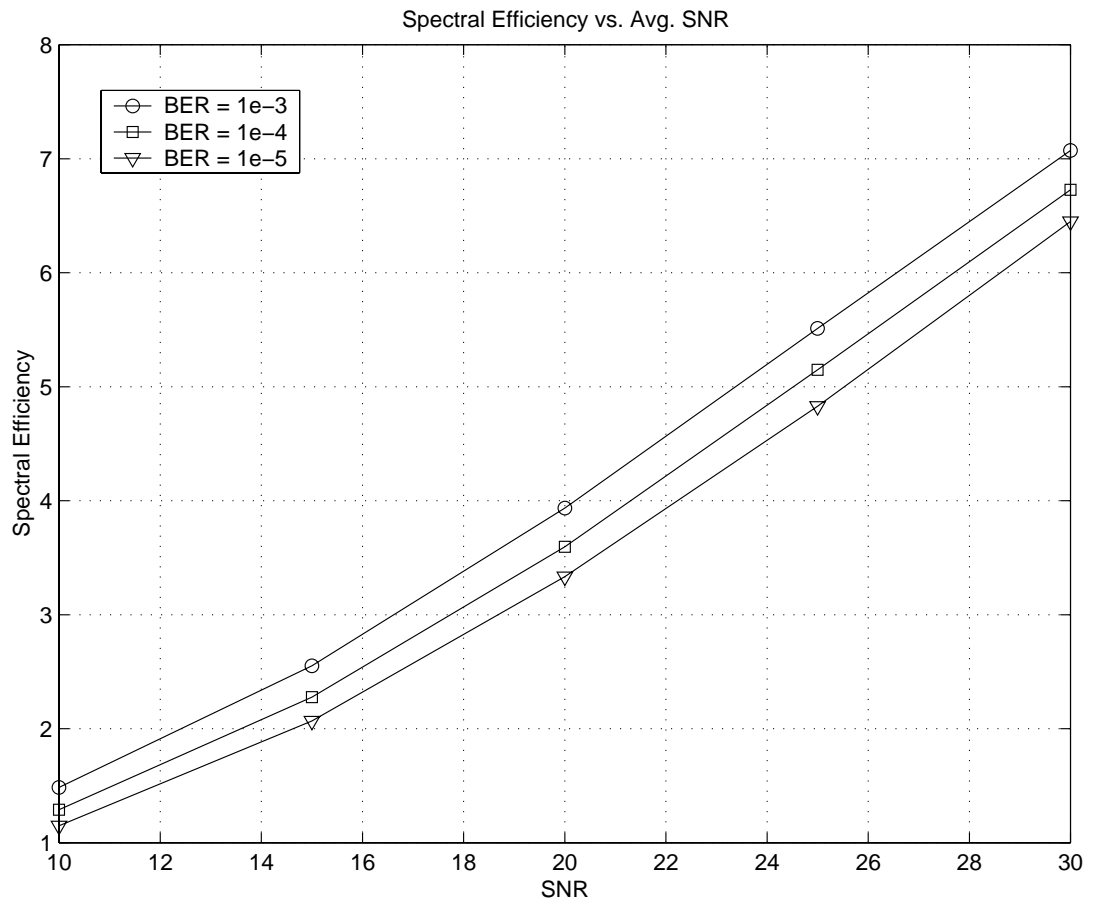


Figure 6-10 Capacity for the frequency-selective channels, MPDP 1.

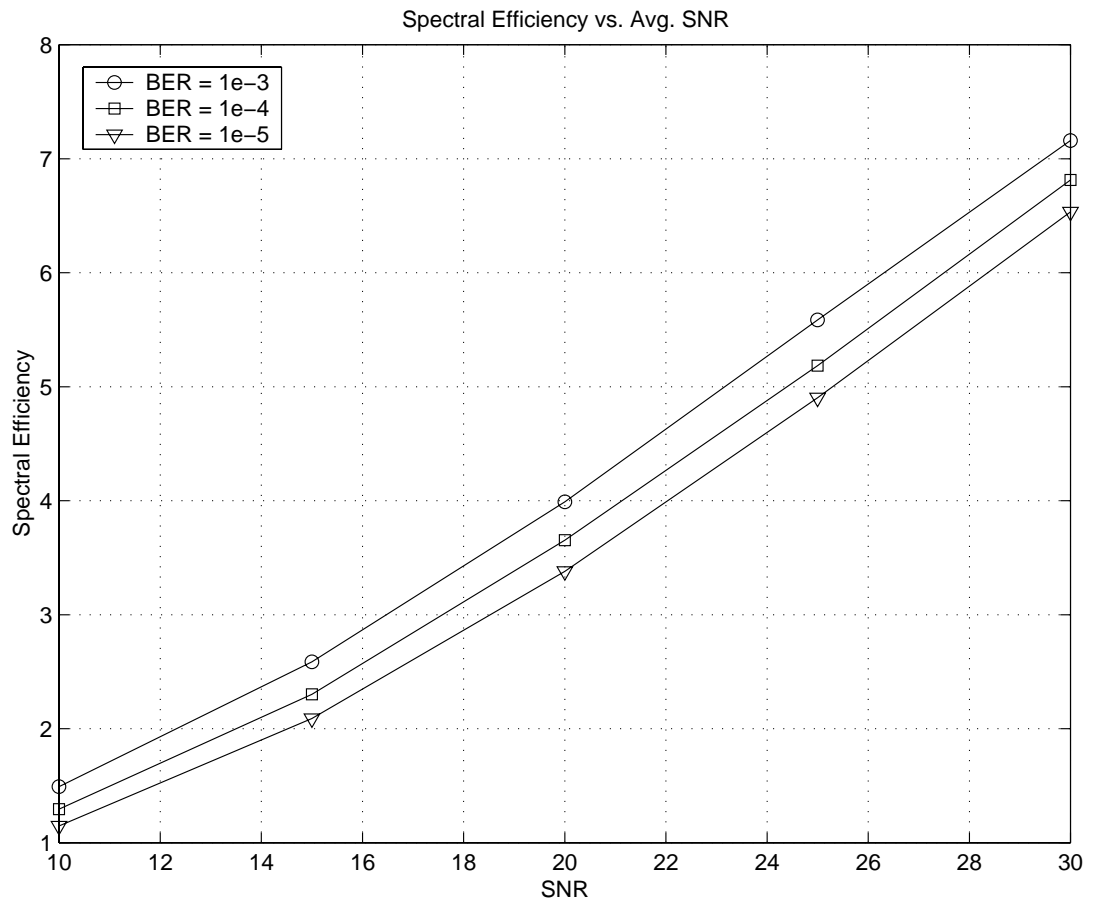


Figure 6-11 Capacity for frequency-selective channels, MPDP 2

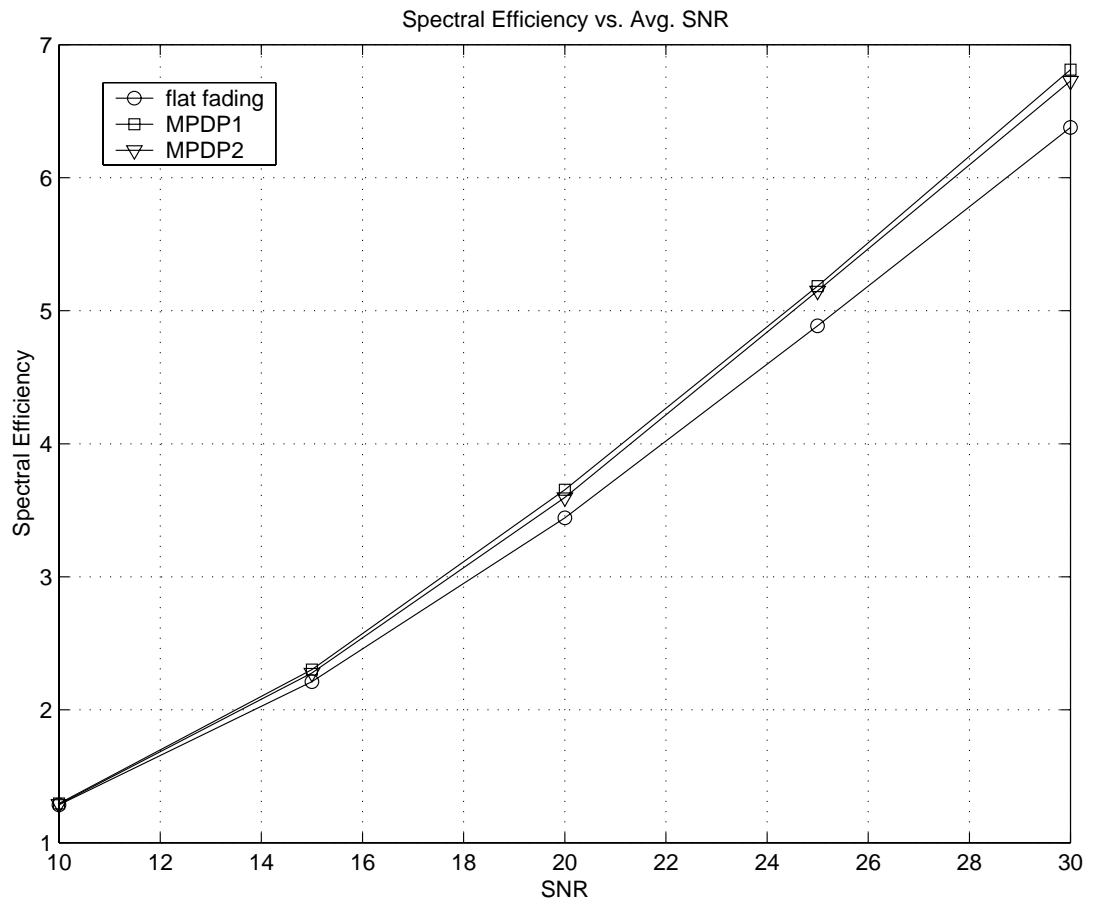


Figure 6-12 Capacity comparison, flat fading, MPDP1 and MPDP2.

## 6.3 Concluding Remarks

In this Chapter, we have derived the lower bounds on symbol error probability using the matched filter SNR for square-QAM signals, transmitted over the diversity frequency-selective channels. These theoretical bounds may not be attainable in reality due to the impractical assumptions made in deriving the bounds. Nonetheless, they provide invaluable information in designing the complex communication systems and analytical tools to provide comparison to the simulation results of the transceiver schemes developed throughout Chapter 4, 5 and 7. Specifically, we shall be able to observe the exact relationship between the asymptotic slopes of SER curves and different MPDPs, and how much an addition of an antenna would affect the SER performance. For future work, we would like to extend these matched filter bound results to the coded transmission cases<sup>1</sup>. Simulation results in Chapter 8 for trellis coded modulation and sequential detection are not compared with any theoretical bounds.

We then derived the capacity of the frequency-selective fading channels. This information provides a meaningful guideline in designing and evaluating the spectrally efficient variable rate and power adaptation protocols.

---

1. Useful literature in this regard includes Chini [40], Cavers [83] and Fechtel [84].

# Appendix A

## Integration of erfc-function over Chi-square distribution

This Appendix briefly reviews basic properties of the Chi-square distributed random variables, and evaluates an integral expression which is useful in deriving the matched filter bounds of symbol error probability. We want to evaluate the following forms of integration

$$E_Y\left(\frac{1}{2}\operatorname{erfc}(\sqrt{Y})\right) = \int_0^{\infty} \frac{1}{2}\operatorname{erfc}(\sqrt{y})Pr(Y = y)dy, \quad (6.73)$$

where  $Y$  is a Chi-square-distributed random variable. We start with evaluating  $Pr(Y = y)$  for number of cases. Then, we evaluate the integral for each case. In particular, we provide a closed form solution for the integral expression, (1) when all the poles of the characteristic function of  $Y$  are distinct; (2) when all the poles of the characteristic function are the same.

Generally, a Chi-square random variable can be constructed from the squared magnitude of Gaussian random variables. The number of real-valued, component Gaussian random variables determines the degrees of freedom of the Chi-square distribution. For example, let

$$Y_1 = \lambda_1|X_1|^2, \quad (6.74)$$

where  $X_1$  is a complex-valued Gaussian r.v. with  $E(X_1) = 0$  and  $Var(X_1) = 1.0$ . Then  $Y_1$  is a Chi-square random variable with 2 degrees of freedom (note that there are two Gaussian random variables, real- and imaginary part of  $X_1$ ).

$Y_1$  has

- $E(Y_1) = \lambda_1 E(|X_1|^2) = \lambda_1$
- $E(e^{j\nu Y_1}) = \frac{1}{1 - j\nu E(Y_1)} = \frac{1}{1 - j\nu \lambda_1}$  (Characteristic function of  $Y_1$ )
- The probability density of  $Y_1$  is then

$$p_1(y_1) = Pr(Y_1 = y_1) = \frac{1}{E(Y_1)} e^{-y_1/E(Y_1)} = \frac{1}{\lambda_1} e^{-y_1/\lambda_1}, y_1 \geq 0. \quad (6.75)$$

Substituting (6.75) into the integral equation (6.73), we have

$$\begin{aligned} E_Y\left(\frac{1}{2}erfc(\sqrt{Y_1})\right) &= \int_0^{\infty} \frac{1}{2}erfc(\sqrt{y})Pr(Y = y)dy \\ &= \int_0^{\infty} \frac{1}{2}erfc(\sqrt{y})\frac{1}{\lambda_1}e^{-y/\lambda_1}dy \\ &= \frac{1}{2}\left(1 - \sqrt{\frac{\lambda_1}{1 + \lambda_1}}\right) \end{aligned} \quad (6.76)$$

For a more general case, we may consider a Chi-square random variable which is defined as

$$Y = \sum_{i=0}^{D-1} Y_i = \sum_{i=0}^{D-1} \lambda_i |X_i|^2, \quad (6.77)$$

where  $X_i$ ,  $i = 0, 1, \dots, D-1$ , are complex-valued *independent identically distributed Gaussian* random variables with  $E(X_i) = 0.0$  and  $Var(X_i) = 1.0$ . Then,  $Y$  is a Chi-square random variable with  $2D$ -degrees of freedom with

$$\bullet E(Y) = \sum_{i=0}^{D-1} E(Y_i) = \sum_{i=0}^{D-1} \lambda_i E(|X_i|^2) = \sum_{i=0}^{D-1} \lambda_i,$$

and the characteristic function of  $Y$ ,

$$E(e^{j\nu Y}) = \prod_{i=0}^{D-1} \frac{1}{1 - j\nu E(Y_i)} = \prod_{i=0}^{D-1} \frac{1}{1 - j\nu \lambda_i}. \quad (6.78)$$

When all the roots are distinct, by the method of partial fraction, (6.78) can be expressed as

$$E\{e^{j\nu Y}\} = \sum_{p=0}^{D-1} \frac{\pi_p}{1 - j\nu \lambda_p}, \quad (6.79)$$

where we have defined

$$\pi_p = \prod_{\substack{q=0 \\ q \neq p}}^{D-1} \frac{1}{(1 - \lambda_q/\lambda_p)}. \quad (6.80)$$

Note that

$$\sum_{p=0}^{D-1} \pi_p = \sum_{p=0}^{D-1} \prod_{\substack{q=0 \\ q \neq p}}^{D-1} \frac{1}{(1 - \lambda_q/\lambda_p)} = 1.0. \quad (6.81)$$

Then, the probability density function of  $Y$  can be written as

$$\begin{aligned} Pr(Y = y) &= \sum_{i=0}^{D-1} \pi_i Pr(Y_i = y) = \sum_{i=0}^{D-1} \pi_i \left( \frac{1}{E(Y_i)} e^{-y_1/E(Y_i)} \right) \\ &= \sum_{i=0}^{D-1} \pi_i \frac{1}{\lambda_i} e^{-y_1/\lambda_i} \end{aligned} \quad (6.82)$$

Substituting (6.82) into the integral equation in (6.73), we have

$$\begin{aligned}
E_Y\left(\frac{1}{2}\operatorname{erfc}(\sqrt{Y})\right) &= \int_0^{\infty} \frac{1}{2}\operatorname{erfc}(\sqrt{y}) \sum_{i=0}^{D-1} \pi_i \frac{1}{\lambda_i} e^{-y/\lambda_i} dy \\
&= \sum_{i=0}^{D-1} \pi_i E_{Y_i} \left\{ \frac{1}{2}\operatorname{erfc}(\sqrt{Y_i}) \right\} \\
&= \sum_{i=0}^{D-1} \pi_i \frac{1}{2} \left( 1 - \sqrt{\frac{\lambda_i}{1+\lambda_i}} \right)
\end{aligned} \tag{6.83}$$

Next, consider when the polynomial has multiple roots of the same values. That is, the characteristic rational polynomial (6.79) is

$$E(e^{j\nu Y}) = \left( \frac{1}{1 - j\nu\lambda_1} \right)^D. \tag{6.84}$$

The probability density function for (6.84) is known as

$$\begin{aligned}
P(Y = y) &= \frac{1}{(D-1)! E(Y_1)^D} y^{D-1} e^{-y/E(Y_1)} \\
&= \frac{1}{(D-1)! \lambda_1} y^{D-1} e^{-y/\lambda_1}.
\end{aligned} \tag{6.85}$$

Substituting (6.85) into the integral equation in (6.73), we have

$$\begin{aligned}
E_Y\left(\frac{1}{2}\operatorname{erfc}(\sqrt{Y})\right) &= \int_0^{\infty} \frac{1}{2}\operatorname{erfc}(\sqrt{y}) \frac{1}{(D-1)! \lambda_1} y^{D-1} e^{-y/\lambda_1} dy \\
&= \left( \frac{1-\Omega}{2} \right)^D \sum_{k=0}^{D-1} \binom{D-1+k}{k} \left( \frac{1+\Omega}{2} \right)^k
\end{aligned} \tag{6.86}$$

where  $\Omega = \sqrt{\frac{\lambda_1}{1+\lambda_1}}$ .

# Chapter 7

## Sequential Detection

In this chapter, we develop an adaptive, low complexity, tree-search sequential-search receiver for the detection of uncoded  $q$ -ary QAM symbols ( $q$  up to 64) transmitted over the time-varying, diversity reception, multipath fading ISI channels. The sequence search method is based on the maximum likelihood sequence detection<sup>1</sup> (MLSD) criterion. Unlike previous research on the sequence-based detection, a symbol-spaced channel is not assumed given *a priori*; instead the receiver utilizes the channel estimation technique developed in Chapter 4 to derive the pre-processing receive filters such that after filtering by pre-processor, the symbol-spaced equivalent channel and the symbol-spaced sufficient statistics become available for the post-processor performing the sequential detection. The new receiver will be extended to the sequential decoding of the channel-interleaved trellis-coded symbols in Chapter 8.

---

1. MLSE, is the other equally commonly used term in the open literature which is an acronym for maximum likelihood sequence estimation. We prefer the terminology *detection* because the technique is employed in detecting the transmitted symbols.

## 7.1 Introduction

We now briefly discuss our motivation for considering the sequence-based search techniques and bring up some critical issues we have to deal with in realizing the benefit of maximum likelihood sequence detection (MLSD).

### 7.1.1 Motivation for sequence based detection

For the detection of a signal having a certain memory structure, a sequence-based detection scheme is the optimum [33]. The ISI channel creates the memory structure of the received signal. A sequence-based detection will enhance the equalization performance greatly and always provide a detection performance better than, or at least equal to, that of the correct decision feedback MMSE-DFE. Namely, the minimum Euclidean detection-distance of MLSD is always larger than or equal to that of the ideal DFE: The difference between the two becomes larger as ISI becomes worse. This is because the DFE follows only a single path amongst all the possible hypothetical paths in the decision tree and thus has to make an early decision, whereas the MLSD follows every possible paths and does not make any early decision until the end of the sequence is reached.

In addition, in practice the DFE has the inherent problem of error-propagation due to decision feedback. This error-propagation problem of the DFE may be tolerable for a small signal constellation such as QPSK or for channels with insignificant ISI. However, the problem becomes catastrophic as the size of signal set grows or as the channel starts to contain severe in-band nulls in the folded-spectrum. In general, this error-propagation problem can be resolved by replacing the feedback filter of the DFE with the modulo-addition feedback filter at the transmitter with exactly the same coefficients calculated for the feedback filter of DFE. This can indeed be a good solution if the channel is not expected to vary much during the reception of the signal burst. We have seen a good example of the

T-H precoder in Chapter 3: The T-H precoder operating on the severe ISI telephone channel shows a significant SNR advantage over the use of the DFE. Unfortunately, the use of the T-H precoder for ISI mitigation in the rapid time-varying channel environment is not a practical solution. For the fast time-varying channel, the receiver might have to send back to the transmitter the updated feedback filter coefficients or the channel-state information as frequently as almost every symbol-epoch, representing an intolerable overhead.

On the other hand, there is a scenario where the transceiver may have to operate in a low average SNR region for example due to shadow-fading. In order to increase the area of coverage to such a region, we might have to consider the use of channel-coding, e.g. the use of a spectrally efficient trellis-code. In this scenario, the optimum receiver must facilitate joint detection and decoding. In this regard, the DFE is not a canonical receiver structure again due to the error propagation problem; although in an ideal situation where no decision feedback error and thus no error propagation are assumed, the use of DFE is believed to be canonical also for the coded transmission [107].

Therefore, in this chapter we start with the feasibility of MLSD for uncoded transmission of spectrally efficient digital signals having a large signaling constellation ( $q$ -QAM signaling up to  $q = 64$ ). In chapter 8, we extend the receiver to sequence detection of trellis-coded modulation that is capable of supporting joint decoding and equalization, as an alternative to the simple case of cascading the DFE with a sequence decoder.

### **7.1.2 Reduced complexity sequence based detection techniques**

In implementing MLSD, the issue of computational complexity and feasibility must be addressed properly. For example consider  $q$ -QAM signaling up to  $q = 64$  and channel memory length of up to  $N_g = 6$  symbol periods. The Viterbi algorithm (VA) is known to be an efficient method to carry out MLSD operations while achieving the full performance

advantage of MLSD: The VA is a complete search method. With MLSD the achieved symbol error rate is very close to the fundamental matched filter bounds. For example, in MLSD over any two tap channel<sup>1</sup> there is no performance loss at all, fully achieving the detection performance of the fundamental matched filter bound. However, the implementation complexity of the complete search VA grows exponentially with the length of channel memory and the size of the signaling set. There are  $q^{N_s}$  states (e.g.  $64^6$  for 64-QAM) and  $q$  branches out of each state in the trellis.

The complexity problem becomes even worse for the time-varying channel. One of the salient features of the VA, when applied to the time-invariant ISI, is that VA can be implemented only with comparisons of metrics, without any multiplications. The multiplication was required only once to obtain the ISI channel output values at each of the  $q \times q^{N_s}$  branches. Later in decoding, they are simply compared with the received sequence. When we have time-varying ISI, however, we need to recompute all ISI channel output values to advance to the next section of the trellis. Even without considering the additional complexity required to perform comparisons, we note that implementing the complete search VA is impractical for a large constellation and for time-varying channels.

A great deal of research has been undertaken to reduce the computational complexity while still achieving a detection performance close to that of the complete search VA. Research in this arena might be addressed as follows, divided largely in two different categories; one approach is to reduce the number of states and the other is to use a sequential search algorithm. The former is to construct a trellis which has a reduced number of states, utilizing the distances among a set of element-symbols defined in the signal constellation. The underlying principle is that the difference of the decision-metrics used in comparing sequences is directly dependent up on the Euclidean-distance of the

---

1. Symbol-spaced tapped delay line channel

element-symbols associated with the paths in comparison. The larger the Euclidean distance is in the element-symbols of any pair of state-transition paths on the original state-trellis, the larger the difference is in decision-metrics associated with the two paths. Thus, amongst those paths in the original state-trellis whose Euclidean metric differences are large enough, early detection-decisions can be made amongst the set of symbol-elements and they can be considered significantly reliable. Those states that belong to the set of involved paths can be collapsed to form a new single state. A subset-trellis is obtained from using the Ungerboeck-like set partitioning rules [98] to collapse a larger number of states into a smaller number of states. It then searches the subset-trellis with the Viterbi algorithm. This technique is called the reduced state Viterbi algorithm (RSVA) [101]. The other obvious method of constructing the subset-trellis to truncate the length of channel response by canceling the contribution of the channel response truncated by the use of previously decided symbols.

The RSVA techniques then utilize the well established VA on the subset trellis. One observation we can immediately point out is that RSVA trades-off the optimality of MLSD with the reduction of number of states because some paths of the full trellis are permanently removed from consideration, and the loss is permanent for a choice of subset-trellis.

We found out that we can achieve better, near-optimal performance-complexity trade-offs by using sequential search algorithms such as M-algorithm, the Fano-algorithm and the T-algorithm [94-96,103,104]. The search algorithms operate on the original trellis and are much more flexible in dealing with the time-varying channels.

The Fano algorithm [92] attempts to expand only the most probable path through the trellis. The Fano metric provides a “fair” measure of goodness at different depths of exploration, unlike the cumulative metric used in VA: it compensates for the depth of an exploration. The value of the Fano metric of a correct path will increase on the average, while those of incorrect paths decrease on the average. We have derived the Fano metric for

the matched filtered ISI channel in Appendix B. However, we found out that there are big drawbacks hindering the use of Fano-algorithm for symbol detection in the time-varying channel. The calculation of the metric becomes too complex due to the time-varying channel and more research insights must be gained to proceed further.

On the other hand, the use of the T-algorithm provides the best performance-complexity trade-offs compared to the use of M-algorithm, Fano-algorithm and RSVA. The intuition regarding our claim will be addressed after we introduce the basic equations and the T-algorithm in 7.3.3.

### 7.1.3 The pre-processing filters

By the pre-processing unit of the MLSD receiver, we imply all the receiver

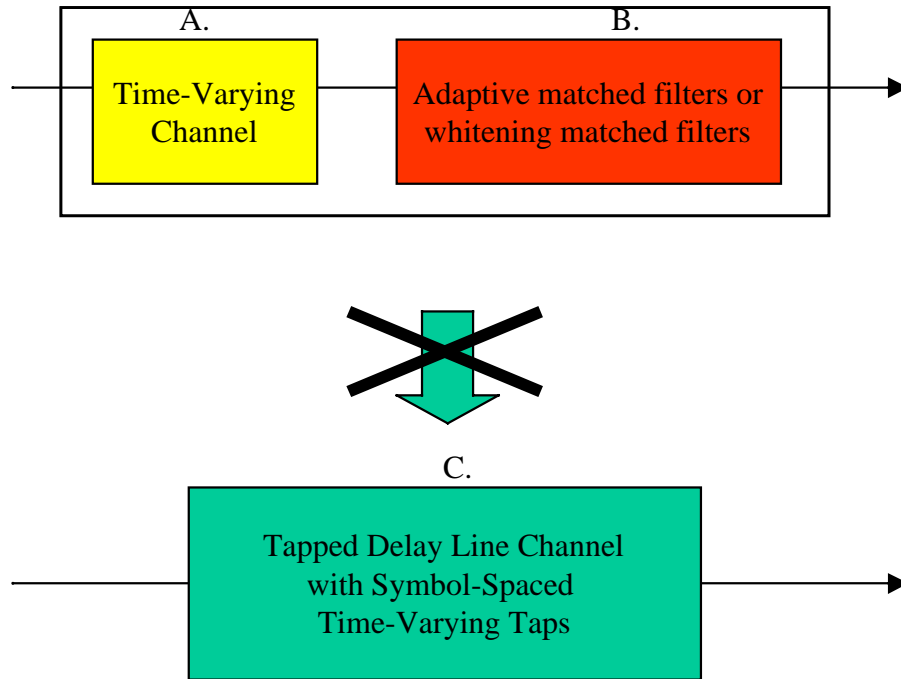


Figure 7-1 The wireless channel models

functions required to bring down the continuous waveform<sup>1</sup> received signal to the symbol-spaced *sufficient statistic* sequence and the equivalent symbol-spaced channel. The sequential search methods are then applied to the equivalent symbol-spaced channel model and the symbol-spaced decision statistics. This pre-processing filtering is largely ignored in the literature of maximum likelihood sequence detection using the so-called *discrete-time white noise model* which models the transmitter, channel, matched filter and the noise whitening filter as a tapped delay line model with symbol-spaced taps. For example, see [123][124][125]. Moreover, each of the symbol-spaced taps is modeled as Rayleigh fading. It will be clear after section 7.2 that such an approach is counter-productive. We emphasize that the pre-processing is very important for wireless channels because

- the channel is time-varying and unknown and
- the efficiency of the reduced complexity post-processing search algorithms depends heavily on the choice of preprocessing.

The channel is time-varying and unknown, and thus the time-varying channel must be estimated prior to the matched filtering i.e. before the function block-B. in Figure 7-1 can be calculated. In addition, with the assumption of excess bandwidth, the channel must be fractionally-spaced taps and thus the matched filter also must be fractionally-spaced. That is, we are claiming that the symbol-spaced channel-model, described in the block-C in Figure 7-1, is invalid for the purpose of fading multipath channel description where the assumption is that the function block-B is already performed and contained in the channel model.

There are a number of different ways to shape the overall ISI by pre-processing.

---

1. Or, the fractionally-spaced sampled received signal. Since the received signal is bandlimited, the fractionally sampled signal is equivalent to the continuous waveform signals once the fractional sampling rate is fast enough, such that the inverse of sampling rate is more than the bandwidth of the signal.

Among them are the whitened matched filter (WMF), the mean square whitened matched filter (MS-WMF) and matched filtering only. The WMF [60] has a nice feature: the output of the WMF forms a non-correlated sufficient statistic sequence for the detection of the input sequence, and thus the branch metric calculation and comparison become relatively simple. However, the use of a WMF in a time-varying channel poses some problems. When the matched filtered ISI contains a null in the Nyquist band, the whitened matched filter may not be well defined [59]. Even when it exists, since the whitening operation is still a channel inversion operation, it may cause some noise enhancement problems in the presence of channel estimation errors. Moreover, in adapting to fast fading the complexity of obtaining the whitened matched filter coefficients becomes non-trivially high. This may be the reason why the whitened matched filter is used mostly in the context of time-invariant channels only.

In the beginning we preferred to try out the last approach of using only matched filters at each diversity branch, followed by combining to give the symbol-spaced sufficient statistics to the post-processors using the Ungerboeck type of metric calculation. The matched filter coefficients are obtained from the channel estimates with a simple Hermitian operation, without the matrix inversion required for the whitening operation and thus without the instability problem involved with inverting the channel. However, we found out that the sequential search algorithms has to consider the full-trellis operating on the matched filtered outputs, and any sub-optimal reduced search effort will result in a large loss in the detection performance. This result is for the channel with a significant ISI. For non-null channels, in any methods work well.

As the proposed approach we use the feedforward filter of a decision feedback equalizer as the pre-processing structure to the MLSD. The feedforward filter takes the role of mean squares WMF (MS-WMF), and shapes the overall channel to be minimum phase. In addition, unlike the WMF, a MS-WMF always exists.

## 7.2 Optimum Diversity Combining MLSD

In this section, we derive the optimal pre-processing blocks for the diversity reception signals. The derivation will provide an opportunity to gain insights on the structure of DC-MLSD receiver, compared with that of the MMSE DC-DFE, and the optimal and sub-optimal pre-filtering solutions.

### 7.2.1 The baseband channel model

Figure 7-2 illustrates the baseband equivalent channel model for the  $L$ -diversity channel receiver. The basic properties of the channel model stays the same as was developed in Chapter 2. The difference is that we now use the polyphase representation of the channel operation, which is suitable for describing the fractional-sampling of the received signals in terms of the symbol-spaced symbol transmission. We briefly describe the channel model, notations and assumptions. We assume the shaping filter employs excess bandwidth, and then the baseband received signal at  $l$ -th diversity branch should be fractionally sampled. We denote the cascade of the transmit pulse shaping filter, the baseband equivalent time-varying channel and any anti-aliasing filter at the receiver (assumed to be an ideal brick wall filter) by the fractionally-spaced sampled filter  $\mathbf{h}^l(k)$ , for  $l = 1, 2, \dots, L$ . We denote the sampling interval as  $T_s = T_B/N_s$ , where  $T_B$  is the symbol period and  $N_s \geq 2$ . We assume the effective span of the overall channel extends over  $N_h$  symbol periods, i.e., the delay dispersion is zero outside of an interval  $[0, N_h T_B]$ . The sampled noise is assumed to be complex-valued additive white Gaussian with zero mean and variance  $\sigma_n^2$ . For the  $k$ -th symbol interval we have  $N_s$  discrete-time received samples of  $x^l(t)$  which can be described by

$$x_{k,i}^l := x^l(t)|_{t=(k+i/N_s)T} = \sum_{j=1}^N I_j h^l((k+i/N_s)T - jT; kT) + u^l((k+i/N_s)T),$$

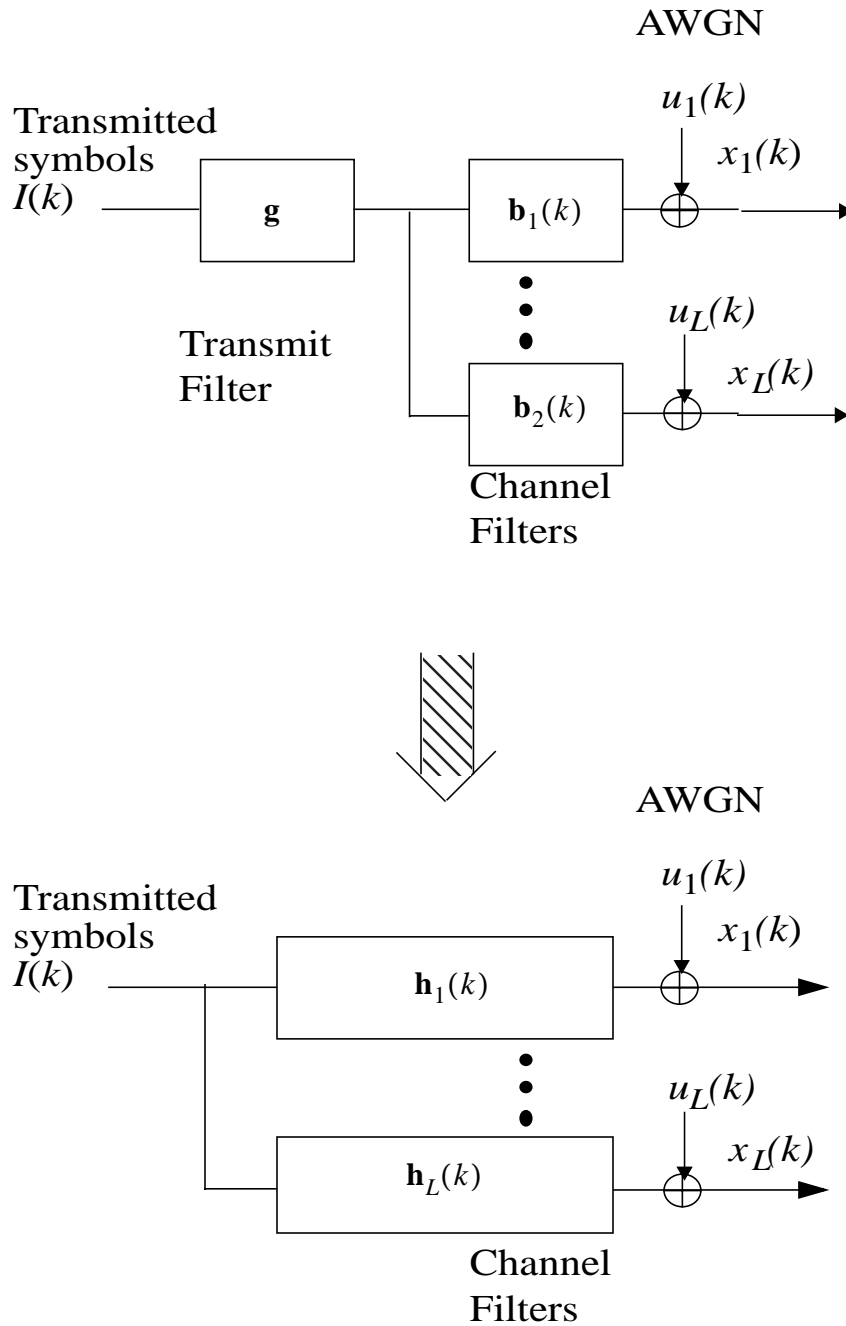


Figure 7-2 The baseband representation of the diversity channels

for  $0 \leq i \leq N_s - 1$  and  $l = 1, \dots, L$ . For convenience of notation, we now define

$$\mathbf{x}_k^l := \begin{bmatrix} x_{k, N_s-1}^l \\ x_{k, N_s-2}^l \\ \dots \\ x_{k, 0}^l \end{bmatrix}, \quad (7.1)$$

$$\mathbf{h}_m^l(k) := \begin{bmatrix} h^l((m + (N_s - 1)/N_s)T ; kT) \\ h^l((m + (N_s - 2)/N_s)T ; kT) \\ \dots \\ h^l(mT ; kT) \end{bmatrix}, \quad (7.2)$$

and

$$\mathbf{u}_k^l := \begin{bmatrix} u^l((k + (N_s - 1)/N_s)T) \\ u^l((k + (N_s - 2)/N_s)T) \\ \dots \\ u^l(kT) \end{bmatrix}. \quad (7.3)$$

Thus, a  $[(N_h + 1)N_s \times 1]$  vector  $\mathbf{h}^l(k)$  represents the non-zero portion of the overall channel impulse response, sampled at the rate of  $N_s/T_B$ , i.e.,

$$\mathbf{h}^l(k) := [\mathbf{h}_0^l(k)^t \mathbf{h}_1^l(k)^t \dots \mathbf{h}_{N_h}^l(k)^t]^t. \quad (7.4)$$

Then, for the time interval of interest,  $0 \leq t \leq (N + N_h)T_B$ , the discrete-time system equation is given by

$$\begin{bmatrix} \mathbf{x}_{N+N_h}^l \\ \mathbf{x}_{N+N_h-1}^l \\ \dots \\ \mathbf{x}_0^l \end{bmatrix} = \begin{bmatrix} \mathbf{h}_0^l(N+N_h) & \mathbf{h}_1^l(N+N_h) & \dots & \mathbf{h}_{N_h}^l(N+N_h) & \mathbf{0} \\ & \mathbf{h}_0^l(N+N_h-1) & \dots & \mathbf{h}_{N_h}^l(N+N_h-1) & \\ & & \dots & & \\ \mathbf{0} & & & \mathbf{h}_0^l(0) & \mathbf{h}_1^l(0) & \dots & \mathbf{h}_{N_h}^l(0) \end{bmatrix} \begin{bmatrix} \mathbf{0}_{N_h} \\ I_{N-1} \\ \dots \\ I_0 \\ \mathbf{0}_{N_h} \end{bmatrix}, \quad (7.5)$$

$$+ \begin{bmatrix} \mathbf{u}_{N+N_h}^l \\ \mathbf{u}_{N+N_h-1}^l \\ \dots \\ \mathbf{u}_0^l \end{bmatrix}$$

or more compactly by

$$\mathbf{x}^l = \mathbf{H}^l \mathbf{I}' + \mathbf{u}^l, \quad (7.6)$$

where

- $\mathbf{x}^l$  is the vector storing the fractionally-sampled received signals during  $0 \leq t \leq (N + N_h)T_B$ ,
- $\mathbf{H}^l$  is the channel matrix,
- $\mathbf{I}' = (\mathbf{0}_{N_h}^t \quad \mathbf{I}^t \quad \mathbf{0}_{N_h}^t)$ ,  $\mathbf{0}_{N_h}$  is the  $(N_h \times 1)$  vector of zeros, and  $\mathbf{I} = (I_{N-1} \dots I_0)^t$  is the transmitted data symbols. The  $\mathbf{0}_{N_h}$  is used in place of the training segments for simplicity.
- $\mathbf{u}^l$  denotes the noise vector.

In this chapter, we again assume the continuous transmission of frames explained in Chapter 4, where a frame consists of training and unknown data segments. The feedforward channel estimation procedure given in Chapter 4 is assumed to provide the estimates of the time-varying channel vectors in (7.5). Briefly, the feedforward channel estimation is comprised of two modes--the snap-shot channel-vector estimation using the

training symbols and then the interpolation of a set of channel estimate vectors to supply the estimates of the channel in-between the training segments. The least squares channel estimator (LSE) in Chapter 4 is used in this chapter.

## 7.2.2 Derivation of the optimum diversity combining MLSD

Figure 7-3 shows the optimum diversity combiner. Each of the  $L$  independent fractionally sampled received signals are fed to the matched filter at each branch, and the matched filtered signals are combined, sampled at the symbol rate to form the sufficient statistics sequence  $\{z_k\}$ . In this section, we provide the standard MLSD derivation and show that the symbol rate sampled, matched-filtered diversity-combining signal  $z_k$  is indeed the sufficient statistic for MLSD processing of the  $L$ -diversity received signals. In addition, in 7.2.3 and 7.2.4, the Ungerboeck and Forney MLSD receivers are derived and compared, and then they are shown to be equivalent in achieving MLSD. When applied to reduced search detection using T-algorithm, however, Forney form turns out to be more efficient, requiring significantly fewer survivors on average. Thus, the derivation of Forney's receiver is emphasized. In 7.2.5 and 7.2.6, finite length whitening filter (WF) and mean-squares whitening filter (MS-WF) are discussed respectively.

Now, we start the standard MLSD derivation. Given the  $L$  independent diversity discrete-time received sequences, we want to find the maximum likelihood sequence  $\hat{\mathbf{I}}$ , i.e.,

$$\begin{aligned}
 \hat{\mathbf{I}} &= \underset{\mathbf{I} \in I}{\operatorname{arg\,max}} \operatorname{Pr}\{\mathbf{x}^1 \dots \mathbf{x}^L | \tilde{\mathbf{I}}\} \\
 &= \underset{\mathbf{I} \in I}{\operatorname{arg\,min}} \left\{ \sum_{l=1}^L \|\mathbf{x}^l - \tilde{\mathbf{x}}^l\|^2 \right\} \\
 &= \underset{\tilde{\mathbf{I}} \in I}{\operatorname{arg\,min}} \{C + M_1(\tilde{\mathbf{I}}) + M_2(\tilde{\mathbf{I}})\}
 \end{aligned} \tag{7.7}$$

where

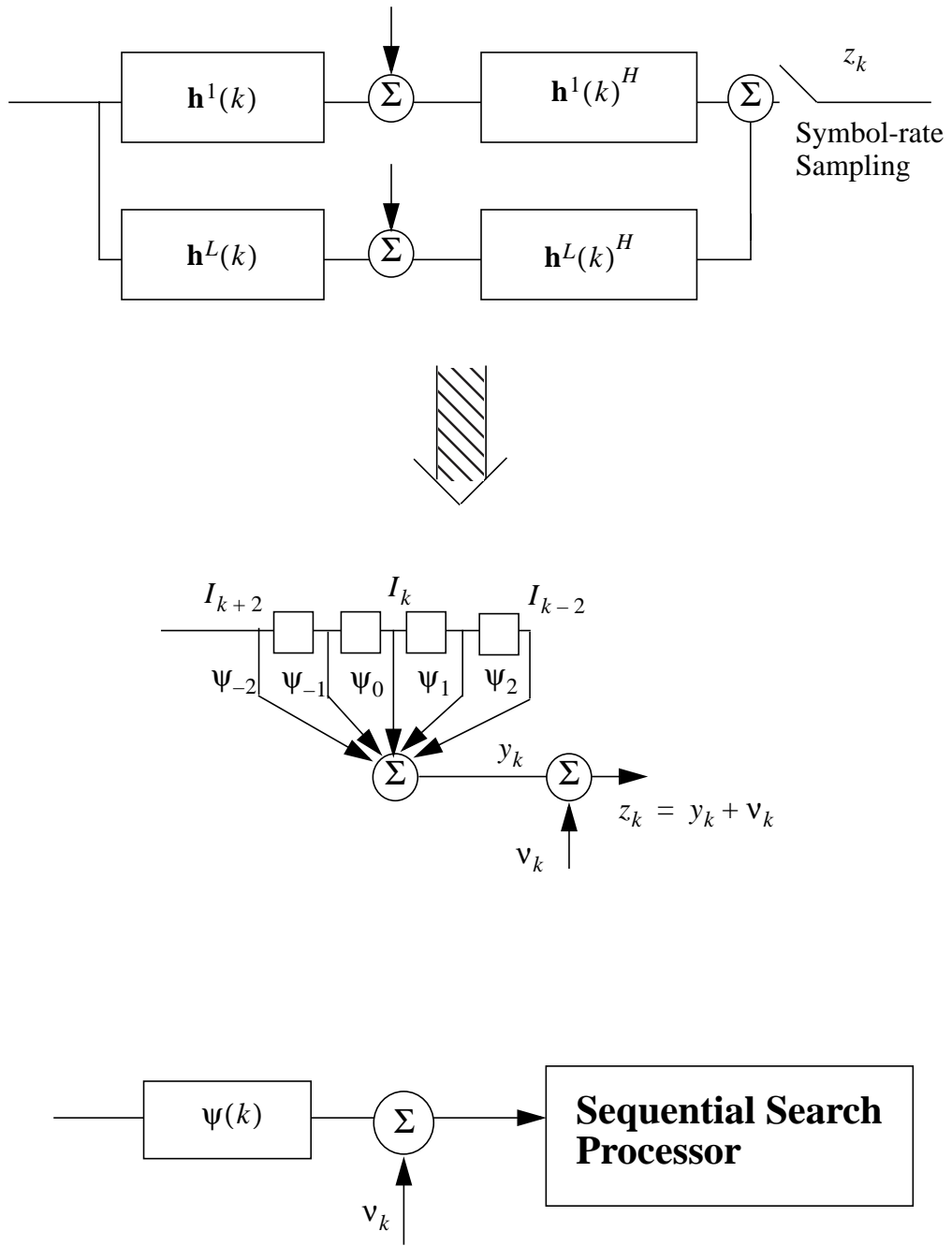


Figure 7-3 The optimum MLSD pre-processing filters, which is again the matched filtering, diversity combining, and symbol-rate sampling.

- the hypothetical channel output sequence  $\tilde{\mathbf{x}}^l$  based on the hypothetical input sequence  $\tilde{\mathbf{I}}'$  is

$$\tilde{\mathbf{x}}^l = \mathbf{H}^l \tilde{\mathbf{I}}' \quad (7.8)$$

- a constant term since it is simply the energy of the received signal

$$C = \sum_{l=1}^L \mathbf{x}^{lH} \mathbf{x}^l \quad (7.9)$$

- the cross term is

$$M_1(\tilde{\mathbf{I}}) = -2Re\left\{\sum_{l=1}^L \tilde{\mathbf{x}}^{lH} \mathbf{x}^l\right\} \quad (7.10)$$

- finally the quadratic term regarding the hypothetical sequence  $\tilde{\mathbf{x}}^l$  is

$$M_2(\tilde{\mathbf{I}}) = \sum_{l=1}^L \tilde{\mathbf{x}}^{lH} \tilde{\mathbf{x}}^l. \quad (7.11)$$

Next, substituting (7.8) into (7.10) and (7.11), we have

$$M_1(\tilde{\mathbf{I}}) = -2Re\left\{\tilde{\mathbf{I}}^H \sum_{l=1}^L \mathbf{H}^{lH} \mathbf{x}^l\right\} = -2Re\left\{\tilde{\mathbf{I}}^H \mathbf{z}\right\}, \quad (7.12)$$

and

$$M_2(\tilde{\mathbf{I}}) = \tilde{\mathbf{I}}^H \left(\sum_{l=1}^L \mathbf{H}^{lH} \mathbf{H}^l\right) \tilde{\mathbf{I}} = \tilde{\mathbf{I}}^H \Psi \tilde{\mathbf{I}}, \quad (7.13)$$

where we have defined

$$\mathbf{z} = \sum_{l=1}^L \mathbf{H}^{lH} \mathbf{x}^l, \quad (7.14)$$

and

$$\Psi = \left(\sum_{l=1}^L \mathbf{H}^{lH} \mathbf{H}^l\right). \quad (7.15)$$

Now, recalling that  $\mathbf{I}' = (\mathbf{0}_{N_h}^t \quad \mathbf{I}^t \quad \mathbf{0}_{N_h}^t)$  and thus ignoring the influences of zero-padded vectors in the final equation, we can write the diversity combining matched filter results  $\mathbf{z}$  in terms of  $\mathbf{I}$ . From (7.14), we note that the multiplication  $\mathbf{H}^{lH} \mathbf{x}^l$  represents the

fractionally-spaced matched filtering operation and symbol-rate sampling at each diversity branch, and the summation implies diversity combining. Therefore,  $\mathbf{z}$  is the symbol-spaced sufficient statistics for the maximum likelihood sequence estimation. Then, the input/output relationship can be rewritten as

$$\mathbf{z} = \Psi \mathbf{I} + \mathbf{v}, \quad (7.16)$$

where the noise vector

$$\mathbf{v} = \sum_{l=1}^L \mathbf{H}^{lH} \mathbf{n}^l \quad (7.17)$$

is the  $[N \times 1]$  noise vector with zero mean vector and the correlation matrix  $E\{\mathbf{v}\mathbf{v}^H\} = \sigma_n^2 \Psi$ . Based on (7.16), the overall system can be described as the symbol-spaced tapped delay line model of Figure 7-3 (b).

### 7.2.3 The Ungerboeck's receiver

Having obtained the symbol-spaced sequence  $\{z_k\}$  of (7.16), Ungerboeck's metric computation method can be applied to implement the VA or T-algorithm, as depicted in Figure 7-3 (c). Ungerboeck's path metric uses only (7.12) and (7.13), i.e, not the constant term. Ungerboeck's MLSD receiver has major advantages over Forney's form. First, it does not require the noise whitening filter of Forney's receiver. In fact, the noise whitening operation is embedded in Ungerboeck's metric computation routine. Considering imperfect channel estimation, any channel inversion effort (to achieve noise whitening) is subject to noise enhancement and instability as well, and is not desirable. Second, the complexity of obtaining the noise whitening filter is relatively large. We either have to solve for the root of the polynomial in a static channel or solve a sufficiently large matrix equation in the time-varying channel case.

The use of Ungerboeck's receiver, however, is not suitable for a reduced complexity

sequential search such as the T-algorithm or M-algorithm. The following analysis helps clarify the reason behind it. Now, consider the branch metric computation using Forney and Ungerboeck form: Forney's metric is calculated from

$$\lambda_k^F = |e_k^F|^2,$$

where

$$e_k^F = y_k - \sum_{m=0}^{N_h} f_m \tilde{I}_{k-m} = \sum_{m=0}^{N_h} f_m \Delta \tilde{I}_{k-m} + \eta_k. \quad (7.18)$$

The Ungerboeck metric is

$$\lambda_k^U = 2Re\{\tilde{I}_k^* e_k^U\}, \quad (7.19)$$

where  $e_k^U = z_k - \sum_{m=0}^{N_h} \Psi_m \tilde{I}_{k-m}$  and thus can be rewritten

$$e_k^U = \sum_{m=0}^{N_h} \Psi_m \Delta \tilde{I}_{k-m} + \sum_{m=1}^{N_h} \Psi_m^* I_{k+m} + v_k. \quad (7.20)$$

As indicated in the second term of right side in (7.20), the Ungerboeck metric is influenced by the future symbols. The VA performs a complete search and thus achieves the full MLSD performance. The VA purges only if there are merged paths to the same states. For the merged paths, the first and the second terms of (7.20) are the same, such that the purging is only based on the cumulative metric difference accumulated before the merge. This is why the Ungerboeck form works in the context of the complete-search VA.

For the case of suboptimal sequential search such as M- or T-algorithms, survivors are dropped based on the metric difference. However, as indicated in the previous paragraph, the Ungerboeck metric is fair only when they are compared among the paths converging to the same state. In fact, the suboptimal search algorithm doesn't work for a severe ISI channel even with zero input noise. The metric difference build-up by the first term in (7.20) is very vulnerable to interference from the second term if the ISI is severe, which implies the magnitudes of off-diagonal terms of summed channel autocorrelation

function  $\{\psi_m, m \neq 0\}$  have large values. Our test simulation results on a severe ISI, static channel,  $(1/2, 1/(\sqrt{2}), 1/2)$  which is a worst ISI channel at the length of 3 [33] with the use of 4-QAM modulation indicates that we need to keep all the paths to get performance close to that of MLSD. With any suboptimal search, the receiver detection performance stays flat even with zero input noise. Thus, we turn to the use of Forney's MLSD receiver.

#### 7.2.4 Forney's MLSD receiver

For static channels, by the use of spectral factorization the summed channel autocorrelation function can be factored into two Hermitian symmetric polynomials, i.e.,

$$\Psi(D) = \sum_{i=-N_h}^{N_h} \Psi_i D^i = F^*(D^{-1})F(D), \quad (7.21)$$

where the  $F(D)$  is the causal, minimum phase response

$$F(D) = \sum_{i=0}^{N_h} f_i D^{-i}. \quad (7.22)$$

Then, the whitening filter is  $1/F^*(D^{-1})$ .

For the time-varying channels, we may want to use Cholesky factorization, which is analogous to spectral factorization. By the use of Cholesky factorization, the positive-definite matrix  $\Psi$  (7.16) can be factored into the upper triangular matrix  $\mathbf{F}$  and its Hermitian transpose,

$$\Psi = \mathbf{F}^H \mathbf{F} \quad (7.23)$$

and

$$\Psi^{-1} = \mathbf{F}^{-1} \mathbf{F}^{-H}. \quad (7.24)$$

Thus, the matched filtered symbol spaced sequence  $\mathbf{z}$  of (7.16) can be rewritten as

$$\mathbf{z} = \mathbf{F}^H \mathbf{F} \mathbf{I} + \mathbf{v}. \quad (7.25)$$

Now, by applying the whitening filter  $\mathbf{F}^{-H}$  to  $\mathbf{z}$  we have:

$$\mathbf{y} = \mathbf{F}^{-H} \mathbf{z} = \mathbf{F} \mathbf{I} + \boldsymbol{\theta}, \quad (7.26)$$

where the noise term,  $\boldsymbol{\theta} = \mathbf{F}^{-H} \mathbf{v}$ , is now whitened having the diagonal correlation matrix

$$\begin{aligned} \mathbf{E}\{\boldsymbol{\theta}\boldsymbol{\theta}^H\} &= \mathbf{E}\{\mathbf{F}^{-H} \mathbf{v} \mathbf{v}^H \mathbf{F}^{-1}\} = \mathbf{F}^{-H} \mathbf{E}\{\mathbf{v} \mathbf{v}^H\} \mathbf{F}^{-1} \\ &= \sigma_n^2 (\mathbf{F}^{-H} \boldsymbol{\Psi} \mathbf{F}^{-1}) = \sigma_n^2 \mathbf{F}^{-H} \mathbf{F}^H \mathbf{F} \mathbf{F}^{-1} = \sigma_n^2 \boldsymbol{\Xi}_N, \end{aligned} \quad (7.27)$$

where  $\boldsymbol{\Xi}_N$  is the  $N \times N$  identity matrix. Now, note that the matrix  $\mathbf{F}$  is an upper triangular matrix and thus it is causal according to our definition equation (7.16). In fact, the non-zero elements of each row of matrix  $\mathbf{F}$  converges to the coefficients of  $F(D)$ , i.e., for  $i = 0, 1, \dots, N_h$

$$\lim_{N \rightarrow \infty} \mathbf{F}_{(N-1; N-1+i)} = f_i. \quad (7.28)$$

The following table summarizes the similarities between the spectral factorization theorem for the static channels and the Cholesky factorization for the time-varying channels.

**Table 7-1: Factorization theorems for static and time-varying channels**

	Static Channel	Time-Varying Channel
<b>Channel</b>	$h(t)$	$\mathbf{H}$
<b>Factorization</b>	$\Psi_k = \int h(t) h^*(t+kT) dt$ $\Psi(D) + N_o = S_o f^*(D^{-1}) f(D)$	$\boldsymbol{\Psi} = \mathbf{H}^H \mathbf{H} + \sigma_n^2 \boldsymbol{\Xi} = \mathbf{F}^H \mathbf{S} \mathbf{F},$ where $\boldsymbol{\Xi}$ is an $N \times N$ identity matrix.
<b>MS- WF</b>	$\frac{1}{S_o f^*(D^{-1})},$ Feedforward filter of DFE $_{\infty}$	$\mathbf{S}^{-1} \mathbf{F}^{-H} \text{ or } S_{N_f-1}^{-1} \mathbf{e}_{N_f-1} \mathbf{F}^{-H}$ Feedforward filter of the NT-DFE
<b>Min. P.R.</b>	$f(D)'$	$\mathbf{F}'$ Upper triangular (band matrix)

The matrix  $\mathbf{F}^{-H}$  is the optimal whitening operator for the entire receive signal  $\mathbf{z}$ . Since it is impossible to obtain  $\mathbf{F}^{-H}$  as the length of the sequence become large, a suboptimal, finite filter length solution should be considered and it will be discussed in 7.2.5.

We continue our derivation of the Forney receiver from the basic MLSD equation (7.7). The three terms in (7.7) can be rewritten as follows

- The constant term: (USE:  $\sum_l \mathbf{H}^l \mathbf{H}^H = \Psi = \mathbf{F}^H \mathbf{F}$  and  $\theta = \mathbf{F}^{-H} \sum_l \mathbf{H}^l \mathbf{u}$ )

$$\begin{aligned}
C &= \sum_l \mathbf{x}^l H \mathbf{x} = \sum_l (\mathbf{H}^l \mathbf{I} + \mathbf{u}^l)^H (\mathbf{H}^l \mathbf{I} + \mathbf{u}^l) \\
&= \mathbf{I}^H \left( \sum_l \mathbf{H}^l \mathbf{H}^H \right) \mathbf{I} + \mathbf{I}^H \sum_l \mathbf{H}^l \mathbf{H}^H \mathbf{u} + \sum_l \mathbf{u}^{lH} \mathbf{H}^l \mathbf{I} + \sum_l \mathbf{u}^{lH} \mathbf{u}^l \\
&= \mathbf{I}^H \mathbf{F}^H \mathbf{F} \mathbf{I} + \mathbf{I}^H \sum_l \mathbf{H}^l \mathbf{H}^H \mathbf{u} + \sum_l \mathbf{u}^{lH} \mathbf{H}^l \mathbf{I} + \sum_l \mathbf{u}^{lH} \mathbf{u}^l \\
&= \mathbf{I}^H \mathbf{F}^H \mathbf{F} \mathbf{I} + \mathbf{I}^H \mathbf{F}^H \left( \mathbf{F}^{-H} \sum_l \mathbf{H}^l \mathbf{H}^H \mathbf{u} \right) + \left( \sum_l \mathbf{u}^{lH} \mathbf{H}^l \mathbf{F}^{-1} \right) \mathbf{F} \mathbf{I} + \left( \sum_l \mathbf{u}^H \mathbf{H}^l \mathbf{F}^{-1} \right) \left( \mathbf{F}^{-H} \sum_l \mathbf{H}^l \mathbf{H}^H \mathbf{u} \right) \\
&= (\mathbf{F} \mathbf{I} + \theta)^H (\mathbf{F} \mathbf{I} + \theta) = \mathbf{y}^H \mathbf{y} \tag{7.29}
\end{aligned}$$

That is,  $C = \mathbf{x}^H \mathbf{x} = \mathbf{y}^H \mathbf{y}$ .

- Next, note the first metric term depends on the hypothetical sequence and can be rewritten as:

$$\begin{aligned}
M_1(\tilde{\mathbf{I}}) &= -2Re\{\tilde{\mathbf{I}}^H \sum_{l=1}^L \mathbf{H}^l \mathbf{x}^l\} = -2Re\left\{ \sum_{l=1}^L \tilde{\mathbf{x}}^l H \mathbf{x}^l \right\}, \tag{7.30} \\
&= -2Re\{\tilde{\mathbf{I}}^H \mathbf{z}\} = -2Re\{\tilde{\mathbf{I}}^H (\mathbf{F}^H \mathbf{F} \mathbf{I} + \mathbf{v})\} \\
&= -2Re\{(\tilde{\mathbf{I}}^H \mathbf{F}^H)(\mathbf{F} \mathbf{I} + \mathbf{F}^{-H} \mathbf{H}^H \mathbf{n})\} = -2Re\{\tilde{\mathbf{y}}^H \mathbf{y}\},
\end{aligned}$$

where  $\tilde{\mathbf{y}} = \mathbf{F} \tilde{\mathbf{I}}$  and  $\tilde{\mathbf{x}} = \mathbf{H} \tilde{\mathbf{I}}$ .

- Thirdly, the last metric term also depends on the hypothetical sequence and can be rewritten as:

$$M_2(\tilde{\mathbf{I}}) = \tilde{\mathbf{I}}^H (\sum_{l=1}^L \mathbf{H}^l H \mathbf{H}^l) \tilde{\mathbf{I}} = \tilde{\mathbf{I}}^H \Psi \tilde{\mathbf{I}} = (\tilde{\mathbf{I}}^H \mathbf{F}^H) (\mathbf{F} \tilde{\mathbf{I}}) = \tilde{\mathbf{y}}^H \tilde{\mathbf{y}}. \quad (7.31)$$

Substituting the three terms (7.29) ~ (7.30) into (7.7), we have

$$\hat{\mathbf{I}} = \underset{\tilde{\mathbf{I}} \in I}{\arg \min} \{ |\mathbf{y} - \tilde{\mathbf{y}}|^2 \} = \underset{\tilde{\mathbf{I}} \in I}{\arg \min} \left\{ \sum_{k=1}^N |y_k - \tilde{y}_k|^2 \right\}. \quad (7.32)$$

The following table summarizes the three terms of the basic MLSD equation (7.7) in each receiver. Note that the only difference between the Ungerboeck and Forney receivers is that the Ungerboeck receiver does not use the constant term of (7.7) in its metric computation routine.

	Constant	$M_1(\tilde{\mathbf{I}})$	$M_2(\tilde{\mathbf{I}})$	Required
Basic Equation	$\sum_{l=1}^L \mathbf{x}^l H \mathbf{x}^l$	$-2Re(\sum_{l=1}^L \tilde{\mathbf{x}}^l H \mathbf{x}^l)$	$\sum_{l=1}^L \tilde{\mathbf{x}}^l H \mathbf{x}^l$	Fractional Sampling
Ungerboeck	Not used	$-2Re\{\tilde{\mathbf{I}}^H \mathbf{z}\}$	$\tilde{\mathbf{I}}^H \Psi \tilde{\mathbf{I}}$	Plus, Matched Filter Bank and Symbol Rate Sampler
Forney	$\mathbf{y}^H \mathbf{y}$	$-2Re\{\tilde{\mathbf{y}}^H \mathbf{y}\}$	$\tilde{\mathbf{y}}^H \tilde{\mathbf{y}}$	Plus, Symbol-Spaced Whitening Filter

**Table 7-2: Comparison of the metric computation for Ungerboeck and Forney**

### 7.2.5 The finite length whitening filter

The whitening operator  $\mathbf{F}^{-H}$  is the optimal solution for the purpose of MLSD for the time-varying channel. However, for large block size  $N$  it is impractical to obtain  $\mathbf{F}^{-H}$  due to high complexity. In this section, we describe the procedure to obtain a finite length whitening filter.

The symbol-rate sampled, matched filtered signal  $z_k$  can be collected for the length of the whitening filter  $N_f$ , and can be written as

$$\begin{pmatrix} z_{k+N_f-1} \\ z_{k+N_f-2} \\ \dots \\ z_k \end{pmatrix} = \begin{pmatrix} \Psi_{-N_h}(k+N_f-1) \dots \Psi_0(k+N_f-1) \dots \Psi_{N_h}(k+N_f-1) & \mathbf{0} \\ \mathbf{0} & \Psi_{-N_h}(k+N_f-1) \dots \Psi_0(k+N_f-1) \dots \Psi_{N_h}(k+N_f-1) \\ & \dots \\ \mathbf{0} & \Psi_{-N_h}(k) \dots \Psi_0(k) \dots \Psi_{N_h}(k) \end{pmatrix} \times \begin{pmatrix} \mathbf{I}_{k+N_h+N_f-1} \\ \mathbf{I}_{k+N_h+N_f-2} \\ \dots \\ \mathbf{I}_{k-N_h} \end{pmatrix} + \begin{pmatrix} v_{k+N_f-1} \\ v_{k+N_f-2} \\ \dots \\ v_k \end{pmatrix}, \quad (7.33)$$

which can be rewritten compactly using the matrix convention<sup>1</sup>

$$\mathbf{z}_{(k+(N_f-1):k)} = \Psi_{(k+N_f-1:k, k-N_h-N_f+1:k+N_h)} \mathbf{I}_{(k+N_h+N_f-1:k-N_h)} + \mathbf{v}_{k+N_f-1:k}. \quad (7.34)$$

Decomposing the first term into three terms, (7.34) is

$$\begin{aligned} \mathbf{z}_{(k+(N_f-1):k)} &= \Psi_A \mathbf{I}_{(k+N_h+N_f-1:k+N_f-1)} \\ &+ \Psi_0 \mathbf{I}_{(k+N_f-1:k)} + \Psi_C \mathbf{I}_{(k-1:k-N_h)} + \mathbf{v}_{k+N_f-1:k}, \end{aligned} \quad (7.35)$$

where we have defined

- $\Psi_A = \Psi_{(k+N_f-1:k, k-N_h-N_f+1:k-N_f)}$ ,
- $\Psi_0 = \Psi_{(k+N_f-1:k, k-N_f+1:k)}$  note this matrix is Hermitian symmetric and the autocorrelation matrix of the combined channel, and
- $\Psi_C = \Psi_{(k+N_f-1:k, k+1:k+N_h)}$ .

Then, the whitening filter  $\mathbf{w}(k)$  is obtained from

---

1. For example, (1:4) implies a vector with elements (1, 2, 3, 4); (4:1) implies (4,3,2,1). In addition, the first field in the parenthesis indicates the row index, the second the column index.

$$\mathbf{w}^t(k)\Psi_0(k) = \mathbf{e}_{N_f-1}^t \quad (7.36)$$

or

$$\mathbf{w}^t(k) = \mathbf{e}_{N_f-1}^t \mathbf{F}_0^{-1}(k) \mathbf{F}_0^{-H}(k), \quad (7.37)$$

where we decomposed the  $N_f \times N_f$  Hermitian symmetric autocorrelation matrix

$$\Psi_0(k) = \mathbf{F}_0^H(k) \mathbf{F}_0(k), \quad (7.38)$$

into multiplication of the lower triangular matrix  $\mathbf{F}_0^H(k)$  and the upper triangular matrix  $\mathbf{F}_0(k)$ .

Now ignoring the epoch terms for brevity. We have

$$\mathbf{w}^t \mathbf{z}_{(k+(N_f-1):k)} = \mathbf{w}^t \Psi_0 \mathbf{I}_{(k+N_f-1:k)} \quad (7.39)$$

$$+ \mathbf{w}^t \Psi_A \mathbf{I}_{(k+N_h+N_f-1:k+N_f-1)} + \mathbf{w}^t \Psi_C \mathbf{I}_{(k-1:k-N_h)} + \mathbf{w}^t \mathbf{v}_{k+N_f-1:k}.$$

Now investigating the properties of each term on the right side of (7.39):

- The first term in (7.39) produces the exact input symbol at the  $k$ -th epoch:

$$\mathbf{w}^t \Psi_0 \mathbf{I}_{(k+N_f-1:k)} = \mathbf{e}_{N_f-1}^t \mathbf{I}_{(k+N_f-1:k)} = I_k, \quad (7.40)$$

where  $\mathbf{e}_{N_f-1}^t = (0, 0, \dots, 1)$  is defined to be the vector of zeros except the value of 1.0 at the location indicated by the subscript.

- The second term indicates the pre-cursor residual ISI terms:

$$\mathbf{w}^t \Psi_A \mathbf{I}_{(k+N_h+N_f-1:k+N_f)} = \sum_{j=0}^{N_f-1} \mathbf{w}^t \Psi_{A(:,j)} I_{k+N_h+N_f-1-j}, \quad (7.41)$$

with sufficient length of  $N_f$  this term becomes close to zero. However, when  $N_f$  is relatively short this pre-cursor residual term becomes significant, especially for channel with a deep in-band null (or nulls).

- The third term corresponds to the strict-causal response:

$$\mathbf{w}^t \Psi_C \mathbf{I}_{(k-1:k-N_h)} = \sum_{j=0}^{N_h-1} \mathbf{w}^t \Psi_{C(:,j)} I_{k-1-j}. \quad (7.42)$$

That is, together with the first term, the third term forms the causal, minimum phase response.

- The last is the noise term, which is supposed to be whitened. Defining

$\boldsymbol{\theta}_k = \mathbf{w}^T(k) \mathbf{v}_{k+N_f-1:k}$ , the correlation function can be obtained as

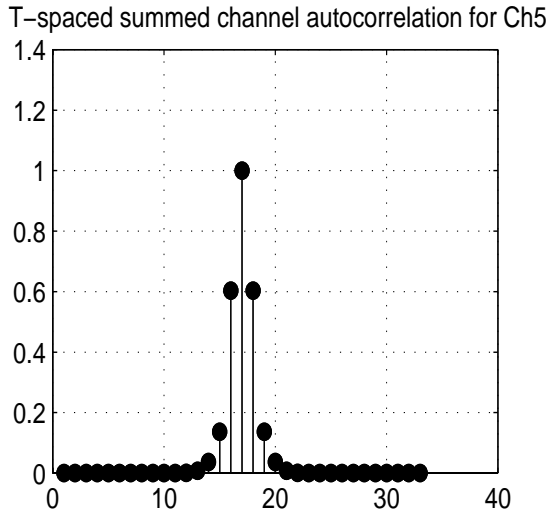
$$\begin{aligned} \mathbf{R}_v(d) &= \mathbf{E}\{\boldsymbol{\theta}_k \boldsymbol{\theta}_{k+d}^*\} = \mathbf{E}\left\{ \mathbf{w}^t \mathbf{v}_{k+N_f-1:k} \mathbf{v}_{k+N_f-1+d:k+d}^H \mathbf{w}^* \right\} \\ &= \begin{cases} \sigma_n^2 \mathbf{w}^t \Psi_0 \mathbf{w}^* = \sigma_n^2 \mathbf{w}_{N_f-1}(k) & , d = 0 \\ 0.0 & , |d| < N_f, \\ \text{small but non-zeros terms} & , |d| \geq N_f \end{cases} \end{aligned} \quad (7.43)$$

such that if we have a large  $N_f$  the cross-correlation terms goes to zero. Figure 7-4 describes the example of whitening matched filtering on a severe ISI channel. Figure 7-4 (a) is the symbol-spaced autocorrelation function for the channel (ACF). The folded-spectrum, Figure 7-4 (b) shows that the channel has about  $-30$  dB in-band null at the normalized frequency of 0.1. Convolution of the ACF with the whitening filter shown in Figure 7-4 (b) results in the response give in Figure 7-4 (c). Figure 7-4 shows the roots of the Z-transform polynomial of the ACF.

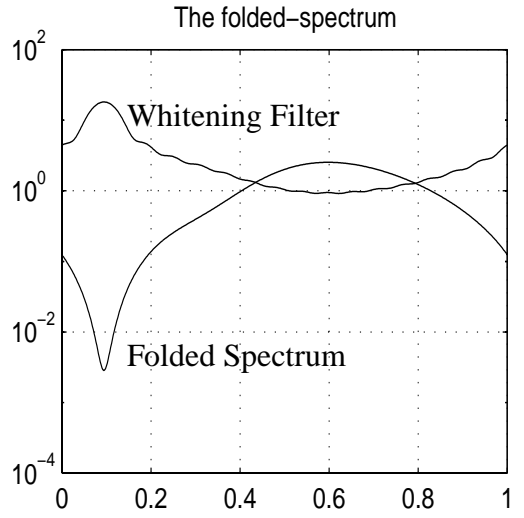
## 7.2.6 The mean-square whitening filter

Now, we consider (7.36) again. When the ISI is severe, and the eigenvalue spread of matrix  $\Psi_0$  is large, such that the channel has a large in-band null in its folded spectrum, the whitening operation would be unstable and enhance the noise and the channel estimation error. Thus, in practice we may have to consider the use of a stable matrix  $\Psi_1 = \Psi_0 + \sigma_n^2 \Xi$  instead of  $\Psi_0$ . In fact, this is analogous to use of the minimum mean

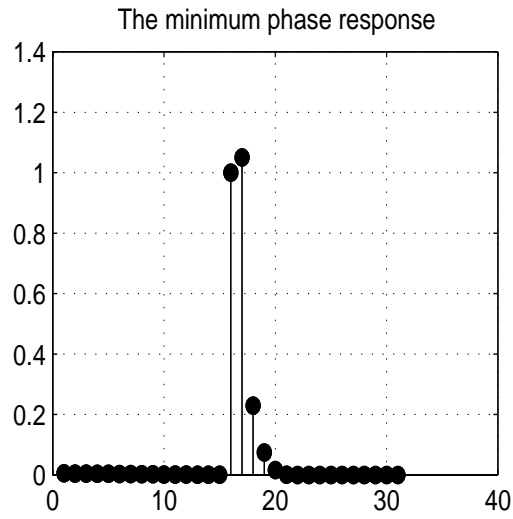
(a)



(b)



(c)



(d)

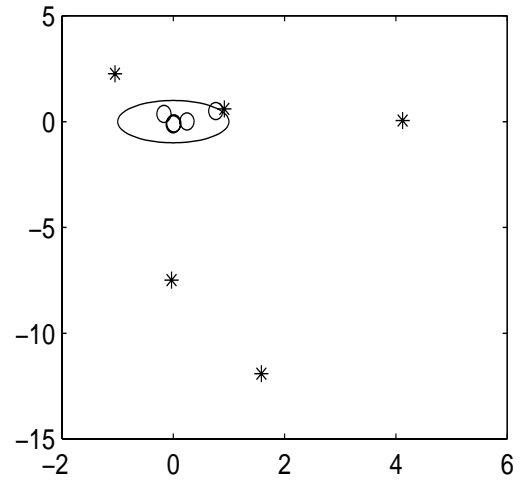


Figure 7-4 The whitening filter (ZF-DFE) example with  $N_f=17$  and zero input noise.

square error criterion (e.g. MMSE-DFE). For example, for the static channel, the following spectral factorization can be used to obtain the feedforward filter  $1/F_1^*(D^{-1})$ :

$$\Psi_{mmse}(D) = \sum_{i=-N_h}^{N_h} \Psi_i D^i + \sigma_n^2 = F_1^*(D^{-1})F_1(D). \quad (7.44)$$

Note this factorization always exists, whereas (7.21) may not.

Using the Cholesky factorization, we have

$$\Psi_1 = \Psi_0 + \sigma_n^2 \Xi = \mathbf{F}_1^H \mathbf{F}_1, \quad (7.45)$$

where again  $\mathbf{F}_1^H$  is the lower triangular matrix and  $\mathbf{F}_1$  is the upper triangular matrix.

The smallest eigenvalue of  $\Psi_1$  is now restricted to be greater than or equal to the noise variance  $\sigma_n^2$ . The MS-WF  $\mathbf{w}_m^t(k)$  is thus obtained as follows:

$$\mathbf{w}_m^t(k) \Psi_1(k) = \mathbf{e}_{N_f-1}^t. \quad (7.46)$$

Note that (7.46) is the same equation that is used to obtain the feedforward filter of the non-Toeplitz DFE (NT-DFE) in Chapter 5. (5.20) translates into the notation of this chapter as

$$(\Psi_0 \Psi_0 + \sigma_n^2 \Psi_0) \mathbf{w}_m^* = \Psi_{0(:, N_f-1)}, \quad (7.47)$$

which provides the solution for obtaining the feedforward filter of NT-DFE. By writing  $\Psi_{0(:, N_f-1)} = \Psi_0 \mathbf{e}_{N_f-1}$  and cancelling  $\Psi_0$  from both side of (7.47), and (7.47) becomes (7.46).

Applying the MS-WF  $\mathbf{w}_m^t(k)$  to  $\mathbf{z}_{(k+(N_f-1):k)}$  we have:

$$\mathbf{w}_m^t \mathbf{z}_{(k+(N_f-1):k)} = \mathbf{w}_m^t \Psi_0 \mathbf{I}_{(k+N_f-1:k)} \quad (7.48)$$

$$+ \mathbf{w}_m^t \Psi_A \mathbf{I}_{(k+N_h+N_f-1:k+N_f-1)} + \mathbf{w}_m^t \Psi_C \mathbf{I}_{(k-1:k-N_h)} + \mathbf{w}_m^t \mathbf{v}_{k+N_f-1:k}.$$

Now, note the following:

- From (7.46), we have  $\mathbf{w}_m^t(k)(\Psi_0 + \sigma_n^2 \mathbf{I}) = \mathbf{e}_{N_f-1}^t$  or  $\mathbf{w}_m^t = \mathbf{e}_{N_f-1}^t \mathbf{F}_1^{-1} \mathbf{F}_1^{-H}$ , and thus

$\mathbf{w}_m^t \Psi_0 = \mathbf{e}_{N_f-1}^t - \sigma_n^2 \mathbf{w}_m^t$ . Therefore, the first term in (7.48) can be written as

$$\begin{aligned} \mathbf{w}_m^t \Psi_0 \mathbf{I}_{(k+N_f-1:k)} &= (\mathbf{e}_{N_f-1}^t - \sigma_n^2 \mathbf{w}_m^t) \mathbf{I}_{(k+N_f-1:k)} = I_k - \sigma_n^2 \mathbf{w}_m^t \mathbf{I}_{(k+N_f-1:k)} \quad (7.49) \\ &= (1 - \sigma_n^2 w_{m, N_f-1}) I_k + \text{precursor ISI terms for } \{k+N_f-1, \dots, k+1\}. \end{aligned}$$

- The second term is the precursor residual ISI terms for  $\{k+N_h+N_f-1, \dots, k+N_f\}$ :

$$\mathbf{w}_m^t \Psi_A \mathbf{I}_{(k+N_h+N_f-1:k+N_f)} = \sum_{j=0}^{N_f-1} \mathbf{w}_m^t \Psi_{A(:, j)} I_{k+N_h+N_f-1-j}, \quad (7.50)$$

with sufficient length of  $N_f$  this term becomes near-zero.

- The third term corresponds to the causal response at the  $k$ -th epoch:

$$\mathbf{w}_m^t \Psi_C \mathbf{I}_{(k-1:k-N_h)} = \sum_{j=0}^{N_h-1} \mathbf{w}_m^t \Psi_{C(:, j)} I_{k-1-j}, \quad (7.51)$$

which is the post-cursor ISI terms for the  $\{k-1, \dots, k-N_h\}$ .

From (7.49) ~ (7.51), we divide the terms for  $\{k+N_h+N_f-1, \dots, k+1, k, k-1, \dots, k-N_h\}$  by  $(1 - \sigma_n^2 w_{m, N_f-1})$  and denote the result

$$f_i(k) = \frac{1}{(1 - \sigma_n^2 w_{m, N_f-1})} \cdot \mathbf{w}_m^t(k) \Psi_{(k+N_f-1:k, k+i)}, \quad (7.52)$$

for  $i = -N_h - N_f + 1, \dots, -1, 0, 1, \dots, N_h$ . Note that  $\{f_i(k)\}_{i \geq 0}$  represents the causal response and the rest the anticausal residual ISI. Also note that the  $f_0(k)$  is 1.0, and for  $1 \leq i \leq N_h$  we have

$$f_i(k) = \frac{1}{(1 - \sigma_n^2 w_{m, N_f-1})} \mathbf{w}_m^t(k) \Psi_{C(:, i-1)}(k). \quad (7.53)$$

$f_i(k)$  will be used in the T-algorithm receiver in section 7.3. Note that the MS-WF asymptotically converges to the WF.

Figure 7-5 illustrates the results of applying the MS-WF to the same channel given

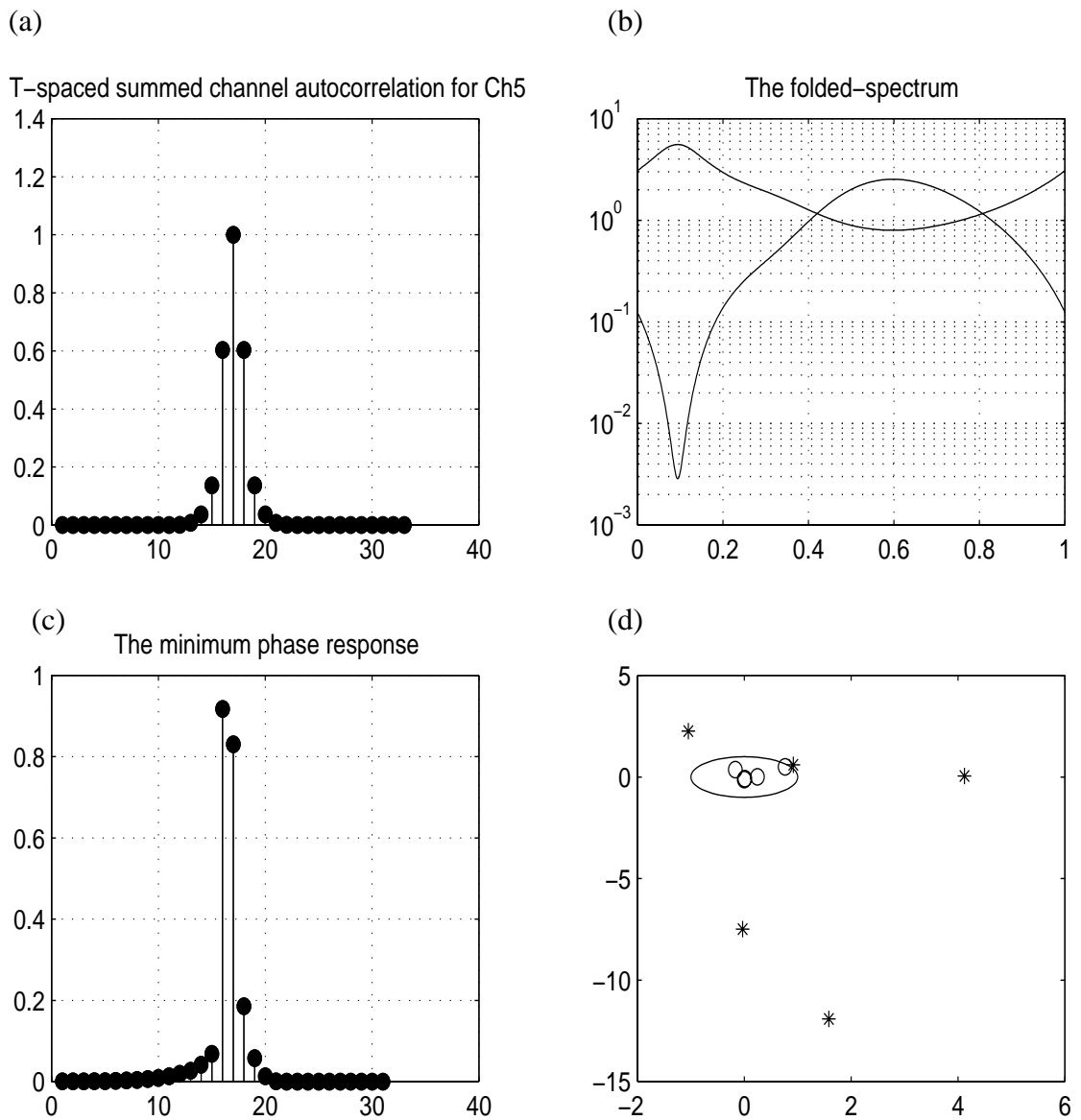


Figure 7-5 The mean-squares whitening filter example with  $N_f=17$  and 10 dB input SNR.

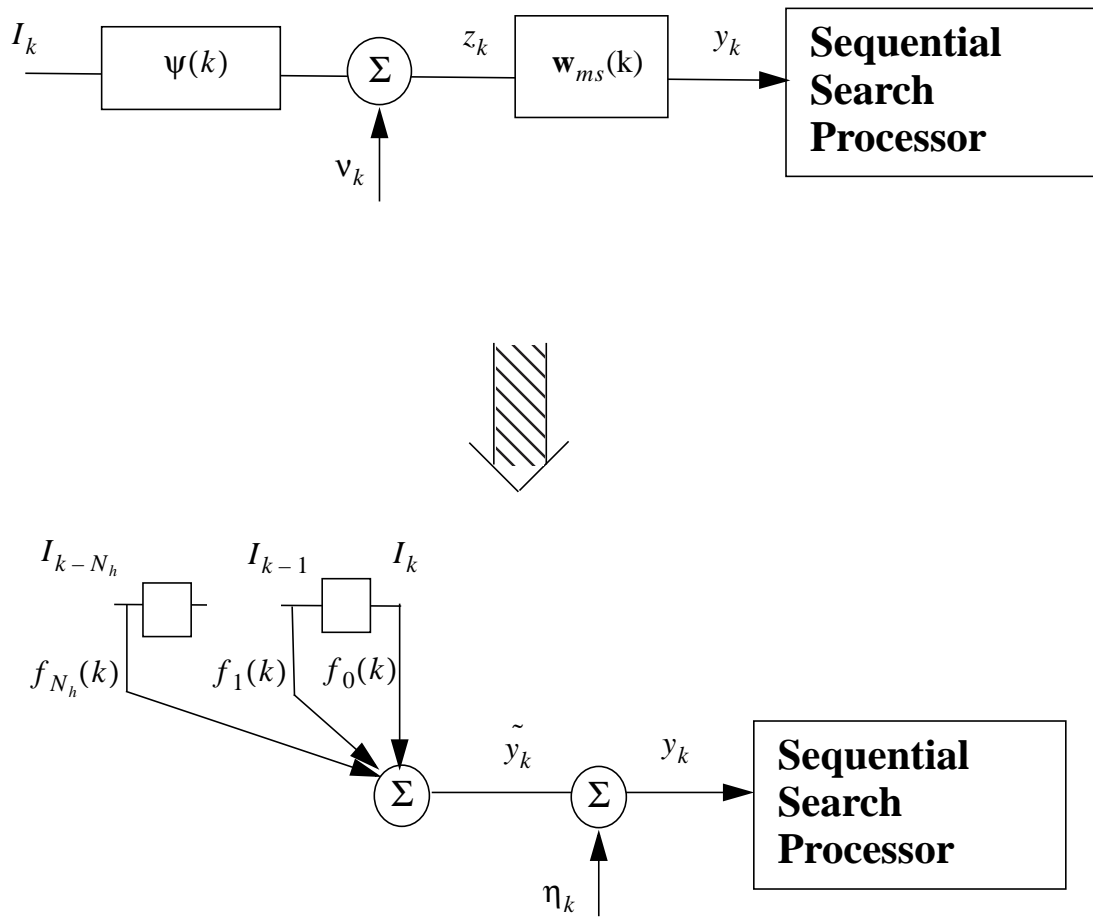


Figure 7-6 The results of pre-processing, the matched filter bank, the combiner and symbol rate sampler, and the (mean-square) whitening filter.

in Figure 7-4. Compare Figure 7-5 (c) with Figure 7-4 (c). Figure 7-5 (c) shows the non-zero pre-cursor responses as well as the difference in the causal responses.

## 7.3 The Proposed MLSD Postprocessor

In this section, it is assumed that the MS-WF is used to perform Forney's MLSD receiver, depicted in Figure 7-6 (a). Since we are using MS-WF, the resulting channel is not minimum phase response, i.e.,  $\{f_i(k)\}_{i < 0}$  are not zero-valued as shown in Figure 7-5. Here we simply ignore the contribution from the non-causal terms  $\{f_i(k)\}_{i < 0}$ . Then, we will use Forney's metric (7.32) to perform the T-algorithm. Then, Figure 7-6 (b) describes the causal symbol-spaced tap filter  $\mathbf{f}(k)$ , which represents the overall channel between  $\{I_k\}$  and  $\{y_k\}$  for the purpose of the T-algorithm search. As this model disregards the anticausal terms resulting from the use of finite length MS-WF as well as any estimation error in the causal response  $\mathbf{f}(k)$  as well, the discrepancies would certainly degrade the detection performance of the complete receiver. By the use of per-survivor processing, discussed in section 7.4, however, some of the performance penalty can be recovered. The T-algorithm is discussed in 7.3.1 and the LMS algorithm per-survivor processing is discussed in 7.4.

### 7.3.1 The equivalent input/output equation

Referring to Figure-5, the input/output relationship including the MS-WF can be written

$$y_k = \sum_{i=0}^{N_h} f_i(k) I_{k-i} + \eta_k, \quad (7.54)$$

where  $\eta_k$  is now assumed to be whitened noise and the  $\{f_i(k)\}$  are as defined in (7.52).

Then, Forney's metric for a hypothetical sequence  $\tilde{\mathbf{I}}_{1:k}$  can be computed from

$$J_k(\tilde{\mathbf{I}}_{1:k}) = J_{k-1}(\tilde{\mathbf{I}}_{1:k-1}) + B_k, \text{ for } k = 0, \dots, N-1 \quad (7.55)$$

where  $B_k$  is the branch metric at the  $k$ -th symbol epoch

$$B_k = \left| y_k - \sum_{i=0}^{N_g} f_i(k) \tilde{I}_{k-i} \right| = |y_k - \tilde{y}_k|. \quad (7.56)$$

Then, the MLSD sequence is determined from

$$\hat{\mathbf{I}} = \underset{\tilde{\mathbf{I}} \in I}{\arg \min} J_N(\tilde{\mathbf{I}}). \quad (7.57)$$

### 7.3.2 The proposed T-algorithm

The tree-search version of the T-algorithm is proposed in this paper. The parameters of importance of the T-algorithm are  $P_{max}$ , the maximum number of paths that can be kept at an epoch, and  $\zeta$ , the threshold value. The following steps describe the T-algorithm used:

- At the zeroth epoch, start from the unique known path that is composed of the training symbols of  $N_h - 1$  and set  $J_k(\tilde{\mathbf{I}}_{1:N_h-1}^0) = 0$ , where the superscript denotes the path index which is from 0 to  $P_{max} - 1$ .
- BEGIN:
- (Step-1) *Path extension*: At  $k$ -th epoch, extend each survived path,  $1 \leq i < P_{max} - 1$ , and calculate the cumulative metric

$$J_k(\tilde{\mathbf{I}}_{1:N_g-1+k}^j) = J_k(\tilde{\mathbf{I}}_{1:N_g-2+k}^i) + B_k^{i,q}, \quad (7.58)$$

for  $j = 0, 1, \dots, P_{max} \cdot M - 1$ , where the branch metric  $B_k^{i,q}$ , from  $i$ -th path to  $j$ -th paths by the  $k$ -th hypothetical input  $\tilde{I}_k \in \text{Alphabet}$  of q-QAM, is defined as

$$B_k^{i,q} = \left| y_k - \sum_{i=1}^{N_g} f_i(k) \tilde{I}_{k-i}^i - \tilde{I}_k \cdot \tilde{f}_0(k) \right|, \quad (7.59)$$

- (Step-2) Update of  $J_{min}$ : Update the minimum metric and its path index  $j(J_{min,k})$ , i.e., for  $j = 0, 1, \dots, P_{max} \cdot M - 1$ ,

$$\text{if } J_k(\tilde{\mathbf{I}}_{1:N_g-1+k}^j) < J_{min,k} \rightarrow J_{min,k} = J_k(\tilde{\mathbf{I}}_{1:N_g-1+k}^j), \quad (7.60)$$

where  $J_{min,k} = 0.0$  is initialized for each  $k$ .

- (Step-3) *Threshold testing and truncation*: Count the number of paths whose path metric difference with  $J_{min,k}$  is less than  $\zeta$  and whose hypothetical input symbol  $\tilde{I}_{k-N_D}^j$  is different with  $\tilde{I}_{k-N_D}^{j(J_{min,k})}$ , where  $N_D$  is the depth of the tree. If the number is greater than the  $P_{max}$ , lower the threshold  $\zeta = \zeta - \zeta_b$  and count again until less than  $P_{max}$  paths remains. Reject all paths that fail.
- (Step-4) Return to Step-3 until the end of the sequence.
- END.

The T-algorithm can be applied to the trellis also. The trellis-search version requires an additional step. First we need to investigate all the survivors if any two survivors have merged. This can be carried out by checking if the last  $N_g$  symbols of the survivors have the same hypothetical symbols. Among those merged, only the minimum metric path survives. Thus, the trellis operation requires additional storage elements and additional set of comparison operations.

### 7.3.3 Why T-algorithm is efficient?

Assuming there is no channel estimation error and based on the metric calculation (7.59), the Forney's metric is calculated from

$$\lambda_k^F = |e_k^F|^2,$$

where

$$e_k^F = y_k - \sum_{m=0}^{N_h} f_m \tilde{I}_{k-m} = \sum_{m=0}^{N_h} f_m \Delta \tilde{I}_{k-m} + \eta_k, \quad (7.61)$$

with  $\Delta\tilde{I}_k = I_k - \tilde{I}_k$  the hypothetical symbol errors associated with a particular survivor path. The simple observation one should make out of (7.61) is that a large Euclidean distance  $\|\Delta\tilde{I}_k\|_2$  in the hypothetical symbols results in a large metric difference  $\|e_k^F\|_2$ . Of course, this is a very loose observation. However, the RSSE is based on this underlying principle such that when states are having a large path-distance they are collapsed into a single state and the VA is applied. One other situation to consider is when the frequency of the error sequence  $\{\Delta\tilde{I}_k\}$  coincides with the null frequency of the channel. The loose relationship surely not hold in such a case as the term,  $\sum_{m=0}^{N_h} f_m \Delta\tilde{I}_{k-m}$ , tends to zero. For this reason, an optimum design of RSSE for time-varying channel requires one to vary the coset labelling and thus the decoding structure to guarantee a detection-distance, which is smaller than the detection-distance of the complete trellis.

Instead of using the distance criterion, we may want to directly use the metric criterion to perform the reduced search. M-algorithm and T-algorithm are in this category. Both use the metric difference as the discard criterion. Briefly illustrating the key aspects of the two algorithms, we note that

- M-algorithm: Use metric difference, but the number of survivors are fixed at each exploration. The metric difference varies at each exploration.
- T-algorithm: Fix the metric difference to keep, but the number of survivors varies.

Thus, the detection performance of the T-algorithm with  $P_{max}$  is the same as the M-algorithm with  $P_{max} = M$ .

## 7.4 Per-Survivor Tracking of the Channel Mismatch

In section 7.3, we apply the T-algorithm to the output sequence of the mean-square whitening filter (MS-WF). The big assumptions are that the channel estimates are perfect and the MS-WF filter closely approximates the WF. Therefore, the output sequence is the

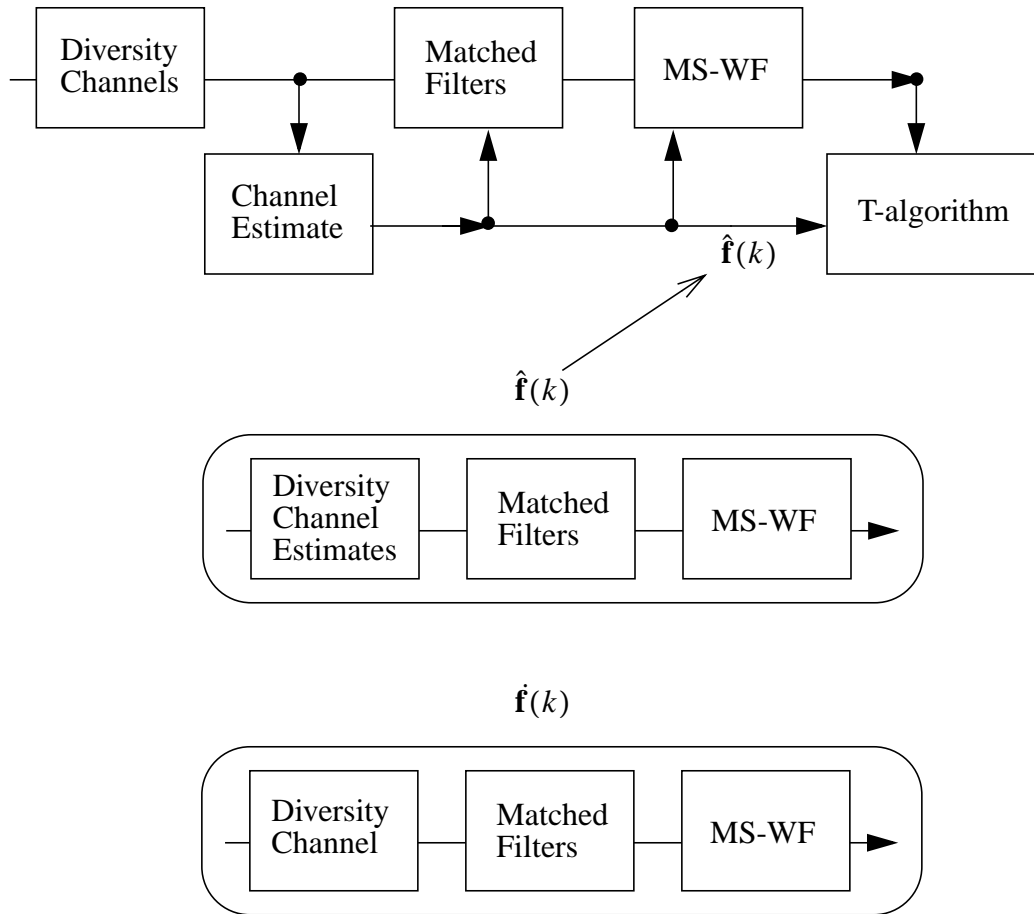


Figure 7-7 Illustration of channel mismatch

set of sufficient statistics, and the resulting overall channel response--including all the diversity channels, the matched filters at the diversity branches and the symbol-spaced whitening filter--is a symbol-spaced minimum phase response and estimated perfectly. In practice, the channel estimate is not perfect, and thus together with the use of finite length MS-WF, a significant channel mismatch may occur between the overall channel that is calculated solely based on the channel estimate and the actual cascades of the unknown channels, matched filters, and the MS-WF. Based on the illustration Figure 7-7, we may

define the channel mismatch as

$$\varepsilon(k) = \hat{\mathbf{f}}(k) - \mathbf{f}(k). \quad (7.62)$$

One of the advantages in dealing with the sequential detection is that one can make use of the hypothetical sequences to improve the channel estimates. The assumption is that there is always one correct sequence in the pool of sequences you are currently considering, and that sequence will provide additional information of the channel. For the purpose of T-algorithm processing, this additional processing helps to reduce the increase in the average number of survivors to keep. That is, the detection performance improves while reducing the complexity. The underlying principle is that in the wrong path, the channel mismatch estimate quickly degrades and this promotes early elimination of the path; while in the correct path, the channel estimate is always improving and thus increases the detection Euclidean distance of the algorithm. In this section, we present the per-survivor estimation of the channel-mismatch.

#### **7.4.1 The channel mismatch and optimal tracking**

Figure 7-8 illustrates the channel mismatch. The channel used is the one for Figure 7-4 and Figure 7-5. Note the asymmetric channel response in Figure 7-8 (a), which is the cascade of the channel and the matched filter obtained from the channel-estimate, the blank dots compared with the filled dots which represent the perfect autocorrelation function using perfect channel estimates. Figure 7-8 (c) shows the results after the MS-WF, one from the channel estimate the other from perfect channel knowledge. Figure 7-8 (d) indicates the difference of the two.

Figure 7-9 illustrates the optimum use of per-survivor processing, for the feedforward channel estimation scheme. We have the continuous set of channel estimates available, and thus the matched filters and the MS-WFs for the duration of the block. The

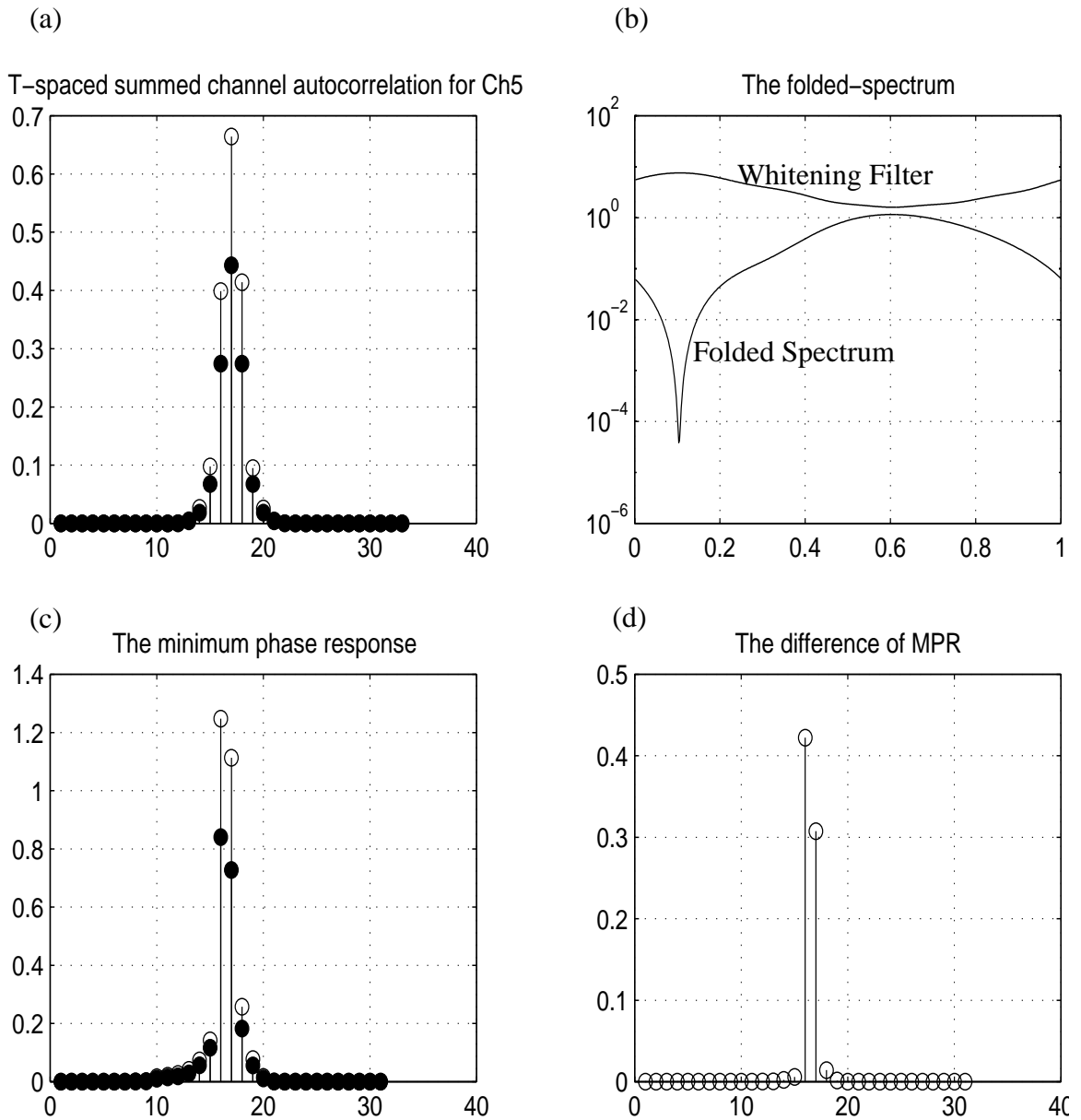


Figure 7-8 The example of channel mismatch, MS-WF with  $N_f=6$  at the input SNR = 10 dB.

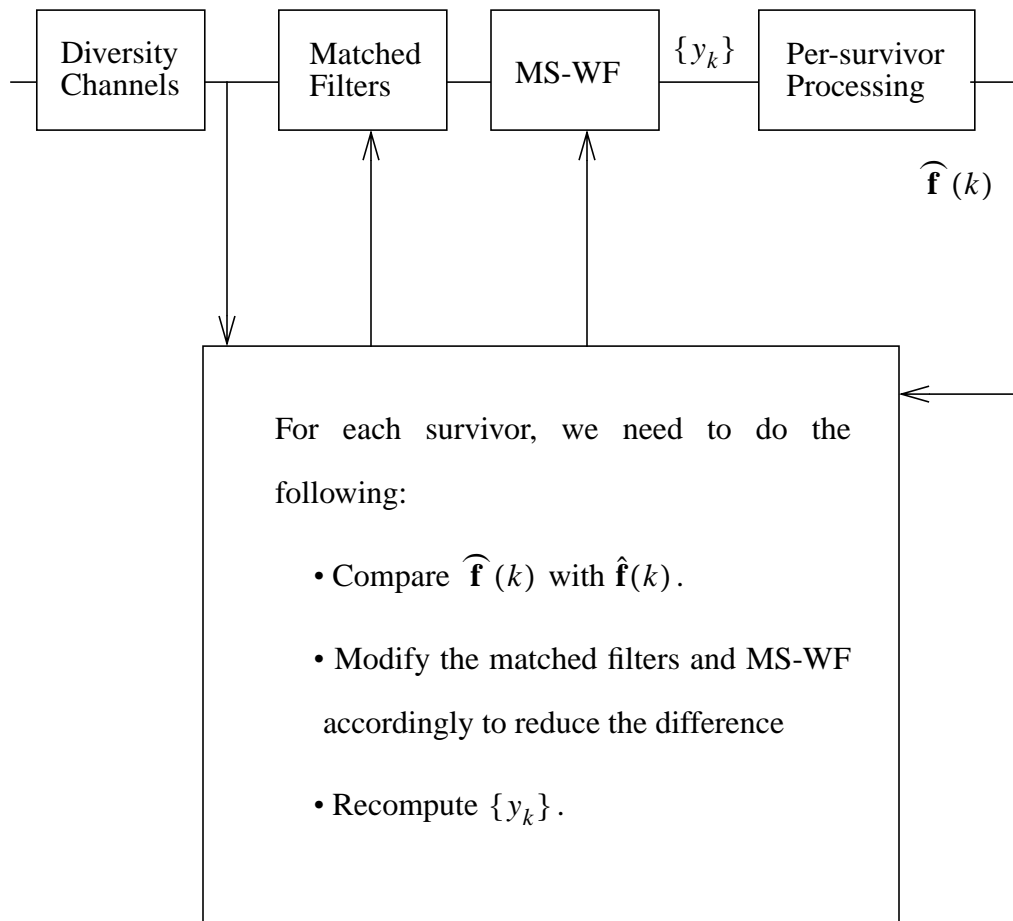


Figure 7-9 Optimal use of PSP is to feedback the channel mismatch information of the overall channel estimate and recompute the matched filters, the MS-WF and finally recompute the output sequence  $\{y_k\}$  at each survivor.

use of per-survivor processing, however, will provide updated channel information in the form of  $\widehat{\mathbf{f}}(k)$ . This information first needs to be compared with the stored  $\hat{\mathbf{f}}(k)$ . The matched filters and the MS-WF need to be updated accordingly. Thus, we need a function that maps the obtained channel mismatch information  $\widehat{\mathbf{f}}(k) - \hat{\mathbf{f}}(k)$  to update the matched filter and MS-WF. This operation must be performed for every survivor path. This is almost impossible for our setting of the problem. If we were assuming the symbol-spaced whitened channel model as commonly used in the open literature, we may be able to perform the optimal processing. However, it is not plausible with the use of realistic pre-processing filters. For this reason, we turn to the use of suboptimal solution that the channel mismatch information is used only once to feedforwardly cancels the channel mismatch, rather than the optimal feedback.

#### 7.4.2 Modeling and suboptimal tracking of the channel mismatch

We now model the channel mismatch. The basic equation (7.54) can be rewritten as

$$y_k = \sum_{i=0}^{N_g} \hat{f}_i(k) I_{k-i} + \eta_k + \sum_{i=-N_f-N_h+1}^{N_g} \varepsilon_i(k) I_{k-i} \quad (7.63)$$

where we have defined:

- $\hat{f}_i(k)$  is the estimated response of the overall channel, the cascade of the channel estimates, the matched filters and combiner and the symbol-spaced MS-WF. Note that the MF and MS-WF are obtained from the channel estimate.
- $\{\dot{f}_i(k)\}$  is the unknown, true response which is the cascade of the channel, the matched filter and the MS-WF.
- The error term  $\varepsilon_i(k)$  is defined as for  $i = -N_h - N_f + 1, \dots, 0, \dots, N_h$

$$\varepsilon_i(k) = \hat{f}_i(k) - \dot{f}_i(k). \quad (7.64)$$

The combined error term can be defined as

$$\xi(k) = y_k - \sum_{i=0}^{N_g} \hat{f}_i(k) I_{k-i} = n_k + \sum_{i=-N_f-N_h+1}^{N_g} \varepsilon_i(k) I_{k-i}. \quad (7.65)$$

As seen in (7.65), the second error term is the convolution of the transmitted signal and the error vector  $\varepsilon$ . Now, we ignore the contribution of the future symbols and only model the contribution from the previous symbols since it can be cancelled with the use of hypothetical symbols in the survivors; while that of future symbols cannot.

Now, define

$$\xi^j(k) = \varepsilon_{0:N_h}^j(k) \cdot \tilde{\mathbf{I}}_{k:k-N_h}^j \text{ and } \xi^J(k) = y_k - \sum_{i=0}^{N_g} \hat{f}_i(k) \tilde{I}_{k-i}^j. \quad (7.66)$$

Then, the LMS algorithm, described in Chapter 4, updates the error vector at each path with the following equation:

$$\varepsilon_{0:N_h}^j(k) = \varepsilon_{0:N_h}^j(k-1) + \Delta \cdot (\xi^j(k) - \xi^j(k)) \cdot \tilde{\mathbf{I}}_{k:k-N_h}^{j*}, \quad (7.67)$$

where  $\Delta$  is the stepsize of the LMS algorithm.

Finally, the causal part of the response is updated using the new estimate  $\varepsilon_{0:N_h}^j(k)$ , i.e.,

$$\hat{f}_i^j(k) = \hat{f}_i(k) + \varepsilon_i^j(k), \quad (7.68)$$

for  $i = 0, 1, \dots, N_h$ . This LMS per-survivor processing estimates the channel mismatch vector in the minimum phase response and lowers the SNR penalty due to the imperfect MF and MS-WF. As mentioned, this method is not optimum. To be optimum, the information should be fed back to recalculate the matched filter and the WF, and re-obtain the minimum phase response. Then as the iteration proceeds the receiver would achieve the performance of the genie-aided receiver operating with perfect channel knowledge. However, the complexity of such a receiver is prohibitively high as iteration is required. At each iteration the matrix inversion must be performed to re-estimate the WF, which is the most intensive

computation. The proposed receiver avoids this problem by an one-step, feedforward adjustment (7.68) to the unknown response  $\{\dot{f}_i(k)\}_{i \geq 0}$ . Significant performance difference has been observed in terms of detection SNR as well as in reducing the number of survivors.

## 7.5 Simulation Results and Discussion

In this section we study the performance of the proposed receiver via computer simulations. First, we examine two sample static channels that are obtained from the ensemble of wireless channels in consideration. These channels have a severe nulls in the folded-spectrum as we desire to test the equalization performance of the proposed receiver. The first channel, denoted as channel-1, has a  $10^{-1}$  null in its folded-spectrum, see Figure 7-10; the other has a  $10^{-2}$  null, see Figure 7-11. We first examine the proposed receiver performance on these channels; in the mean time, we may tune the parameters of the proposed receivers, such as the feedforward filter length, feedback filter length of MS-WMF, the threshold value, the maximum path allowed, and the stepsize of LMS channel estimation error tracking. Later, we apply the receiver to the time-varying ISI channels.

We now briefly review the simulation parameters and assumptions. A fractionally sampled system, i.e.,  $N_s = 2$  in (7.1), is assumed. The SRRC filter uses 35% rolloff factor and is represented with the column vector

$$\mathbf{f} = (0.0404 \ -0.0953 \ -0.0600 \ 0.4297 \ 0.7749 \ 0.4297 \ -0.0600 \ -0.0953 \ 0.0404)^t, \quad (7.69)$$

which is four symbol truncation of the SRRC filter. For both fading and static channels, a Monte Carlo method with 2,000-50,000 independent trials was used. To evaluate the adaptation on continuously transmitted frames, each trial consisted of 5-16 frames, where a frame is a block of  $B = 80$  symbols including the  $N_t = 11$  training symbols. The sum of nine-sinusoids described in Chapter 2 was used to generate the  $L$  independent diversity

channels coefficients, which is continuously varied at a given fading rate. The half symbol-spaced complex-valued additive noise samples were independently generated. The channel interpolation is performed using two future and two past channel estimates. The training symbols are also the same as defined in Chapter 4, i.e.,

$$\mathbf{I}_T = ((\sqrt{q}-1) + i(\sqrt{q}-1))(1 \ 1 \ -1 \ -1 \ -1 \ 1 \ -1 \ 1 \ 1 \ 1 \ 1)^t, \quad (7.70)$$

for  $q$ -QAM  $q = 4, 16, \text{ and } 64$ . Finally, assuming a symbol rate of 24 ksps, fast fading corresponds to  $f_{dm} = 100$  Hz ( $f_{dm}T = 0.0042$ ) and slow fading to  $f_{dm} = 10$  Hz ( $f_{dm}T = 0.00042$ ).

### 7.5.1 Static channel simulation

The static channel examples are

$$\mathbf{b}_1 = (-0.2695+0.3785i \ 0.9619+0.0303i \ 0.0730-0.2938i)^t \quad (7.71)$$

and

$$\mathbf{b}_2 = (0.3236-0.7876i \ 0.3222+0.8566i \ -0.0155+0.1278i)^t \quad (7.72)$$

in  $T_B/2$ -spaced sampled response. Then, the overall channels can be obtained from convolution of the SRRC filter, i.e.,  $\mathbf{h}_i = \mathbf{b}_i \otimes \mathbf{f}$ , which spans five symbol periods. The folded spectrum of the channel  $\mathbf{h}_1$  and  $\mathbf{h}_2$  are given in Figure 7-10 (a) and Figure 7-11 (a) respectively.

Figure 7-10 (b) and Figure 7-11 (b) show the 4-QAM symbol error simulation results using the T-algorithm receiver over channel-1 and channel-2 respectively, compared with the fundamental matched filter bound (solid line). The feedforward and feedback filter lengths of NT-DFE or the MS-WF of the T-algorithm receiver are  $(N_f, N_b) = (6, 6)$  for each of the six different receivers. First, let's compare results of the T-algorithm and the NT-

DFE with the channel perfectly known as a benchmark. Since the channel is static, the NT-DFE is the same as the conventional DFE. We observe there is about 1.5 ~ 2.0 dB SNR penalty (at  $10^{-4}$ ), even for the correct decision feedback DFE (CDF-DFE), for both channels. The T-algorithm uses  $(P_{max}, \zeta) = (1000, 4.0)$  and achieves the performance of the VA for both channels. As the folded spectrum of channel-2 exhibits a deeper null than the channel-1, the SNR penalty of the DFE is larger for the channel-2.

- Next, compare the rest of the curves where the channel is estimated using the least squares estimator (LSE). Observe that the use of the T-algorithm receiver with  $(P_{max}, \zeta) = (100, 3.0)$  improves detection SNR by 2.0dB over the use of a DFE or about 0.5 to 1.0 dB over the use of the correct decision feedback-DFE for both channels. The T-algorithm receiver employing the per-survivor LMS channel mismatch tracking is denoted as T-*alg*-LMS receiver. The receiver's simulation parameters are  $(P_{max}, \zeta, \rho) = (100, 3.0, 0.005)$  for the maximum allowed paths, the threshold value, and the stepsize of the LMS algorithm. LMS stepsize is chosen according to  $q$ , i.e.,  $\Delta < \frac{1}{\sigma_I^2(q)}$  or  $\Delta < \frac{1}{N_f \cdot \sigma_I^2(q)}$ . T-*alg*-LMS receiver achieves an additional 1.0 to 1.5 dB SNR advantage over the use of T-algorithm without the use of LMS tracking. That is, about 3.0 dB SNR advantage compared to the DFE.

The static channel simulation results can be summarized as follows:

- The T-*alg*. closely achieves VA's performance when used with a sufficiently large number of paths and a large threshold value. With the ideal channel estimates available, the T-*alg* (1000,4.0) achieves the performance of the VA as indicated in Figure 7-10 and Figure 7-11.
- This performance is obtained with the average number of paths of only a few tens of paths for simulations with the input SNR greater than 9 dB.

- The symbol error rate (SER) of the T-algorithm is lower than that of the correct decision feedback DFE (CDF-DFE).
- The LMS tracking of the channel estimation error helps reduce the number of paths and provide further SNR advantage, recovering some of the SNR penalty due to imperfect channel estimation.

## 7.5.2 The Rayleigh fading ISI channel

The rms delay spread of the Rayleigh fading channel that are used in the simulation is  $0.3257 T_B$ . The diagonal term of the channel autocorrelation matrix is the MPDP. The matrix is

$$E\{\mathbf{b}'\mathbf{b}^H\} = \text{diag}(0.6652, 0.2447, 0.0900). \quad (7.73)$$

The following table summarizes the receiver parameters used in simulations.

**Table 7-3: Simulation parameters and results**

$q$ -QAM	Threshold	Maximum Paths	SNR region	LMS stepsize	Average Paths	SER
4	2.5 - 4.0	100	15-25	0.05	1.0~30.0	$1e-2 \sim 1e-4$
16	4.0	200	20-30	0.01	10.0	$1e-2 \sim 1e-4$
64	4.5-5.5	200	25-35	0.001	30-40.	$1e-2 \sim 1e-4$

Figure 7-12 is the symbol error rate (SER) simulation results of 4-QAM signalling, compared with the matched bound calculated for the 4-QAM modulation format over the Rayleigh fading ISI channel. The T-*alg*-LMS receiver shows very robust symbol error rate performance for the fading channel. At the fastest fading rate (100 Hz, the vehicle speed of 120 km/hr), the SNR degradation from the slow fading (1 Hz, quasi-static channel) is only about 3.0 dB, whereas in the case of NT-DFE it was about 6.0 dB at  $10^{-4}$  SER.

Figure 7-13 and Figure 7-14 are the SER simulation results for 16-QAM and 64-QAM signalling over the Rayleigh fading ISI channels, compared with the matched filter bound. While maintaining the superiority to the NT-DFE receiver, we now observe that the SER for the fast fading reaches irreducible error floors. Figure 7-15 is the SER simulation results for 64-QAM signalling when 2-independent diversity channel is available. From these figures, we observe that the proposed receiver does bring a significant SNR advantage over the NT-DFE.

Looking at the fading channel simulation results, we conclude that the proposed T-algorithm using the LMS-per-survivor channel mismatch tracking indeed is superior to the use of the NT-DFE receiver developed in chapter 5. In addition, the computational complexity problem of MLSD can be controlled by the use of a reduced search algorithm. However, we immediately note that the receiver could not overcome the limitation imposed by the channel estimation error. This was one reason we explored the possibility of feedback of the channel mismatch information obtained from the LMS per-survivor processing stage. As mentioned earlier this is extremely unrealistic due to our realistic multi-stages of pre-processing receive filtering to produce the sufficient statistics.

Another point worthy to note is that the advantage of MLSD over the DFE does not stand out as much as those of static channels given in Figure 7-10 and Figure 7-11. In fact, the performance of MLSD stands out only when the channel develops a severe ISI channel or in other word contains a deep null (or nulls) in the folded spectrum. For a channel with no nulls in the folded spectrum, there is little performance difference among MMSE-LE, MMSE DFE or MLSD. The simulated multipath ISI fading channels with the multipath power delay profile (MPDP) given in (7.73) would occasionally develop such deep in-band nulls just like the static channel examples of Figure 7-10 and Figure 7-11 and this is when a large performance difference can occur. For other occasions when there are no nulls, the performance of the NT-DFE should be comparable with that of T-algorithm receiver. Since

the simulation results for fading ISI channels are the averaged results over all the possible channels, it is understandable that the advantage in detection SNR over the use of NT-DFE is not as large as the static channel case.

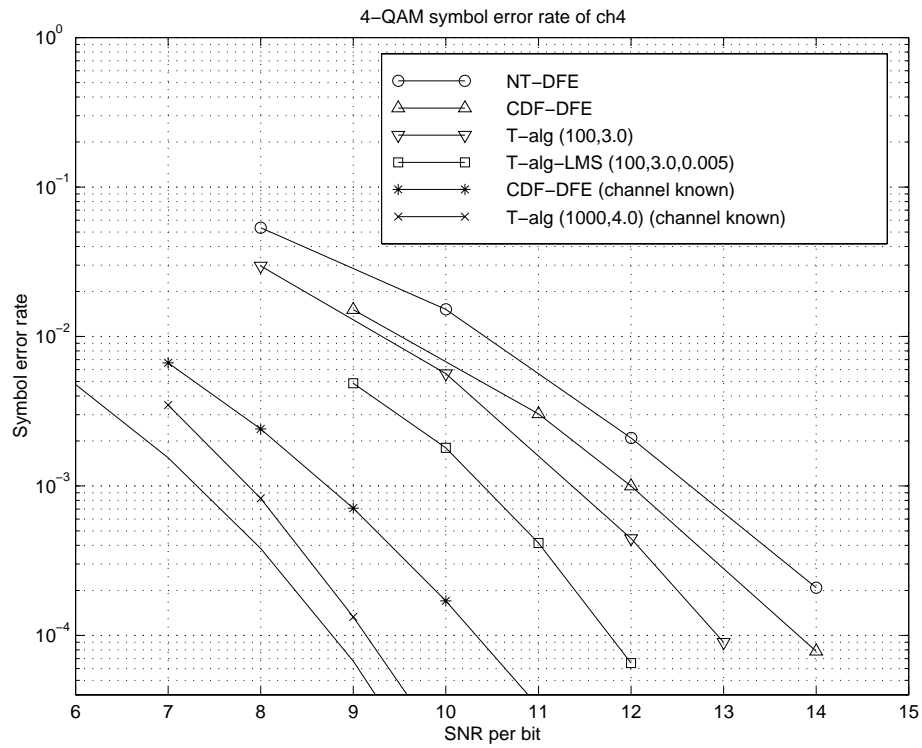
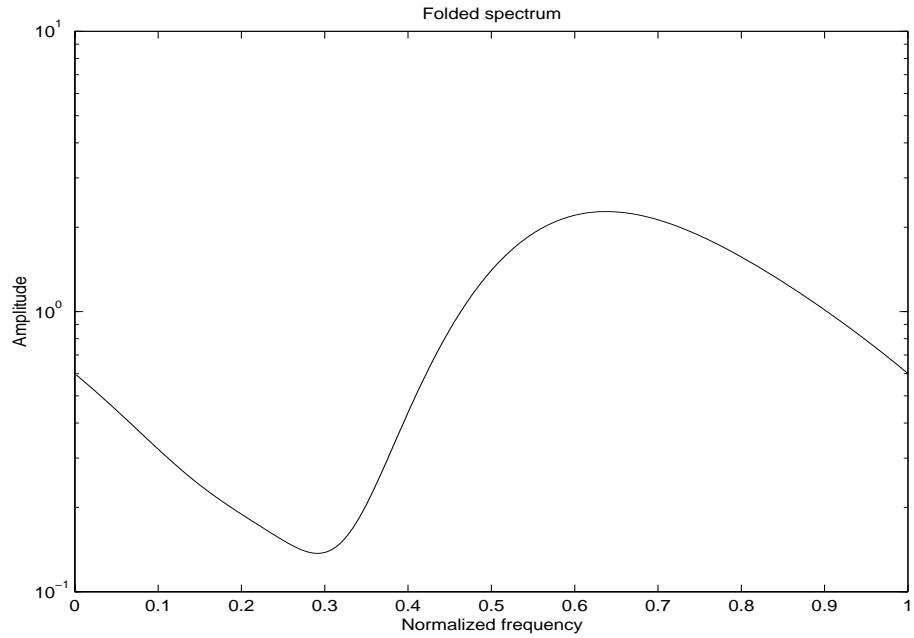


Figure 7-10 Simulation results for channel-1

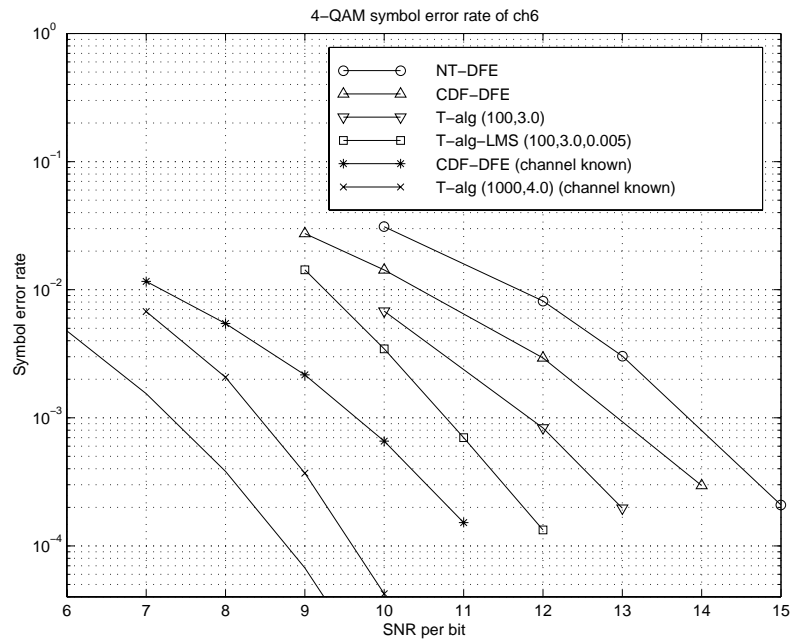
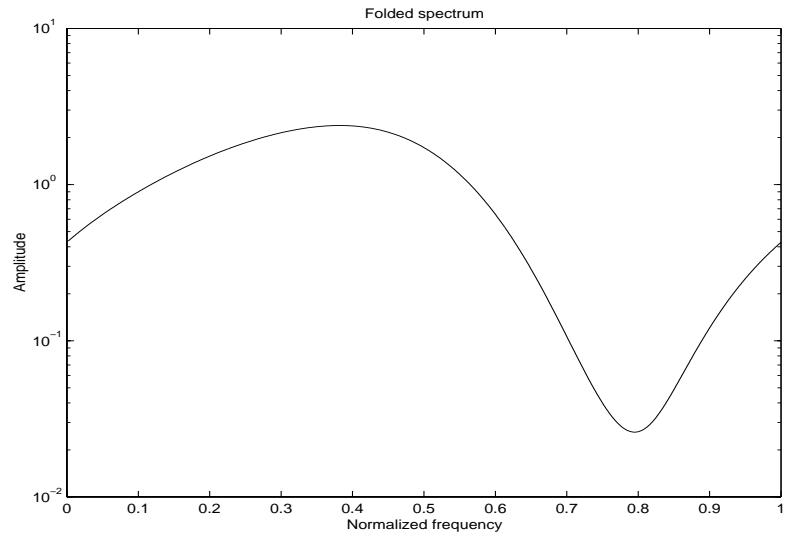


Figure 7-11 Simulation results for channel-2

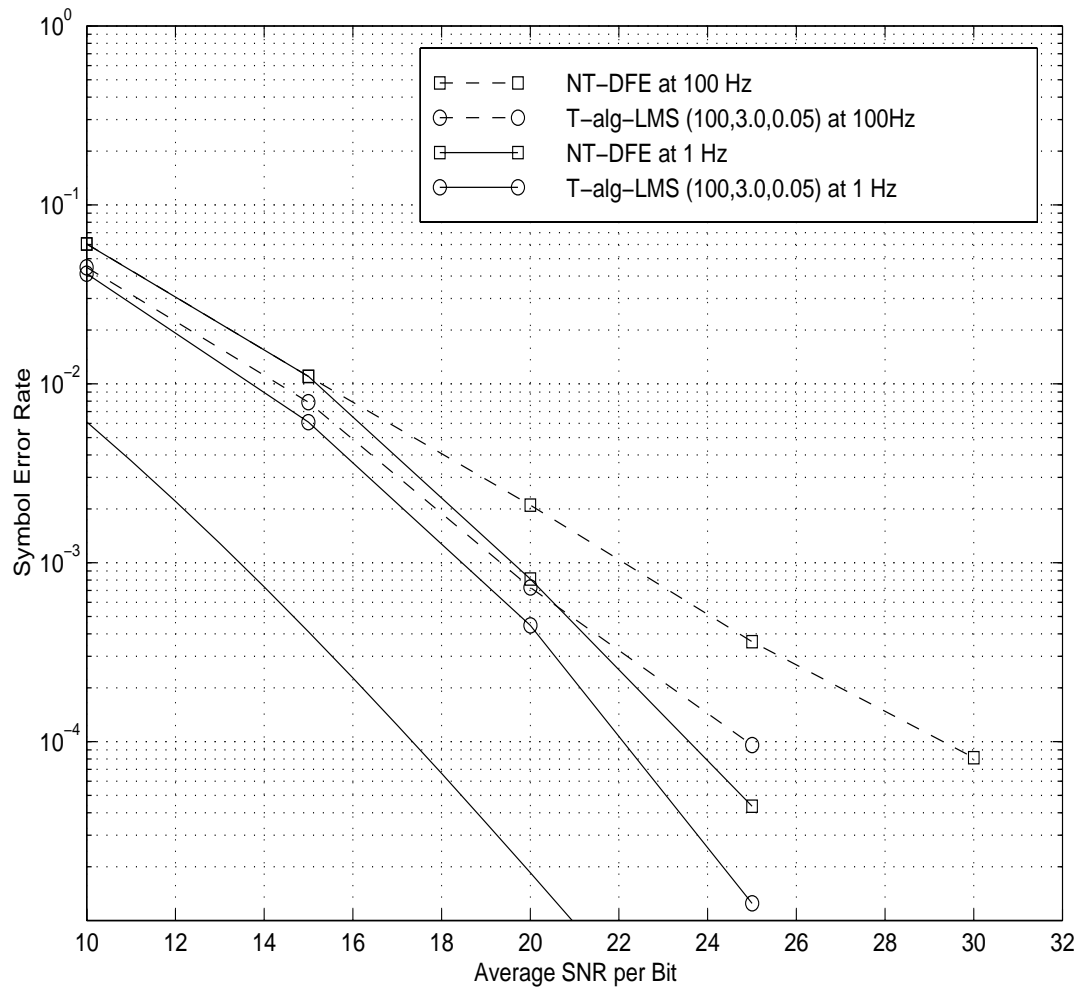


Figure 7-12 4-QAM simulation results for the fading ISI channel

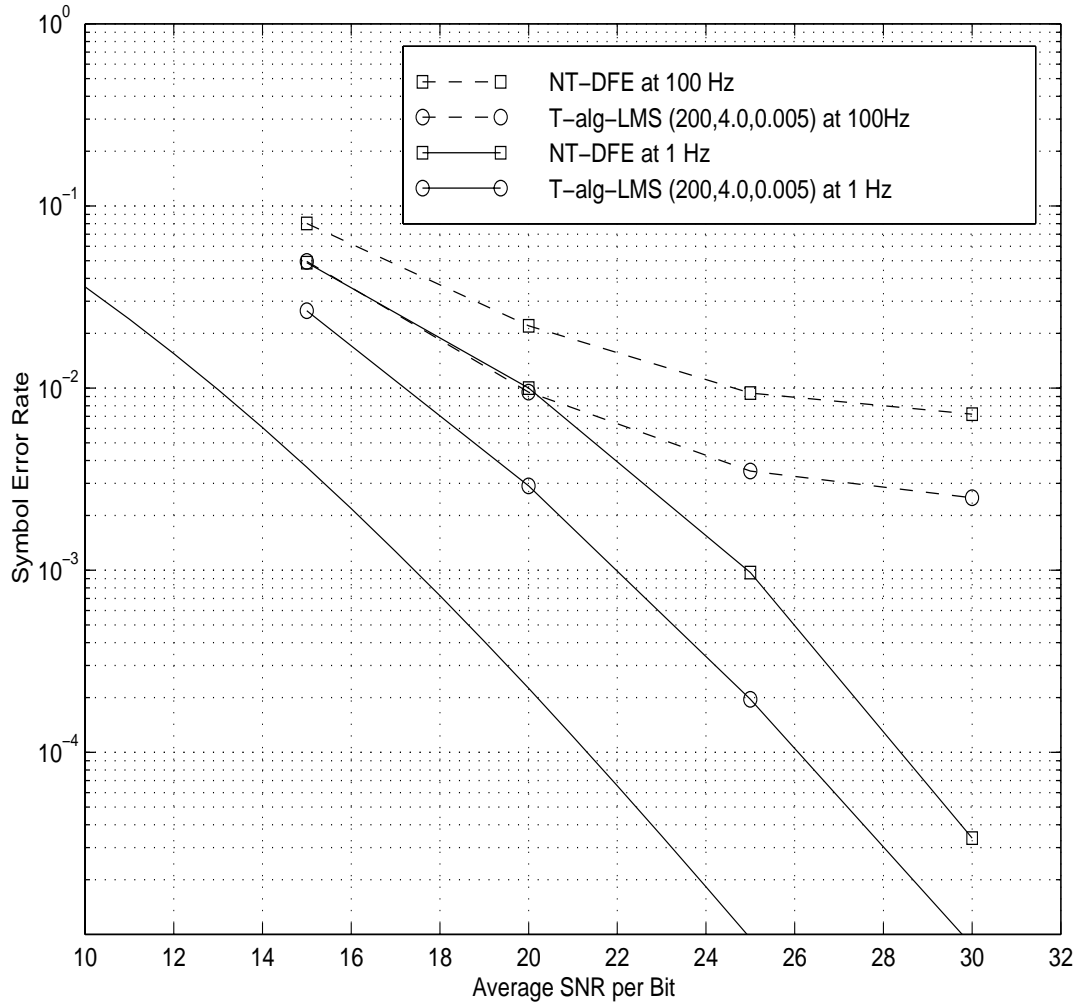


Figure 7-13 16-QAM simulation results for the fading ISI channel

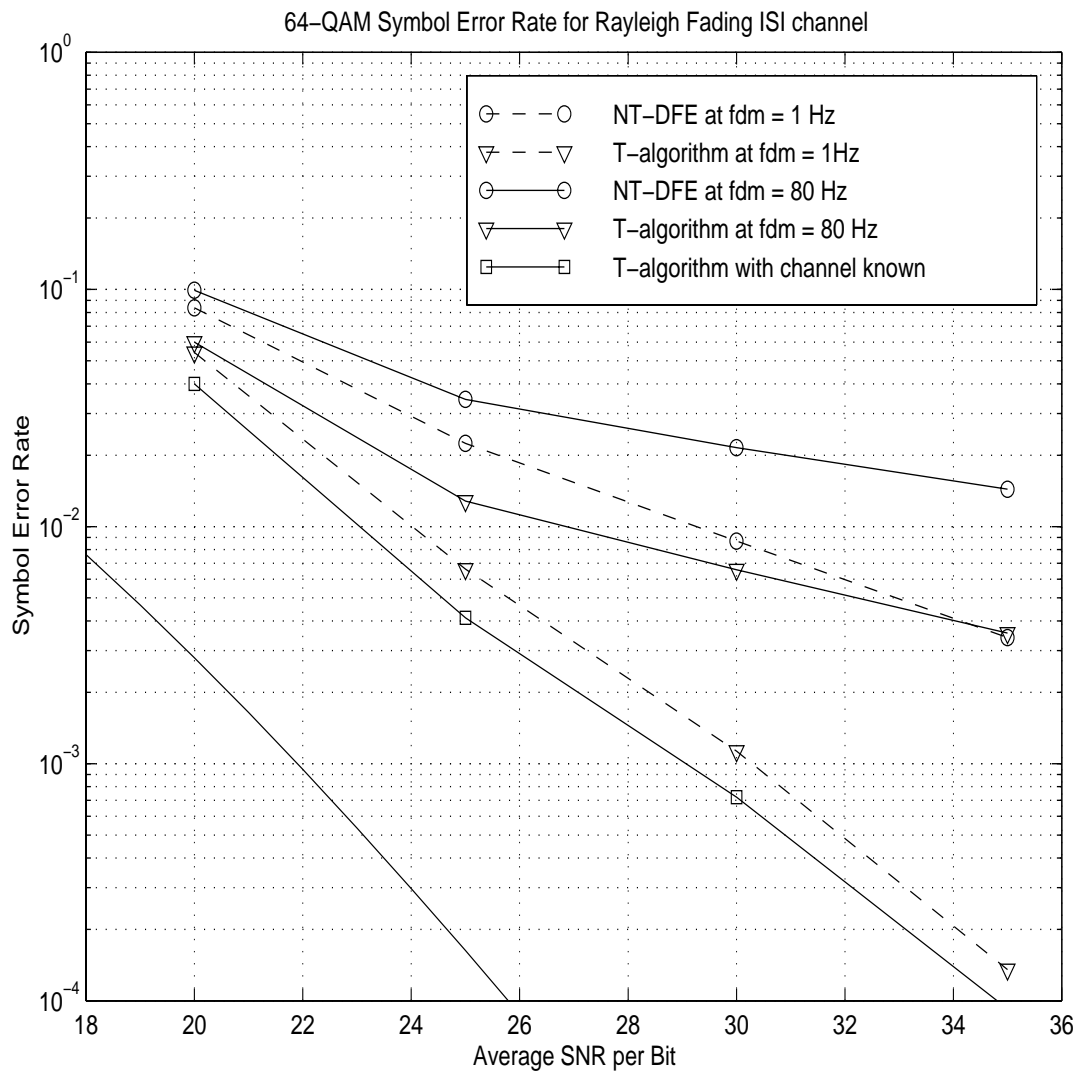


Figure 7-14 64-QAM simulation results for the fading ISI channel

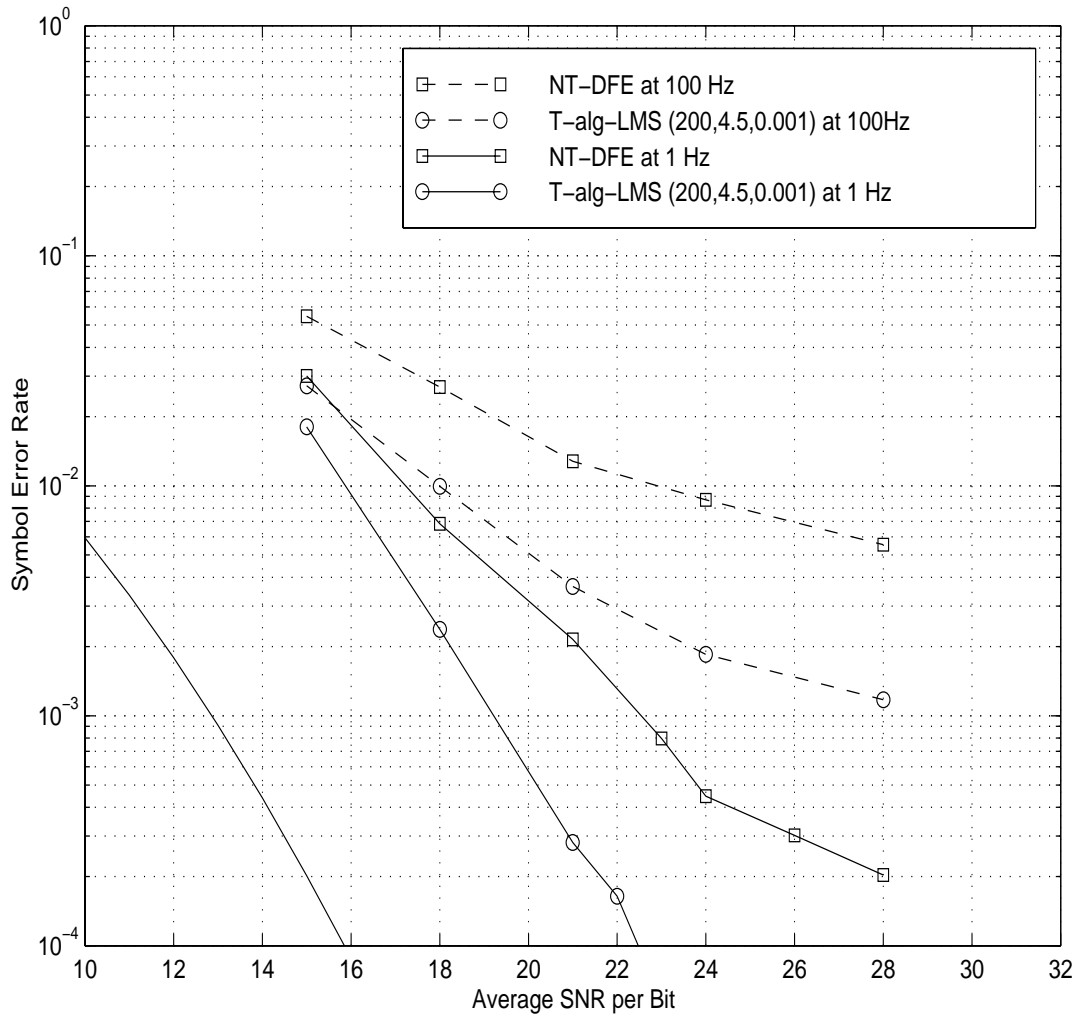


Figure 7-15 64-QAM simulation results for the fading ISI channel ( $L = 2$ ).

## 7.6 Concluding Remarks

In this section, we have proposed the reduced complexity MLSD receiver architecture, where the feedforward channel estimation and interpolation, front-end filter derivation, and the application of the T-algorithm are integrated. First, we have investigated a number of different receiver schemes using different front-end filters (e.g., the matched filter, the WF, or MS-WF). Among them we determined the cascade of matched filters, combiner and the MS-WF, which is suitable for the T-algorithm. Ungerboeck receiver operates only with the matched filtering and diversity combining, but it turned out that the sequential search methods using Ungerboeck metric, such as T-algorithm or M-algorithm, required exploration of every possible path, especially for a channel with a deep in-band null. Thus, we proposed use of the finite length MS-WF to approximate the WF, where the T-algorithm receiver was shown to exhibit desirable error-rate versus average-computational-complexity behavior. In addition, we also proposed the use of per-survivor channel mismatch tracking using the LMS algorithm in conjunction with the T-algorithm. The per-survivor channel mismatch tracking helps further reduce the average-complexity while achieving higher SNR advantage. The developed receiver was shown to be operational for a large  $q$ -QAM signalling,  $q$  up to 64.

In Chapter 8, the pre-processing filters and the T-algorithm receiver will be extended to decode the trellis-coded signal transmitted over the time-varying ISI channel. Since the coded sequence has a larger minimum distance than uncoded sequences, a near-optimum MLSD performance can be obtained without significantly increasing the average number of survivors that the T-algorithm receiver must consider.

## Appendix B The Fano metric

In this section, we derive the Fano metric for the *symbol*-spaced matched filter ISI model. For the derivation of the Fano metric we follow the random tail method of Massey [93]. We assume a forward search which explores the trellis from the beginning for the description of the Fano metric. That is, we consider the Fano metric for the input sequence of length  $n$ ,  $1 \leq n \leq N$ , where  $N$  is the total length of the transmitted input sequence. It should be recognized that a backward search, a search started from the end of the trellis, has exactly the same property as the forward search. Since the matrix  $\Psi$  is Toeplitz Hermitian symmetric, the state machine exhibits the same distance property for both directions. Thus, bidirectional sequential decoding [104] can be applied to alleviate the variability of detection effort.

The Fano metric is in fact obtained from a maximum *a posteriori* probability density regarding an input sequence of length  $n$  given the sequence of matched filter output samples. Following the random tail method [93], the MAP measure of a hypothetical sequence  $I_1 \dots I_n$  given the observation  $z_1 \dots z_N$  is

$$Pr(y_{1:n} | z_{1:N}) = \frac{Pr(z_{1:n} | y_{1:n})Pr(y_{1:n})}{Pr(z_{1:n})}. \quad (7.74)$$

After taking the logarithm and defining the log MAP measure as the Fano metric, we have

$$\phi(I_1 \dots I_n) = \log Pr(z_{1:n} | y_{1:n}) - \log Pr(z_{1:n}) + \log Pr(y_{1:n}). \quad (7.75)$$

The third term in (7.75) can be readily computed since we assume an *iid* input sequence, i.e.,

$$Pr(y_{1:n}) = \prod_{i=1}^{n-1} Pr(y_{i+1} | y_i) Pr(y_1) = \prod_{i=1}^n Pr(I_i) = M^{-n}, \quad (7.76)$$

and thus  $\log Pr(y_{1:n}) = -n \log_2 M$ , where  $M$  is the size of modulation constellation set.

The second term in (7.75) is a pure observation. If we are comparing the MAP measure for the same length of sequence, it can be consolidated to the universal constant term. However, the Fano metric is supposed to give a fair distinction among different lengths of hypothetical input sequences. Thus, we should include the second term in comparison of different length sequences.

The first term of the Fano metric is the likelihood function. We define the first term as

$$\begin{aligned}
L_n &:= \log Pr(z_{1:n} | y_{1:n}) = \text{Const} \\
&- \frac{1}{2} \{ z_{1:n}^H R_n^{-1} z_{1:n} - y_{1:n}^H R_n^{-1} z_{1:n} - z_{1:n}^H R_n^{-1} y_{1:n} + y_{1:n}^H R_n^{-1} y_{1:n} \}, \quad (7.77) \\
&= \text{Const} - \frac{1}{2} \left\{ z_{1:n}^H R_n^{-1} z_{1:n} - \frac{1}{\sigma_n^2} [2 \text{Re}(I_{1:n}^H z_{1:n}) - I_{1:n}^H \Psi_n I_{1:n}] \right\},
\end{aligned}$$

where we have used  $R_n = \sigma_n^2 \Psi$ . We can show that the first component  $z_{1:n}^H R_n^{-1} z_{1:n}$  can be computed from the fractionally sampled received samples, i.e.,

$$z_{1:n}^H R_n^{-1} z_{1:n} = x_{v:v+n-1}^H x_{v:v+n-1}. \quad (7.78)$$

It should be recognized that the rest of terms in (7.77) are the same as Ungerboeck's MLSD cross-correlation measure. In fact, the metric for the M-algorithm is the likelihood function  $L_n$  without the term  $z_{1:n}^H R_n^{-1} z_{1:n}$ . Specifically, we define

$$J_n = L_n - z_{1:n}^H R_n^{-1} z_{1:n}.$$

Then, we can show that  $J_n$  can be computed recursively from

$$J_n = J_{n-1} + \hat{\lambda}_{n-1,n}, \text{ for } n = 1, 2, \dots, N, \text{ with } J_0 = 0; \quad (7.79)$$

where the cumulative metric  $J_n$  is

$$J_n = \sum_{i=1}^n \sum_{j=1}^n I_i^* I_j \Psi_{i-j} - 2Re \left\{ \sum_{i=1}^n I_i^* z_i \right\}, \quad (7.80)$$

and the branch metric,  $\lambda_{n-1, n}$ , from the  $(n-1)$ -th node to  $n$ -th node is

$$\lambda_{n-1, n} = -2Re\{I_n^* z_n\} + I_n^* I_n \Psi_0 + 2Re\{I_n^* \sum_{i=1}^L I_{n-i} \Psi_i\}.$$

## Chapter 8

# Decoding of Trellis Coded Modulated Signals

In this chapter, a new receiver is proposed for decoding trellis coded modulation signals transmitted over fast fading ISI channels. The feedforward channel estimation and the adaptive matched and whitening filters developed in previous chapters are used to combine diversity signals and obtain the estimate of the causal, symbol-spaced FIR channel. Then, the proposed receiver performs the T-algorithm search over the combined tree, which includes the code, the deinterleaver and the causal FIR channel. In Chapter 7, the T-algorithm is used as an equalizer and is shown to achieve near-optimal performance (in the MLSD sense) for uncoded systems at a reduced complexity. We show that the T-algorithm can be applied to a joint decoding/equalization problem, and the coding benefit can be achieved without increasing the complexity. We use the 8-PSK, 8-state trellis code [98] with modest block interleaving to show that the proposed receiver achieves the available time-diversity benefit of the code for the fast Rayleigh fading ISI channel. The proposed receiver is also compared to the other suboptimal receivers, using the T-algorithm

for equalization and the Viterbi decoder for the deinterleaved soft-equalized symbols. Simulation results indicate that the proposed joint receiver is superior in terms of both BER and complexity.

## 8.1 Introduction

Trellis coded modulation is an efficient coding technique, which achieves coding benefit at no cost in bandwidth. This makes the use of TCM very attractive for any wireless communications applications where the spectrum and the battery power are limited resources.

TCM was originally designed and optimized for additive white Gaussian noise (AWGN) channels [98]. The design goal is to increase the free Euclidean distance  $d_{free}$  of the coded sequence. One method of decoding is the Viterbi algorithm (VA) which searches the code trellis for the maximum likelihood sequence having the minimum Euclidean metric. For a static channel with intersymbol interference (ISI) in addition to AWGN, optimum decoding can be achieved by first forming a joint trellis which combines the code and ISI trellises and then employing the Viterbi algorithm to search the joint trellis for the minimum Euclidean metric path. Suboptimal but reduced complexity search techniques such as the reduced state sequence estimation (RSSE), the M-algorithm or the T-algorithm, can also be considered when the number of states of the joint trellis is large.

For Rayleigh or Rician flat-fading channels, the TCM design criterion is to obtain as much signal diversity as possible. Thus, first it is desirable to have the encoded symbols interleaved so as to provide independent fading on adjacent symbols. Then, the primary code design criterion is to increase the length of the shortest error event path; the secondary one is to increase the product of branch distances along that path, to achieve as large as possible time-diversity. The Viterbi decoder or other reduced search techniques can be used

to search the deinterleaved sequence.

For fading ISI channels, such as the frequency-selective Rayleigh fading channels we are considering in this paper, the optimum decoder must again search the combined trellis of the encoder and the ISI. However, the use of the interleaver/deinterleaver forbids the formation of a joint trellis due to the prohibitive complexity. Provided an interleaver is not used, the joint trellis can be formed but little signal diversity can be achieved from the use of TCM. It was reported that TCM designed for the flat fading channel may bring worse bit error rate (BER) performance than an uncoded modulation, where the receiver uses the VA to search the joint trellis without interleaving [49].

In this paper, we propose a new receiver scheme to decode TCM signals which are interleaved and transmitted over fast Rayleigh fading frequency-selective channels. The receiver employs the feedforward channel estimation techniques in Chapter 4 and the front-end filters developed in Chapter 7 which optimally combine diversity antenna signals and provide a symbol spaced, causal overall channel estimate to the sequence estimator using the T-algorithm. The T-algorithm receiver then searches the combined tree of the TCM encoder, the deinterleaver and the ISI formed by the overall channel estimate. In Chapter 7 it was shown that for uncoded signal transmission over the fading ISI channels the T-algorithm receiver brings a substantial SNR benefit over a decision feedback equalizer at a moderate increase in complexity. We show here that by the use of T-algorithm the joint decoding can be performed even for interleaved sequences and the efficiency of T-algorithm search is further enhanced while achieving the coding benefit.

This chapter is organized as follows. Section 8.2 describes the system in consideration. Section 8.3 explains the receivers. Section 8.4 presents the simulation results. Section 8.5 provides the conclusion of the chapter.

## 8.2 The system description

Figure 8-1(a) describes the baseband equivalent system used for the simulation. It is a part of the complete system, from A to B in Figure 8-2. The complete system will be used to explain the operation of the decoding processes in which the detailed system (a) is replaced with the simplified tapped delay line (TDL) model (b). More explanation will be followed later in this section.

In Figure 8-1, the modulated symbol sequence  $\{I_k\}$  is transmitted using the transmit shaping filter (TX) with 35% excess bandwidth. Then, the transmitted signal is received through the  $L$  frequency-selective channels, assumed to be mutually independent by the use of  $L$  space-diversity antennas. Since the shaping filter employs excess bandwidth, a half symbol period sampling of the received signal is assumed. Accordingly, the TX, diversity channels and matched filters ( $MF^l$ ) are realized with half symbol-spaced finite impulse response (FIR) filters.  $MF^l$  at each diversity branch is matched to the cascade of TX and the  $l$ -th channel  $Ch^l$ . Then, the matched filtered signals are combined and symbol-rate sampled.

The mean-square whitening filter (MS-WF) is an anticausal, symbol-spaced FIR filter, which whitens the noise colored by the matched filtering at each diversity branch and provides the “quasi” minimum phase overall channel response between the input symbols  $\{I_k\}$  and the output symbols  $\{y_k\}$ .

In Chapter 5, the same diversity combining structure of Figure 8-1 is derived under the criterion of minimum mean squares error-DFE. In Chapter 7, the same structure is also shown to be the optimum (in MLSE sense) pre-processor to be used with the T-algorithm post-processor for uncoded use. In fact, by the use of a finite length MS-WF, instead of using an infinite length WF, the overall channel is generally not minimum phase nor is the resulting noise perfectly whitened. The non-causal part of the response tends to vanish but

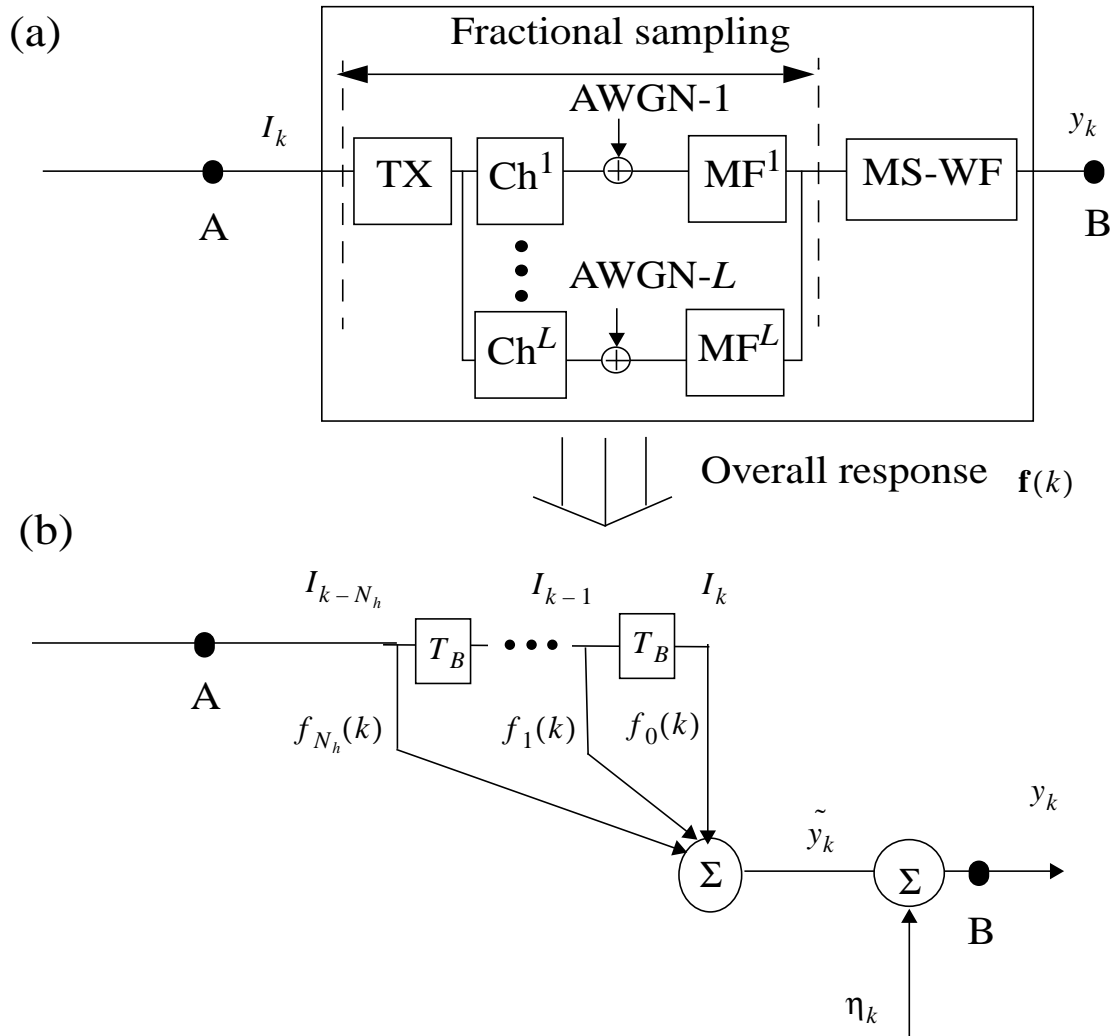


Figure 8-1 (a) Baseband system description of the system from A to B in Figure 8-2. (b) The symbol-spaced TDL is the model representing the system from A to B for the operation of T-algorithm receiver.

not exactly zero-valued, even with perfect knowledge of the channel. As was shown in Chapter 7, however, the MS-WF provides a practical and stable solution suitable for use in the presence of channel estimation error and for channels with a null (nulls) in the folded spectrum (i.e. severe ISI).

For the purpose of T-algorithm search, therefore, the non-causal part of the overall response  $\mathbf{f}(k)$  is ignored, and the noise is assumed to be whitened. Then, the input/output relationship between  $\{I_k\}$  and  $\{y_k\}$  is given by as depicted in Figure 8-1 (b)

$$y_k = \sum_{i=0}^{N_h} f_i(k) I_{k-i} + \eta_k, \quad (2)$$

where  $N_h$  is the length of  $\mathbf{f}(k)$  and  $\eta_k$  is assumed to be white Gaussian noise.

To update the MF, MS-WF and thus  $\mathbf{f}(k)$ , we use the channel estimation and tracking methods described in Chapter 4. That is, we assume a contiguous transmission of frames, where a frame constitutes a training segment and an unknown data segment. A set of four channel estimates obtained during the training segments is interpolated to track the channel variation for the second data block. From the interpolated channel estimates, the MF<sup>l</sup> and the MS-WF are obtained. Readers are directed to Chapter 7 for further details of the pre-processing receiver and the procedure to obtain the MF, MS-WF and  $\hat{\mathbf{f}}(k)$  from the channel estimates.

Figure 8-2 provides the description of the complete system where the detailed system given inside the box of Figure 8-1 (a). is replaced with the overall channel estimate  $\mathbf{f}(k)$  and the equivalent noise  $\eta_k$ . The equally-likely uncoded bits are mapped to the encoded symbol sequence and the modulated sequences are interleaved by the  $(N_I \times N_J)$  interleaver before being transmitted. The training sequence of length  $N_t$  is inserted into each row of the interleaved sequence as described in Figure 8-3, and transmitted row by row. These training symbols are used for the feedforward channel estimation as well as for the start and end of a decoding process (i.e., a sequence starts with a known state and ends

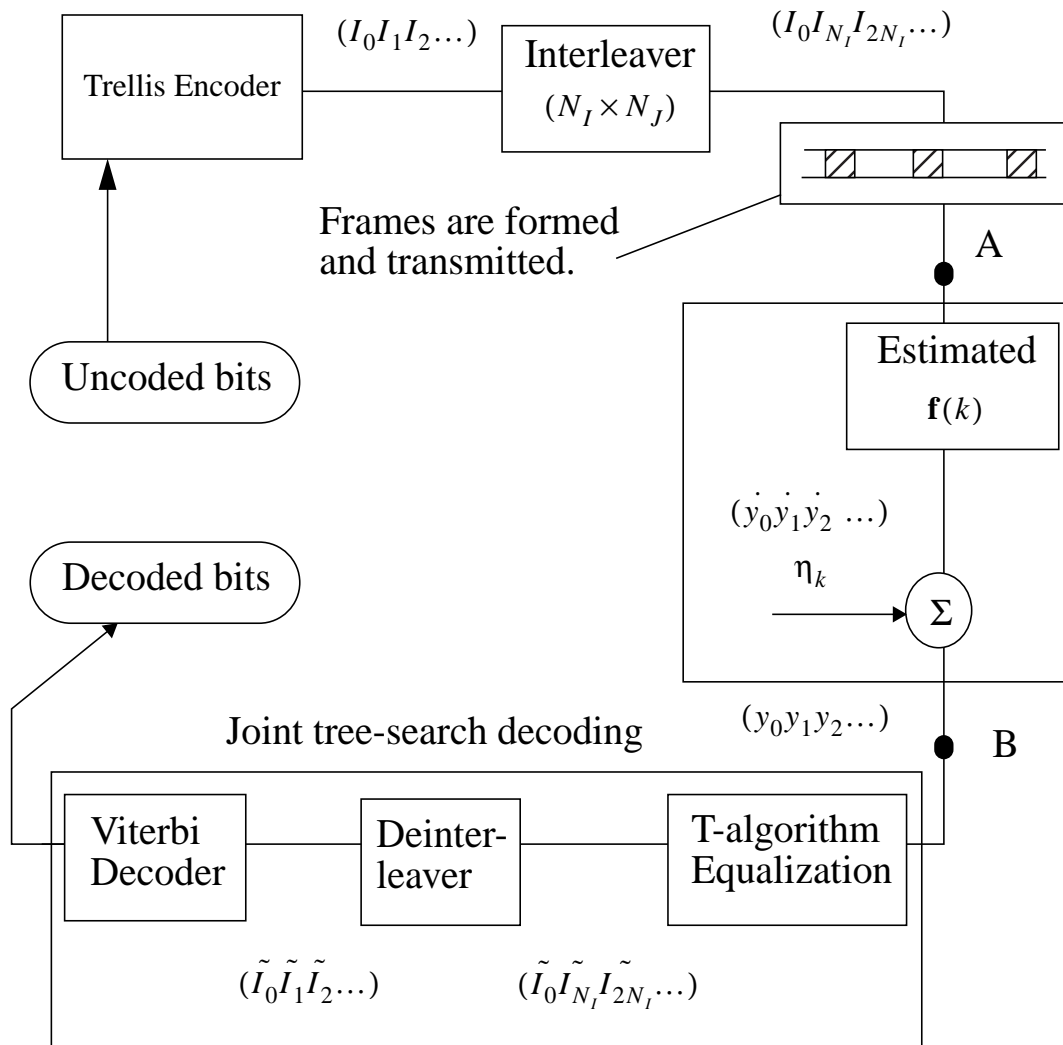


Figure 8-2 The block diagram of the overall system: the details of the system from A to B are described in Figure 8-1 (a).

in a known state.)

## 8.3 The receivers

In this section, we describe the proposed receiver and the other suboptimal receivers that are in comparison. All of the receivers use the Euclidean distance metric, obtained under the criterion of maximum likelihood sequence estimation (MLSE). Thus, we first begin with the derivation of the metric.

### 8.3.1 The Euclidean distance metric from MLSE

The maximum likelihood bit-sequence can be determined from

$$\hat{\mathbf{b}} = \underset{\mathbf{b} \in \mathbf{B}}{\arg \max} \Pr\{\mathbf{y} | \mathbf{b}\}, \quad (8.1)$$

where  $\mathbf{b}$  is the sequence of independent, equally likely bits and  $\mathbf{B}$  is the set of all possible bit sequences. The code trellis provides a one-to-one mapping from a sequence of bits  $\mathbf{b}$  to a sequence of trellis coded modulation symbols  $\mathbf{I}(\mathbf{b})$ . Therefore, (8.1) can be rewritten as

$$\hat{\mathbf{b}} = \underset{\mathbf{I} \in \{\mathbf{I}(\mathbf{b}): \mathbf{b} \in \mathbf{B}\}}{\arg \max} \Pr\{\mathbf{y} | \mathbf{I}\}. \quad (1)$$

Then, from the relationship given by (2) we have

$$\hat{\mathbf{b}} = \underset{\mathbf{I} \in \{\mathbf{I}(\mathbf{b}): \mathbf{b} \in \mathbf{B}\}}{\arg \min} \{|\mathbf{y} - \hat{\mathbf{y}}|^2\} = \underset{\mathbf{I}}{\arg \min} \left\{ \sum_{k=0}^{N-1} |y_k - \hat{y}_k| \right\} \quad (2)$$

where we used  $\hat{\mathbf{y}} = (\hat{y}_{N-1} \dots \hat{y}_0)^t$  and  $\hat{y}_k = \sum_{i=0}^{N_g} f_i(k) I_{k-i}$ . The second equality follows from the assumption that  $\eta_k$  is white.

### 8.3.2 Joint decoder without the use of interleaver

Now consider a situation where no interleaver is used, i.e.  $N_I = 1$ . Then, the ISI trellis with  $q^{N_g}$  states and the encoder trellis with  $S$  states can be readily combined to form

a super-trellis, and the complete search of (2) can be performed by the use of VA which searches over the joint-trellis with  $O(S \times q^{N_s})$  states. When the number of trellis state become too large for the VA to be of any practical use, reduced search techniques can be considered. In [117], the M-algorithm, the T-algorithm and RSSE are applied to decode trellis coded signals transmitted over a static ISI channel, and it is reported that the T-algorithm which operates on the joint trellis achieves the performance of RSSE at much less average computational cost.

When applied to fading channels, however, the joint trellis decoder may not provide any coding benefit [124] since the interleaver is not used. In the design of trellis-coded signals for fading channels the primary objective is not to obtain a large free Euclidean distance but to achieve as large a diversity order as possible. Then the potential diversity gain of the code can be achieved fully for an ideal system operating on an independent fading channel, and partially for systems which use a finite length interleaver to implement independent signal fading. The asymptotic BER performance of the ideal system would behave proportional to  $SNR^{-D}$  where the power exponent  $D$  is the order of diversity provided by the code for flat Rayleigh fading channels.

The joint decoder without an interleaver uses the same T-algorithm with  $N_I = 1$ , described in section 8.3.4. This joint decoder employs the least mean squares (LMS) per-survivor channel tracking scheme developed in Chapter 7 to enhance the channel estimate and thus improve the decision. The intermittent training symbol sequence enforces the sequence to start from and end in a known state within a frame, and thus the decoding is performed on a per frame basis. We refer to this receiver as ‘no interleaver joint T-algorithm’ (NI Joint T-*alg*).

### **8.3.3 Separate equalization and decoding with the use of an interleaver**

In this system the interleaver-deinterleaver is employed to achieve the diversity

benefit provided by TCM. The sequence of symbols  $(I_0 I_1 I_2 \dots)$  are interleaved and the interleaved sequences  $(I_0 I_{N_I} I_{2N_I} \dots)$  are transmitted over the multipath fading channel as shown in Figure 8-2. Then the equalization and the decoding steps are separated at the receiver. The T-algorithm equalization in Chapter 7 is first performed on the received signals, which are corrupted by the overall channel  $\mathbf{f}(k)$ . The T-algorithm searches on the interleaved sequence without exploiting the sequence constraint imposed by the code trellis. The sequence estimator also works on a per frame basis using the training symbols at both ends. The T-algorithm equalization provides hard decisions  $(\hat{I}_0 \hat{I}_{N_I} \hat{I}_{2N_I} \dots)$  on the transmitted symbols in the expanded signal set. These hard decisions are then used to cancel the ISI and generate the sequence of soft equalized outputs  $(\tilde{I}_0 \tilde{I}_{N_I} \tilde{I}_{2N_I} \dots)$  where

$$\tilde{I}_{kN_I+i} = \frac{y_k - \sum_{p=1}^{N_h} f_p(k) \hat{I}_{k-pN_I}^i}{f_0(k)} = \hat{I}_{kN_I+i} + noise \quad (8.2)$$

for  $k = 0, 1, \dots, N_J - 1$  and  $i = 0, 1, \dots, N_I - 1$ . The LMS per-survivor channel tracking is again used to reduce the number of survivors and improve on the hard decisions.

The deinterleaved soft output sequence  $(\tilde{I}_0 \tilde{I}_1 \tilde{I}_2 \dots)$  is fed to the Viterbi decoder which searches the code trellis with  $S$  states to decide the minimum metric path. We refer this receiver as the ‘T-*alg.* & VA’ receiver.

### 8.3.4 The proposed joint tree searching T-algorithm receiver

We now describe the proposed T-algorithm receiver which performs jointly the decoding, deinterleaving and equalization. Since it is a joint search of the maximum likelihood path, there is no information loss due to early decisions (definitely there is some information loss due to the use of the suboptimal T-algorithm search, instead of complete search) nor is “turbo” like iteration required between the ISI trellis and the code trellis. It is the case that for a separate equalization and decoding scheme, a turbo-iteration would be

beneficial since the two state machines are separated by the deinterleaver. The results of the iterations would converge to that of the joint-search.

As elaborated more in the sequel, the T-algorithm follows the code tree, while cancelling the contribution of post-cursor ISI by the use of the tentative decision symbols stored in the survivor-sequence, or by the use of the decided symbols when the depth of the T-algorithm is shorter than  $N_I N_h$ . The decided symbols are quite reliable since they are the results of sequential search, not a symbol by symbol decision as in the case of DFE. That is, the ISI cancelling is carried out in each of the survivors.

We now describe the proposed receiver algorithm. The following receiver parameters can be selected by the receiver designer:

- $P_{max}$  denotes the maximum number of survivors allowed.
- $\zeta$  denotes the threshold value and  $\zeta_b$  denotes the reduction value.
- $N_g$  determines the depth of the tree, i.e.,  $N_D = N_g \cdot N_{row}$ .

Then for the description of the algorithm we use the following notation.

- $i$  denotes the survivor index, i.e.,  $i = 0, 1, 2, \dots, P_{max} - 1$ .
- $j$  denotes the contender index, i.e.,  $j = 0, 1, 2, \dots, MP_{max} - 1$ .
- $\mathbf{I}_k^i$  denotes the  $i$ -th survivor,  $i = 0, 1, 2, \dots, P_{max} - 1$ , a  $(N_D \times 1)$  vector which stores a history of hypothetical encoded symbols.
- $\mathbf{S}_k^i$  denotes the history of encoder-states of the  $i$ -th survivor.
- $B_{met}(i, q)$  denotes the metric of the branch which is the  $q$ -th transition from the state of  $i$ -th survivor, and is computed by

$$B_{met}(i, q) = \left| y_k - \sum_{p=1}^{N_h} f_p(k) \mathbf{I}_{k-pN_I}^i \cdot \tilde{f}_0(k) \right|, \quad (3)$$

where  $\mathbf{I}_k$  represents the modulation symbol defined in the encoder-trellis for the transition.

- $J_{cum}(i)$  the cumulative metric of the  $i$ -th survivor.
- $J_{cont}(j)$  denotes the cumulative metric of the  $j$ -th contender, i.e.,

$$J_{cont}(j = iN_b + q) = J_{cum}(i) + B_{met}(i, q), \quad (4)$$

where  $N_b$  is the number of branches out of a state.

- $\mathbf{D}_I$  denotes the decided symbol sequence.
- $\mathbf{D}_E$  denotes the decided encoder-state sequence.
- $P$  denotes the length of survivor list that is updated at each epoch.

Then, the joint-tree searching T-algorithm can be described as:

- (Step-1) Start from the state-0 of the encoder, and thus set  $J_{cum}(0) = 0.0$ ,  $\hat{S}_{N_d}^0 = 0$  and the length of the survivor  $P = 1$ .

Then for each  $k = 0, 1, \dots, N_I \cdot N_J - 1$  the following steps are taken:

- (Step-2) For  $i = 0, \dots, P - 1$ , extend the  $i$ -th survivor into  $N_b$  contenders. At each extension step,  $J_{cont}(j)$  is computed by (4), the minimum metric  $J_{min}$  and the best survivor index  $i_{min}$  are updated by a binary comparison ( $J_{min} = J_{cont}(0)$ ), and the survivor-path index  $i$ , i.e.  $P_{id}(j) = i$ , are recorded.
- (Step-3) Mark and count the contenders which pass the threshold test

$$J_{cont}(j) - J_{min} < \zeta \quad (5)$$

and possess the same path-history symbol as the one in the best metric path. If the counter  $p$  reaches  $P_{max}$  before  $j$  reaches  $PN_b$ , stop and lower the threshold by  $\zeta_b$ , and then mark and count again. From the marked paths, generate a survivor list which records the contender's index  $S_{id}(p) = j$ .  $P$  is the size of the survivor list.

- (Step-4) For  $p = 0, 1, \dots, P - 1$  obtain the index of the survivors using  $S_{id}$  and  $P_{id}$ , i.e.  $r = P_{id}(S_{id}(p))$ , and form the new survivors  $\hat{\mathbf{I}}_{k+1}^p$  and  $\hat{\mathbf{S}}_{k+1}^p$  by concatenating the new symbol and the new encoder-state which are obtained from the trellis to  $\hat{\mathbf{I}}_k^r$

and  $\mathbf{S}_k^r$  respectively.

- (Step-5) For  $k \geq N_D$ , release the symbol and the encoder-state of the best metric path to  $\mathbf{D}_I$  and  $\mathbf{D}_E$ .

## 8.4 Simulation Results and Discussion

In this section we study the performance of the proposed receiver via computer simulations. Let's briefly explain the simulation environment and parameters.

- We use the  $T_B/2$ -spaced sampled system for the fractionally sampled system.
- The transmit filter uses a nine tap square root raised cosine filter with 35% roll-off, which is a 4-symbol period truncation.
- Each diversity channel is a three tap filter, and each independent Rayleigh fading tap is realized with the sum of nine-sinusoids method as explained in Chapter 2.
- The average powers of the three fading taps are (0.6652,0.2447,0.0900), for which the rms delay spread is about 0.3257 the symbol period.
- During reception of the signal the channel taps are continuously varied according to the given fading rate  $f_{dm}$ . As a worst case scenario of 120 km/hr vehicle speed, the fading rate reaches 100 Hz. This requires the frequency of training to be at least every 120 symbols for the purpose of channel interpolation.
- In this chapter we use the eleven training symbols for every 69 symbols, so that a frame consists of 80 symbols. The training sequence used is  $(N_t, N_c) = (11, 6)$  as defined in Chapter 4 which is

$$\mathbf{I}_T = (1 \ 1 \ -1 \ -1 \ -1 \ 1 \ -1 \ 1 \ 1 \ 1 \ 1)^t. \quad (6)$$

- The MF and the MS-WF use 12 taps and 6 taps respectively.
- A Monte Carlo method with 2,000-50,000 independent trials was used to obtain an

averaged performance over the randomly varied channel. To evaluate the adaptation on continuously transmitted frames, each trial consisted of 5-16 frames.

- We use the 8-PSK, 8 state code given in Figure 8-4. The length of the shortest error event path in the trellis is 2 and the square product Euclidean distance is equal to 8.0. Thus, it provides a potential diversity gain of order 2. The code has 3.6 dB asymptotic coding gain over AWGN.

We simulate different receiver schemes for the purpose of comparison with our proposed receiver. All the following receivers use the same number of taps for the front-end filters. In particular, the matched filter at each diversity branch uses 12 half symbol-spaced taps. The symbol-spaced MS-WF uses 6 symbol-spaced taps.

- The ‘NT-DFE’ represents the non-Toeplitz DFE in Chapter 5 which is used to decode Gray-mapped 4-QAM signals. The feedback filter uses six taps.
- The ‘NI-Joint T-alg.’ stands for the joint T-algorithm receiver described in 8.3.2. The T-algorithm parameters are  $(P_{max}, \zeta, N_D, \Delta) = (1000, 2.5, 50, 0.005)$ , where  $\Delta$  is the stepsize of the least mean squares (LMS) algorithm.
- The ‘T-alg. & VA’ implies the receiver scheme described in section 8.3.3 in which the T-algorithm of Chapter 7 is employed to obtain the equalized, soft-output sequence  $\{y'_k\}$ , then deinterleaved and fed to the VA decoder which searches the 8-state trellis. That is, the equalization and the decoding are separated by the use of deinterleaver as shown in Figure 8-2. The T-algorithm parameters are  $(P_{max}, \zeta, N_D, \Delta) = (100, 2.5, 50, 0.005)$ .
- The ‘Joint T-alg.’ represents the proposed receiver where the equalization and decoding are jointly performed by the joint T-algorithm. The joint T-algorithm searches the combined tree formed by the encoder trellis, the interleaver/deinterleaver and ISI. The T-algorithm parameters are  $(P_{max}, \zeta, N_D) = (100, 2.5, 50)$ .
- The ‘Ideal Joint T-alg.’ is the Joint T-alg. operating with perfect knowledge of the fad-

ing channel. Doppler fading at 200 Hz is used to simulate an ideal interleaving. The T-algorithm parameters are  $(P_{max}, \zeta, N_D) = (1000, 2.5, 50)$ .

Figure 8-5 shows the average BER performance of different receivers at the fast fading rate  $f_{dm} = 100$  Hz. First we note that the NI-Joint T-alg. receiver achieves no coding benefit at all, showing only a slight performance advantage over the NT-DFE at high SNR. On the other hand, the receivers with the use of interleaver/deinterleaver show drastic performance difference. The 'T-alg. & VA' and 'Joint T-alg.' receivers shows substantial SNR benefit, which is about 5 - 6 dB for  $L = 1$  and 3 - 4 dB for  $L = 2$  at the average BER  $10^{-4}$  over the NT-DFE. Comparing the 'Joint T-alg.' receiver with the 'Ideal' receiver the SNR loss due to channel estimation error can be estimated, which is about 5 dB SNR loss for  $L = 1$  and 4 dB for  $L = 2$ .

Comparing the 'T-alg. & VA' and the proposed 'Joint T-alg', it seems that there is not much noticeable difference in terms of BER. The 'Joint T-alg' receiver provides an SNR benefit less than 1.0 dB compared to the T-alg. & VA receiver. The BER advantage of the Joint T-algorithm, however, is obtained by keeping a far smaller number of survivors on average. Figure 8-6 indicates the average number of survivors required for the T-algorithm employed in different receivers. The 'T-alg. & VA' receiver requires more than 60 survivors for equalization alone to obtain the BER performance presented in Figure 8-5. Additional complexity is required for the VA decoding. In addition, the overflow percentage of this receiver reaches 100%, suggesting the need to lower the threshold value at the expense of bit error rate increase. On the other hand, the Joint T-alg receiver shows very low average number of survivors, requiring about 10 average survivors in the SNR region where BER is acceptable. The overflow percentage is less than 0.1%.

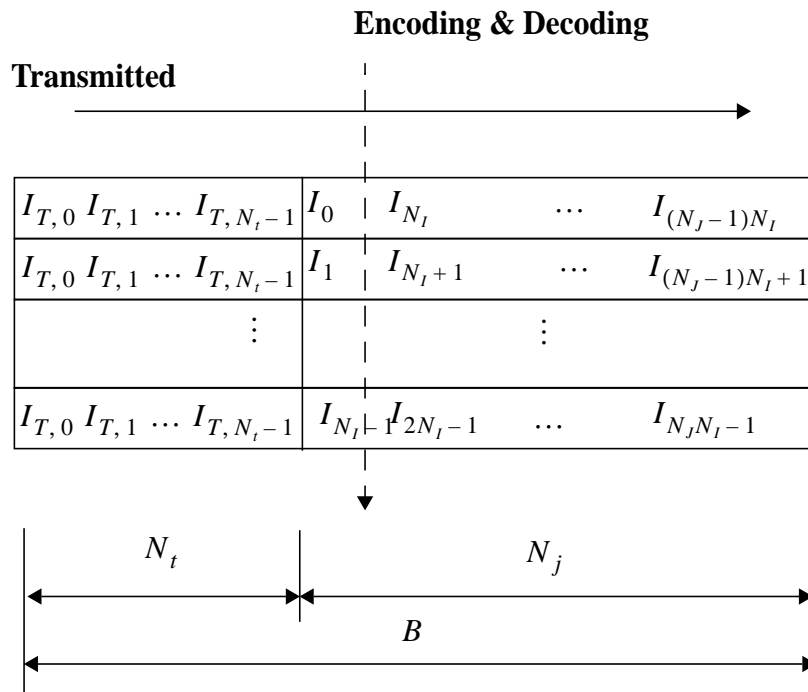


Figure 8-3  $(N_t \times B)$  transmitted symbols. Each row is  $B$  symbols,  $N_t$  training symbols and  $N_j$  unknown symbols.

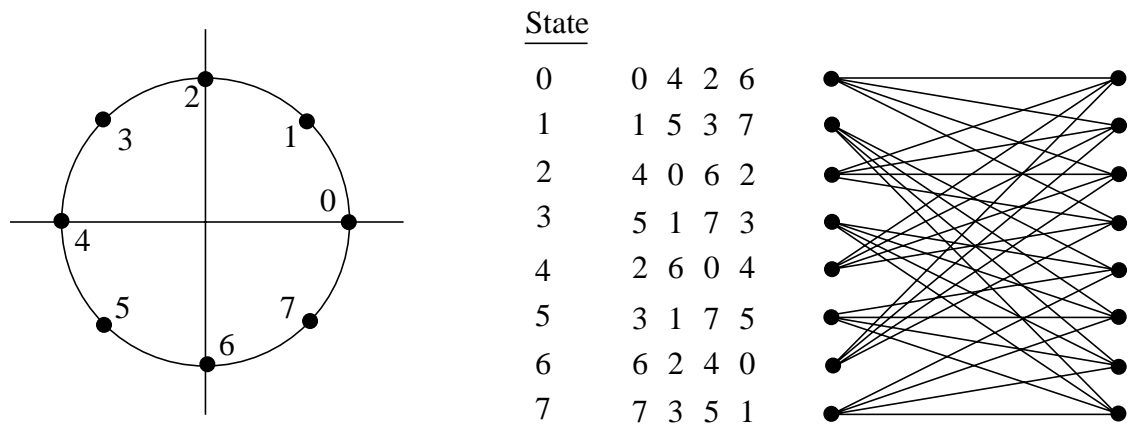


Figure 8-4 The signal set and trellis for 8-PSK, eight-state code. This code has time-diversity order of two.

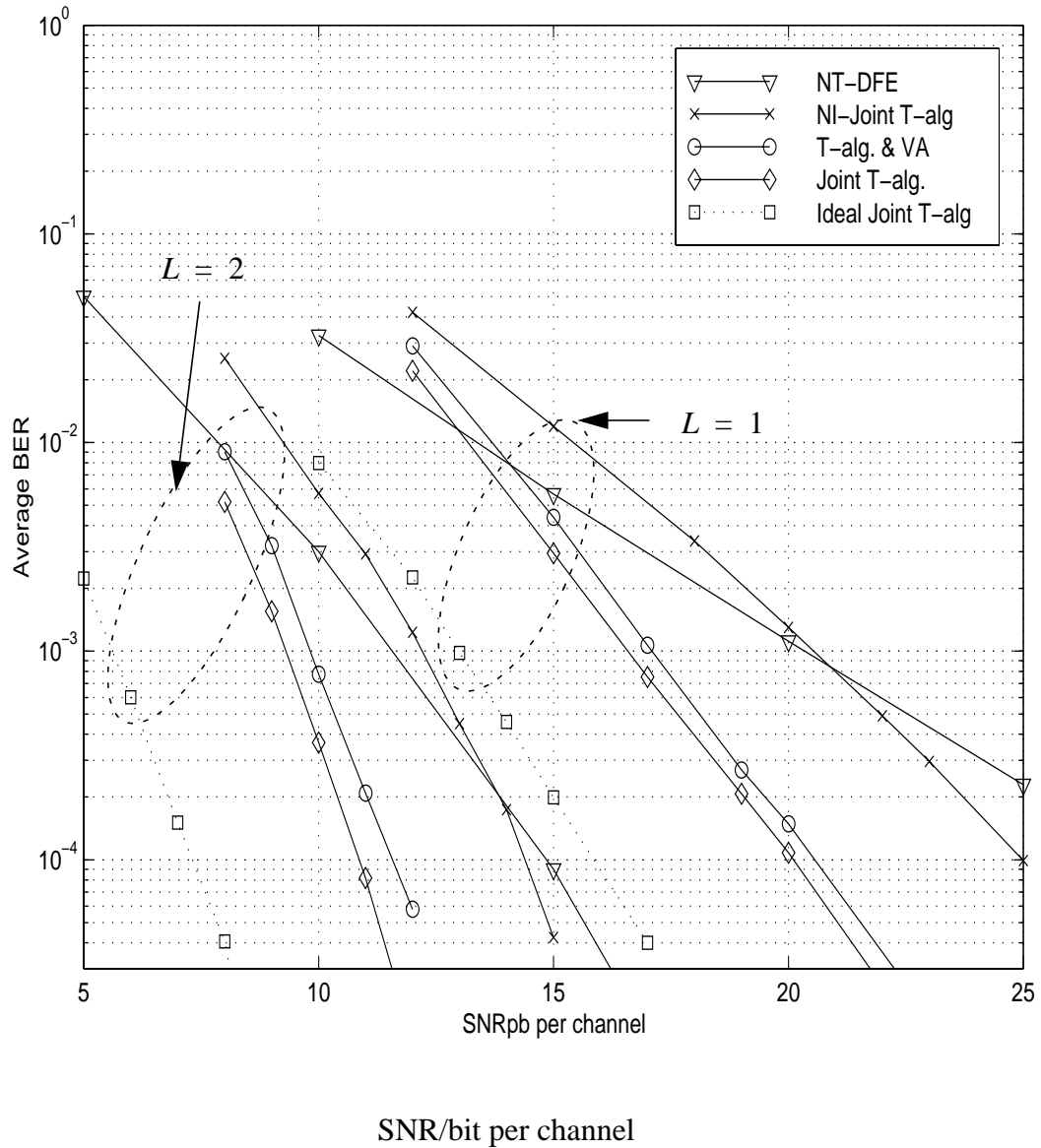


Figure 8-5 Average BER performance over the fading ISI channels (100 Hz). 4-QAM Gray coding is the signalling format for NT-DFE and 8-states 8-PSK trellis modulation for the other receivers, T-alg. & VA, joint-T-alg and Ideal Joint-T-alg. The Ideal receiver is the same as the joint-T-alg., but the channel is perfectly known to the receiver, which is fading at 200 Hz to implement the ideal interleaving.

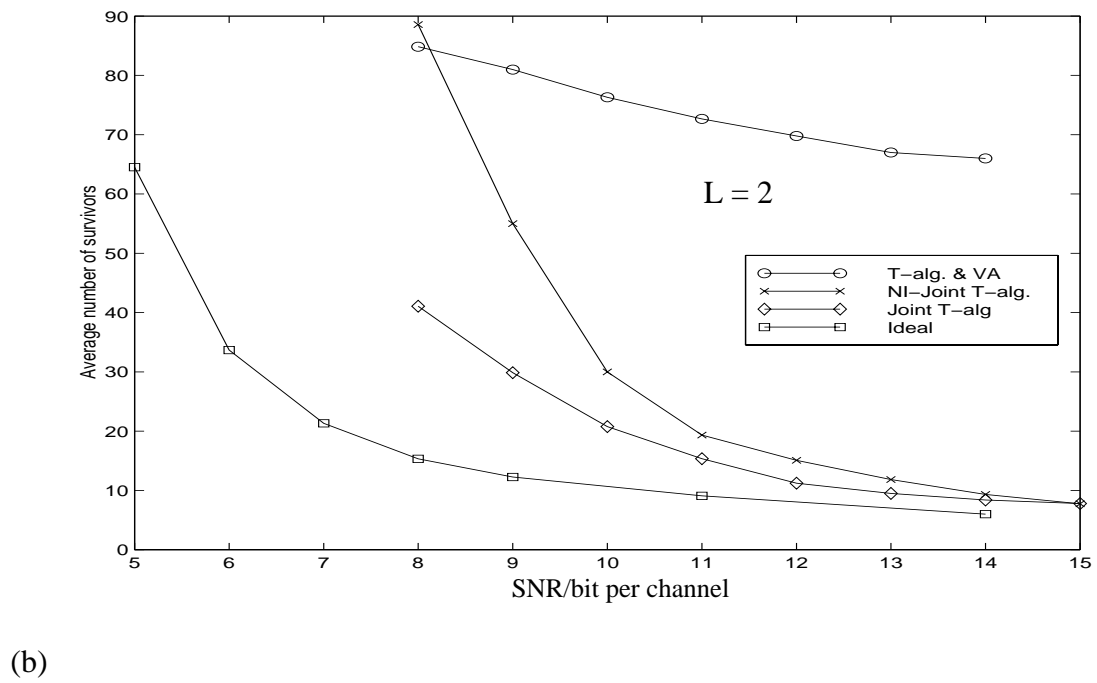
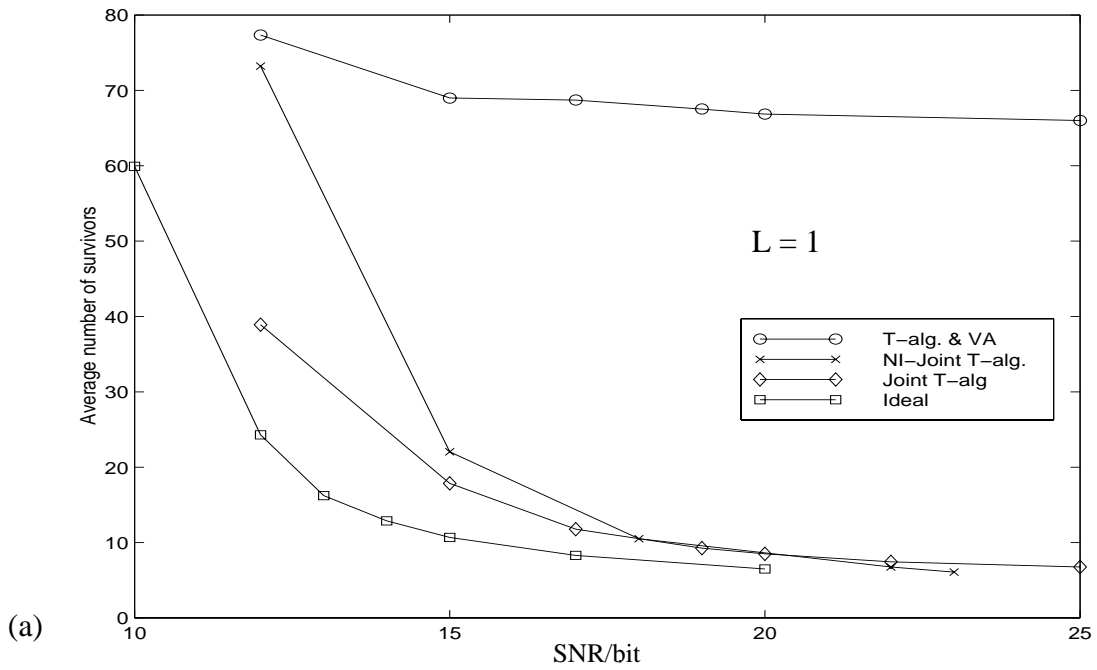


Figure 8-6 Average number of survivors vs. SNR for each receivers. (a) is for  $L = 1$  and (b) is for  $L = 2$ .

## 8.5 Concluding Remarks

We proposed a new receiver scheme which may be used to decode the coded symbol sequences transmitted over fast fading frequency-selective diversity channels. It consists of the pre-processing receiver discussed in Chapter 7 and the post-processing sequence decoder using the T-algorithm.

The pre-processing receiver optimally combines the diversity channel outputs and provides the symbol-spaced sufficient statistic to the post-processing receiver. Using the pre-processing receiver, the overall channel response can be approximated as a quasi minimum-phase ISI with the additive-noise term whitened (approximately). This is desirable for the T-algorithm processor. The efficiency of T-algorithms depend on the channel response. It makes early decisions to purge based on the metric difference. If the channel has the larger energy taps early in the response, then the metric difference will be larger between the correct and incorrect paths, and a more reliable early decision can be made.

Provided with the sufficient statistic sequence and the estimate of the minimum phase overall response at our disposal, in this Chapter we designed a new receiver that jointly and computationally-efficiently decodes the trellis-codes which had been channel-interleaved and transmitted over the fast time-varying multipath fading ISI channels. The use of the interleaver is necessary to realize the potential diversity benefit of the trellis-code designed for a fading channel. The problem of joint decoding and equalization is not a trivial problem since the use of interleaver hinders a formation of a super trellis and make the decoding process difficult. The separate decoding/equalization receiver is suboptimal, due to early decision made at the equalization step.

The proposed T-algorithm is a tree-searching receiver, thus the formation of a joint-trellis is not required and the ISI cancellation and deinterleaving can be performed on a per

survivor basis. The decoder follows the code tree and at each survivor cancels the contribution of the minimum phase ISI using the hypothetical symbols stored in the survivor. This differentiates the proposed receiver from the separate equalization and decoding receiver, where the ISI cancellation is performed using the hard decision symbols in the extended signal set and the decisions are made without the knowledge of the sequence constraint of the code.

Our simulation results show that the proposed joint tree-search T-algorithm brings out the available coding benefit at a very moderate complexity in terms of the average number of survivors that the algorithm had to keep.

# Chapter 9

## Conclusion

The vision of universal communication networking and computing systems provided in the introduction of this dissertation requires many technical breakthroughs. In this dissertation, we have focused on the design of reliable, efficient wireless communication techniques at the link-layer. In particular, we have proposed a TDMA based systems where using the intermittent training symbols, the receiver estimates the channel and obtains the optimum filter coefficients to process the received signals. We paid special attention to ensuring robust receiver performance in fast time-varying fading channel conditions and for signal modulation with a large constellation to improve spectral efficiency. The development of the transceiver was extended to support the trellis-coded modulation, which would be useful in extending the coverage area of the transceiver. The transceiver techniques introduced in the dissertation may be a stepping stone towards the realization of the envisioned wireless networking systems. We now conclude the dissertation with summary of research contribution and a list of possible future research topics.

## 9.1 Research Contributions

This dissertation presents advances in the design of wireless transceiver in a number of areas. A summary of these contributions is given below.

1. We have proposed a novel channel estimation scheme, where the *a priori* information of the transmit shaping filter was used to reduce the number of unknown parameters in the channel parameter estimation problem. This brings about a number of benefits. First, with fewer unknown parameters, a shorter observation window is needed. Second, with a shorter observation period the snap-shot channel estimation performs robustly in fast fading. Since a snap-shot channel estimation problem relies on a fixed channel during the observation period, a long observation may become counterproductive [10, 20]. Finally, the estimates will be more accurate when there are fewer parameters to be estimated. Having obtained the estimates of the channel, the overall channel can be computed from the convolution of the estimate and the filter.
2. Based on the new channel estimation equation, we have obtained the channel estimators under least squares estimation (LSE), maximum likelihood estimation (MLE), and maximum *a posteriori* estimation (MAP) criteria. Theoretical as well as simulation mean squares channel estimation errors are evaluated for each of the channel estimators.
3. We have proposed the use of a matched filtered diversity combining decision feedback equalization (DFE) instead of the “straightforward” diversity combining DFE [72] for symbol detection in a relatively small constellation such as QPSK and DQPSK. We have explicitly shown the theoretical equivalence of the two structures by deriving the matched filter form from the straightforward form under the assumption of perfect channel estimates. We have also identified the eigenvalue spread problem of the straightforward form, which significantly degrades the performance of the overall receiver in the presence of channel estimation error. A large scale channel estimation noise enhancement occurs. The matched filtered form solves the eigenvalue problem, and requires less computation than the straightforward form does.

4. To cope with the fast time-varying ISI channel, we have proposed a new DFE computation algorithm for the matched filtered diversity combining DFE, termed the non-Toeplitz DFE (NT-DFE). This is obtained by incorporating the channel variation during the decision delay into the minimum mean square error criterion. For time-invariant channels, the longer the DFE filters the better the ISI suppression capability. However, in fast time-varying channel, long DFE filters might become counter-productive due to the channel variation during the DFE length [58].
5. Simulation was performed to evaluate the DFE receivers, which employ the proposed channel estimation and the diversity combining DFE methods. The proposed receiver has been shown superior to the receiver that employs a recursive least square channel tracking receiver and diversity combining DFE. The feasibility of a suboptimal matched filtered DFE, suitable for a handset application since it requires significantly less computations, was also evaluated.
6. We have derived the matched filter bound symbol error rate expressions for  $q$ -ary QAM signalling. With this theoretical expression, we were able to observe how an addition of an antenna and the change of the channel's MPDP may affect the overall detection performance of the transceiver and the expected order of diversity. In addition, we continued the results of matched filter SNR to derive the spectral efficiency limit of the frequency-selective channel for variable rate  $q$ -QAM signaling.
7. We have identified the symbol spaced equivalent ISI channel model which combines the  $L$  explicit diversity branches with only matched filtering required at each branch. This will provide the sufficient statistics and the necessary ISI trellis for the maximum likelihood sequence detection (MLSD).
8. We developed an adaptive, low complexity tree-search detection receiver for uncoded (or gray-coded) modulation signals using the T-algorithm for the fast fading multipath ISI channels. Unlike previous research on sequence based detection receiver, a symbol spaced receiver is not assumed a priori, rather the receiver utilizes the feedforward channel estimation to derive the matched filter, and obtains the symbol-spaced channel taps and the sequence of sufficient statistic to be used in the T-algorithm search.

9. We have proposed the use of per-survivor processing in conjunction with the use of the T-algorithm to reduce the average number of survivor paths, which at the same time brings a further SNR advantage over the DFE receiver. The reason for the win-win situation is that in a correct path, the channel estimate is enhanced; while in the wrong paths, the channel estimate degrades quickly, promoting early elimination of the path from the survivor list.
10. We have extended the tree-search receiver using the T-algorithm for the decoding of the channel-interleaved trellis-code transmitted over the fast fading multipath ISI channels. Since the receiver uses a tree-search version of the T-algorithm, joint decoding of the trellis code over the de-interleaver and the ISI trellis can be performed. The simulation results indicate that the receiver achieves the available time-diversity benefit of the code for the fast Rayleigh fading ISI channels, with a very moderate increase in the decoding complexity compared to the uncoded DFE.

In total, these contributions significantly extend the ability to achieve spectrally efficient and reliable communications over wireless channels.

## 9.2 Future Work

Much work remains to be solved to realize the envisioned universal communications networks. The following three layers of future work may be meaningful extension to this dissertation. They are VLSI implementation at the chip level, further improvement at the system design level, and system integration of the transceiver with higher networking layers such as power and medium access controls.

We note that VLSI implementation of the T-algorithm is possible [127]. Thus, the post-processor receiver techniques developed for Chapter 7 and Chapter 8 can be implemented in VLSI chips. The most challenging problem is to reduce the number of operations required to implement the pre-processing filtering of the received signals, especially the matrix inversion operation required to obtain the mean-square whitening

filter.

In recent research it was shown that the spectral efficiency of the wireless transceiver can be improved dramatically by the use of multiple transmit diversity antennas along with the use of multiple receive diversity antennas. It was shown in [128] that the use of both transmit and receive diversity antennas creates a new degree of freedom (space-dimension) to play with in Shannon-theoretic capacity calculations, and the capacity of the wireless channel can be increased multiple times, as much as linearly with the number of antennas used at the transmitter, compared to the single transmit antenna system. The use of multiple diversity antennas was considered only at the receiver in this dissertation. An explosively growing body of publications [129][130] repeatedly confirms the benefits of using multiple transmit and multiple receive antennas.

We have focused on spectrally efficient systems only at the link-layer in this dissertation. In the context of multiple users sharing the same allocated frequency spectrum and physical spaces, we should be able to come up with an area efficient networking scheme which implements efficient controls of transmit power, medium access and sharing taking full benefit of the link-flexibility the new transceiver provides.

# Glossary

## List of Acronyms and Abbreviations

<b>AMPS</b>	Advanced Mobile Phone Service
<b>AWGN</b>	Additive white Gaussian noise
<b>BER</b>	Bit error rate
<b>CDMA</b>	Code division multiple access
<b>DCA</b>	Dynamic channel allocation
<b>DCR</b>	Digital cellular radio
<b>DECT</b>	Digital European Cordless Telecommunications
<b>DPCA</b>	Dynamic power and channel allocation
<b>DQPSK</b>	Differential quadrature phase-shift keying
<b>DS</b>	Direct sequence
<b>FCC</b>	Federal Communications Commission (U. S.)
<b>FDMA</b>	Frequency division multiple access
<b>FEC</b>	Forward error correction
<b>FH</b>	Frequency hop

<b>GSM</b>	Groupe Spécial Mobile or Global System for Mobile Communication
<b>IS-54</b>	Interim Standard 54 (TIA/EIA TDMA cellular standard, U. S.)
<b>IS-95</b>	Interim Standard 95 (TIA/EIA CDMA cellular standard, U. S.)
<b>ISDN</b>	Integrated Services Digital Network
<b>ISI</b>	Inter-symbol interference
<b>ISM</b>	Industrial, Scientific, and Medical (bands, devices)
<b>LAN</b>	Local area network
<b>MPDP</b>	Multipath Power-Delay Profile
<b>MTSO</b>	Mobile telephone switching office
<b>PBX</b>	Private branch exchange
<b>PCN</b>	Personal Communications Network (Europe)
<b>PCS</b>	Personal Communications Services (U. S.)
<b>PN</b>	Pseudo-noise
<b>PDC</b>	Personal Digital Cellular (Japan)
<b>PSTN</b>	Public Switched Telephone Network
<b>QAM</b>	Quadrature amplitude modulation
<b>QOS</b>	Quality of service
<b>SIR</b>	Signal-to-interference ratio
<b>SNR</b>	Signal-to-noise ratio
<b>SS</b>	spread spectrum
<b>TCM</b>	Trellis coded modulation

<b>TDMA</b>	Time division multiple access
<b>TIA</b>	Telecommunications Industry Association (U. S.)

## Definitions

**Baud:** The unit of number of bits per symbol.

**Bit error rate:** The ratio of the number of bits incorrectly received to the total number of bits transmitted.

**BCH Codes:** A large class of cyclic block codes that include both binary and nonbinary alphabets.

**Block codes:** A type of error correcting code of fixed length  $N$ . These  $N$  symbols represents  $K$  symbols of information and  $(N - K)$  parity or redundancy symbols where  $N \geq K$ .

**Blocking:** New users to the system are declined services due to the lack of channel resources.

**Capacity:** In the context of networking, power control or medium access control, it implies the maximum number of users a system can support. In the context of link-layer, it implies the maximum number of bits a channel can support with an arbitrary small error.

**Cellular Radio:** A system in which a service area is divided into smaller areas called cells where users in each cell communicate with a base station usually located near the center of the cell.

**Channel coding:** Adding controlled redundancy to the information sequence to improve reliability of data transmitted through a noisy channel.

**Coherence bandwidth:** A statistical measure of the range of frequencies over which the channel passes all spectral components with approximately equal gain and linear phase.

**Coherent detection:** Detection using a reference signal that is synchronized in frequency and phase to the transmitted signal.

**Convolutional codes:** A type of code in which output sequence consists of a selected set of linear combinations of the input sequence.

**Code division multiple access:** A way of sharing a common spectrum in which signals from different transmitters are distinguished by a code known to the intended receiver. It is usually divided into two categories: direct sequence (DS) and frequency hop (FH).

**Differential quadrature phase-shift keying (DQPSK):** A digital modulation scheme that uses the phase changes of multiples of ninety degrees or  $\pi/2$  from the previous symbol to carry two bits of information.

**Dispersion:** The spreading, separation, or scatter of a waveform during transmission.

**Diversity:** The reception of different versions of the same information, each is usually with independent fading levels.

**Down-link:** The radio link where the base station is transmitting to a user in the coverage area. Also known as the forward link.

**Erlang:** A unit-less measure of the offered load.

**Fading:** The variation of the intensity or relative phase of any frequency component of a received signal due to changes in the characteristics of the propagation path with time.

**Finite impulse response (FIR) filter:** A discrete-time filter of which the coefficients represents the sampled, truncated impulse response of a filter.

**Flat fading:** Fading resulting in similar attenuation of all frequency components of signal.

**Forward link:** The radio link where the base station is transmitting to a user in the coverage area. Also known as the down-link.

**Frequency diversity:** A transmission technique used to minimize the effects of fading wherein the same information signal is transmitted and received simultaneously on two or more independent carrier frequencies.

**Frequency reuse:** The scheme of assigning different frequencies to adjacent cells so that users communicating at the same frequency would not be too close to one another.

**Frequency-selective fading:** Fading in which not all frequency components of the received radio signal are attenuated equally.

**Hand-off (HO):** The process of a user changing the base station it communicates with as it moves across the cell boundaries. Also known as hand-over.

**Integrated services digital network (ISDN):** An integrated digital network which can establish connection for data and telephony services using the same transmission equipment.

**Interleaving:** A method of spacing successive symbols of a given codeword at wide intervals in time to overcome burst errors.

**Offered load:** The ratio of the new user arrival rate divided by the system service rate. It may be normalized to the number of channels are available to the system.

**Modulation:** The process of varying certain characteristics of a carrier in accordance with a message signal.

**Multilevel trellis coded modulation:** A modified trellis coded modulation where the uncoded bits are coded often with an error correcting code that explore the geometric properties of the signal constellations.

**Multipath:** The large set of propagation paths that the transmitted signal takes to the receiver. The multiple paths could be caused by scattering.

**Multipath fading:** Fading that results when radio signals reach the receiving antenna by two or more paths.

**Multiple-Access:** A sharing scheme that enables dispersed users to simultaneously access a common channel resource.

**Network:** An organization of terminals capable of intercommunication.

**Outage:** A condition wherein a user is deprived of service due to unavailability of the communication system.

**Parity-check code:** A simple forward error correcting block code of rate  $(N, N-1)$ . It adds a parity bit at the end of  $(N-1)$  information bits so that the  $N$ -bit block would have even number of ones. This code can be decoded using a simple two-state trellis decoder.

**Personal Communication Services (PCS):** For standard purposes, it is an umbrella term to describe services and supporting systems that provide users with the ability to communicate anytime, anywhere, and in any form.

**Power control (PC):** A technique employed to adjust the transmit power from every radio link to the minimum level required for reliable transmission.

**Quadrature amplitude modulation:** A coherent digital modulation technique that uses the amplitude in both the I-channel and the Q-channel of the signal to represent information.

**Reverse link:** The radio link where a user is transmitting to a base station. Also known as the up-link.

**Signal-to-Interference Ratio (SIR):** The ratio of the desired signal power divided by the total power of the interference and the background noise.

**Spread Spectrum (SS):** A signaling scheme in which the transmission bandwidth is much greater than the information rate.

**Transceiver:** A contraction of “transmitter/receiver.” The term is used when a communication device can both transmit and receive.

**Trellis coded modulation (TCM):** A digital bandwidth-efficient modulation technique that incorporates the concept of set partitioning and channel coding.

**Up-link:** The radio link where a user is transmitting to a base station. Also known as the reverse link.

**White noise:** Noise whose frequency spectrum is uniform over a wide frequency band.

**Wireless Communications:** General term for communication without wires.

# References

## For Chapter 1

- [1] J.V. Cuttag, “Communications Chameleons (MIT Laboratory for Computer Science’s Oxygen Project: Cover Story),” *Scientific American*, v.281, n2, p. 58-9, August 1999.
- [2] M.L. Dertouzos, “The Future of computing. (MIT Laboratory for Computer Science’s Oxygen Project: Cover Story),” *Scientific American*, v.281, n2, p. 52-5, August 1999.
- [3] V. Zue, “Talking with your computer (MIT Laboratory for Computer Science’s Oxygen Project: Cover Story),” *Scientific American*, v.281, n2, p. 56-7, August 1999.
- [4] A. Agarwal, “Raw Computation (MIT Laboratory for Computer Science’s Oxygen Project: Cover Story),” *Scientific American*, v.281, n2, p. 60-3, August 1999.
- [5] G. Christian Hill, “First voice, now data,” Section R: The Internet cuts the cord, *The Wall Street Journal Reports*, Sept. 20, 1999.
- [6] S.N. Mehta, “Putting it all together,” Section R: The Internet cuts the cord, *The Wall Street Journal Reports*, Sept. 20, 1999.

- [7] K. Swisher, "Tethered once more," Section R: The Internet cuts the cord, The Wall Street Journal Reports, Sept. 20, 1999.
- [8] P. Kam, "Bit error rate probabilities of MDPSK over the nonselective Rayleigh fading channel with diversity reception," *IEEE Trans. Comm.*, vol. 39, pp. 220-224, Feb. 1991.
- [9] TIA/EIA IS-54, "Cellular system dual-mode mobile station-base station compatibility standard," Telecommunications Industry Association, December, 1991.
- [10] Heinrich Meyr and Ravi Subramanian, "Advanced digital receiver principles and technologies for PCS," *IEEE Commun. mag.*, pp. 68- 78, Jan. 1995.

## **For Chapter 2**

- [11] R.B. Ertel, et al, "Overview of spacial channel models for antenna array communication systems," *IEEE personal commun. mag.*, pp. 10 - 22, Feb. 1998.
- [12] Jørgen Bach Andersen, Theodore S. Rappaport, and Susumu Yoshida, "Propagation measurements and models for wireless communications channels," *IEEE Commun. mag.*, pp. 42- 49, Jan. 1995.
- [13] J.C. Chuang, "The effects of time delay spread on portable radio communications channels with digital modulation," *IEEE J. Sel. Areas in Comm.* vol. SAC-5, no.5, pp. 879-889, June 1987.
- [14] H. Hashemi," Simulation of the urban radio propagation channel," *IEEE Trans. Vehic. Technol.*, vol. VT-28, Aug. 1979.

- [15] W.C. Jakes, ed., *Microwave Mobile Communications*. New York, NY: Wiley, 1974.
- [16] Edward A. Lee and D.G. Messerschmitt, *Digital Communication*, Kluwer Academic Publishers: Boston/Dordrecht/London, 2nd Edition, 1994.
- [17] R. Steel, *Mobile Radio Communications*. New York: IEEE press, 1992.
- [18] S. E. Alexander, "Characterising buildings for propagation at 900 MHz," *Electronics Letters*, Vol. 19, No. 20, pp. 860, Sep. 1983.
- [19] D. C. Cox, "Wireless network access for personal communications," *IEEE Communications*, pp. 96-115, Dec. 1992.
- [20] H. Hashemi, "The indoor radio propagation channel," *Proceedings of the IEEE*, Vol. 81, No. 7, pp. 943-68, July 1993.
- [21] H. Hashemi, "Impulse response modeling of indoor radio propagation channels," *IEEE JSAC*, Vol. 11, No. 7, pp 967-78, Sep. 1993.
- [22] H. Hashemi, D. Tholl, G. Morrison, "Statistical modeling of the indoor radio propagation -- part I," *Proc. of IEEE Vehicular Technology Conf.*, pp. 338-342, VTC 92, May 1992.
- [23] H. Hashemi, D. Tholl, G. Morrison, "Statistical modeling of the indoor radio propagation -- part II," *Proc. of IEEE Vehicular Technology Conf.*, pp. 839-842, VTC 92, May 1992.
- [24] G. Janssen and R. Prasad, "Propagation measurements in an indoor radio environment at 2.4 GHz, 4.75 GHz and 11.5 GHz," *Proc. IEEE Vehicular Technology Conf.*, VTC 92, Denver, CO., May 1992, pp. 621-624.
- [25] W. C. Y. Lee, *Mobile Communications Design Fundamental*, Wiley and Sons, New York, New York, 1993.
- [26] J. C. Liberti and T. S. Rappaport, "Statistics of shadowing in indoor radio

- channels at 900 and 1900 MHz,” *Proc. of IEEE*, pp. 1066-70, 1992.
- [27] T. S. Rappaport, S. Y. Seidel, K. Takamizawa, “Statistical channel impulse response models for factory and open plan building radio communication system design,” *IEEE Tran. on Comm.*, Vol. 39, No. 5, pp 794-806, May 1991.
- [28] A. A. M. Saleh and R. A. Valenzuela, “A statistical model for indoor multipath propagation,” *IEEE JSAC*, Vol. AC-5, No. 2, pp. 128-137, 1987.
- [29] S. Y. Seidel and T. S. Rappaport, “900 MHz path loss measurements and prediction techniques for in-building communication system design,” *IEEE Tran. on Vehicular Technology*. pp 613-618, 1991.
- [30] A. F. de Toledo and A. M. D. Turkmani, “Propagation into and within building at 900, 1900 and 2300 MHz,” *Proc. of IEEE Vehicular Technology Conf.* pp. 633-36, VTC 92, May 1992.
- [31] G. L. Turin, “Introduction to spread-spectrum antimultipath techniques and their application to urban digital radio,” *Proc. of IEEE*, Vol. 68, No. 3, pp. 328-353, Mar. 1980.
- [32] G. L. Turin, “The Effects of multipath and fading on the performance of direct-sequence CDMA systems,” *IEEE JSAC*, Vol. SAC-2, No. 4, pp. 597-603. July 1984.
- [33] J. G. Proakis, *Digital Communications*, new york: McGraw-Hill, 1983.
- [34] European digital cellular telecommunications system (Phase 2); Radio transmission and reception (GSM 05.05) Draft prETS 300 577, European Telecommunications Standard Institute, Fifth Edition, Dec. 1995.
- [35] B. Sklar, “Rayleigh fading channels in mobile digital communication systems Part I: Characterization”, *IEEE Communications Magazine*, pp. 90

~ 100, July 1997.

### **For Chapter 3**

- [36] Draft Recommendation V.34, A Modem Operating at Data Signalling Rates of Up to 28800 bit/s for Use on the General Switched Telephone Network and on Leased Point-to-Point 2-Wire Telephone-Type Circuits,
- [37] D. Hughes-Hartogs, Ensemble Modem Structure for Imperfect Transmission Media, United States Patent 4,679,227. Jul. 1987.
- [38] Eyuboglu et al., Line Probing Modem, United States Patent 5,048,054, Sep. 10, 1991.
- [39] I. Kalet, "The multitone channel," *IEEE Tran. on Comm.*, Vol. 37, No. 2, pp. 119-124, Feb, 1989.
- [40] A. Chini, Multicarrier modulation in Frequency-Selective Fading Channels, Ph.D. Dissertation, Department of Electrical Engineering, Carleton University, Ottawa, ON, Canada, Sept. 1994.
- [41] S.K. Wilson, Digital Audio Broadcasting in a Fading and Dispersive Channels, Ph.D. Dissertation, Department of Electrical Engineering, Stanford University, Stanford, CA, Aug. 1994.
- [42] K. Yao, Lecture note provided in class EE 230 C, Department of Electrical Engineering, University of California, Los Angeles, Los Angeles, Fall quarter, 1995.
- [43] Gregory J. Pottie, Lecture note provided in class EE 230B, Department of Electrical Engineering, University of California, Los Angeles, Los Angeles, Spr. quarter, 1994.

- [44] M. Tomlinson, "New automatic equaliser employing modulo arithmetic," *Electronics Letters*, vol. 7, (no. 5-6), p. 138-9, March 1971.

#### **For Chapter 4**

- [45] Guanghua Deng, Jim Cavers, and Paul Ho, "A reduced dimensionality propagation model for frequency selective Rayleigh fading channels," *IEEE Glovecom 95*, pp. 1158-1162, 1995.
- [46] G.K. Kaleh, "Channel estimation for block transmission systems," *IEEE S. Areas in Commun.*, vol. 13, no. 1, pp. 110-121, Jan. 1995.
- [47] J. Lin, J.G. Proakis, F. Ling, and H. Lev-Ari, "Optimal tracking of time-varying channels: A frequency domain approach for known and new algorithms," *IEEE Trans. on Sel. Areas in Comm.*, Vol. 13, no.1, pp.141-153, Jan. 1995.
- [48] R.A. Ziegler and J.M. Cioffi, "Estimation of time-varying digital radio channels," *IEEE Trans. on Vehic. Tech.*, vol. 41, no. 2, pp. 134-151, May 1992.
- [49] K.A. Hamied, Mushfiqur Rahman, and Mohamed S. El-Hennawey, "A new channel estimator for fast start-up equalization," *IEEE Trans. on Commun.*, vol. 39, no.2, pp.177-181, Feb. 1991.
- [50] C. Rao, *Linear Statistical Inference and Its applications*. New York: John Wiley & Sons, 1973.
- [51] A.S. Khayrallah, R. Ramésh, G. Bottomley, and D. Koilpillai, "Improved channel estimation with side information," *IEEE 47 th Vehic. Tech. Conf. Proc.*, vol 2, pp. 1049-1053, May 1997.

## For Chapter 5

- [52] P. Balaban and J. Salz, "Optimum diversity combining and equalization in digital data transmission with applications to cellular mobile radio - Part I: Theoretical considerations and Part II: Numerical results," *IEEE Trans. Comm.*, vol. COM-40, no. 5 pp. 885-907, May 1992.
- [53] S.N. Crozier, Short-block, data detection techniques employing channel estimation for fading, time-dispersive channels, PhD thesis, Dept. of systems and computer engineering, Carleton University, Ottawa, ON, Canada, May 1990.
- [54] G.W. Davidson, D.D. Falconer and A.U.H. Sheikh, "An investigation of block-adaptive decision feedback equalization for frequency selective fading channels," *Can.J.Elect. & Comp. Eng.*, Vol. 13, no. 3-4, 1988.
- [55] E. Eleftheriou and D.D. Falconer, "Adaptive equalization tech. for HF channels", *IEEE J. Sel. Areas in Comm.*, vol. SAC-5, no.2, pp.238-247, Feb. 1987.
- [56] D.D. Falconer, Fumiyuki Adachi, and Björn Gudmundson, "Time division multiple access methods for wireless personal communications," *IEEE Comm. Mag.*, pp. 50-57, Jan. 1995.
- [57] S. Fechtel and Heinrich Meyr, "Optimal parametric feedforward estimation of frequency-selective fading radio channels," *IEEE Trans. on Comm.*, vol. 42, no. 2/3/4, pp. 1639-1650, Feb./Mar./Apr. 1994.
- [58] S. Fechtel and Heinrich Meyr, "An investigation of channel estimation and equalization techniques for moderately rapid fading HF-channels," in *Proc. ICC '91*, pp. 768-772.

- [59] S. Fechtel and Heinrich Meyr, "Optimal feedforward estimation of frequency-selective fading radio channels using statistical channel information," in *Proc. ICC '92*, vol.2, pp. 677-681.
- [60] B. Glance and L.J. Greenstein, "Frequency-selective fading effects in digital mobile radio with diversity combining," *IEEE Trans. on Comm.*, vol. COM-31, no.9, pp. 1085-1094, Sep. 1983.
- [61] N.W.K. Lo, D.D. Falconer and A.U.H. Sheikh, "Adaptive equalization and diversity combining for mobile radio using interpolated channel estimates," *IEEE Trans. Vehic. Tech.*, vol. VT-40, no.3, pp. 636-645, Aug. 1991.
- [62] P. Mosen, "Feedback equalization for fading dispersive channels," *IEEE Trans. on Inform. Theory*, pp. 56-64, Jan. 1971.
- [63] P. Mosen, "Theoretical and measured performance of a DFE modem on a fading multipath channel," *IEEE Trans. Veh. Technol.*, vol.COM-25, no. 10, pp. 1144-1153, Oct. 1977.
- [64] P. Mosen, "Digital transmission performance on fading dispersive diversity channels," *IEEE Trans. on Comm.*, vol. COM-21, no. 1, pp. 33-39, Jan. 1973.
- [65] J.G. Proakis, *Digital Communications*. New York, NY: McGraw-Hill, 3rd Edition, 1989.
- [66] J. Salz, "Optimum mean-square decision feedback equalization," *Bell Syst. Tech., J.*, vol. 52, no. 8, pp. 1341- 1373, Oct. 1973.
- [67] P.K. Shukla and L.F. Turner, "Channel-estimation-based adaptive DFE for fading multipath radio channels," *IEE Proceedings-I*, vol. 138, no.6, pp., 525-543, Dec. 1991.
- [68] P.K. Shukla, and L.F. Turner, "Examination of an adaptive DFE and MLSE/

- near-MLSE for fading multipath radio channels,” *IEE Proceedings-I*, vol. 139, no. 4, pp. 418-428, Aug. 1992.
- [69] M. Stojanovic, J. G. Proakis, and J. Catipovic, “Analysis of the impact of channel estimation errors on the performance of a decision-feedback equalizer in fading multipath channels,” *IEEE Trans. on Comm.*, vol. 43, no. 2/3/4, 877-886, Feb./Mar./Apr. 1995.
- [70] A.A. Abu-Dayya and N.C. Beaulieu, “Micro- and macrodiversity MDPSK on shadowed frequency-selective channels,” *IEEE Trans. on Commun.*, vol. 43, no. 8, pp. 2334-2343, Aug. 1995.
- [71] Heung-No Lee and Gregory J. Pottie, “Channel estimation based adaptive equalization/diversity combining for Time-varying dispersive channels,” *IEEE 47 th Vehic. Tech. Conf. Proc.*, vol 2, pp. 884-888, May 1997.
- [72] Heung-No Lee and Gregory J. Pottie, “Fast adaptive equalization/diversity combining for time-varying dispersive channels,” *IEEE Trans. on Commun.* vol. 46, pp. 1146-62, Sept. 1998.

## **For Chapter 6**

- [73] A.D. Whalen, *Detection of Signals in Noise*. San Diego: Academic Press, Inc., 1971.
- [74] F. Ling, “Matched filter-bound for time-discrete multipath Rayleigh fading channels,” *IEEE Trans. Veh. Technol.*, vol. 43, no. 2/3/4, pp. 710-713, Feb./Mar./Apr. 1995.
- [75] J. H. Hayes, “Adaptive feedback communications,” *IEEE Trans. on Commun. Technol.*, vol. COM-16, pp. 29-34, February 1968.

- [76] J. K. Cavers, "Variable-rate transmission for Rayleigh fading channels," *IEEE Trans. on Commun.*, vol. COM-20, pp. 15-22, February 1972.
- [77] Mohamed-Slim Alouini and Andrea Goldsmith, "Adaptive M-QAM modulation over Nakagami fading channels," submitted to *Globecom 97*.
- [78] Mohamed-Slim Alouini and Andrea Goldsmith, "Capacity of Rayleigh fading channels under different adaptive transmission and diversity-combining techniques," submitted to *IEEE Trans. Veh. Technol.*
- [79] Andrea Goldsmith and Pravin Varaiya, "Increasing spectral efficiency through power control," *IEEE ICC 93' Proc.*, vol.1, pp. 600-604, May 1993.
- [80] Soon-Ghee Chua and Andrea Goldsmith, "Variable-rate variable-Power MQAM for fading channel," To appear *IEEE Trans. on Commun.*
- [81] W.T. Webb and Raymond Steele, "Variable rate QAM for mobile radio," *IEEE Trans. on Commun.*, vol. 43, no. 7, pp. 2223 - 2230, July 1995.
- [82] K. Raith, "Capacity of digital cellular TDMA systems," *IEEE Trans. on Vehicular Technology*, Vol. 40, No. 2, pp. 323-332, May 1991.
- [83] J.K. Cavers et. al., "Exact calculation of the union bound on performance of trellis-coded modulation in fading channels," *IEEE Trans. on Commun.*, vol. 46, no.5, p. 576-579, May 1998.
- [84] S.A. Fechtel and Heinrich Meyr, "Matched filter bound for trellis-coded transmission over frequency-selective fading channels with diversity," *European Trans. on Telecommun. and Related Technol.*, vol.4, (no.3):343-54, May-June 1993.

## For Chapter 7 & 8

- [85] N. Al-Dhahir and J.M. Cioffi, "MMSE decision feedback equalizers: Finite length results," *IEEE Trans. Information Theory*, vol. 41, no.4, pp. 961-975, July 1995.
- [86] G.E. Bottomley and S. Chennakeshu, "Unification of MLSE receivers and extension to time-varying channels," *IEEE Trans. on Commun.*, vol. 46, no. 4, pp. 464-472, April 1998.
- [87] K.C. Chang and W.H. Lam, "An adaptive reduced-state channel equalizer with T-algorithm," *Proc. of IEEE 44th VTC*, vol.2, pp. 1237-40, Jun 1994.
- [88] G.D. Forney, "Maximum-likelihood sequence estimation of digital sequences in the presence of intersymbol interference," *IEEE Trans. on Inform. Theory*, vol. IT-18, no.3, pp. 363-378, May 1972.
- [89] Heung-No Lee and Gregory J. Pottie, "Adaptive sequence detection using T-algorithm for multipath fading ISI channels," *Proc. of IEEE ICC 1999, CTMC*, in print.
- [90] Heung-No Lee and Gregory J. Pottie, "Adaptive sequence detection of channel-interleaved trellis-coded modulation signals over multipath fading ISI channels," *Proc. of IEEE 49 th Vehic. Tech. Conf.*, in print.
- [91] Samir Kallel and Kaiping Li, "Bidirectional sequential decoding," *IEEE Trans. on Inform. Theory*, vol.43, no. 4, pp. 1319-1326, July 1997.
- [92] Robert M. Fano, "A heuristic discussion of probabilistic decoding," *IEEE Trans. on Inform. Theory*, vol. IT-9, pp. 64-73, April 1963.
- [93] J. Massey, "Variable-length codes and the Fano metric," *IEEE Trans. Inform. Theory*, pp. 196-198, Jan. 1972.

- [94] Ettie Katz and Gordon L. Stüber, “Sequential sequence estimation for trellis-coded modulation on multipath fading ISI channel,” *IEEE Trans. on Commun*, vol. 43, no. 12, pp. 2882-2885, december 1995.
- [95] Fuqin Xiong, Ali Zerik, and Ed Shwedyk, “Sequential sequence estimation for channels with intersymbol interference of finite or infinite length,” *IEEE Trans. on Commun*, vol. 38, no. 6, pp. 795-804, June 1990.
- [96] Fuqin Xiong, “Sequential decoding of convolutional codes in channels with intersymbol interference,” *IEEE Trans. on Commun*, vol. 43, no 2/3/4, pp. 828-Feb./March/April 1995.
- [97] G. Ungerboeck, “Adaptive maximum-likelihood receiver for carrier-modulated data-transmission systems,” *IEEE Trans. on Commun*, COM-22, no. 5, pp. 624-636, May 1974.
- [98] G. Ungerboeck, “Channel coding with multilevel/phase signal,” *IEEE Trans. on Inform. Theory*, IT-28, no. 1, pp. 55-66, May 1982.
- [99] G. Ungerboeck, “Trellis-coded modulation with redundant signal sets. Part I: introduction,” *IEEE Comm.*, Vol. 25, No. 2, pp. 5-11, Feb. 1987.
- [100] G. Ungerboeck, “Trellis-coded modulation with redundant signal sets. Part II: state of art,” *IEEE Comm.*, Vol. 25, No. 2, pp. 12-21, Feb. 1987.
- [101] M. Vedat Eyuboglu, “Reduced-state sequence estimation for coded modulation on intersymbol interference channels,” *IEEE Journal on Sel. Areas in Commun.*, vol. 7, no. 6, pp. 989-995, August 1989.
- [102] Raafat E. Kamel and Yeheskel Bar-Ness, “Reduced-complexity sequence estimation using state partitioning,” *IEEE Trans. on Commun.*, vol. 44, no. 9, pp. 1057-1063, Sept. 1996.
- [103] Gregory J. Pottie and Desmond P. Taylor, “A comparison of reduced

- complexity decoding algorithms for trellis codes,” *IEEE Journal on Selected Areas in Commun.*, vol. 7, no. 9, pp. 1369-1380, Dec. 1989.
- [104] Samir Kallel and Kaiping, “Bidirectional sequential decoding,” *IEEE Transactions on Inform. Theory*, vol. 43, no. 4, pp. 1319-1326, July 1997.
- [105] A. M. Michelson and A.H. Levesque, *Error-control techniques for digital communication*, New York, John Wiley & Sons, 1985.
- [106] J. Cioffi, G. Dudevoir, M. Eyuboglu, and G. D. Forney, “Minimum mean-square-error decision feedback equalization and coding-part I: Equalization results,” *IEEE Transactions on Commun.*, vol. 43, no. 10, pp. 2582-2594, Oct. 1995.
- [107] J. Cioffi, G. Dudevoir, M. Eyuboglu, and G. D. Forney, “Minimum mean-square-error decision feedback equalization and coding-part II: Coding results,” *IEEE Transactions on Commun.*, vol. 43, no. 10, pp. 2595-604, Oct. 1995.
- [108] Yonghai Gu and Tho Le-Ngoc, “Adaptive combined DFE/MLSE techniques for ISI channels,” *IEEE Transactions on Commun.*, vol. 44, no. 7, pp. 847-857, July 1996.
- [109] J. B. Anderson and S. Mohan, *Source and Channel Coding: An Algorithmic Approach*, Kluwer Academic Pub., Boston, MA, 1991.
- [110] S. Benedetto, E. Biglieri, V. Castellani, *Digital Transmission Theory*, Prentice-Hall, Englewood Cliffs, NJ, 1987.
- [111] E. Biglieri, D. Divsalar, P. J. McLane, M. K. Simon, *Introduction to Trellis-Coded Modulation with Applications*, Macmillan Pub. Co., New York, NY 1991.
- [112] A. R. Calderbank and N. J. A. Sloane, “New trellis codes based on lattices and cosets,” *IEEE Transactions on Information Theory*, Vol. IT-33, No. 2, pp. 177-

195, March 1987.

- [113] T. M. Cover and J. A. Thomas, *Elements of Information Theory*, John Wiley and Sons, Inc., New York, NY, 1991.
- [114] G. D. Forney, "Coset codes -- part I: Introduction and geometrical classification," *IEEE Tran. on Information Theory*, Vol. 34, No. 5, pp. 1123-51, Sep. 1988.
- [115] K.D. MacNeill and S.J. Simmons, "Performance of reduced computation trellis decoders for mobile radio with frequency-selective fading," *IEEE ICC 91*, vol.2, pp. 784-788, Jun 1991.
- [116] S.J. Simmons, "Breadth-first trellis decoding with adaptive effort," *IEEE Trans. on Commun.*, vol. 38, no.1, pp. 3-12, Jan 1990.
- [117] S.J. Simmons, "Alternative trellis decoding for coded qam in the presence of ISI," *IEEE Trans. on Commun.*, vol. 42, no. 2/3/4, pp. 1455-1459, Feb/Mar/Apr 1994.
- [118] G. J. Pottie and A. R. Calderbank, "Channel coding strategies for cellular radio," *Proc. of IEEE Int. Symposium on Information Theory*, San Antonio, TX, Jan. 1993. (submitted to *IEEE Trans. on Vehicular Technology*).
- [119] G. J. Pottie and D. P. Taylor, "Multilevel codes based on partitioning," *IEEE Tran. on Information Theory*, Vol. 35, No. 1, pp. 87-98, Jan. 1989.
- [120] A. J. Viterbi, "Convolutional codes and their performance in communication systems," *IEEE Tran. on Comm. Technology*, Vol. COM-19, No. 5, pp. 751-772, Oct. 1971.
- [121] E. Katz and G. L. Stüber, "Sequential sequence estimation for trellis-coded modulation on multipath fading ISI channels," *IEEE Trans. Commun.*, vol. 43, no. 12, pp 2882-2885, Dec. 1995.

- [122] R. Raheli and A. Polydoros, "Per-survivor processing: A general approach to MLSE in Uncertain environment," *IEEE Trans. Commun.*, vol. 43, no. 2/3/4, pp 354-364, Feb./Mar./Apr. 1995.
- [123] T. Vaidis and C.L. Weber, "Block adaptive techniques for channel identification and data demodulation over band-limited channels," *IEEE Trans. on Commun.*, vol. 46, no. 2, pp. 232-243, Feb 1998.
- [124] K.A.Hamied and G.L. Stüber, "Performance of trellis-coded modulation for equalized multipath fading ISI channels," *IEEE Trans. Veh. Technol.*, vol. 44, no.1, pp 50 - 58, Feb. 1995.
- [125] W.-H. Sheen and G.L. Stüber, "MLSE equalization and decoding for multipath-fading channels," *IEEE Trans. Commun.*, vol. 39, no. 10, pp. 1455 ~ 64Oct. 1991.
- [126] M.V. Eyuboglu and S.U.H. Qureshi, "Reduced-state sequence estimation with set partitioning and decision feedback," *IEEE Trans. Commun.*, vol. COM-36, pp. 13-20, Jan. 1988.

## **For Chapter 9**

- [127] P.A. Bengough and S.J. Simmons, "Sorting-based VLSI architecture for the M-algorithm and T-algorithm trellis decoders," *IEEE Trans. Commun.*, vol. 43, no.2-4, pp 514-22, Feb./Apr. 1995.
- [128] J.H. Winters, "The impact of Antenna diversity on the capacity of wireless communication systems," *IEEE Trans. Commun.*, vol. 42, no.2-4, pp 1740-51, Feb./Apr. 1994.
- [129] G.J. Foschini, "Layered space-time architecture for wireless

communication in a fading environment when using multi-element antennas,” Bell Labs Technical Journal, pp. 41 - 59, Autumn 1996.

- [130] A.F. Naguib et al, “A space-time coding modem for high-data-rate wireless communications,” *IEEE Journal on sel. areas of commun.*, vol. 16, no.8, pp 1459-78, Oct. 1998.